Advances in Oil and Gas Exploration & Production

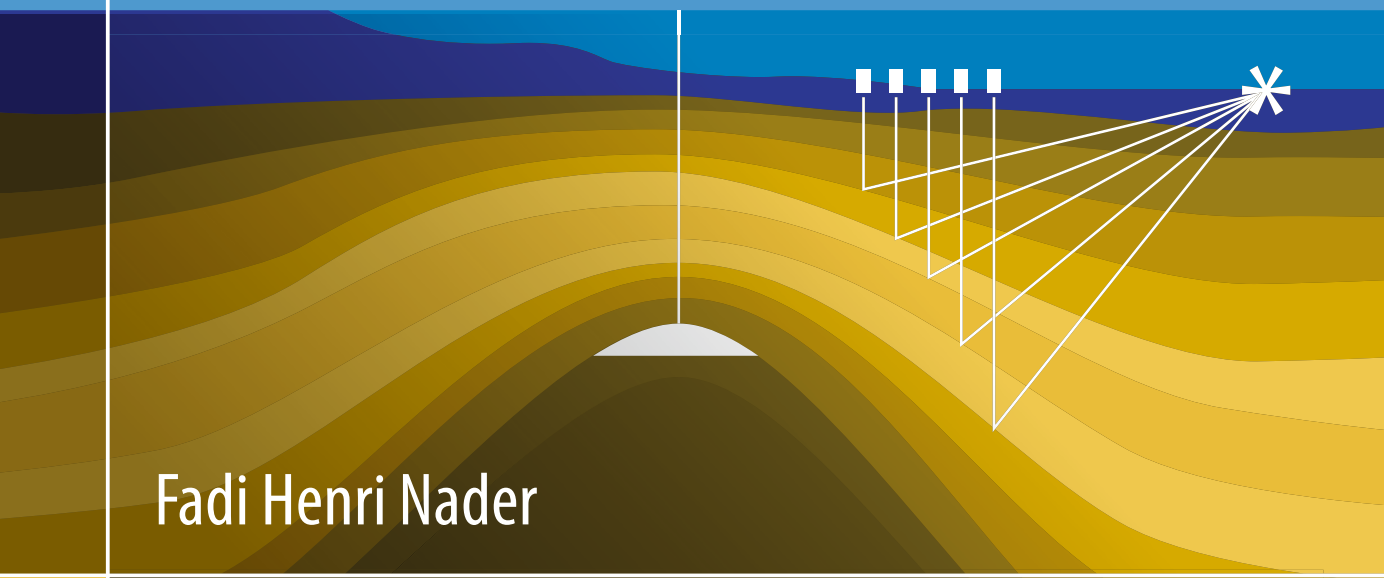

Fadi Henri Nader

Multi-scale Quantitative Diagenesis and Impacts on Heterogeneity of Carbonate Reservoir Rocks

Springer

Advances in Oil and Gas Exploration & Production

Series editor

Rudy Swennen, Department of Earth and Environmental Sciences, K.U. Leuven, Heverlee, Belgium

The book series Advances in Oil and Gas Exploration & Production publishes scientific monographs on a broad range of topics concerning geophysical and geological research on conventional and unconventional oil and gas systems, and approaching those topics from both an exploration and a production standpoint. The series is intended to form a diverse library of reference works by describing the current state of research on selected themes, such as certain techniques used in the petroleum geoscience business or regional aspects. All books in the series are written and edited by leading experts actively engaged in the respective field.

The Advances in Oil and Gas Exploration & Production series includes both single and multi-authored books, as well as edited volumes. The Series Editor, Dr. Rudy Swennen (KU Leuven, Belgium), is currently accepting proposals and a proposal form can be obtained from our representative at Springer, Dr. Alexis Vizcaino (Alexis.Vizcaino@springer.com).

More information about this series at http://www.springer.com/series/15228

Fadi Henri Nader

Multi-scale Quantitative Diagenesis and Impacts on Heterogeneity of Carbonate Reservoir Rocks

Springer

Fadi Henri Nader
IFP Energies nouvelles
Rueil-Malmaison, Paris
France

ISSN 2509-372X ISSN 2509-3738 (electronic)
Advances in Oil and Gas Exploration & Production
ISBN 978-3-319-46444-2 ISBN 978-3-319-46445-9 (eBook)
DOI 10.1007/978-3-319-46445-9

Library of Congress Control Number: 2016951649

Printed on acid-free paper

This Springer imprint is published by Springer Nature
The registered company is Springer International Publishing AG
The registered company address is: Gewerbestrasse 11, 6330 Cham, Switzerland

Foreword 1

Recent technological advances in reservoir characterization and new developments of numerical tools have induced the needs for more integration between various disciplines, allowing sedimentologists, geochemists and modellers to work together and propose innovative workflows aiming at quantifying properly carbonate rocks porosity at various scales, and better predicting reservoir characteristics as a function of long-term burial history and overall evolution of regional fluid flow and chemical transfers.

During the last ten years or so, Fadi H. Nader and his numerous Ph.D.'s and postdoctorants have explored many of the new analytical techniques described in this book on real case studies around the world, coupling lab measurements with accurate sedimentological observations at outcrop scale with subsurface data such as well logs and cores, as well as with seismic stratigraphy at basin scale. Also, Fadi has been constantly interacting with other IFPEN colleagues involved in the development of new numerical tools, allowing him to proceed with coupled thermal, fluid flow and diagenetic modelling, thus allowing full quantitative and predictive approaches.

After all this work, it is now a real pleasure to read this very comprehensive and didactic book on the characterization and prediction of carbonate reservoirs.

I would like to thank and congratulate Fadi for sharing here his wide expertise to the benefit of a wide range of end-users, this book being dedicated to young students in geosciences as well as to more senior scientists from a wide range of disciplines, both at the university and in the industry.

Rueil-Malmaison, France
February 2016

François Roure

Foreword 2

In this book, that relies on the HDR thesis of the author, Dr. Fadi Nader, the different steps in diagenetic research of reservoir rocks, particularly carbonate rocks, at different scales are addressed. For this accomplishment, the author relied on a broad spectrum of expertise, e.g. his own research, his experiences gained as researcher affiliated at the Institut Français du Pétrole—Energies nouvelles (IFP-EN), his role as mediator affiliated as geology consultant at the Ministry of Energy and Water in Lebanon at the time of the preparation for the first Lebanese offshore licensing round and finally as catalyser initiating a large number of scientific studies in the Levant Basin and offshore Cyprus.

In contrast to many books addressing the effect of diagenesis on reservoir properties, as said before with a focus on carbonate systems, the author not only addresses the classical and upcoming techniques to unravel the paragenesis (Chap. 1: including petrographical, geochemical, mineralogical, and fluid microthermometrical techniques) but also addresses the way how these acquired data need to be quantified and integrated into quantitative diagenesis (Chap. 2) as well as how they need to be upscaled. In Chap. 2, he addresses several techniques that are used at different scales, which make this book very relevant since developing an upscaling philosophy is one of the key items in "advances in oil and gas production and exploration". Of particular interest here relates to computerized tomography which bridges the classical petrography approach in geology to the 3D approach of reservoir engineers. At the end, even the bridge to geophysics (seismic and wireline logging) is presented in a comprehensive way. Of peculiar interest are the strategies the author proposes to upscale certain observations based on integrating remote sensing and photogrammetry techniques as well as integrated data analysis tools. He pleads clearly for a quantitative approach of diagenetic research to bridge the gap between reservoir geologists and reservoir engineers. In Chap. 4, he provides a comprehensive overview of different numerical modelling approaches on diagenesis based on geometry-based modelling, geostatistical modelling and geochemical modelling where he can rely on the extensive expertise acquired at his home institute IFP-EN. He closes this session with some outlook to advancements in numerical modelling of diagenesis, which likely will be developed at the moment the reader is reading these chapters.

The work is nicely illustrated with a number of case studies carried out by the author on hydrothermal dolomites in Lebanon, Northern Spain, the UAE, … However, also reference is made to some of the key studies carried out by other researches that were published in peer-reviewed international journals. The author also gives a nice overview of the software packages developed at IFP-EN over the last years with regard to sedimentological, structural geological and reaction transport modelling.

In the last chapter, the author pays a lot of attention to the workflows that need to be developed, not only with regard to the characterization and quantitative techniques but also addressing the modelling techniques aiming at developing integrated modelling workflows. With this contribution, the author likes to share his experiences to present his view on how advances in gas and oil production and exploration can be achieved based on a thorough development of quantitative diagenesis, reservoir and reaction transport modelling and development of an upscaling as well as downscaling research approach in reservoir studies.

Heverlee, Belgium Rudy Swennen
March 2016

Preface

The starting point of the worldwide interest in "Diagenesis"—especially for carbonate rocks—can be traced back to 1975, when R. Bathurst published the book entitled "Carbonate Sediments and their Diagenesis" including the famous statement: "*Carbonate rocks are as much the products of diagenesis as they are of primary deposition*". Alteration of sedimentary rocks after sediment deposition due to various processes of diagenesis is crucial in reshaping their mineralogical and petrophysical properties. The petroleum industry, since that early time, needed workflows and means to understand and predict the heterogeneous flow properties of reservoir rocks. Henceforth, a considerable amount of research work has been dedicated to the investigation of diagenetic processes, environments and products. Diagenetic processes are inherently related to the rock–fluid interactions and attract multi-disciplinary researchers. This is quite demonstrated by the wide spectrum of the nature of published work on diagenesis and by the difficulty in integrating all aspects related to diagenesis research.

Sedimentologists have extensively described the results of diagenetic processes ("diagenetic phases") in surface-exposed rocks and subsurface well cores across the planet. The aim was set at matching processes and products, and being able to come up with conceptual models that would allow at least constraining the geometry/dimension as well as the fluid flow history of the altered rocks. In addition, since the 1970s and the original paper of Choquette and Pray (1970)—entitled "Geologic nomenclature and classification of porosity in sedimentary carbonates"—efforts were spent to understand the impact of diagenesis on porosity and permeability of carbonate rocks.

To date, classical diagenesis studies make use of a wide range of descriptive methods and analytical techniques converging into conceptual models that explain specific, relatively time-framed, diagenetic processes, and deduce their impacts on carbonate reservoir rocks (e.g. Nader et al. 2004; Nader et al. 2008). Currently used techniques combine petrographic (conventional, cathodoluminescence, fluorescence, scanning electron microscopy with energy dispersive spectrometer—SEM/EDS and 3D computed tomography, CT), geochemical (major/trace elements, stable oxygen and carbon isotopes, strontium isotopes, Mg and clumped isotopes) and fluid inclusion analyses (microthermometry, Raman spectrometry, crush-leach analysis, laser ablation), providing independent arguments to support or discard any of the proposed models. More recently, the use of basin modelling is

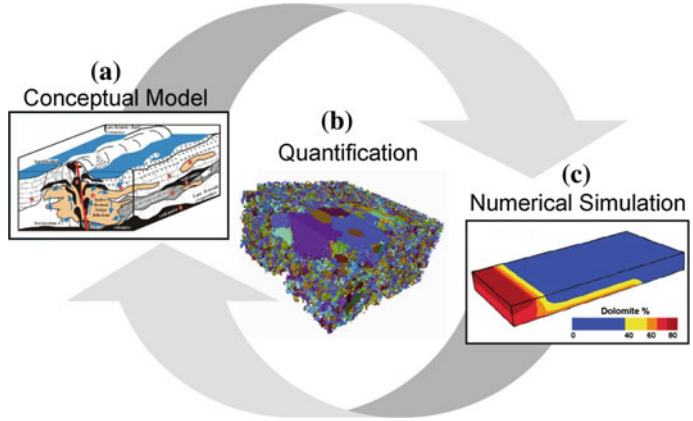

Fig. 1 From conceptual to numerical modelling of diagenesis, quantifying diagenetic phases remains essential. **a** Conceptual studies of diagenesis—for example hydrothermal or high-temperature dolomitization (HTD; Nader et al. 2004, 2007). **b** Quantification methods—e.g. micro-computed tomography (micro-CT) image analyses (De Boever et al. 2012). **c** Numerical simulations of diagenetic processes such as reactive transport modelling of dolomitization (e.g. Consonni et al. 2010)

employed (e.g. Fontana et al. 2014; Peyravi et al. 2014) to support the burial history evolution (including temperature and pressure boundary data) and the proposed paragenesis (i.e. the sequence of diagenetic phases in chronological order). Still, conceptual models lack exact dating frameworks (or specific timing constraints for the described processes). They are qualitative and do not yield quantitative data to be directly used by reservoir engineers for rock-typing and geological modelling (Nader et al. 2013). New analytical techniques (e.g. U/Pb for dating) and advances in numerical modelling may provide better tools for achieving time-constrained, quantitative diagenetic studies. The operational workflow that aims at predicting the impact of relevant diagenetic processes on reservoir properties, henceforth, consists of three main iterative stages (Nader et al. 2013): (i) constructing a conceptual diagenesis model, (ii) quantifying the related diagenetic phases and (iii) modelling the diagenetic processes (Fig. 1).

While most of the concepts of diagenetic processes operate at the larger, basin scale, the description of the diagenetic phases (products of such processes) and their association with the overall petrophysical characteristics of sedimentary rocks remain at reservoir (and even outcrop/well core) scale. Hence, "upscaling" becomes another major challenge for sedimentologists and reservoir engineers in the coming decades. Recently, massive work has been undertaken to propose methods capable of defining representative elementary volumes (REV) of carbonate reservoir rocks. REVs would then be used to represent the whole rock type at various scales (reservoir and basin scales).

Between the years 2000 and 2003, I worked, during my Ph.D. project (KU Leuven, Belgium), on the "Dolomitization Problem" as one of the significant processes of diagenesis in carbonate rocks (Nader 2003). About 50 % of the

world's known carbonate reservoirs are in dolostones. Based on my local field knowledge, I have investigated the Jurassic dolostones that are exposed in Lebanon (part of the Jurassic carbonate platform on the southern margin of the Neo-Tethys ocean) and ascribed them to conceptual models (eogenetic reflux and mesogenic high-temperature fracture-associated) invoking the fluid flow characteristics and rock–fluid interactions (Nader et al. 2004). From 2003 to 2007, I have extended this work upon my appointment as assistant professor at the American University of Beirut (Lebanon) by further studying the Jurassic hydrothermal dolomitization fronts and the Cretaceous sabkha-style dolostones in Lebanon (Nader et al. 2006, 2007). I have also supervised projects on diagenesis of carbonate rocks (Doummar 2005), hydrocarbon assessments based on petrography and geochemistry of source rocks (Al Haddad 2007), and diagenesis of sandstones Bellos (2008).

In 2007, I joined IFP Energies nouvelles (*Institut Français du Pétrole* at that time), and I worked first within the "Reservoir Characterization" mega project and Enhanced Oil Recovery Joint Industry Project. Most of my work at that time concerned with characterization of diagenetic phases and their relationship with reservoir properties. This involved field investigation of some of the world-class outcrops of hydrothermal dolomites (e.g. Ranero, Spain; Apennines, Italy; e.g. Shah et al. 2010, 2012; Swennen et al. 2012), as well as studies of actual oilfields and outcrop-analogues (e.g. Gashsaran oilfield, Iran). Other than characterization studies, I got myself involved in upgrading analytical methods for petrography and fluid inclusion analyses as well as X-ray diffraction quantifying methods and atomic absorption spectrometry of mixed dolomite/calcite samples. This was the beginning of quantitative diagenesis workflows for carbonate rocks at IFPEN (e.g. Turpin et al. 2012).

I have started applying numerical modelling to dolomitization as of the first years I spent at IFPEN. We tried to model hydrothermal dolomitization fronts with ArXim-Coores™ (coupled geochemical and transport reactive software packages). Geostatistical modelling was also applied to the Ranero hydrothermal fault-associated dolomites by coupling Fraca™ and GOCAD software packages.

In 2009, we embarked on larger-scale studies of diagenesis, concerning basin-scale processes. Fluid inclusion analyses across the Apennines Jurassic platform as well as the petrographic and mineralogic investigations of the Cretaceous Mannville tight sandstones gave a larger framework for the investigated diagenetic processes (Deschamps et al. 2012). At that time, I initiated my second Ph.D. project which consisted of a basin-scale diagenesis study of the Permo-Triassic Khuff carbonates in the United Arab Emirates (Fontana et al. 2010, 2014). I was also involved in the CAPSARK project (BRGM, IFPEN, GeoGreen), which aimed at proposing sites for CO_2-storage in the Kingdom of Saudi Arabia. This project allowed me to undertake a comprehensive stratigraphic and structural geology review at the scale of Saudi Arabia (Jaju et al. in press).

In 2010, two new aspects of diagenesis research were added to our ongoing projects. The first consisted in developing more advanced techniques on quantifying diagenetic phases by means of 2D and 3D image

analyses with micro-CT and MATLAB™ tools. We became capable of quantifying diagenetic phases from high-resolution scans of thin sections and 3D scanned rock samples. The postdoctoral project of Eva de Boever, which I have conceived, allowed us also to link the micro-CT approach to (reactive) Pore-Network Modelling to establish a possibility to model dissolution of carbonates or precipitation of anhydrite based on 3D scanned images at the scale of plugs (De Boever et al. 2012). The second aspect of diagenesis also concerned quantifying techniques, but at a larger, reservoir scale. Here, we benefited from collaboration with the Petroleum Institute in Abu Dhabi (UAE) in order to analyze a huge petrographic and petrophysical database across an oilfield (Morad et al. 2012). We constructed maps showing the proportional distribution of diagenetic phases (such as dolomite and anhydrite) and relative abundance of cements, such as syntaxial calcite overgrowth (Nader et al. 2013). Such maps were essential and preceded geostatistical modelling (with CobraFlow™) which helped in illustrating the reservoir heterogeneity based on quantitative diagenesis at the oilfield scale (MSc. Thesis of Morad 2012). Henceforth, I have put together a workflow whereby quantifying tools (such as 2D/3D image analyses) can be used to achieve quality control on industrial petrographic and petrophysical data, and then statistical analyses of the data sets are done by EasyTrace™ software before undertaking geostatistical modelling with CobraFlow™.

In 2011 and 2012, I had the opportunity to work as a geology consultant at the Ministry of Energy and Water in Lebanon at the time of the preparation for the first Lebanese offshore licensing round. I discovered basin-wide reflection seismic data (2D and 3D) and their major importance, not only for hydrocarbon exploration assessment but also for stratigraphic and structural studies. At that time, Petroleum Geo-Services (PGS) and Spectrum Geo Ltd. were busy acquiring 2D and 3D seismic surveys covering the whole Lebanese offshore exclusive economic zone (EEZ; exceeding 19,000 km^2). I learned about the wealth of data provided by these surveys in the frontier gas-bearing Levant Basin (Nader 2011, 2014a). I have initiated three Ph.D. projects based on such seismic data and fieldwork onshore Lebanon. These projects are to be integrated, and cover the stratigraphic (Hawie et al. 2013), structural (Ghalayini et al. 2014) and petroleum (Bou Daher et al. 2014) aspects of Levant Basin. Having established the basin-scale framework for the Levant Basin research with various European academic and industrial partners, I am looking forward eventually to tackle reservoir-scale studies once exploration well data will be made accessible.

Upon my return to IFPEN (end of 2012), I worked on extending my research network over the Eastern Mediterranean region (including new Ph.D. projects offshore Cyprus; Ph.D. projects of N. Papadimitriou and V. Symeou, 2014–2017). Additional 2D and 3D seismic interpretations were carried out on the first seismic profiles onshore Lebanon and the Messinian salt in the Levant Basin, respectively. Numerical modelling of diagenesis also took a considerable part of my work, including geostatistical modelling at the reservoir-scale and geochemical reactive transport modelling of dolomitization. We developed simple examples of rock-water geochemical simulations with ArXim. For instance, geochemical modelling can provide

simple estimations of porosity destruction or enhancement in the freshwater lens during carbonate platform growth. Such modules can be eventually plugged in forward stratigraphic modelling tools (e.g. DionisosFlow™) and help in predicting the effect of diagenetic processes during the growth of a carbonate platform. The eventual goal for geochemical RTM is the predictive modelling of diagenetic processes and their impacts on reservoir properties. They ought to be used as tools to question certain scenarios and to infer about the sensitivity of specific parameters.

Today, we have an operational workflow for proposing conceptual models of diagenetic processes based on studying surface-exposed rocks and well cores. We are able to quantify the diagenetic products in carbonate rocks with various techniques and on varying scales. In addition, we have the possibility to use distinct software packages for numerical modelling. I have been involved in all aspects of this workflow by undertaking and supervising research projects on plug, reservoir and basin scales.

On a more global level, the way forward, seems evident to me as the integration of workflows at different scales. I would like to improve such integration by planning research projects that go from a basin scale (using seismic data, outcrop-analogues, well cores, etc.) to a reservoir scale, and eventually the plug scale. Such integration will bring more constrains on the boundary data, better validation for models, and less uncertainty.

This book is based on the thesis I have defended on the 19 March 2015, for acquiring my Habilitation diploma (HDR) at the Université Pierre et Marie Curie (UPMC, Sorbonne Universities, Paris, France), and about 12 years of research work—mainly on carbonate rocks. The present book composed of five chapters. First, an introductory chapter outlines the general topics of diagenesis (i.e. characterization, quantitative diagenesis and numerical modelling) that will be further investigated in this work. Three chapters follow consecutively bringing appropriate emphasis on the actual state of the art and the future perspectives for each of these three topics, respectively. In addition, future development trends are discussed at the end of each chapter. Chapter 5 presents major conclusions and general perspectives, which are grouped in five sections (i.e. characterization techniques, quantitative methods, modelling workflows, integration of modelling workflows and the way forward). It is my belief that the larger, basin-scale picture is of importance to carbonate rock diagenesis studies, as it provides the broader framework for fluid migrations and can help in setting the boundary conditions for reservoir-scale studies. This contribution aims to highlight the multi-scale aspect of diagenesis and provide a road map for future research projects (including techniques, workflows and tools).

Rueil-Malmaison, Paris, France Fadi Henri Nader

References

Al Haddad, S. (2007). Petrographic and geochemical characterization of the Hasbaya asphalt and related host rocks (Senonian Chekka Formation), South Lebanon: MSc Thesis, American University of Beirut, Beirut, Lebanon, 121p.

Bellos, G.S. (2008). Sedimentology and diagenesis of some Neocomian-Barremian rocks (Chouf Formation), Southern Lebanon: MSc Thesis, American University of Beirut, Beirut, Lebanon, 251p.

Bou Daher, S., Nader, F.H., Strauss, H., and Littke, R. (2014). Depositional environment and source-rock characterization of organic-matter rich upper Santonian - upper Campanian carbonates, northern Lebanon. Journal of Petroleum Geology, 37 (1), 5-24.

Choquette, P.W., and Pray, L.C. (1970). Geologic nomenclature and classification of porosity in sedimentary carbonates. AAPG Bulletin, 54, 207-250.

Consonni, A., Ronchi, P., Geloni, C., Battistelli, A., Grigo, D., Biagi, S., Gherardi, F., and Gianelli, G. (2010). Application of numerical modelling to a case of compaction-driven dolomitization: a Jurassic palaeohigh in the Po Plain, Italy. Sedimentology, 57, 209-231.

De Boever, E., Varloteaux, C., Nader, F.H., Foubert, A., Bekri, S., Youssef, S., and Rosenberg, E. (2012). Quantification and prediction of the 3D pore network evolution in carbonate reservoir rocks. Oil & Gas Science and Technology (OGST), 67(1), 161-178.

Deschamps, R., Kohler, E., Gasparrini, M., Durand, O., Euzen, T., and Nader, F.H. (2012). Impact of mineralogy and diagenesis on reservoir quality of the Lower Cretaceous Upper Mannville Formation (Alberta, Canada). Oil & Gas Science and Technology (OGST), 67 (1), 31-58.

Doummar, J. (2005). Sedimentology and diagenesis of the Albian rock sequence (Upper Hammana-Lower Sannine Formations), northern Lebanon. MSc. Thesis, American University of Beirut, Beirut, Lebanon, 199p.

Fontana, S., Nader, F.H., Morad, S., Ceriani, A., Al-Aasm, I.S., Daniel J.-M., and Mengus, J.-M. (2014). Fluid-rock interactions associated with regional tectonics and basin evolution. Sedimentology, 61, 660-690.

Fontana, S., Nader, F.H., Morad, S., Ceriani, A., and Al-Aasm, I.S. (2010). Diagenesis of the Khuff Formation (Permian-Triassic), northern Uinted Arab Emirates. Arab J. Geosci. (Springer), 3, 351-368

Ghalayini, R., Daniel, J.-M., Homberg, C., Nader, F.H., and Comstock, J.E. (2014). Impact of Cenozoic strike-slip tectonics on the evolution of the northern Levant Basin (offshore Lebanon). Tectonics, 10.1002/2014TC003574.

Hawie, N., Gorini, C., Deschamps, R., Nader, F.H., Montadert, L., Granjeon, D. Baudin, F. (2013). Tectono-stratigraphic evolution of the northern Levant Basin (offshore Lebanon). Marine and Petroleum Geology, 48, 392-410.

Morad, D. (2012). Geostatistical Modeling of the Upper Jurassic Arab D Reservoir Heterogeneity, Offshore Abu Dhabi, United Arab Emirates. MSc. Thesis, Uppsala University, Sweden, 113p.

Morad, S., Al-Aasm, I.S., Nader, F.H., Ceriani, A., Gasparrini, M., and Mansurbeg, H. (2012). Impact of diagenesis on the spatial and temporal distribution of reservoir quality in the Jurassic Arab D and C members, offshore Abu Dhabi oilfield, United Arab Emirates. GeoArabia, 17(3), 17-56.

Nader, F. H., Abdel-Rahman, A.-F. M., and Haidar, A. T. (2006). Petrographic and chemical traits of Cenomanian carbonates from central Lebanon and implications for their depositional environments. Cretaceous Research, 27, 689-706.

Nader, F. H., Swennen R. and Ellam, R. (2004). Stratabound dolomite versus volcanism-associated dolomite: an example from Jurassic platform carbonates in Lebanon. Sedimentology, 51(2), 339-360.

Nader, F.H. (2003). Petrographic and geochemical study of the Kesrouane Formation (Jurassic), Mount Lebanon: Implications on dolomitization and petroleum geology, Katholieke Universiteit Leuven, 386p.

Nader, F.H. (2011). The petroleum prospectivity of Lebanon: an overview. Journal of Petroleum Geology, 34 (2), 135-156

Nader, F.H. (2014a). Insights into the Petroleum Prospectivity of Lebanon. In: Marlow, L., Kendall, C., and Yose, L. (eds): Petroleum systems of the Tethyan region. AAPG Memoir 106, 241-278.

Nader, F.H., De Boever, E., Gasparrini, M., Liberati, M., Dumont, C., Ceriani, A., Morad, S., Lerat, O., and Doligez, B. (2013). Quantification of diagenesis impact on reservoir properties of the Jurassic Arab D and C members (offshore, U.A.E.). Geofluids, 13, 204-220.

Nader, F.H., Swennen, R., and Ellam, R. (2007). Field geometry, petrography and geochemistry of a dolomitization front (Late Jurassic, central Lebanon). Sedimentology, 54, 1093-1110.

Nader, F.H., Swennen, R., and Keppens, E. (2008). Calcitization/dedolomitization of Jurassic dolostones (Lebanon): results from petrographic and sequential geochemical analyses. Sedimentology, 55, 1467-1485.

Peyravi, M., Rahimpour-Bonab, H., Nader, F.H., and Kamali, M.R. (2014). Dolomitization and buriql history of lower Triassic carbonate reservoir-rocks in the Persian Gulf (Salman offshore field). Carbonates and Evaporites, DOI 10.1007/s13146-014-0197-2

Shah, M.M., Nader, F.H., Dewit, J., Swennen, R., and Garcia, D. (2010). Fault-related hydrothermal dolomites in Cretaceous carbonates (Cantabria, northern Spain): Results of petrographic, geochemical and petrophysical studies. Bull. Soc. geol. Fr., 181(4), 391-407.

Shah, M.M., Nader, F.H., Garcia, D., Swennen, and Ellam, R. (2012). Hydrothermal dolomites in the Early Albian (Cretaceous) platform carbonates (NW Spain): Nature and origin of dolomites and dolomitising fluids. Oil & Gas Science and Technology (OGST), 67(1), 97-122.

Swennen, R., Dewit, J., Fierens, E., Muchez, P., Shah, M.M., Nader, F.H., and Hunt, D. (2012). Multiple dolomitisation events along the Pozalagua Fault (Pozalagua Quarry, Basque – Cantabrian Basin, Northern Spain). Sedimentology, 59, 1345-1374.

Turpin, M., Nader, F.H., and Kohler, E. (2012). Empirical calibration for dolomite stoichiometry calculation: Application on Triassic Muschelkalk-Lettenkohle carbonates (French Jura). Oil & Gas Science and Technology (OGST), 67(1), 77-95.

Contents

List of Figures

List of Tables

Introduction

1

Diagenesis refers to any physical, chemical, and/or biological process that alters carbonate rocks after deposition (until metamorphic conditions are reached). When the ambient conditions of the rocks and intrinsic fluids change, or upon migration of extrinsic fluids into a rock-mass, processes such as dissolution, precipitation and mineralogical changes may occur. These so-called diagenetic processes have been already investigated and described through hundreds of studies covering the whole sedimentary rock-record, and practically anywhere on our planet.

1.1 Diagenetic Realms

The concept of "diagenetic realms" has been proposed in order to better characterize the diagenetic processes in carbonate rocks (Longman 1980; Moore 2001). A "diagenetic realm" is defined as a distinct environment that can be described by specific physico-chemical and spatiotemporal conditions, where explicit processes prevail (Fig. 1.1).

Carbonate sediment petrologists employ this concept to be able to recognize and even predict similar patterns of diagenesis in such specific environments. Yet, the investigated rocks that are initially subjected to one diagenetic realm and subsequent processes may also be subjected to different realms throughout the basin history. Accordingly, carbonate diagenetic evolution could be progressive, abrupt or even cyclic (Parker and Sellwood 1994).

The main carbonate diagenetic realms are marine, meteoric, and burial (Fig. 1.1), each of which is inherently associated with the prevailing type of fluids. The marine realm comprises a stagnant zone and an active zone, both with marine-related fluids. While the former zone, represents areas with no considerable water circulation, and is characterized by minor cementation (rather micritization), the latter active zone, includes pervasive cementation—e.g. isopachous fibrous aragonite—chiefly due to considerable water circulation and subsequent replenishment of seawater aqueous species. The meteoric (freshwater) realm is divided into (upper) vadose and (lower) phreatic environments. The former includes a zone of carbonate dissolution by undersaturated meteoric water (e.g. development of cavernous porosity, karst), and a zone of precipitation where minor meniscus, pendent and spelean cementation occurs. The freshwater phreatic environment is characterized by three distinct zones (i.e. dissolution, precipitation, stagnant), whose limits are chiefly function of the aquifer's water-table position. Mouldic and vuggy porosities are the result of intense dissolution by undersaturated waters in the dissolution zone (or high pCO_2), while little cementation is commonly recorded in the stagnant zone (due to

F.H. Nader, *Multi-scale Quantitative Diagenesis and Impacts on Heterogeneity of Carbonate Reservoir Rocks*, Advances in Oil and Gas Exploration & Production, DOI 10.1007/978-3-319-46445-9_1

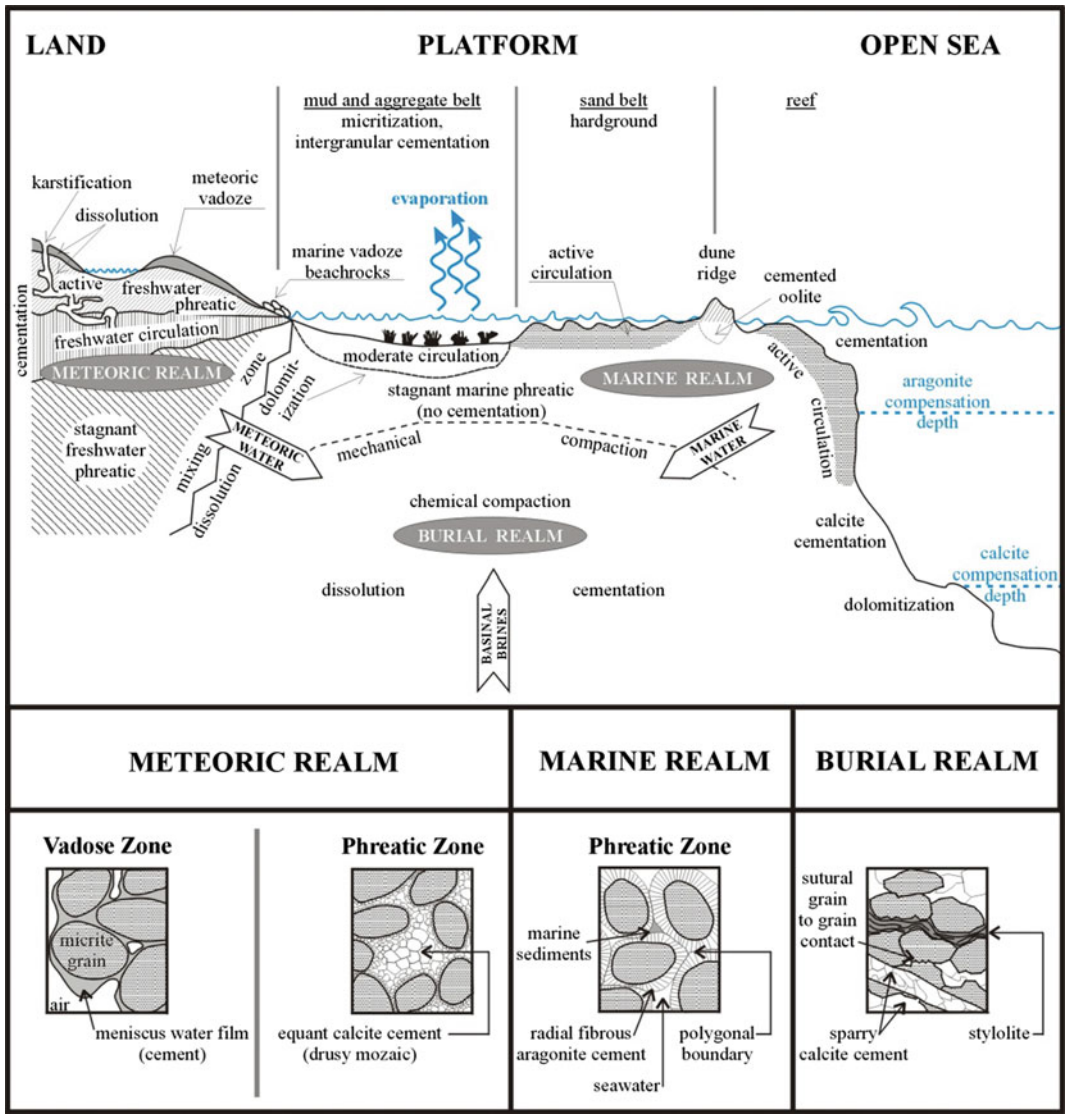

Fig. 1.1 Schematic representation of major carbonate diagenetic realms, related processes and resulting products in a carbonate platform (Longman 1980; Parker and Sellwood 1994; Moore 2001)

absence of water circulation and replenishment). This is quite contrasted to active water circulation and rapid cementation within the precipitation zone, usually leading to considerable porosity destruction. Equant calcite cement (completely replacing aragonite and occluding pores) characterizes this zone. If burial conditions prevail within the context of freshwater phreatic zone, the special patterns of drusy mosaic and syntaxial overgrowth and poikilotopic cements may occur. Note that drusy mosaic and syntaxial overgrowth cements are also formed in marine settings. The burial (subsurface) realm is mainly characterized by lithology-dependant compaction and pressure solution. Sparry calcite cement (relatively coarsely-sized) characterizes subsurface diagenesis (Fig. 1.2a). In addition, mineral replacement

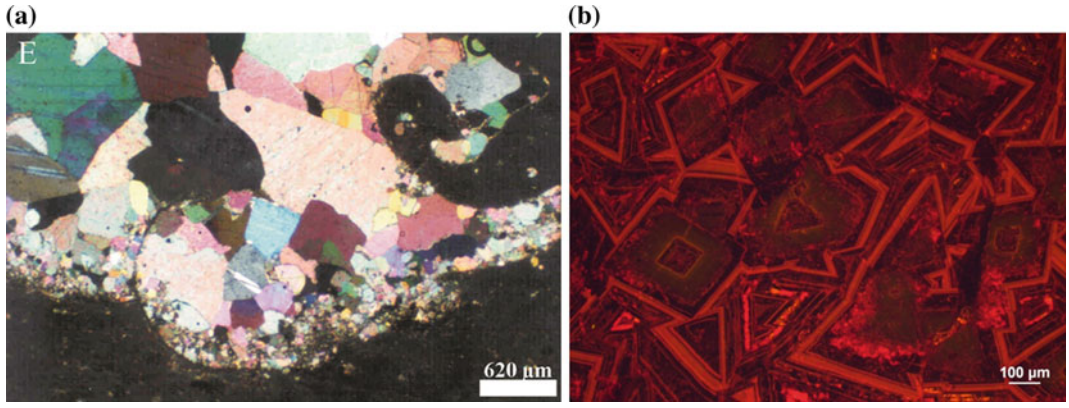

Fig. 1.2 Photomicrographs of diagenetic phases characteristic of the Jurassic shallow marine carbonates in Lebanon (Middle-East): **a** Plane-polarized transmitted light view of mosaic/interlocking sparry calcite cement typical of burial diagenesis; and **b** Replacive, coarse-crystalline planar subhedral dolomite interpreted to be of hydrothermal origin, viewed under cathodoluminescence microscopy

(e.g. dolomitization, silicification) as well as early chemical reactions (e.g. illite/smectite) often occur within the burial realm (Fig. 1.2b).

Other diagenetic realms include special marine-related environments (e.g. marine vadose, sabkha; McKenzie 1981) and mixing zones (e.g. Ward and Halley 1985; Humphrey 1988). 'Sabkhas' are "low-lying salt encrustrated surfaces sometimes adjacent to perennial/ephemeral bodies of brine—e.g. the Arabian/Persian Gulf, Gulf of Suez and the Red Sea, Australia, North Africa, Mexico" (Reading 1996). Fault-related zones can also be regarded as a special type of localized diagenetic realm for fluid-flow and mixing of intrinsic and extrinsic fluids. The hydrothermal dolomitization processes and what has been referred to as HTD (high-temperature dolomite; e.g. Davies and Smith 2006) possess distinctive genetic conditions that allow them to be considered in a separate group of diagenetic environments.

Themes related to the microbial effects on diagenesis have attracted the attention of many scientists in the last decade (e.g. Riding and Awramik 2000). Microbes (bacteria, small algae, fungi and protozoans) may produce acids that alter/dissolve pre-existing minerals, or set chemical environments that favour (induce and enhance) mineral precipitation. In other words, these abundant organisms are capable of generating, modifying and sustaining sediments (e.g. Freytet and Verrecchia 2002; Foubert and Henriet 2009). Accordingly, microbial processes associated with early phases of diagenesis (during, and/or just after sediment deposition) may produce extensive sedimentary structures and geo-bodies of interest for hydrocarbon exploration (Fig. 1.3; Immenhauser et al. 2005).

Diagenetic processes are also grouped according to their temporal characteristics (Fig. 1.4). 'Eogenesis' is a term given to the diagenetic processes occurring just after sediment deposition and before burial—it invokes 'early diagenesis'. Yet, sedimentary rocks spend most of their time under burial conditions and this is referred to as 'Mesogenesis'. Finally, when the rocks are uplifted and exposed to surface processes, 'Telogenesis' is frequently used to describe the associated diagenetic phases. Caution must be taken when using such terms since the temporal factor remains a relative one. For instance, we could imagine a fracture-associated hydrothermal dolomitization event affecting a prevailing eogenetic or telogenetic environment. Besides, similar diagenetic processes, such as cementation, dissolution, mineral replacement, can occur in any of these realms. Since this classification approach does not take

Fig. 1.3 Field photograph showing the Lower Cretaceous microbialithes of the Qishn Formation in Wadi Baw (Oman) during a field visit with Petrobras (in 2007). The index photos represent analogue modern build-ups (from Freytet and Verrecchia 2002)

into account the intrinsic fluids for each of the environments, the associated processes/phases remain un-constrained.

The concept of diagenesis realms and zones equally applies to silici-clastics (sand and shale) as well as evaporites, and should not be restricted to carbonate rocks. This idea is certainly adopted by the author, though this book tackles specifically carbonate diagenesis.

1.2 Porosity and Diagenesis

Choquette and Pray (1970) followed by Lucia (1995) established the main foundations of what is called today "Porogenesis", invoking the evolution of porosity during carbonate diagenesis. The basic types of porosity in carbonate rocks were first grouped as *fabric* and *not fabric* selective (Choquette and Pray 1970). In the first category, primary porosity types include inter- and intra-particle, fenestral, shelter and growth framework. Mouldic and intercrystalline porosity types are considered secondary (post-deposition) fabric-selective. *Not fabric* selective porosity types are all secondary and they include fractures, channels, vugs (and caverns). In addition, a genetic approach to the porosity development and evolution was achieved by providing clues regarding the major diagenetic process (cementation/filling versus dissolution) and its magnitude/extent (Fig. 1.5). Lucia (1995) and later on Lønøy (2006) go even further and try to associate grain types (and size) to porosity types. Using porosity/permeability relationships, they aimed to better understand the permeability of carbonate rocks (attempts towards better rock-typing).

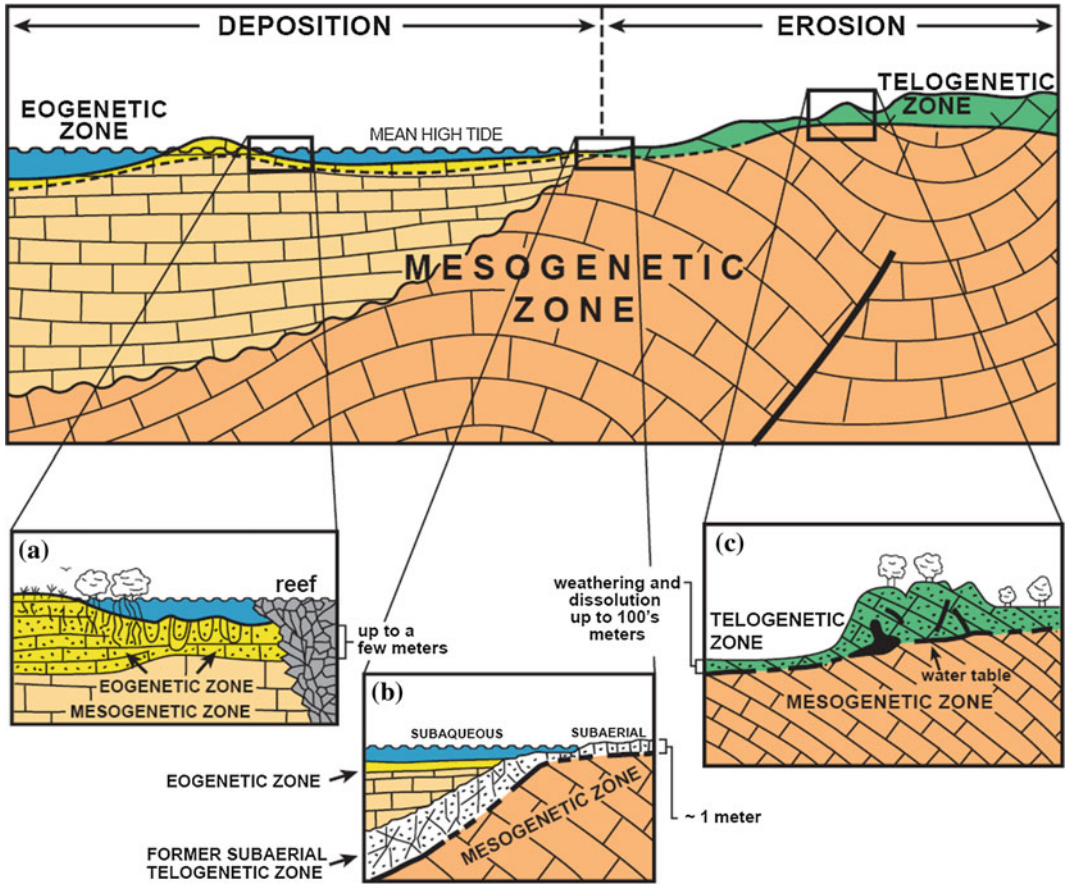

Fig. 1.4 Carbonate diagenesis occurs in depositional and erosional environments with distinct spatiotemporal zones: Eogenetic, Mesogenetic and Telogenetic. Schematic illustration not to scale (slightly modified from Choquette and Pray 1970)

Decades ago, porosity was chiefly investigated by petrographers through microscopic examinations of thin-sections representing only 2D views of the three-dimensional pore space. Petrophysicists measure independently the flow properties (e.g. MICP, Air-Permeability) of the same bulk rocks, hence taking into account the three-dimensional aspect of the macro-porosity. Besides, wireline logs, petro-acoustic and seismic data are routinely used for modern reservoir characterization and rock-typing (discussed further in Chap. 3). This mismatch in analytical measurements (2D vs. 3D) brought a major challenge for precise quantitative description of flow properties (porosity and permeability) in carbonate rocks. It often represented a difficulty in integrated studies and communication between the petrographer, the petrophysicist and the reservoir engineer.

Today, with advances in X-ray computed tomography and new generations of scanning electron microscopes, the bridge between petrophysics and petrography has been provided (discussed further in Chap. 2). The pore space can be investigated with 3D scanning and micro-scanning, and eventually linked to the 3D flow properties of sedimentary rocks (Fig. 1.6). Such approach is at the micro-scale and needs to be brought up to the scale of reservoirs. To do so, one major step remains and that is to constrain correctly the challenging representative elementary volumes (REV). Pore Network Modelling

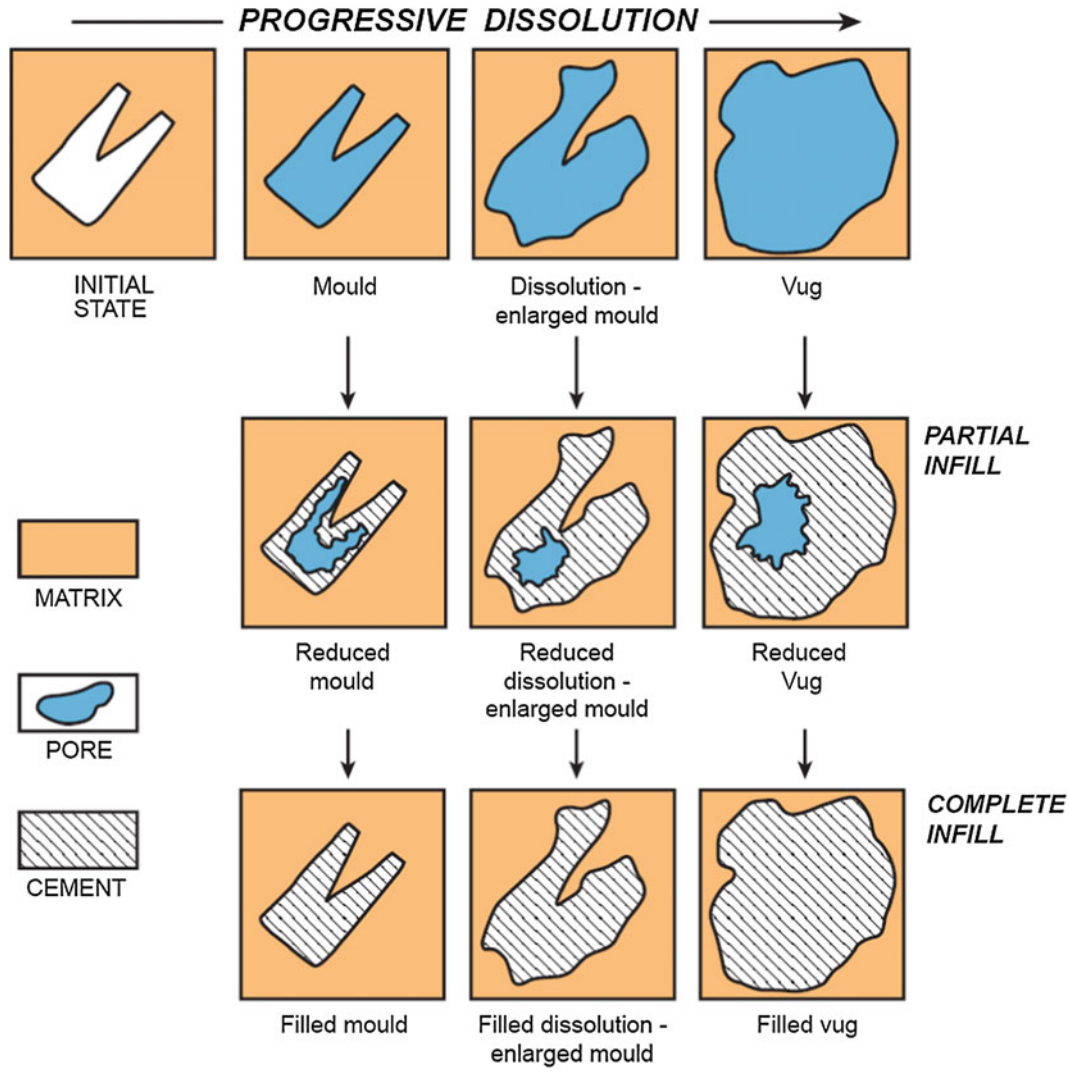

Fig. 1.5 Schematic illustration of porosity evolution during diagenesis: progressive dissolution (from mould to vug) and porosity reduction by cementation (slightly modified from Choquette and Pray 1970)

(PNM) can also be used to analyse the pore structure evolution in carbonate rocks. More recently reactive-PNM and micro-CT techniques have been used to investigate the evolution of flow properties influenced by diagenesis, e.g. dissolution/precipitation (Fig. 1.7; Algive et al. 2012; De Boever et al. 2012). Alternatively, numerical flow simulations can also be undertaken through 3D pore-space models.

1.3 Quantitative Diagenesis

Diagenesis is indeed one the major factors that influence porosity/permeability distribution within hydrocarbon reservoirs (and aquifers). Certainly, it remains the least used in today's numerical modelling techniques—most of the time because of seldom quantitative description.

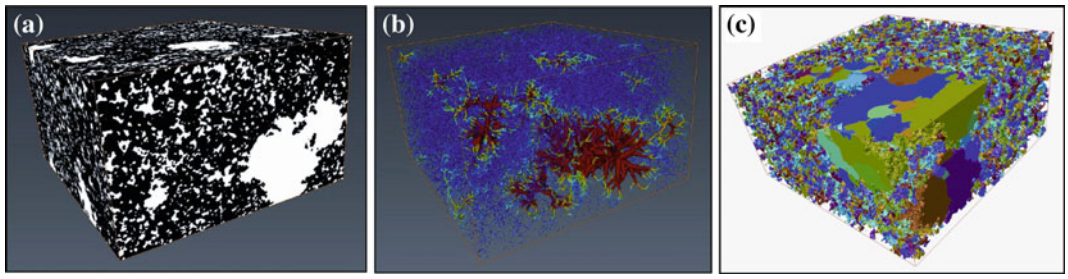

Fig. 1.6 3D Porosity network building based on micro-CT and image analyses (from De Boever et al. 2012): **a** Image binarisation revealing the extent and (intercrystalline/vuggy) types of porosity—in *white*; **b** Skeleton representation of porosity (assigned minimum distance to porosity border; *blue* to *red colours* express increasing "minimum distance to porosity border"); and **c** partitioned pore space illustrating the dual porosity (1000 × 1000 × 1000 pxls; separate colours for specific pore clusters)

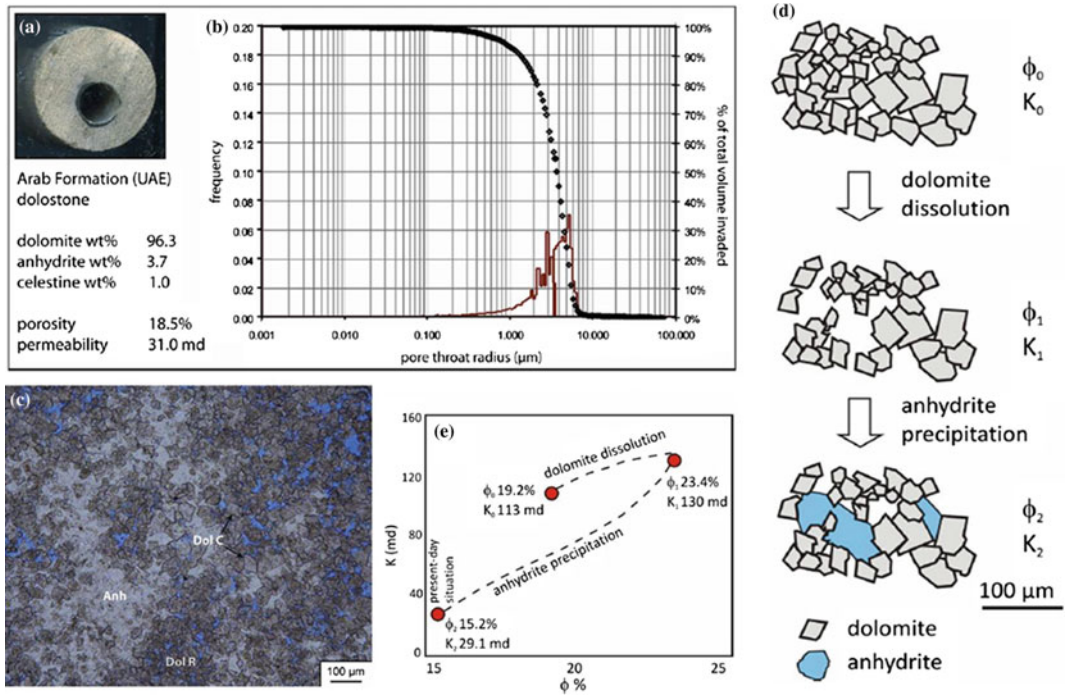

Fig. 1.7 Integrated techniques for constraining flow properties (porosity and permeability) during dissolution of dolomite and successive anhydrite cementation of a reservoir rock (De Boever et al. 2012): **a** Image of sample plug (diameter 23 mm), quantitative XRD data, classical porosity and permeability measurements; **b** Pore-size distribution through MICP; **c** Transmitted light microscopic image (2D thin-section) showing the dolostone (Dol; C = cement; R = replacive) texture and anhydrite (Anh); **d** and **e** Schematic illustration of rock fabrics as a result of dissolution/precipitation and deduced porosity/permeability evolution

Assessing precisely the diagenetic sensitivity of sedimentary rocks, especially the highly reactive carbonates (Wilson 1975), is a crucial task for reservoir geologists. Quantitative diagenesis (Parker and Sellwood 1994) emerged as an approach to quantify processes and responses (e.g. geochemical mass-balances, thermal evolution) from micro- to basinal scales. Quantifying

Fig. 1.8 Photograph showing the extent of hydrothermal dolomites (*dark brown*) in platform carbonates (Ranero, northern Spain)

diagenetic phases (representing processes) has become a widespread activity, which is commonly applied at varying scales (Fig. 1.8).

The volumes of dolostone bodies at the outcrop-scale can be quantified by means of geo-referenced (aerial) photographs coupled with digital elevation models (e.g. Shah et al. 2012). Ground-based hyperspectral imaging combined with lidar scanning has also been used to reveal distinct diagenetic as well as lithological facies on the almost vertical faces (50 m × 15 m) of the Ranero Pozalagua Quarry (Cantabria Spain; Kurz et al. 2012). Quantifying such "diagenetic" geobodies and heterogeneous carbonate reservoirs can be also done at the seismic-scale (Sagan and Hart 2006), offering the possibility to integrate quantitative diagenesis to seismic interpretation. This step is very rewarding for providing reservoir-analogues for the less known subsurface reservoirs.

At the sample-scale, dolomite/calcite relative abundance can be measured with X-ray diffractometry (XRD) and petrographic techniques. Furthermore, 3D high resolution scanning can yield the 3D volume of major mineralogical phases (e.g. micro-CT technologies; Fig. 1.9). Together with image analyses and modelling, such 3D quantitative assessment can be applied for several diagenetic steps and could illustrate the porosity evolution through the deduced paragenesis. Quantitative approaches also include geochemical and isotopic analyses as well as measurements carried out on fluid inclusions (discussed in Chap. 3). All of these techniques lead to somehow quantitative data representing frequency (e.g. volumes of chemical species or mineralogical phases) and/or physico-chemical conditions (e.g. temperature, pressure). Progress in technology, leading to higher resolution and better precision of measurements (e.g. Mees et al. 2003; De Boever et al. 2012), will certainly promote quantitative diagenesis studies. Yet, a new rising challenge is related to upscaling

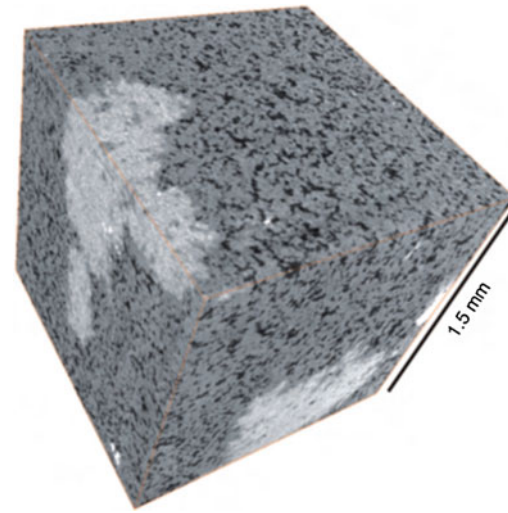

Fig. 1.9 3D cube of a typical Jurassic Arab C dolostone sample (Middle East), which have been scanned with micro-CT at resolution of 1.5 µm. Dolomite is in *grey*, anhydrite in *white* and the pore space in *black*

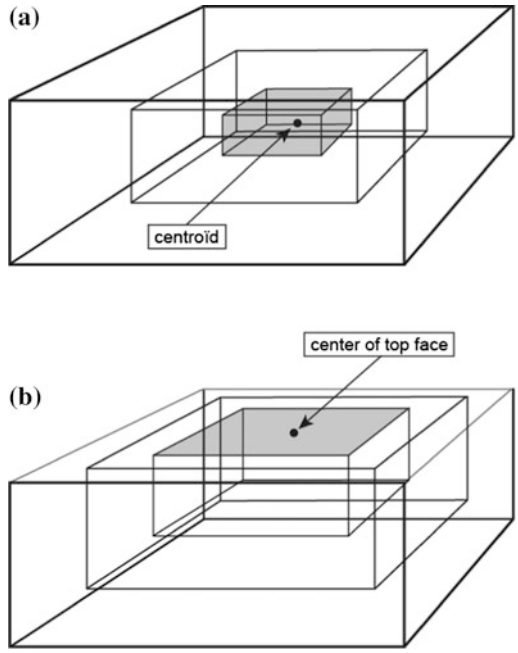

Fig. 1.10 Illustrations showing subsampling schemes for determining the Representative Elementary Volume (REV). Calculation of a certain parameter (e.g. macro-porosity%) is undertaken for volumes increasing either around the centroid ("Central out"; **a**) or downwards from the upper surface of the data-set ("Top down"; **b**)

and/or downscaling the quantitative data, and associating them together. One of the first step in taking up such a challenge remains the adequate definition of the representative elementary volume (REV) of especially heterogeneous carbonate rocks (Fig. 1.10; e.g. Nordahl and Ringrose 2008).

1.4 Numerical Modelling of Diagenesis

For many years, numerical modelling has been considered to be a useful way for predicting and further explaining diagenetic processes (e.g. Boudreau 1997). For instance, forward modelling aims at providing substantial information about the porosity/permeability heterogeneous evolution in a certain reservoir due to specific diagenetic processes. Still, such models should be regarded as numerical tools capable of answering certain questions and assessing sensitivity issues rather than mimicking natural processes.

Numerical modelling of diagenetic processes can focus on a variety of spatiotemporal scales, applying different, custom-tailored techniques. Basin modelling is already used in order to confirm or refute certain conceptual diagenetic models; e.g. a proposed hydrothermal dolomitization may be ruled out if no considerable differences in host-rock and fluid temperatures prevail. Such powerful techniques can also give valuable insights on the fluid flow and thermal evolution at the basin-scale. Numerical models therefore help in deducing whether precipitation or dissolution of a certain phase is more likely to occur. Numerical models can be constructed on reservoir-scale aiming at the prediction of heterogeneous distributions of the diagenetic phases, such as dolomite fronts and CO_2-based dissolution. Furthermore, numerical simulations of cement precipitation and plugging the reservoir's pore-space coupled with experimental analyses could be achieved at the micro-scale.

Today, modelling diagenesis is chiefly undertaken with three different approaches: (i) geometry-based; (ii) geostatistical; and (iii) geochemical. Once a certain diagenetic process has been demonstrated to have played a major role in shaping up the heterogeneous character of reservoir rocks, whereby the resulting impacts are well apprehended, numerical modelling can be safely undertaken. Geometry-based modelling helps in explaining geometric heterogeneity distribution. Karstification and fracture-related diagenesis are good candidates for this approach. For example, certain privileged dissolution directions/planes are assumed to be associated with karstic conduits formation, and the numerical model will implement the conduit geometries accordingly (e.g. models constructed with GoKarst/GOCAD software packages). Studies on fracture-related dolomitization also benefit from this type of modelling, whereby certain fractures may represent sites of presence of dolomites or their dissolution (Fig. 1.11; discussed further in Chap. 4).

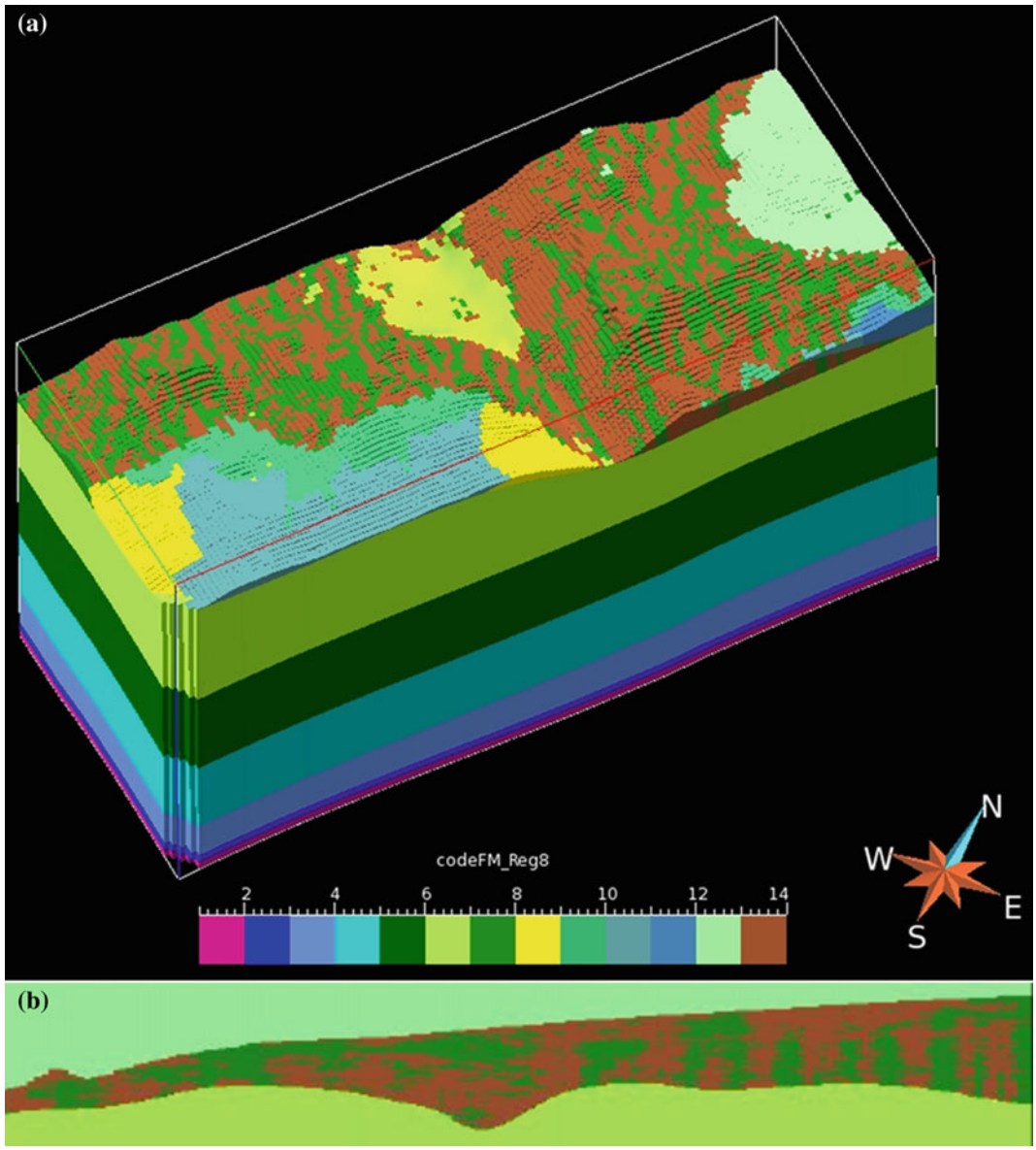

Fig. 1.11 Geometry-based modelling of the fracture related Ranero hydrothermal dolomites (northern Spain): **a** 3D model (6000 × 2000 m), whereby the distribution of dolomites (*brown*) within the limestone facies has been associated to NW-trending fractures/faults; **b** NE-SW cross-section (*diagonally*) across the model (**a**) showing the distribution of dolomites and original limestone host rock

Geostatistical methods are often used for reservoir-scale modelling and make use of considerable amount of data. Generally speaking, modelling precision relates to the quantity of input data (e.g. well cores description, wireline logs, petrographic analyses, MICP, permeability). In any case, geostatistical modelling aims to fill in (via *intelligent* extrapolation; e.g. plurigaussian, multiple point) the space between control points with known 'exact' data. Hence, the resulting simulation consists of having cells filled with the most probable facies/phase.

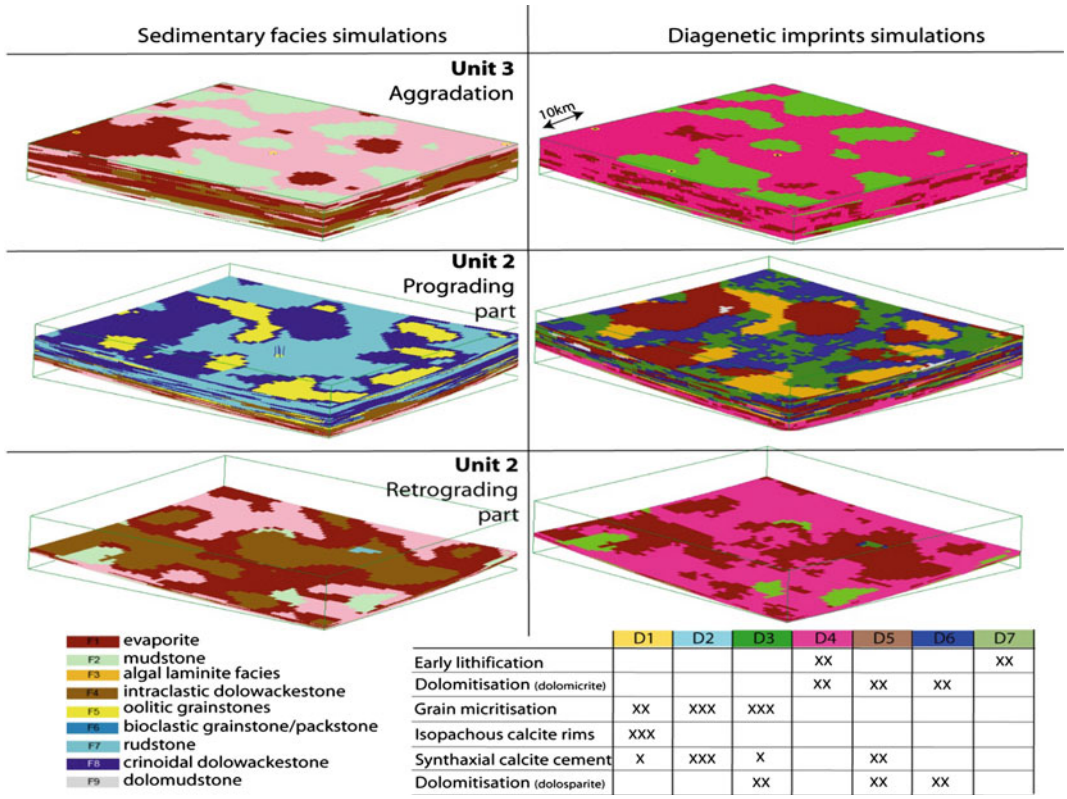

	D1	D2	D3	D4	D5	D6	D7
Early lithification				XX			XX
Dolomitisation (dolomicrite)				XX	XX	XX	
Grain micritisation	XX	XXX	XXX				
Isopachous calcite rims	XXX						
Synthaxial calcite cement	X	XXX	X		XX		
Dolomitisation (dolosparite)			XX		XX	XX	

Fig. 1.12 Results of geostatistical stochastic joint simulations of sedimentary facies and diagnetic imprints of the three stratigraphic units in the Madison Formation, Wyoming—USA; Barbier et al. 2012)

This is not a predictive approach but rather an extrapolation workflow based on probability. It certainly helps in illustrating a probability-based reservoir heterogeneity, ahead of flow simulations (Fig. 1.12; discussed further in Chap. 4).

Geochemical modelling makes use of thermodynamic and kinetic rules and data-bases to simulate chemical reactions and fluid-rock interactions. This can be done through a 0D model (e.g. ArXim, PHREEQ-C), whereby a certain chemical process is tested and analysed. Hence, the method is process-based. It can also consist of changing parameters through time (e.g. thermal/flux variations) while remaining in the same dimensional configurations. The results are usually in two groups, those related to the fluids and those related to the mineral phases. They could be used as arguments to support or refute proposed outcomes of fluid-rock interactions, and to clarify the distinct assumptions of open versus closed system diagenesis or better still, to discuss degrees of open-ness as a function of time and specific chemical species type (e.g. Ca, Mg, CO_2, SO_4, H_2S).

Coupling geochemical modelling with reactive-transport allows the simulation of fluid-flow and associated processes. Geochemical RTM are attractive as they provide forward simulations of diagenetic processes and resulting phases (see Fig. 1.13; discussed further in Chap. 4). Yet, they need to be validated since most of these processes occurred in different temporal and physico-chemical conditions. This remains today a weak point for the geochemical approach in modelling diagenesis.

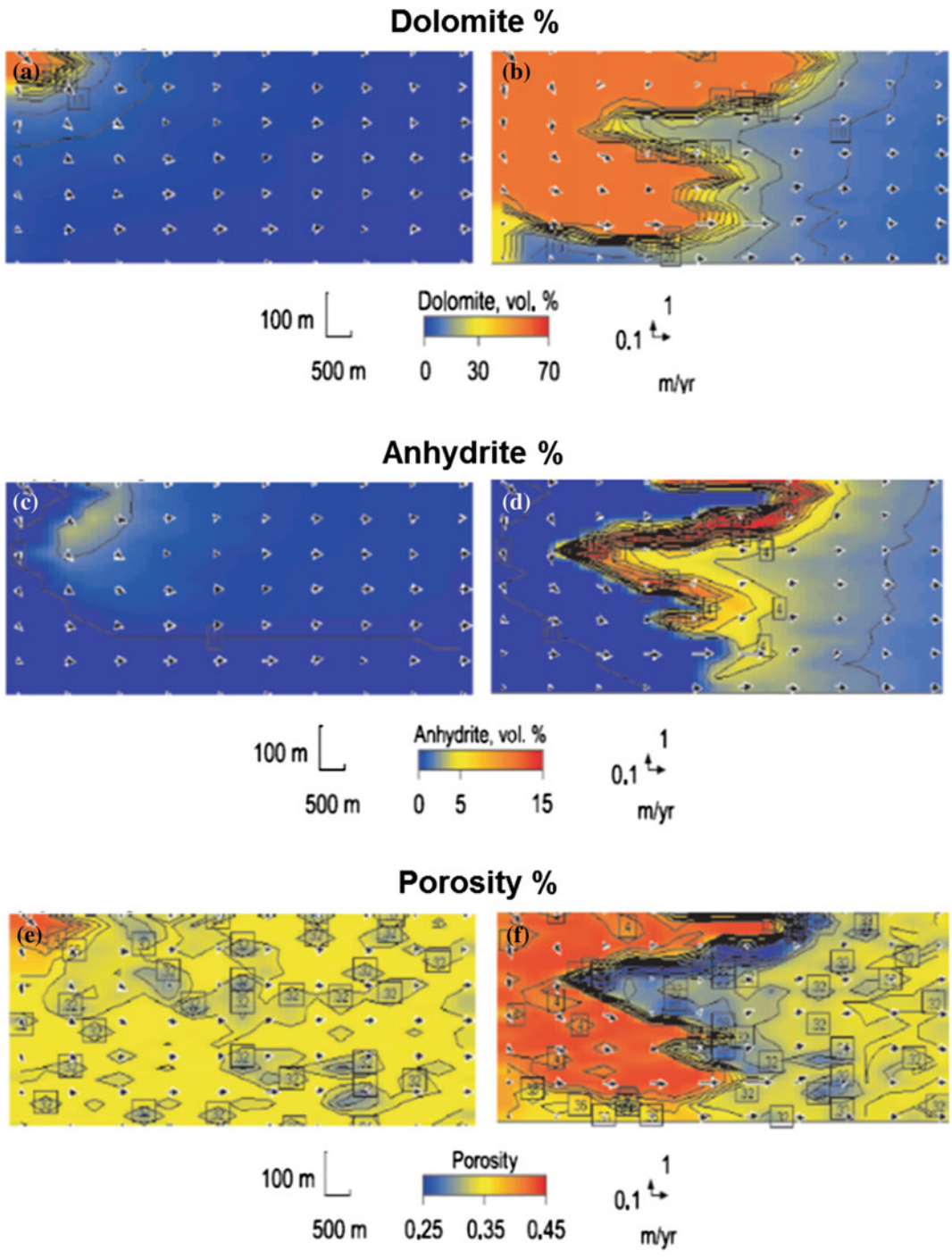

Fig. 1.13 Results of reactive transport modelling of reflux dolomitization showing the volumetric evolution (in %) of dolomite, anhydrite and porosity upon the formation of dolomite front (from Jones and Xiao 2005): **a**, **b** Simulated spreading of the dolomite front from 0.2 to 2.0 m.y. after injection of dolomitizing fluids; **c**, **d** Anhydrite precipitates at the front of the propagating dolomite body decreasing drastically the bulk rock porosity; **e**, **f** The associated porosity evolution from 0.2 to 2.0 m.y. showing the increased porosity within the dolomite body

1.5 Objectives

Through this contribution, the actual state of the art for characterizing diagenetic processes and providing conceptual models (Chap. 2) is presented to the best knowledge of the author. A variety of tools and approaches for quantitative assessments of diagenetic processes at various scales, and their impacts on the porosity of sedimentary rocks will be discussed in Chap. 3. Numerical modelling of diagenesis will be further discussed in Chap. 4. This chapter ends with a proposed workflow for integrated basin and reservoir modelling, aiming to further assess the impacts of multi-scale diagenesis on the heterogeneity of carbonate reservoir rocks.

No finalized workflows are present here, but rather work in progress. More emphasis will be set on the utility of the different sorts of modelling approaches and their challenges. This contribution is both a review and a look to the future presenting aspects of diagenesis studies that have been well understood so far, and highlighting future challenges for better predicting quantitatively diagenesis on a wide range of scales. The heterogeneous reservoir properties of carbonate rocks—as well that of silici-clastics—need to be well appreciated in order to achieve sustainable use of our underground realms (e.g. enhanced oil recovery, geothermal energy, CO_2/gas/water storage). Several new techniques and numerical tools will be tailored to reach such goals in the near future.

Characterization of Diagenesis

2

Several inter-related factors lead to complicated heterogeneities in sedimentary rocks, including the depositional settings, diagenetic processes, as well as tectonics and burial/thermal evolution of the basin (Cantrell et al. 2001; Roure et al. 2005; Ehrenberg et al. 2007; Rahimpour-Bonab et al. 2010). Substantial heterogeneities are often associated with carbonate reservoir rocks, resulting in a significant challenge for the optimization of hydrocarbon production and recovery (Ahr 2008), underground storage of gas (e.g. carbon capture and storage—CCS), freshwater and geothermal energy applications. In order to characterize properly such heterogeneities, studies of diagenetic phases (products) have to be combined to classical sedimentological investigations and basin analyses (e.g. burial history).

By 'characterization', description and classification are invoked. The diagenetic phases, which are produced by certain processes under specific conditions, are precisely described and then ascribed to carbonate diagenetic realms (see above, Chap. 1). Accordingly, predictive deductions could be applied concerning the extent of such phases and their impacts on the host-rocks at various scales. Diagenetic phases cover a wide range of types, some of which are: (i) mineralogical phases, such as cements; (ii) fluid phases, such as trapped fluid inclusions; (iii) transformed matter, such as dissolved material; and (iv) and resulted pore space. They are commonly investigated with a variety of tools, somehow specific to the type of phases at hand, which make the state of the art of today's characterization workflows for diagenesis.

2.1 State of the Art (Characterization of Diagenesis)

Classical carbonate diagenesis studies make use of a wide range of analytical techniques and aim to describe and explain specific, relatively time-framed, diagenetic processes (e.g. Nader et al. 2004; Gasparrini et al. 2006; Fontana et al. 2010; Ronchi et al. 2011; Swennen et al. 2012). Currently used techniques combine petrographic (conventional, cathodoluminescence, fluorescence, scanning electron microscopy with energy dispersive spectrometer—SEM/EDS, and 3D X-ray micro-computed tomography, micro-CT), geochemical (major/trace elements, stable oxygen and carbon isotopes, strontium isotopes, magnesium isotopes, clumped isotopes), and fluid inclusion analyses (microthermometry, Raman spectrometry, crush-leach analysis), providing the state of the art characterization tools and further independent arguments to support or discard any of the proposed conceptual models.

Diagenetic studies usually follow classical sedimentological descriptions of sedimentary rocks. Various techniques are used in order to describe the diagenetic phases. Here, descriptions—seldom

F.H. Nader, *Multi-scale Quantitative Diagenesis and Impacts on Heterogeneity of Carbonate Reservoir Rocks*, Advances in Oil and Gas Exploration & Production, DOI 10.1007/978-3-319-46445-9_2

quantitative, rather qualitative—are made on rock textures, primary sedimentary and diagenetic features as well as cements (in matrix and fractures/veins). Mineral replacements (e.g. dolomitization) and porosity are also investigated. A proper diagenetic study should lead to the following results: (i) identifying and defining the various diagenetic phases; (ii) organizing the diagenetic phases in chronological order—i.e. constructing a paragenesis (usually based on cross-cutting relationships and relative dating); (iii) inferring about the nature of original fluids that are responsible for the diagenetic processes and, subsequent, phases; and (iv) reconstructing the physico-chemical conditions that have prevailed during the respective diagenetic processes. Such results are inherent to develop conceptual models that explain the evolution of fluid-rock interactions and the sequence of diagenetic processes. Recently, this is also associated with burial modelling in order to constrain the spatiotemporal settings of the diagenetic processes (e.g. Lopez-Horgue et al. 2010; Fontana et al. 2014; Peyravi et al. 2014).

Several techniques are commonly used when describing diagenetic phases in carbonate rocks. The classical ones are presented here.

2.1.1 Fieldwork

Whether the study concerns subsurface well cores or surface-exposed rocks, the first step consists of describing the accessible rocks and selecting representative samples for further, laboratory investigation. The field description of the diagenetic geo-bodies—sometimes of seismic-scale—(e.g. dolomite fronts) and facies (e.g. zebra dolomites) provides the basic building blocks for

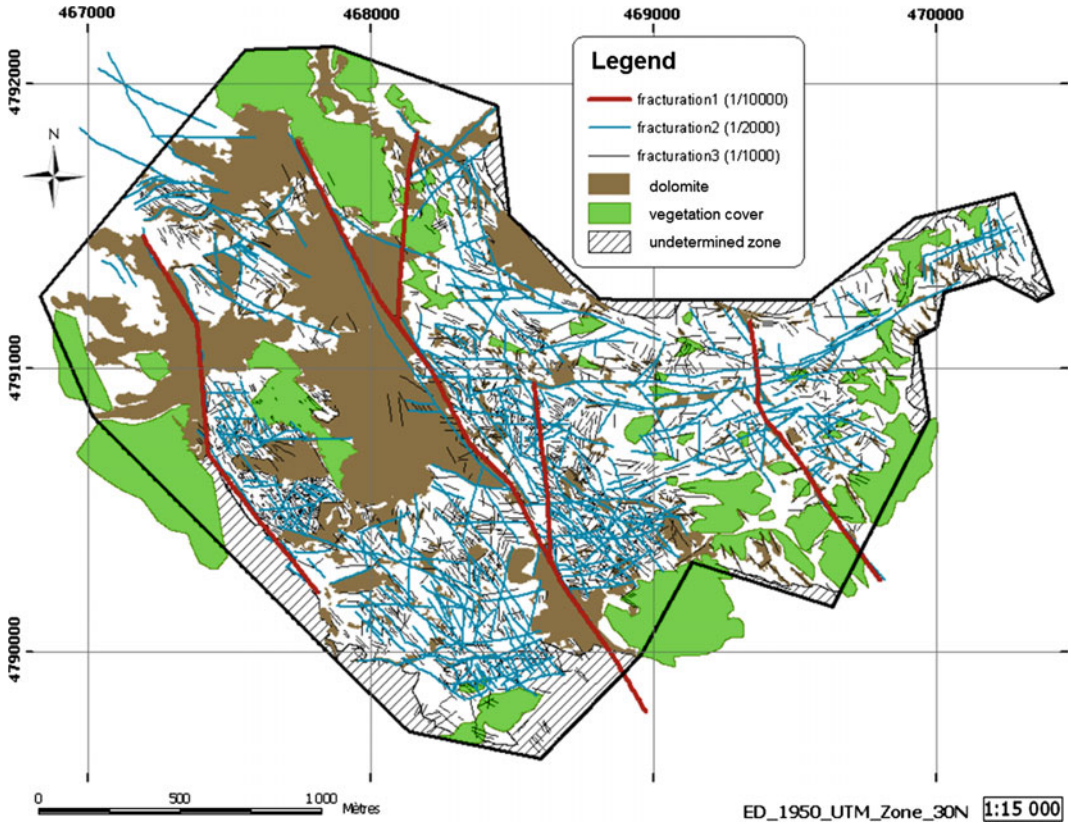

Fig. 2.1 Map showing dolomite occurrence and fracture (fault) lineaments in Cretaceous platform carbonate rocks exposed in Ranero (NE Spain), based on aerial photographs and fieldwork

any study. Here, mapping of diagenetic features is essential in order to understand the associated fluid-flow and the conceptual rock-fluid interactions (Shah et al. 2012; Nader et al. 2012; Fig. 2.1). In some cases, petrographic analyses can be achieved at the outcrop-scale (Fig. 2.2).

Many samples are usually collected by hammering pieces of rocks out of outcrops, whereas others are drilled out (with a micro-drillers) to retrieve detailed diagenetic cross-cutting features (e.g. distinct veins/fractures, stylolites) and/or to decrease the sample weight. Drilled samples are usually termed 'plugs', while hand-specimens are simply referred to as 'samples'. When needed, oriented sampling is performed (i.e. measuring the sample position with respect to bedding and/or magnetic north). Table 2.1 lists the bulk material of a typical study—i.e. number of samples, thin sections, geochemical and mineralogical analyses, microthermometry and samples for crush-leach analyses. Sampling is usually performed either vertically across stratigraphic columns, and/or laterally along sedimentological and/or diagenetic facies changes. It is usually planned on the m/cm scale across cross-cutting features considered to be of importance for the objectives of the study. For well-cores, detailed sedimentological logs are needed as background, based on which, sampling is performed.

2.1.2 Petrography

Petrographic analyses remain the basics of any diagenetic study. Carbonate rocks are investigated routinely with microscopic techniques to describe their textures, fabrics, and porosity. The various diagenetic features (replacive minerals, cements, dissolution, pressure-solution, etc.), are detailed and placed in chronological order based on cross-cutting relationships. Subsequently, a

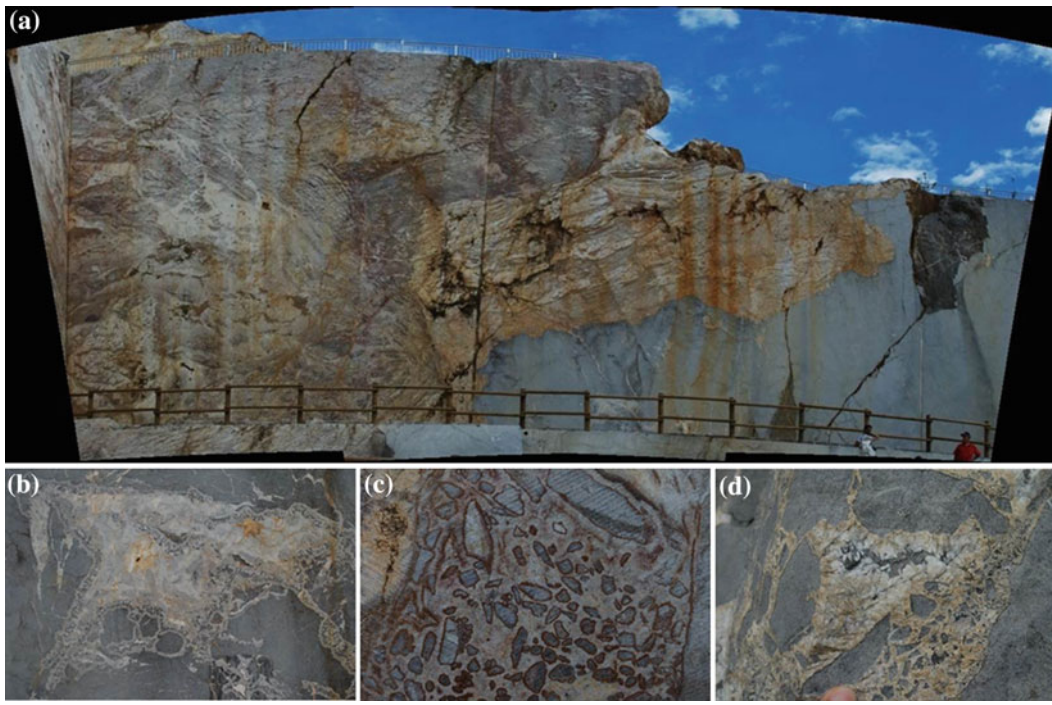

Fig. 2.2 Out-crop scale petrographic observations on the world class fault-associated dolomites in the Ranero, Pozalagua quarry/auditorium (NE Spain): **a** Overall view of the dolomite front in bluish-grey limestone; **b** Cemented paleo-karst cavity in the limestone; **c** Limestone clasts in distinct dolomite cement phases; **d** Various calcite and dolomite cement phases

Table 2.1 Total list of material used throughout a typical diagenetic study (Nader 2003)

Sections locations	Samples (thin sections)	AAS	AES	O/C isotopes (sequential)	Sr isotopes	XRD	Wafers	Crush-leach
Jeita-Metn	226 (160)	140	14	125 (21)	19	33	8	12
N. Ibrahim	191 (106)	48		83 (2)	2	25	4	5
Qadisha	83 (32)	42		56		14		
Total	500 (241)	230	14	264 (23)	21	72	12	17

paragenesis is proposed and will be further refined with geochemical and mineralogical investigations as well as fluid inclusions analysis.

Samples are systematically subjected to preliminary preparation and 'pre-microscopic' observation (of cut-faces) before thin section preparation and subsequent conventional microscopic examination (Nader 2003). In general, plugs are less often processed through this scheme, and frequently anticipated to thin section preparation.

2.1.2.1 Pre-microscopic Observations

'Pre-microscopic observations' encompass a series of steps necessary for providing larger scale petrological information of a sample, and for efficiently locating representative two-dimensional thin sections. Accordingly, sample preparation first consists of sawing the pieces or plugs in order to produce flat cut-faces or 'slabs', which are then processed for polishing, etching, staining (and peeling, see Nader 2003), all combined with low magnification binocular macroscopic investigation. Staining carbonate rock slabs is usually done by applying a solution of potassium ferricyanide blue and alizarin red S (Dickson 1966). This is done in order to distinguish (ferroan) calcite and (ferroan) dolomite (Fig. 2.3). Other types of solution may be used to distinguish other minerals (e.g. feldspars, anhydrite/gypsum; e.g. Doummar 2005). The practical result of the 'pre-microscopic' procedures for each sample is to be able to decide whether thin section(s) is (are) to be prepared, and to choose the optimal location for the thin section(s).

When thin-sections are available for the study, best is to stain them (see above) and scan them with a high resolution scanner, in order to provide high-quality images for further quantitative measurements.

Recently the computerized tomography CT technique provides the possibility to scan bulk rocks (or well cores) in 3D in order to select the optimal sampling locations, before destroying the bulk sample. Then, smaller plugs can be drilled out of the bulk rocks and scanned with higher resolution. This technique should also be coupled with classical microscopic investigations.

2.1.2.2 Microscopic Observations

Thin sections are studied through conventional, fluorescence and cathodoluminescence microscopy (e.g. CL: Technosyn Cold Cathodoluminescence Model 8200 Mark II; operation conditions were 16–20 kV gun potential, 350–600 μA beam current, 0.05 Torr vacuum and 5 mm beam width). Cathodoluminescence is simply the luminescence emitted by minerals when they are excited with radiation caused by an electron beam (Machel et al. 1991; Fig. 2.4). Microscopic viewing under fluorescent light can be used to investigate organic matter, to emphasis the porosity of carbonate rocks (impregnated with fluorescent dye), and to identify HC-rich fluid inclusions. Both fluorescence and cathodoluminescence (CL) microscopy should only be performed after the completion of conventional microscopic examination. Usually, for each CL and fluorescence photomicrograph a transmitted-light double is also taken. These

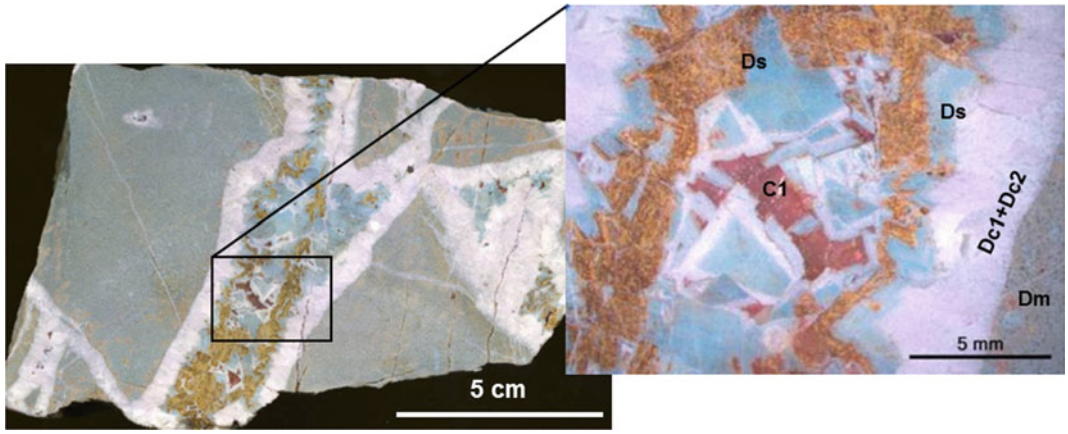

Fig. 2.3 *Stained polished*, *etched* slab of dolomite from the Ghalilah Formation (*Upper Triassic*) in Ras Al Khaimah (UAE), showing the host dolomite "*Dm*" together with fracture-filling non-ferroan (*unstained*) dolomite cements (*Dc1* and *Dc2*) and a later phase of ferroan saddle dolomite cement (*stained in blue*, *Ds*), and a later calcite cement phase (*C1*), *stained in red* (from Fontana et al. 2014)

techniques proved to be very useful for pre-set targets (e.g. determination of specific cement types, emphasis porosity, comparison between similar diagenetic phases present in different samples, assessing the homogeneity of the sample for precise isotopic and/or chemical analyses).

Scanning electron microscopy (SEM) is a technique that allows the petrographic examination under three-dimensional viewing and higher magnifications (10–100,000 times). The relatively old JEOL-JSM 6400 Scanning Electron Microscope unit is an example of SEM devices with operating conditions of 15–40 kV accelerating voltage, 2.10^{-7} to 10^{-9} A probe current, and working distance of 8–39 mm. The newer, EVO MA10 Zeiss SMT equipment has a computer-motorized five axis stage, enabling rapid sample observation. It operates with a tungsten filament at 15 kV and 100 mA, and a probe current of 150–700 pA (for SE imaging and EDS analysis, respectively). Combined with an Energy Dispersive X-ray Spectrometer (EDS), relative determination of compositional elements, based on the X-ray energy, may be performed. The SEM works by producing a high energetic electron beam in vacuum (inside an electron gun; LaB_6 or tungsten filament) that is accelerated towards the specimen surface (Fig. 2.5). The electron bombardment of the specimen surface results in two types of electrons—low energy secondary electrons (SE) and high energy backscatter electrons (BE). The former electrons are captured in a photomultiplier tube and transformed into an image on the screen, while the latter backscatter electrons (BE) are used to detect compositional variations (given that the intensity of the BE is composition dependent, i.e. related to the mean atomic number of the target).

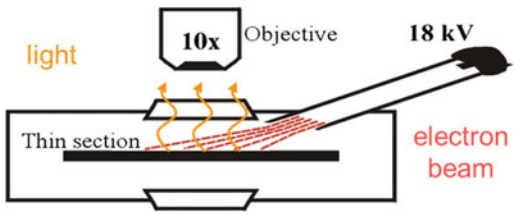

Fig. 2.4 A sketch showing the elementary constituents of cathodoluminescence (CL) microscopic technique: An electron beam focused on the *upper face* of a *thin-section* (or *polished* sample surface), which emits light (CL-pattern) that is observed under a microscope

High resolution 2D compositional analyses are performed with new SEM-EDS (and/or microprobes; EPMA) equipment (e.g. Zeiss EVO SEM, Oxford ESS), by applying punctual analysis for chemical composition and mineral mapping on thin-sections (Fig. 2.6). The time counting of 1000 microseconds can be set for spectral

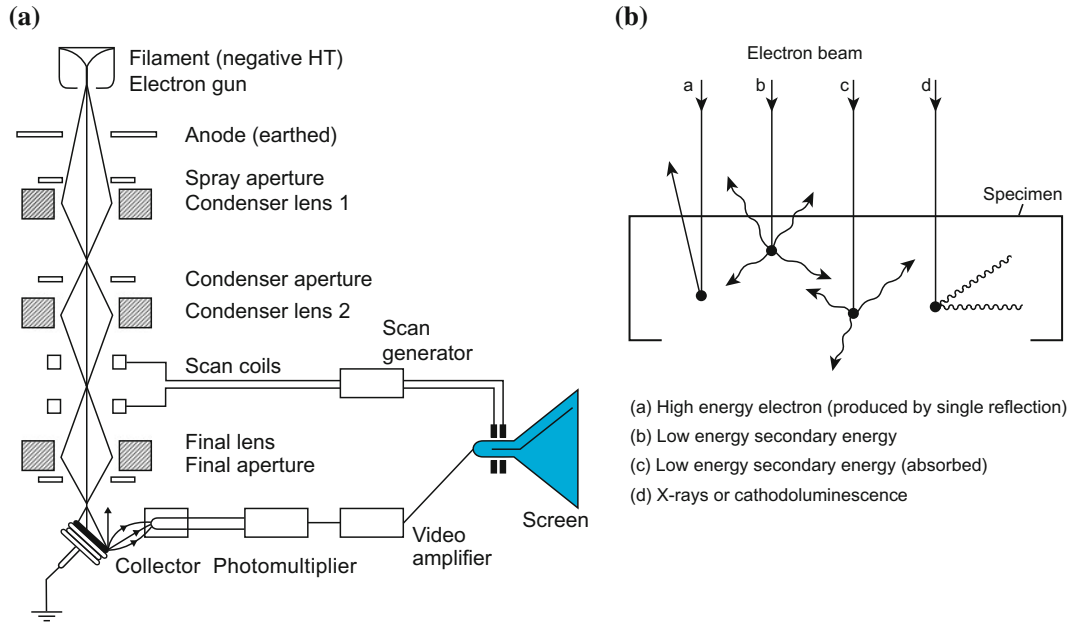

Fig. 2.5 Simplified illustration of the interior of a scanning electron microscope (SEM; **a**) and the resulting detected forms of energy (**b**). Sketch from Emery and Robinson (1993)

imaging, and the acquisition time for 86 × 128 pixels in the order of 1 h 30 min. Accordingly, mineral assemblages can be mapped, and the porosity change associated to mineralogical transformations through diagenesis can be determined. X-ray intensity maps of all elements are transformed to oxide wt.% by means of software packages (e.g. AZtecEnergy, produced by Oxford Instruments) constrained by EDS standardization. Statistical cluster analysis is commonly used to identify the different phases occurring in the samples (see below). Data output (from SEM-EDS analyses) can be further analysed with Matlab™ software based on De Andrade et al. (2006).

2.1.3 Geochemistry

A large variety of geochemical analyses are used in order to describe the chemical patterns of the diagenetic phases and to infer about the original fluids (at the time of precipitation or recrystallization). This quest remains very difficult and tricky due to the subtle "resetting" of the geochemichal signatures of carbonate minerals during diagenesis (e.g. Frisia et al. 2000). Only some of the major geochemical analyses that are routinely used for diagenesis studies are presented below.

2.1.3.1 Major and Trace Element Analyses

Major and trace elements allow defining the chemical characteristics of the diagenetic mineral phases, and eventually better constraining the fluid systems occurring during related diagenetic processes. Subsequently, they can also help in understanding the overall physico-chemical conditions and evolution through the proposed paragenesis.

Major and trace element analyses are carried out by flame Atomic Absorption Spectrometry (AAS), Atomic Emission Spectrometry (AES), and Inductively Coupled Plasma Mass Spectrometery (ICP-MS) which can be also coupled to a Laser Ablation device (LA-ICP-MS) to allow direct analysis of solid phases. In fact without Laser ablation, the rock samples need to be dissolved in solutions prior to analysis. Bulk samples (e.g. limestone/dolostone rock matrix), uni-phase samples (e.g. dolomite or calcite veins)

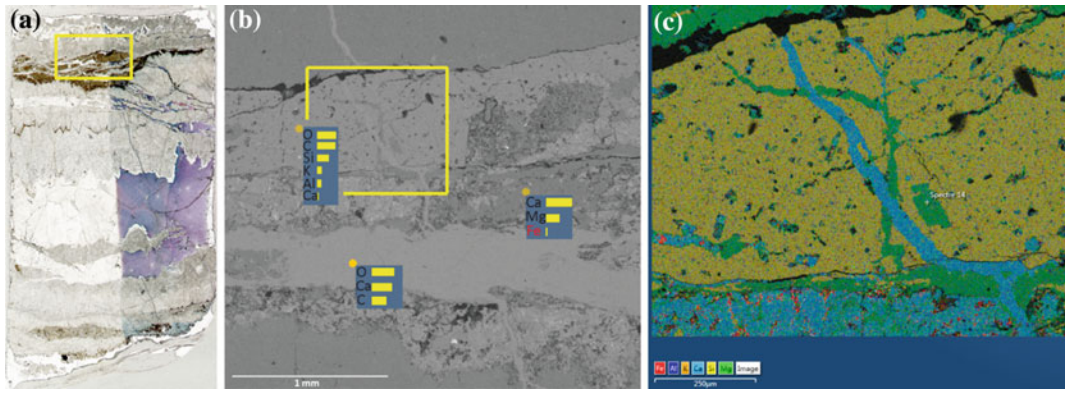

Fig. 2.6 Results of high resolution 2D elemental compositional SEM-EDS analysis performed on a stylolite in a dolostone from Latemar, northern Italy (courtesy of Katreine Blomme, KU Leuven): **a** *stained thin-section* with ferroan dolomite cement and clay-filled stylolite; **b** SEM photomicrograph showing a *close-up view* of the *yellow rectangle* in (**a**) together with 3 spots of EDS analysis on clay, dolomite and calcite zones; and **c** EDS map of the area indicated by the *yellow rectangle* in **b**, showing a dolomite veinlet (rich in Mg) cross-cut by a calcite veinlet (rich in Ca) within the silica-rich clay of the stylolite

and multi-phase samples (e.g. dolomite/calcite of a calicitized dolostone) could be analysed by AAS (Fig. 2.7; Nader 2003; Maussen 2009). Due to their non-carbonate impurities and mixed volumes of calcite and dolomite, carbonate rocks are very problematic when it comes to determining their major and trace elemental distribution. The designed analytical procedures for sample preparation are the result of tedious trial and error lab-work.

2.1.3.2 IFPEN Protocol for AAS (Maussen 2009)

Flame atomic absorption spectrometry (AAS: Varian SpectrAA 240FS) is perfectly adequate to determine major and trace elements composition

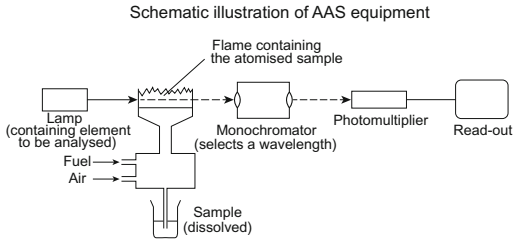

Fig. 2.7 Simplified diagram of AAS equipment and constituents—courtesy of Maussen (2009) (from A. Walsch: http://www.hsc.csu.edu.au/chemistry/core/monitoring/chem943/943net.html)

of sedimentary rocks (e.g. Ca, Mg, Fe and Mn contents among others). For major and trace element analyses, dolostone and limestone powdered samples (1 g of each) are leached in 40 ml (1 M) HCl and left on hot plates until evaporation. The residues are dissolved for a second time in 20 ml (1 M) HCl. Samples containing both calcite and dolomite are subjected to a sequential extraction procedure modified from Nader (2003) prior to geochemical analyses (Maussen 2009). Samples are leached in 60 ml of 4 %v/v. acetic acid to remove the calcite phase. After reaction, the remaining samples are evaporated. The residue is dissolved in 20 ml of 25 %v/v. nitric acid, the calcite evaporate is then dissolved with 20 ml of 25 %v/v. nitric acid. After filtering and rinsing, the resulting solution is considered to represent the calcite phase. The remaining solids (assumed to represent the dolomite phase and clays) are subjected to similar leaching procedures: dissolution in 20 ml of 25 %v/v. nitric acid, evaporation and dissolution in 20 ml of 25 %v/v. nitric acid. After filtering and rinsing, the resulting solution is considered to represent the dolomite phase and the remaining solids are clays. Calibration of the AAS needs to be achieved by means of a multi-element standard solution (in a 5 %v/v. nitric acid matrix). The multi-element standard solutions and sample

solutions are commonly matrix corrected for Ca and Mg. Analytical precision on ppm contents is generally less than 5 % for both mixed calcite/dolomite and dolomite samples.

2.1.3.3 Stable Oxygen and Carbon Isotopic Analyses

Oxygen and Carbon isotopic analyses help in shedding lights on the original type of fluids and temperature prevailing throughout diagenesis. Stable oxygen isotopes reflect the original fluids and the temperature during precipitation of the analysed carbonate phase. Thus, an independent argument is needed in order to estimate one of these two variables. Stable carbon isotopes are inherently related to the original seawater and soil-derived carbon. Often the $\delta^{13}C$ signature of the investigated diagenetic phase is buffered by that of the host-rocks (e.g. pointing towards its marine origin).

Stable isotope analyses are frequently done in specialized laboratories (e.g. Université Pierre et Marie Curie UPMC, Paris—France; Institute of Geology and Mineralogy, University of Erlangen —Germany). Samples are usually micro-drilled or micro-milled from the stained rock-slabs (or directly from thin sections), and sent to the qualified laboratory. The carbonate powders are commonly reacted with 100 % phosphoric acid (density > 1.9; Wachter and Hayes 1985) at 75 °C in an online carbonate preparation line (Carbo-Kiel—single sample acid bath) connected to a Finnigan Mat 252 mass-spectrometer. All values are reported in per mil relative to Vienna Pee Dee Belemnite (V-PDB) by assigning a $\delta^{13}C$ value of +1.95‰ and a $\delta^{18}O$ value of −2.20 ‰ to NBS19. Oxygen isotopic compositions of dolomites are usually corrected using the fractionation factors given by Rosenbaum and Sheppard (1986). Reproducibility based on replicate analysis of laboratory standards is better than ±0.02 ‰ for $\delta^{13}C$ and ±0.03 ‰ for $\delta^{18}O$.

For the samples that contain calcite and dolomite phases together (inseparable; e.g. dedolomite), a special double collection procedure can be performed (e.g. Nader et al. 2008). The same sample (about 10 µg, powdered) is first reacted with 100 % phosphoric acid for 2 h in a water-bath at 25 °C. The extracted CO_2 is assumed to represent the calcite phase. Then, the reaction with the acid continues for 36 h (same operating conditions), or at higher temperatures (for a shorter time duration), before a second extraction of CO_2 considered to represent the dolomite phase.

2.1.3.4 Strontium Isotope Analyses

Strontium isotope ratios are usually used in order to determine either the age of the investigated diagenetic phase (compared to the evolution of the marine Sr curve; Fig. 2.8) or to infer about rock-fluid interactions (e.g. mixing and interaction with radiogenic Sr fluids).

Sr isotope analyses are also carried out in specialized laboratories (e.g. BRGM, Orléans—France; SARN-CNRS, Nancy—France; SUERC, Glasgow—United Kingdom). Carbonate samples are leached in 1 M ammonium acetate prior to acid digestion. Calcite is digested in 1 M acetic acid, and dolomite in 6 M HCl. Sr is separated in 2.5 M HCl using Bio-Rad AG50W X8 200–400 mesh cation exchange resin. Total procedure blank for Sr samples prepared using this method is <200 pg. In preparation for mass spectrometry, Sr samples are loaded onto single Ta filaments with 1 M phosphoric acid. Sr samples are analysed on a VG Sector 54–30 multiple collector mass spectrometer. A ^{88}Sr intensity of 1 V (1×10^{-11}A) ± 10 % is maintained and the $^{87}Sr/^{86}Sr$ ratio is corrected for mass fractionation using $^{86}Sr/^{88}Sr = 0.1194$ and an exponential law. The VG Sector 54–30 mass spectrometer is operated in the peak-jumping mode with data collected as 15 blocks of 10 ratios.

2.1.4 Mineralogy

Mineralogical investigations are usually done by means of X-ray diffraction (XRD) technique for various purposes: (i) determination of clay minerals, (ii) determination of amounts (%) of mineral phases in a rock (e.g. calcite, dolomite, anhydrite), and (iii) assessment of dolomite nonstoichiometry and crystal ordering.

The relative determination of calcite/dolomite percentage in a carbonate rock is possible by

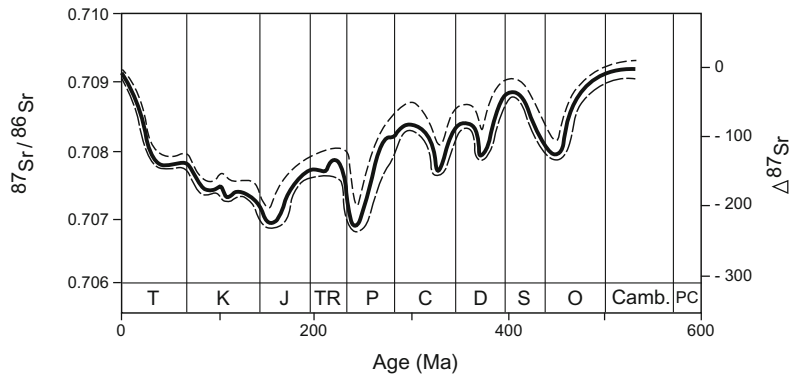

Fig. 2.8 Variations of $^{87}Sr/^{86}Sr$ in seawater throughout the geologic time (from Emery and Robinson 1993). *Detached lines* represents the approximate limits of uncertainties

means of relative comparison of calcite/dolomite peak surfaces and Rietveld modelling. Optimized workflows have been designed based on several authors (e.g. Hutchison 1971; Royse et al. 1971; Tucker 1988), and experimental laboratory work. Dolomite nonstoichiometry—mole (M) % $CaCO_3$—is often calculated using the relationship between calcium content and $d_{[104]}$ spacing (Goldsmith and Graf 1958) and applying the equation of Lumsden to the measured $d_{[104]}$ spacing (Lumsden 1979):

$$N_{CaCO3} = M\,d + B$$

where N_{CaCO3} is the mole% $CaCO_3$ in the dolomite crystal lattice, d is the diffractogram's peak d spacing in Angstrom units, M is 333.33 and B is −911.99.

Dolomite crystal ordering can be assessed by calculating the FWHM (full width of half maximum intensity) of the main dolomite peak on X-ray diffractograms. Experience showed that, within the context of relative assessment, this method yields better results than those of other traditional methods (described in Tucker 1988), where the surface area of the accessory dolomite smaller peaks are used to determine ordering ratios (Nader 2003). Jones et al. (2001) proposed a methodology for assessment of 'heterogeneous' dolostones, which exhibit multiple peaks and/or shoulders.

2.1.4.1 IFPEN Protocol for XRD (Turpin 2009; Turpin et al. 2012)

Small portions of each sample are uniformly ground in an agate mortar for XRD measurements. Alumina from NIST is added to each powder sample for use as an internal standard (50 weight %) and the mixture is again ground until it becomes homogeneous. The Alumina cell parameters are taken from the NIST information (SRM 676a). XRD patterns are collected using Cu radiation with step size of 0.017°2θ and counting time in the order of 91 s.$2\theta^{-1}$ (with a position-sensitive detector on an X'pertPro Panalytical diffractometer). The identification of minerals is performed on the measured digitized diffractograms, using the ICDD database (PDF4+). XRD analyses in θ–2θ configuration is performed with a parallel beam focused by an elliptic W/Si crystal mirror. The measurements are undertaken on the powder samples enclosed in a 1 mm glass capillary, to enable the analysis of the whole sample.

Structure and cell refinements are then performed on the resulting diagrams. The structure refinement method (Rietveld 1969) is based on a least-squares refinement procedure which employs directly the profile intensities obtained from step-scanning measurements of the powder diagram. It allows making some quantitative judgment of the agreement between observed and calculated integrated intensities instead of profile intensities. A fair approximation to the observed integrated intensities can be made by separating the peaks according to the calculated values of the integrated intensities. Based on all diffraction peaks, the Rietveld refinement is used to quantify the relative proportions of coexisting phases in samples and cell refinement, to determine the unit cell parameters of the dolomite crystals. The peak positions of the NIST Alumina

are used to correct the peak shift error (in two-theta) for the various constituent of each sample between experimental and calculated profiles. The relative error on quantification via Rietveld refinement has been already calculated for common minerals. The uncertainty is logically linked to the phase proportion in the sample: when abundance is <5 %, uncertainty is >75 % while it is <10 % when proportion is >80 %.

2.1.4.2 Electron Microprobe

Electron microprobe analyses (EMPA) are usually undertaken only on key samples. Their use aims to map mineralogical assemblages (and possible evidence of incorporated Fe and Mn in the carbonate minerals). EMP (mapping) analyses are achieved using a Cameca SX100 microprobe under the following analytical conditions: 15 kV, 100nA, 0.3 s for all analysed elements (e.g. Ca, Mg, Fe, Mn, Sr), with 1 μm spot size and 5 μm step size.

The electron microprobe is standardized on diopside for magnesium and calcium, garnet for iron, rhodonite for manganese and celestine for strontium. X-ray intensity maps of all elements were transformed into oxide weight% concentration maps according to the procedure of De Andrade et al. (2006), using high quality point analyses. A statistical cluster analysis could identify the different major mineral phases occurring in the samples. For carbonate clusters, a structural formula is calculated for each pixel using a 1 oxygen basis, and assuming all iron to be divalent (Fig. 2.9). The maps of structural formulas are then filtered to remove pixel analyses located at the limit between different homogeneous phases (mechanical mixing on contaminated analyses). The remaining structural formulas were filtered using the following equations: (i) $0.96 < Ca < 1.14$; (ii) $0.86 < Mg < 1.04$; and (iii) $0.0 < Fe < 0.1$ (per formula unit with 0.1 as standard analytical error). This set of constraints are defined by natural variation of typical dolomite compositions between two end members; i.e. $Ca_{0.96}Mg_{1.04}(CO_3)_2$ and $Ca_{1.14}Mg_{0.86}(CO_3)_2$ calculated for 48 and 57 % dolomite nonstoichiometry, respectively.

2.1.5 Fluid Inclusions

Analyses of fluid inclusions trapped in diagenetic minerals (and cements) provide one of the few tools that allow a direct reconstruction of the thermal and fluid composition history of a sedimentary basin (e.g. Ceriani et al. 2002; Swennen et al. 2003; Nader et al. 2004).

2.1.5.1 Microthermometry

Microthermometric analyses of fluid inclusions are performed on double-polished sections using a Linkam THMSG 600 heating cooling stage mounted on an Olympus BX60 microscope. The liquid-vapor homogenization temperatures (T_h) of two-phase primary and pseudo-secondary aqueous fluid inclusions are studied in order to estimate the temperature of precipitation for the host crystal. Assuming that the investigated minerals derive from a certain fluid system (such as NaCl-H_2O), the final melting temperatures of ice (T_m) are used to infer about the salinity of the fluid itself (Fig. 2.10). Measurement accuracy is usually in the order of 1 °C for T_h values and 0.2 °C for T_m values. T_h values are also used in association with $\delta^{18}O$ isotopic data in order to reconstruct $\delta^{18}O$ composition of the parent fluids.

2.1.5.2 Crush-leach Analyses

Specific sample phases are carefully cut from core or hand sample using a saw and then cleaned with a dentist's drill, mainly representing phases whose fluid inclusions were properly investigated. The samples are crushed and sieved to give a 1–2 mm grain size fraction and hand-picked under a binocular microscope to obtain 2 g of a clean mineral separate where possible. The samples are then washed in 18.2 ml water, heated overnight on a hot plate, electrolytically cleaned for 1 week and then dried in an oven. 1–2 g of sample are ground to a fine

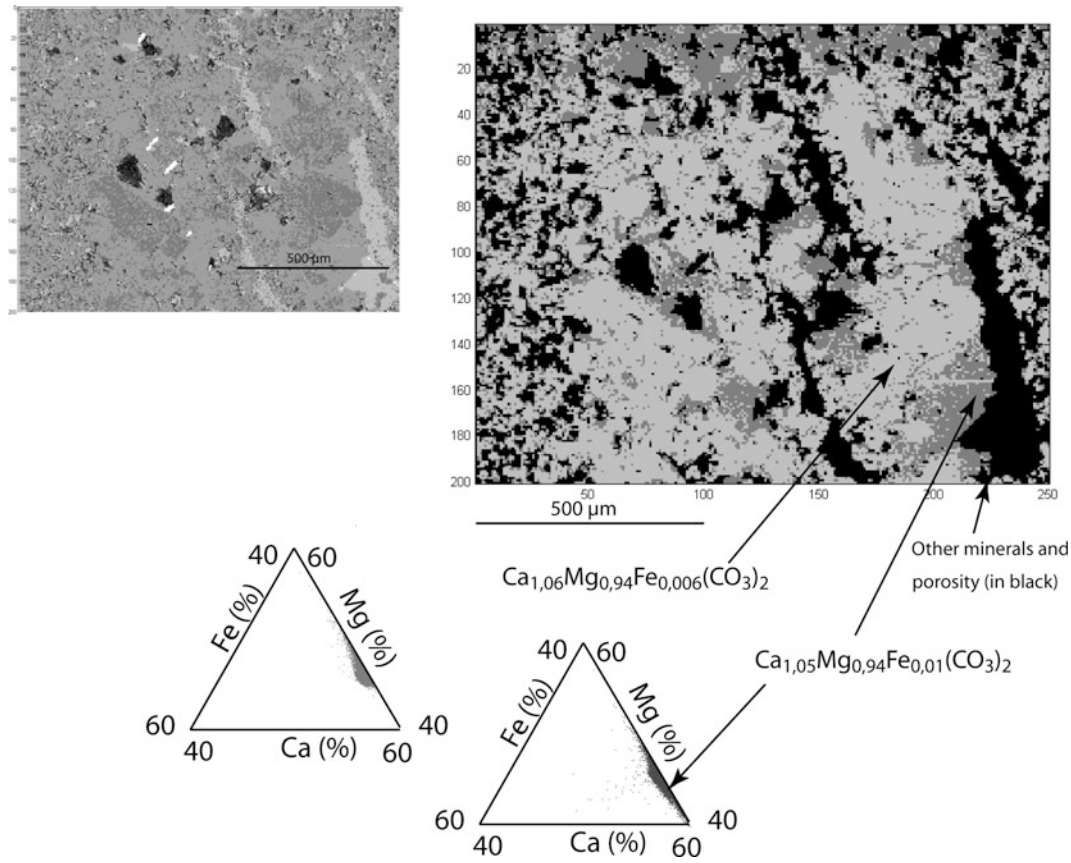

Fig. 2.9 SEM backscattered electron image (*left*) and cluster analysis of electron microprobe map (*right*), as well as mean structural formula for two different dolomites with varying chemical composition in Ca–Mg-Fe ternary diagram. Triassic dolomite rock sample (well core) from the French Jura (Turpin 2009)

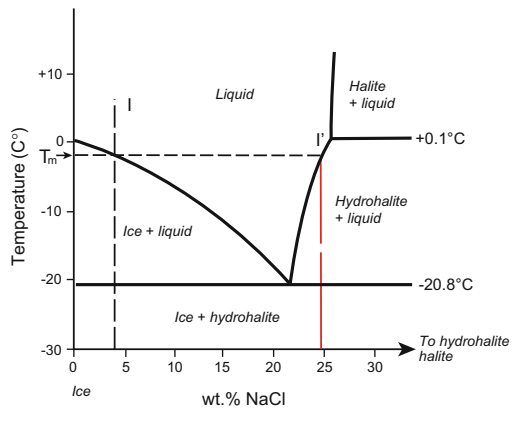

Dissolved species	Eutectic temperature (°C)	Eutectic composition (wt. %)	Solid phases		
			H_2O	ice	hexagonal colorless RI e 11.3 w 1.30
NaCl	-20.8	23.3% NaClN	aCl.2H_2Ohydrohalitem		onoclin//ic colorless RI 1.416
			NaCl	halite	cubic colorless RI 1.544
KCl	-10.6	19.7% KCl	KCl	sylvite	cubic colorless yellowish RI 1.490
$CaCl_2$	-49.8	30.2% $CaCl_2$	$CaCl_2.6H_2O$	antarcticiteh	exagonal colorless RI e 1.39 w 1.41
$MgCl_2$	-33.6	21.0% $MgCl_2$	$MgCl_2.12H_2O$		
NaCl-KCl	-22.9	20.17% NaCl 5.81% KCl			
NaCl-$CaCl_2$	-52.0	1.8% NaCl 29.4%$CaCl_2$			
NaCl-$MgCl_2$	-35.0	1.56% NaCl 22.75% $MgCl_2$			
NaCl-$CaCl_2$-$MgCl_2$					

Fig. 2.10 Typical phase diagram for NaCl-H_2O fluid systems and selected phase data for aqueous solutions of chloride species commonly found in fluid inclusions (modified from Emery and Robinson 1993)

powder in an agate mortar and pestle in a clean and controlled environment. Half the powder is transferred to an unreactive vial and 5 ml of clean water was added. These samples are shaken, and filtered through 0.2 micron filters to give a clean leachate. Anions (Cl, Br, F and sulfate) are analysed using a Dionex DX600 ion chromatograph or ICP-MS (see above). Na and K and other cations are analysed on the same leachate using atomic absorption spectroscopy or ICP-MS.

2.1.6 Integrated Techniques for Building Conceptual Models

Through the application of various techniques, independent arguments are collected to describe the diagenetic features and organize the respective phases (and processes) in chronological order. Hence, a paragenesis can be presented, and it is commonly associated with a porogenesis (evolution of porosity, see above). It spans the time since the deposition until burial and/or surface exposure—practically until sampling took place (Fig. 2.11).

Each of the documented diagenetic phase represents a certain process that is pigeon-holed in a diagenetic realm with specific physico-chemical conditions. Then a conceptual model could be associated with the defined process. Based on detailed petrographic analyses with geochemical characterization of the key diagenetic phases and fluid inclusion analyses, Nader et al. (2007) constructed the paragenesis of a hydrothermal dolomite front in Jurassic platform carbonate rocks. The cross-cutting relationships as well as the petrographic and geochemical characteristics of the dolomite phases helped in relative-dating the process of front emplacement. Accordingly, a conceptual model could be presented illustrating the spatial/temporal evolution of the hydrothermal dolomite front (Fig. 2.12).

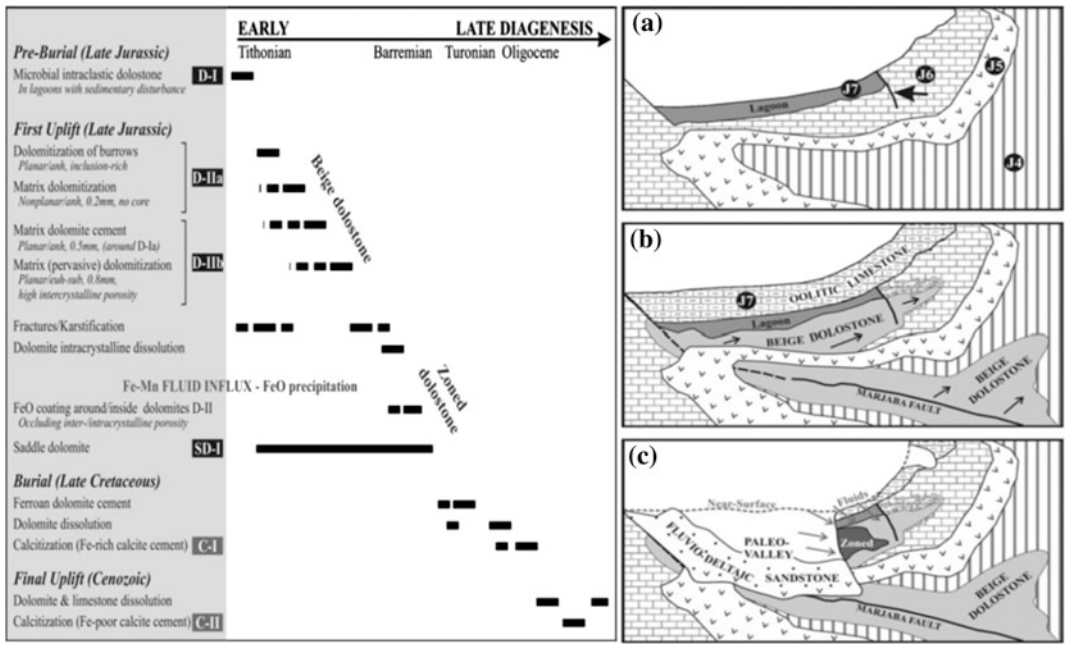

Fig. 2.11 Proposed sequence of diagenetic phases (paragenesis) for the dolostones of the Marjaba HDT front (central, Lebanon) based on petrographic, geochemical and fluid inclusion analyses. Cartoons **a**–**c** represent the proposed conceptual model of the dolostone front emplacement and evolution (beige dolomite, ferroan zoned dolomite, dolomite cementation/dissolution) during the Kimmeridgian-Tithonian, Tithonian-Early Cretaceous, and early Cretaceous, respectively (Nader et al. 2007)

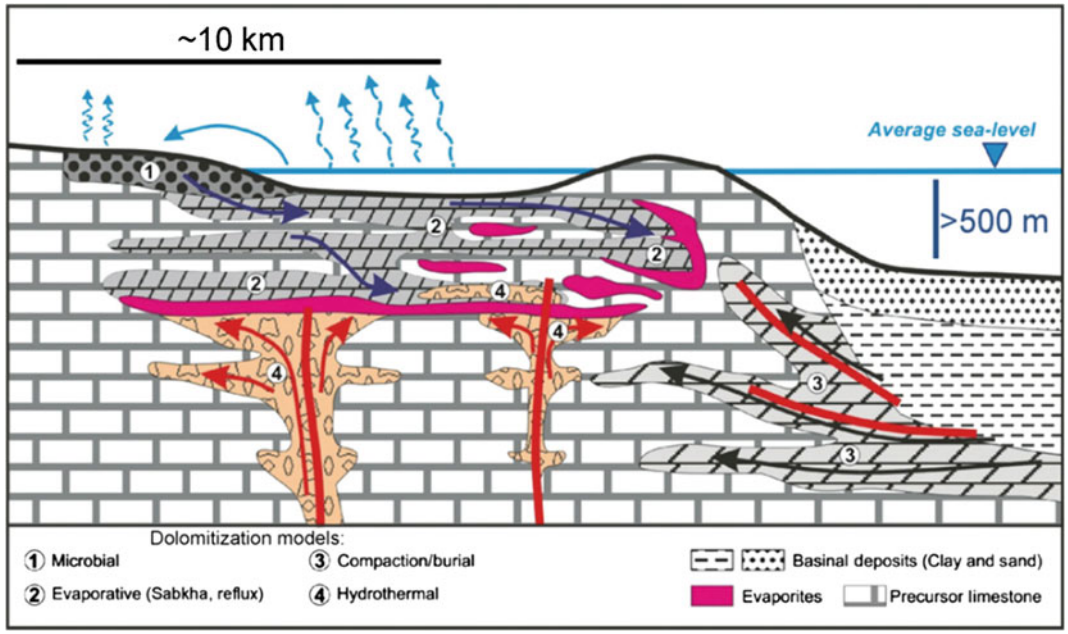

Fig. 2.12 Examples of conceptual dolomitization models and their schematic geometries and extent. The expected fluid flow pathways are indicated with *arrows* (from Nader et al. 2013)

Alternatively, reflux, burial or fracture-related dolomitization models (Fig. 2.12) may be invoked to explain a certain dolomite phase, whose petrographic and geochemical characteristics have been detailed. By following similar workflows, and through the comparison with other similar study cases, further constraints on the geometry (extent) and timing of the process may be reached. In addition, the hydrodynamic settings during the operation of such process may be proposed. The spatial heterogeneity in the host rock is eventually qualitatively estimated together with the impacts on reservoir properties (namely, porogenesis).

2.2 Future Perspectives

At this stage, it is fair to state that the various characterization methods for diagenesis and overall workflows are well advanced. Additional analytical techniques will certainly bring more precision and better constrains to diagenesis, namely through quantitative techniques. Indeed, some new, promising analytical techniques are currently being developed, building up further the state of the art of diagenesis studies (e.g. clumped oxygen and magnesium isotopic analyses). In addition, new cutting edge technologies in investigating porosity will undoubtedly bring a new era. Until today, the analyses of porosity in sedimentary rocks often is based on the rock textures—see above, the classifications of Choquette and Pray (1970) and Luccia (1995) and Lønøy (2006). The coming years will probably reveal another approach to understand the porosity evolution by focusing on the investigations of the pore space itself. This is becoming possible through advances in computed tomography techniques capable of capturing the porous space in 3D at the macro-scale (intergranular) and micro-scale (intra-granular).

2.2.1 Clumped Oxygen Isotopic Analyses

Oxygen stable isotopic analyses infer about the nature of the original fluids and the temperature during precipitation of carbonate minerals. Such

results are hindered by two variables (original fluids chemistry and precipitation temperature, as presented above). Fluid inclusions analyses are often used as an independent approach to constrain the precipitation temperatures, and, together with stable oxygen isotopic results, confirm the original nature of the precipitating fluid. Yet, carbonate rocks in general (and dolomites in particular) have fluid inclusions that often are damaged by leakage or stretching. A new paleo-thermometer is therefore needed, one that can be used on several types of cement fabrics/types, and that is not associated to any other unknown variable. The 'clumped' oxygen isotopic analyses are believed to provide such paleo-thermometry approach, and are expected to have great analytical potentials in the near future.

While the classic stable isotopic analyses (e.g. $\delta^{18}O$, $\delta^{13}C$) aim to estimate the difference between the isotopes' ratio (e.g. $^{18}O/^{16}O$, $^{13}C/^{12}C$) of the rock sample compared to that of an international standard, the 'clumped' isotopic analyses distinguishes specific 'isotopologues'—i.e. molecules of similar chemical composition but different isotopic composition. Practically, the isotoplogue of CO_2 with a mass of 47—i.e. Δ47—(where the heavy, rare isotopes of carbon and oxygen, ^{13}C and ^{18}O, are substituted in the CO_2 molecule; i.e. $^{13}C^{18}O^{16}O_2{}^{2-}$) is measured representing the amount of 'clumping' of the heavy isotopes in the crystal lattice (Fig. 2.13). This is achieved by simultaneous measurement of $\delta^{18}O$ and $\delta^{13}C$ to Δ47 in the same sample, with no comparison with external references.

The amount of 'clumping' can be known at a specific temperature according to the laws of thermodynamics. Ghosh et al. (2006) demonstrated that a single calibration line could be derived for the Δ47 values of different carbonate minerals that have precipitated at distinct temperatures (Fig. 2.14; Eiler 2007). Hence, 'clumped' isotopes are free of mineral specific fractionation effects in contrast to $\delta^{18}O$ and $\delta^{13}C$ measurements. Δ47 is independent of the original fluid $\delta^{18}O$ composition; it only reflects temperature.

Accordingly, the carbonate 'clumped' isotope paleo-thermometry is based on the temperature-

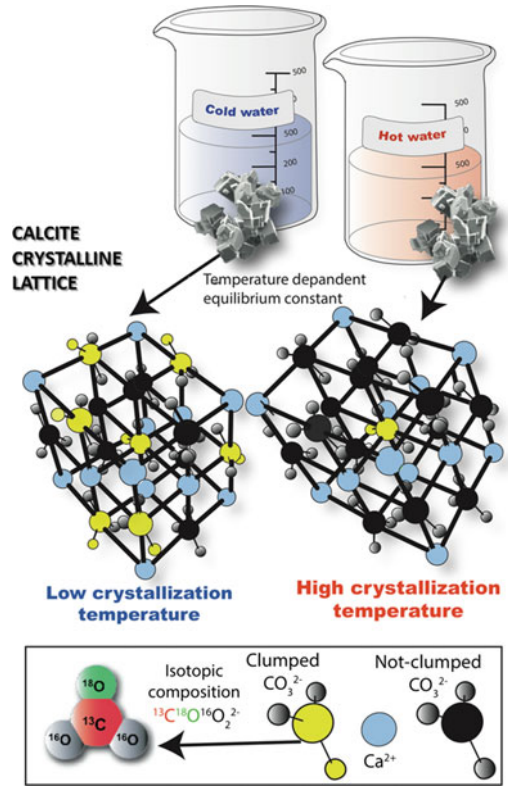

Fig. 2.13 The amount of "clumped" oxygen isotopes is calculated by the measuring the quantity of Δ47 isotoplogues of CO_2 in a calcite lattice (i.e. $^{13}C^{18}O^{16}O_2{}^{2-}$), which is a function of temperature of crystallization (illustration courtesy of Xavier Mangenot, IFPEN 2015)

dependent formation of an isotoplogue of CO_2 with a mass of 47 within the carbonate minerals ($^{13}C^{18}O^{16}O_2{}^{2-}$ ionic groups, as presented above). This is done by determining Δ47 values of CO_2 extracted from the minerals, and comparing results with the temperature calibration line.

More recently, analyses of clumped isotopes have been made possible and standardized for calcite and dolomite (e.g. Dennis et al. 2011). Henceforth, estimations of the crystallization temperatures of diagenetic calcites at temperatures varying from 14 to 123 °C (Huntington et al. 2011) and synthetic dolomites at temperatures between 25 and 350 °C (Bonifacie et al. 2013, 2014), have been achieved and published. The calibration lines for calcite and dolomite are currently being improved with additional

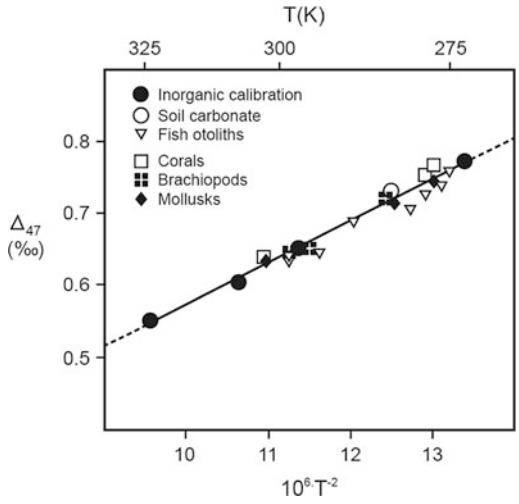

Fig. 2.14 *Interpolated* (*solid*) *line* of Δ47 values (in ‰) and corresponding temperatures (in K) for inorganic and organic carbonates (from Eiler 2007)

published data (*pers. communication* Xavier Mangenot, IFPEN 2015).

2.2.2 Mg Isotopic Analyses

Magnesium (Mg) is a major rock-forming element in terms of its abundance (second, after oxygen). It is ubiquitously present in the seawater, where most of carbonate rocks are formed. It is also present in the hydrological and biological systems (Young and Galy 2004). The multiple-collector inductively coupled plasma-source mass spectrometers (MC-ICP-MS) is capable to properly measure the Mg isotopic ratios $^{25}Mg/^{24}Mg$ and $^{26}Mg/^{24}Mg$ in dissolved samples (e.g. Young and Galy 2004). Besides thermal ionization mass spectrometry (TIMS) allows precise measurements of the differences in $^{26}Mg/^{24}Mg$ from a fixed "terrestrial" value.

Li et al. (2012) measured the Mg isotope fractionation between Mg-bearing calcite and Mg in aqueous solutions over a range of temperatures (4–45 °C). Their results, together with those of other workers (e.g. Schauble 2011; Rustad et al. 2010) allowed to constrain furthermore the Mg isotope fractionation factors between carbonates and solution (see Fig. 2.15). They have also demonstrated that the $\Delta^{26/24}Mg_{cal-sol}$ fractionation is insensitive to pCO_2, solution chemistry, and calcite composition, and that it is only slightly affected by temperature. Therefore, the Mg isotopes can be used to constrain Mg fluxes (including continental weathering) in modern and ancient marine systems.

Mg isotopic compositions of carbonate minerals could be compared to the $\delta^{26}Mg$ of modern carbonates, and become of interest for diagenesis studies (e.g. Lavoie et al. 2011; Li et al. 2012). For instance, they can offer important insights into the sources of Mg (necessary for the dolomitization processes), and thus, they can validate some conceptual models of dolomitization (Fig. 2.16). Often $\delta^{26}Mg$ isotopic analyses are done after securing other classical geochemical analyses (e.g. $\delta^{18}O$, $\delta^{13}C$, $^{87}Sr/^{86}Sr$) and fluid inclusions. Lavoie et al. (2011) revealed

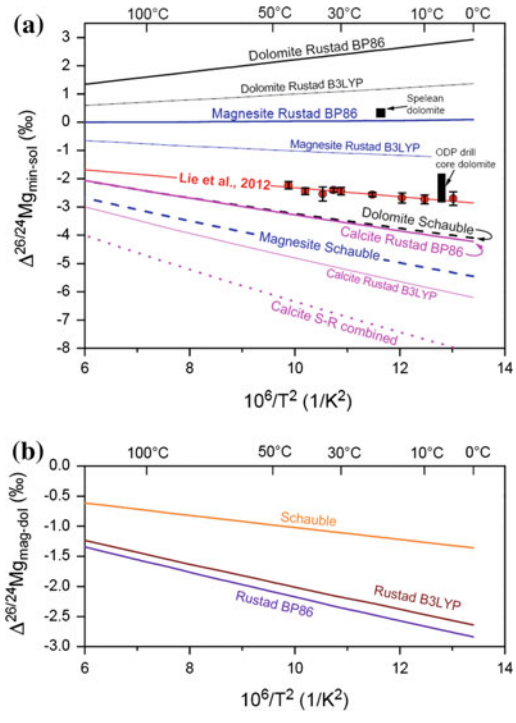

Fig. 2.15 Theoretically predicted Mg isotope fractionation factors (from Li et al. 2012 and references therein): **a** Mg isotope fractionation factors between carbonates and solution with respect to temperature. **b** Mg isotope fractionation factors between magnesite and dolomite relative to temperature

linear relationships between the $\delta^{26}Mg$, $\delta^{18}O$, and $^{87}Sr/^{86}Sr$ values for the Paleozoic dolomites of eastern Canada. Accordingly, they were able to constrain the nature of the dolomitizing fluid and its probable source from mafic and ultra-mafic volcanic rocks.

2.2.3 U-Pb Dating

U-Pb dating method of carbonate minerals is actually applicable to almost the entire geologic time scale, while it was previously somehow restricted to Pleistocene speleothems (e.g. Verheyden et al. 2008). Smith et al. (1991) succeeded U-Pb radiometric age determination of secondary calcite phases in Middle Devonian carbonate rocks and corals (Ontario, USA), paving the way to direct dating of carbonate diagenesis. Advanced technology for the new versions of MC-ICP-MS coupled with laser ablation, and the new thermal ionization mass spectrometers (TIMS) allowed higher precision and adequate measurements even if the U and Pb quantities are minute in the investigated samples. Thus, U-Pb dating has been undertaken successfully on carbonates from a broad range of depositional and diagenetic environments. Rasbury and Cole (2009) presented the state of the art in terms of laboratory techniques and analytical protocols for achieving U-Pb dating on carbonate minerals. There is no doubt that this method has a great potential for dating diagenetic phases and inferring related processes.

Grandia et al. (2000) succeeded in U-Pb and Th–Pb dating of carbonates that are associated with Mesozoic MVT ore deposits. Since, most carbonates are somehow affected by diagenetic alterations, the main difficulty in applying such radiometric isotope dating is in distinguishing the time of formation of the deposit from its diagenetic alteration (Jahn and Cuvellier 1994; Rasbury and Cole 2009). This relies more on the petrographic investigations—and other diagenetic characterization techniques—than on the precision of radiometric dating. Indeed, the U-Pb dating technique abides by the necessary considerations common to most of used radioisotopic systems for dating. These are: (i) daughter isotopes are initially homogeneous; (ii) parent/daughter ratios are well spread; (iii) relevant half-life decay of the parent [with respect to the measured age]; and (iv) prevailing closed system. In addition, some problematic issues have to be taken into consideration when applying U-Pb dating for carbonates (Jahn and Cuvellier 1994):

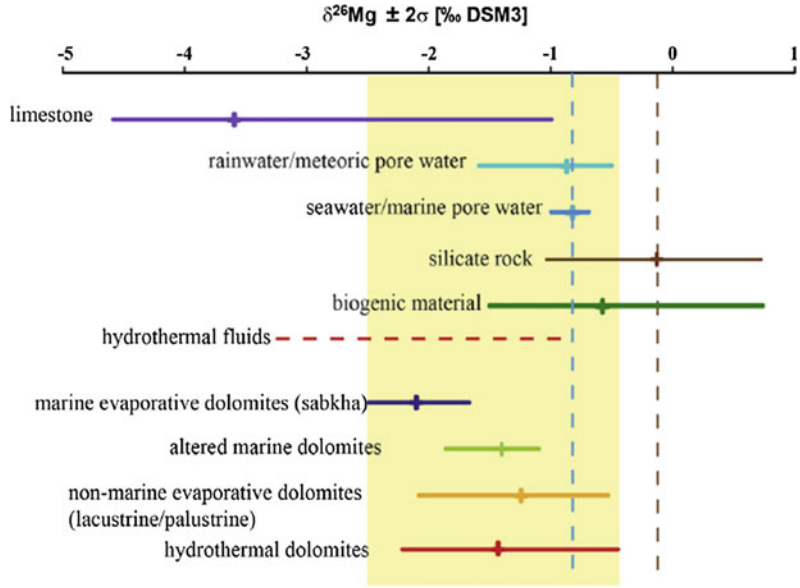

Fig. 2.16 Magnesium isotopic composition ($\delta^{26}Mg$ DSM3) of different Mg sources (e.g. limestones, seawater, rainwater, silicate rocks, plant material), as well as resulting sabkha-, mixing zone and lacustrine dolomites (from Geske et al. 2015)

(i) U-Pb incorporation during carbonate rock deposition/formation; (ii) identification of the U-carriers in the carbonates; (iii) time interval between deposition and diagenesis as mentioned above (e.g. dolomitization); and (iv) diagenesis influence on Pb isotopic homogenization and U-Pb redistribution.

The resulting isochrones represent, for a specific age, the parent-daughter ratio on x-axis while the y-axis shows the ratio of the daughter isotope over the same denominator used for the x-axis (Fig. 2.17).

More recently, Li et al. (2014) undertook U-Pb dating on early calcite cements in Mesozoic ammonites with LA-ICP-MC-MS technique. The analyzed cements resulted in U-Pb ages that are close to 159 Ma (Fig. 2.18a) and 165 Ma (Fig. 2.18b, c), about 10 and 15 Myr younger than the Bajocian and Toarcian strata where the ammonites are found, respectively (the stratigraphic intervals have numerical ages of 168.3–170.3 Ma, and 179–180 Ma; Gradstein et al. 2012). Li et al. (2014) interpreted the measured ages to be the time at which the walls and internal structures of the ammonites as well as the early-diagenetic fringing cements inverted from aragonite to calcite and distributed their uranium content into the fringing cements as they recrystallized during late diagenesis. This study shows the subtlety of this method and the necessity to interpret the produced analytical results with critical reasoning, taking into consideration other independent arguments.

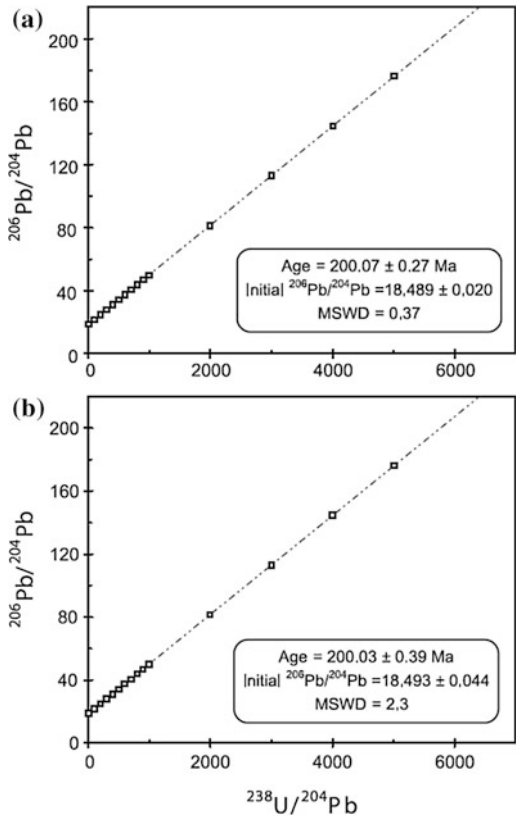

Fig. 2.17 Examples of isochrones evolved to a same age, i.e. 200 Ma from both, homogeneous (**a**) and heterogeneous (**b**) starting conditions. These results show demonstrate that "correct" ages can be obtained even with initial scatter in Pb isotopes (represented here by higher MSWD values; from Rasbury and Cole 2009)

2.2.4 3D Porosity

The flow properties of carbonate rocks are difficult to characterize, and to subsequently predict. Various classifications attempt to associate different types of porosity (partially based on the textures of rocks and their constituents) with measured permeability values (e.g. Lucia 1995; Lønøy 2006). Statistical analyses are usually performed on industrial well cores data-bases of thin section porosity typing with the corresponding flow properties measurements (e.g. MICP, Air-Permeability, Helium-Porosity). These analyses lead to rock-typing throughout the investigated reservoirs, which is a necessary step for reservoir-modelling. Subsequently, reservoirs are subdivided into zones with specific porosity/permeability characteristics (among other properties).

The current applied workflow for classical reservoir rock-typing is about to evolve with the advances in X-ray computed tomography capable of providing high resolution, three-dimensional imaging of the pore networks. Micro-CT approach coupled with 3D-image analyses allow, indeed, the characterization of the pore space in 3D irrespectively of the rock

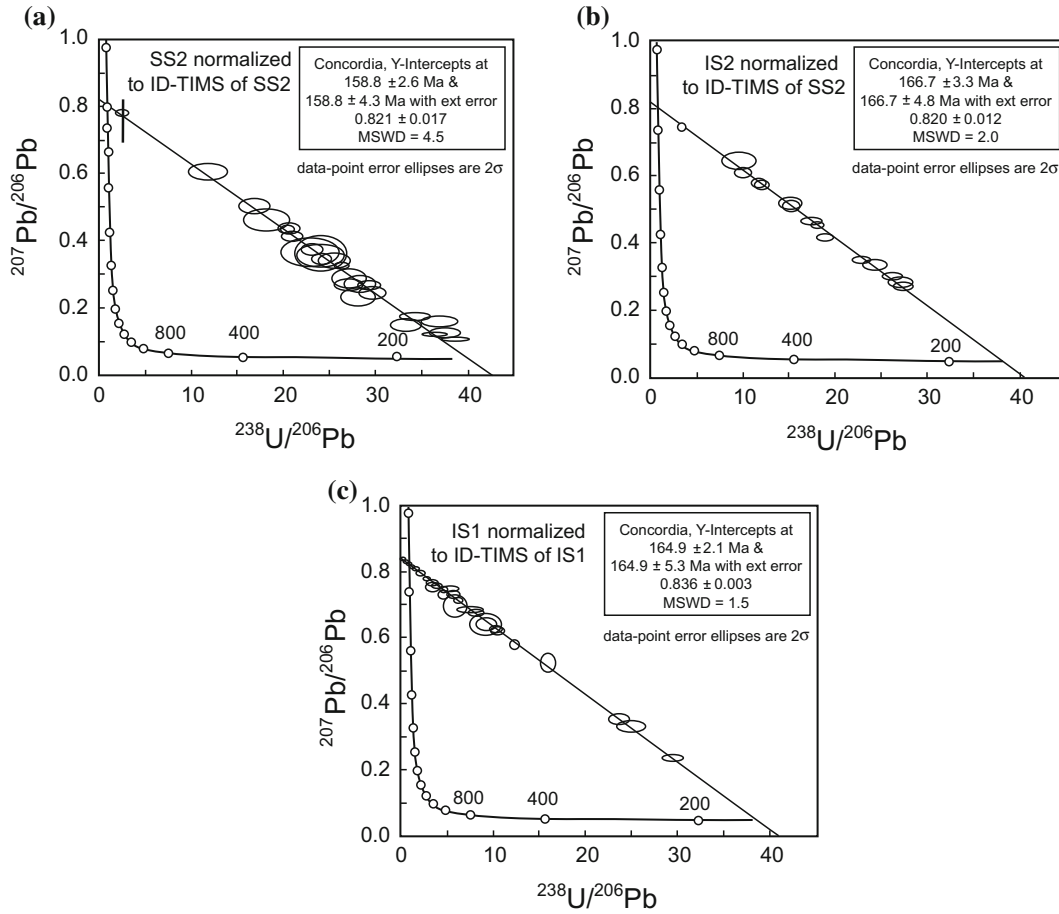

Fig. 2.18 Diagrams of LA–ICP–MC–MS–Pb data that has been normalized to TIMS measurements of early calcite cement in Jurassic ammonites (from Li et al. 2014). See text for details

texture itself. Porosity becomes a 3D network of isolated and/or connected space (Fig. 2.19), through which flow modelling can also be achieved (Talon et al. 2012).

2.2.4.1 Micro-CT Setup and 3D-Image Reconstruction

CT scan is commonly applied on a 23 mm core (plug) sample permitting the optimal selection of a representative miniplug of 5 mm diameter. This miniplug, which is micro-drilled in the core (plug) sample, will be subject to micro-CT scanning. Hence, 3D images could be acquired using a Nanotom high resolution X-ray micro-CT from PHOENIX X-Ray (e.g. De Boever et al. 2012). The sample is fixed on a horizontal rotation axis, placed between the source and the detector. 2D projections are acquired by rotating the sample over 360° at rotation steps of 0.2°. Parameters during acquisition are a tube voltage of 90 kV and a current of 170 µA. The detector consists of a Hamamatsu flat detector (110 mm × 110 mm) made up of a 2304 × 2304 pixels (pxls) grid, with a step of 50 µm. The source-object distance is 11.8 mm and the source-detector distance 200 mm, providing a resolution of 3 µm (pixel size). The presence of very fine pores and pore throats however required an even lower pixel size. To increase the resolution, the detector acquisition

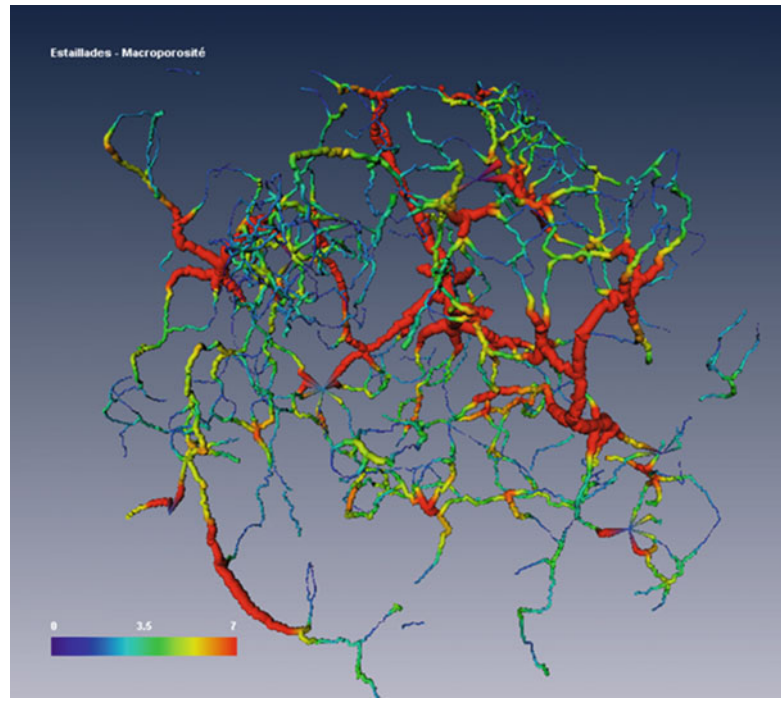

Fig. 2.19 Extracted macro-pore network for the Estaillades carbonate rock standard (France). The scale bar represents the width in microns of the pore space (courtesy of the IFPEN Petrophysics group)

mode is applied. By shifting the detector along the projection plan it creates a virtual detector of 2304 × 4608 pxls, allowing a larger field of view. Then the source-object distance is adjusted to 6.2 mm to double the magnification ratio. With this set up the resulting resolution is 1.5 µm. In counterpart, the acquired data size and the acquisition time double. Further improved conditions may lead to higher resolutions, in the order of 0.5 µm—this certainly necessitates longer acquisition time.

Each acquisition (with a 1.5 µm resolution) generates 1800 TIFF projections that are used for the numerical reconstruction of volumetric data. The maximum volume that can be reconstructed and stored at full resolution is 1000 × 1000 × 1000 pixels. The reconstruction (PHOENIX algorithm) uses a cone beam Feldkamp algorithm. The beam hardening effect is corrected by using a metal Cu-filter (0.1 mm) and by applying a mathematical correction during the reconstruction process.

2.2.4.2 Building an Equivalent Pore Network from the Actual Pore Space

The workflow for the image treatment and analysis of the reconstructed 3D-volumes consists of (1) visualizing, isolating (segmentation) and quantifying the resolved pore space and different mineral phases, (2) the reconstruction of an equivalent pore network and description of its parameters, and (3) the reconstruction of ancient pore networks.

The volume is visualized and analysed using the Avizo software package (version 6.2, VSG, France). In order to reduce noise, increase image contrast and facilitate thresholding, the image histograms are stretched and the images are filtered if appropriate (noise reduction, application of brightness/contrast filter). This results in an improved separation of the grey level peaks in the image histograms (Fig. 2.20). Segmentation of the grey level image to accurately separate each grey class one by one includes a

thresholding step, followed by filtering operations (removal of islands) and morphological operations (smoothing, shrinking and growing). More details can be found in Youssef et al. (2008). This creates a binary 3D image of each phase or grey class and allows calculating the volumetric percentages of the sample constituents. The quality of the image segmentation can be evaluated by comparing the calculated volumetric percentages with results of laboratory measurements on the 23 mm plug.

Porosity is compared to He-porosity measurements. Quantitative XRD results are used to calibrate the volumetric percentages for the different mineral constituents. The result of image segmentation is a 3D labelled binary image that allows visualizing the spatial distribution of each sample constituent. The pore space is typically composed of several, independent clusters. To further proceed, the pore space should include at least one, important percolating cluster to acquire representative results during transport property simulations.

Once a binary 3D image of the resolved pore space is captured, an equivalent network of pore bodies and pore throats can be built, which can be used in network models for the calculation of petrophysical properties. The procedure consists in three principal steps: skeleton extraction, pore space partitioning and parameter extraction (Fig. 2.21).

The skeleton extraction step uses the Distance Ordered Homotopic Thinning algorithm implemented in Avizo. The algorithm computes the shortest distance of each point of the foreground (void space) to the background (solid phase). The resulting distance map is then used to guide the thinning algorithm, resulting in a thin, centralized skeleton that preserves the topography of the original pore space. By means of the distance map, each voxel of the skeleton is marked with the minimum distance to the boundary of the void space. The skeleton of the pore space is then partitioned into groups of lines belonging to the same pores and separated by throat points that correspond to the restrictions between pores. Subsequently, the different pores are geometrically separated and labelled by adding the binary image of the pore space to the labelled line set image using a voxel growth constrained algorithm. The process of pore network reconstruction allows defining several statistical parameters of the equivalent pore network, e.g. the pore size distribution, based on the pore radii and the coordination number of each pore (Youssef et al. 2008).

In addition, the ancient pore networks (shape, dimension, and inter-connectivity) could be reconstructed from 3D micro-CT images. Their transport properties may then be simulated (e.g. Talon et al. 2012). The procedure consists of an additional segmentation and pore network building step analogues to the procedure outlined above. The segmentation step involves a double thresholding operation. The present pore space is

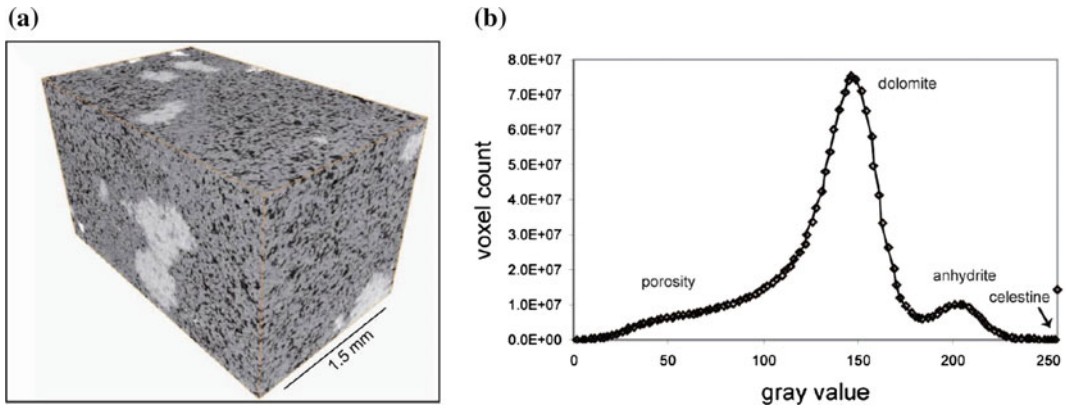

Fig. 2.20 **a** 3D grey scale view of micro-CT scan (2000 × 1000 × 1000 pxls) of a typical Jurassic Arab C dolostone (Middle East). **b** Grey level histogram (De Boever et al. 2012)

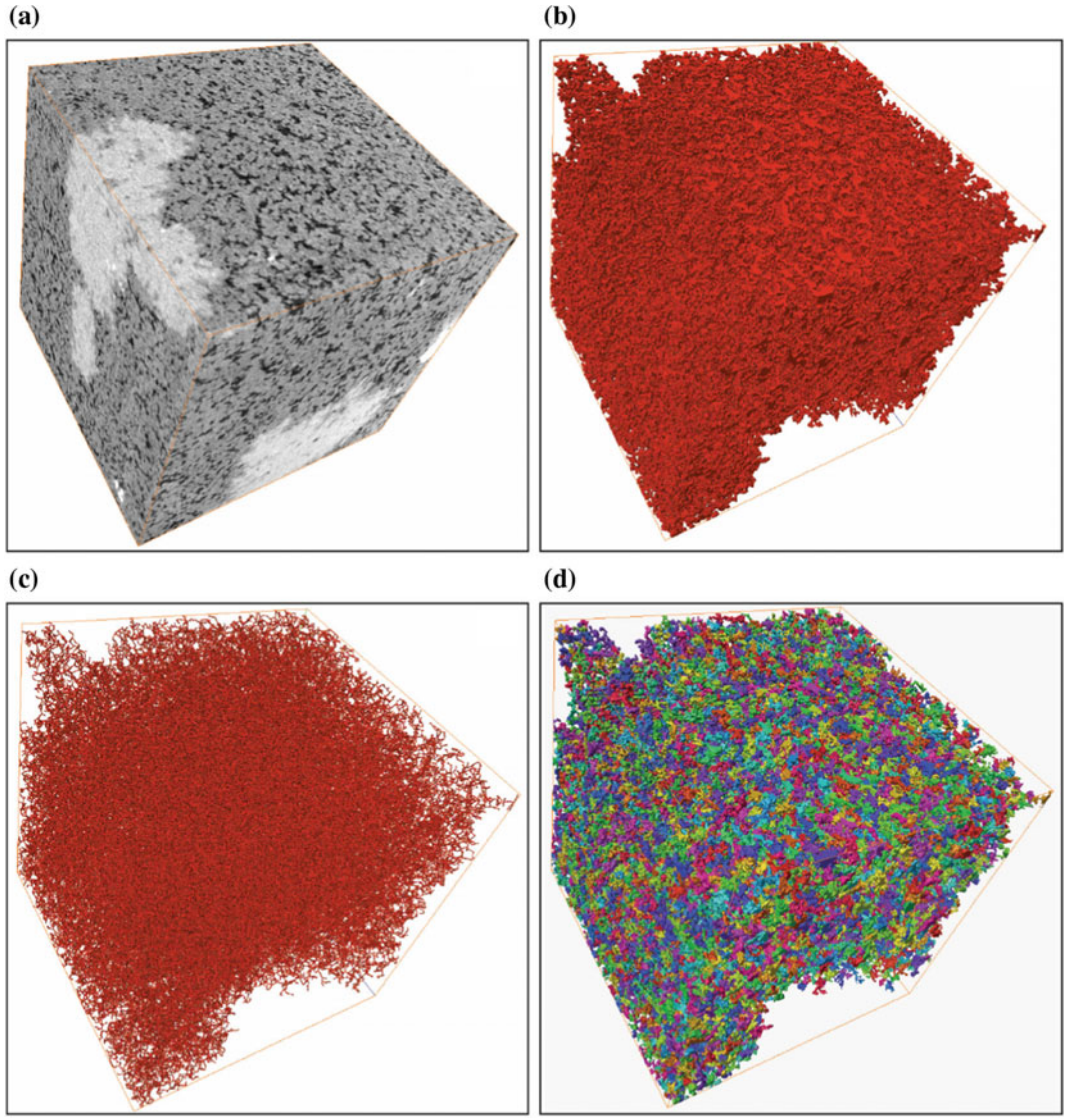

Fig. 2.21 Equivalent network building of the actual pore structure of a typical Jurassic Arab C dolostone (Middle East): **a** 3D grey scale view of micro-CT scan (1000 × 1000 × 1000 pxls); **b** Segmented image with porosity in *red*, following the binarisation step; **c** 3D skeleton representation as *lines* in the *centre* of pores, preserving the original pore topography; **d** partitioned pore space of the entire volume

isolated and merged with the segmented volume of a second mineral phase. This approach has been applied on the typical (Jurassic) Arab C dolostones, whose intercrystalline porosity is plugged by anhydrite. The pore space before anhydrite precipitation (see Figs. 2.20 and 2.21), was accordingly reconstructed (for more details see De Boever et al. 2012).

2.2.4.3 Numerical Simulation of Mercury Intrusion and Permeability

Following pore space partitioning, a connection matrix is built that is used to simulate mercury intrusion and calculate the permeability. A full drainage curve is obtained through a step by step invasion of an entire pore volume that is

accessible via its throat radius for a fixed capillary pressure (Pc). The procedure is explained in detail by Youssef et al. (2007). Comparison of simulation results with lab permeability and Purcell mercury porosimetry measurements are used to validate the quality of the reconstructed pore network and pore partitioning (Fig. 2.22).

2.3 Discussion

Diagenetic processes can be unveiled through the detailed description of the related diagenetic phases. For example, petrographic examination of dolomite crystals together with geochemical and fluid inclusions analyses lead to suggest specific processes for their formation (i.e. conceptual models of dolomitization). In addition, dolomite studies have benefitted from exceptionally well exposed outcrops, where the geometry of the dolomitized geo-bodies could be apprehended (e.g. Shah et al. 2012; Dewit 2012). At Ranero (northern Spain), we have achieved relatively detailed mapping of such dolomite geo-bodies through analysis of aerial photographs and field observations (cf. Fig. 2.1). Still, petrography takes the largest share when conducting a typical study on diagenesis. Description and classification schemes of diagenetic phases (cements, replacive minerals, porosity) remain basically the outcome of classical petrographic examinations whether with conventional, cathodoluminescence and/or scanning electron microscopic techniques.

A series of geochemical, mineralogical and fluid inclusion analyses are also carried out systematically within the framework of common diagenesis studies on carbonate rocks. Major and trace element compositions are frequently measured through geochemical analysis or electron microprobes. A variety of laboratory workflows (adapted to specific instruments: AAS, AES, LA-ICP-MS) are available, but I have chosen to highlight the 'sequential extraction' procedure that concerns samples containing both calcite and dolomite phases, in order to measure separately the major and trace elements of each phase (Nader 2003). Stable oxygen and carbon isotopic analyses are very common nowadays and they are carried out at specialized laboratories. Here, the 'special double collection' procedure that is applied on calcitized dolomites is presented (Nader et al. 2008). Though more expensive, strontium isotope analyses are also routinely carried out at specialized research centres, and the results of which illustrate most of the published work on diagenesis. XRD analysis is an old technique, yet today it benefits from Rietveld modelling, and results in a better assessment of the stoichiometry of dolomite crystals and quantified mineral volumes (further discussed in Chap. 3). New experimental protocols,

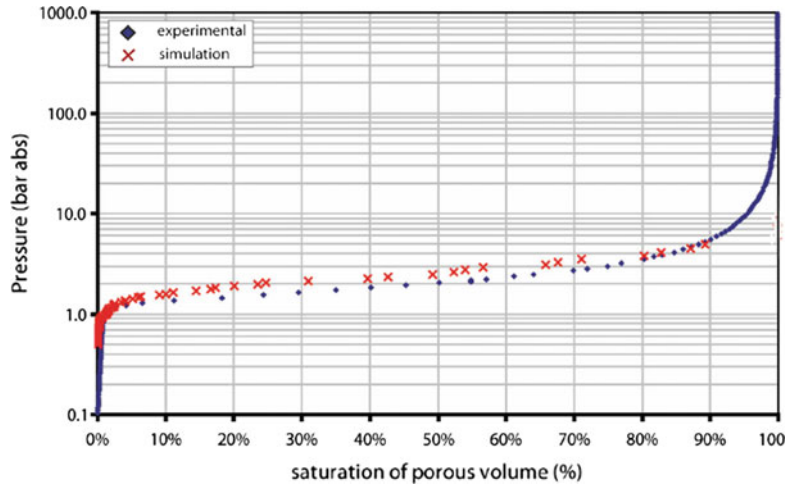

Fig. 2.22 Simulated and measured mercury injection capillary pressure curve of the actual pore structure of a typical Jurassic Arab C dolostone (Middle East)

developed at IFPEN are decribed in this chapter; they basically couple XRD and Rietveld refinement for studying dolomites. Microthermometry and crush-leach analyses involving fluid inclusions trapped in diagenetic minerals are also more or less frequently undertaken (especially the former method involving heating cooling stages mounted on microscopes). All of these techniques result in further characterizing the diagenetic phases and related diagenetic fluids, and the physico-chemical conditions prevailing at the time of their formation.

The optimal approach consists of integrating many—if not all—of these techniques. For example, oxygen isotopic ratios corresponding to specific cements are dependent on the original fluids from which they have precipitated and the prevailing temperatures. Combined with the measured liquid-vapour homogenization temperatures of relevant fluid inclusions trapped in these cements, the temperature at the time of precipitation can be constrained and therefore the original fluid oxygen isotopic ratio known (Friedman and O'Neil 1977; Land 1983; Fontana et al. 2010). Numerous papers illustrate well this approach (e.g. Nader et al. 2004, 2007, 2008; Fontana et al. 2014; among other published contributions). Besides, constraining the conditions of precipitation/formation of the diagenetic phases and their timing (for example with Sr isotopic ratios), together with petrographic examination lead to shaping up the paragenesis (check Fig. 2.11) and confirming the proposed conceptual model (Fig. 2.12). Ultimately, we are able to superpose the proposed sequence of diagenetic phases onto the burial curve (Fig. 2.23; Peyravi et al. 2014).

While recognizing that the field of 'diagenesis characterization' with its commonly used techniques is quite mature, some advancement and future perspectives appear to be very attractive. Measurements of 'Clumped' oxygen isotopes are becoming available for calcite and dolomite minerals (Dennis et al. 2011). This approach overcomes the dependence of classical oxygen isotopic ratios on both original fluids and temperatures (two variables, discussed above), providing estimations of the crystallization temperatures based on the 'clumped' isotope standardized paleo-thermometry (check Figs. 2.13 and 2.14). Another interesting analytical technique involves magnesium isotopic analyses. Here, the source of Mg (major rock-forming element in terms of abundance) could be theoretically traced (Fig. 2.16). Today, this method is applied together with classical oxygen and strontium isotopic analyses and is proving to be of interest for constraining dolomitization processes (e.g. Lavoie et al. 2011). Better analytical precision with new techniques (LA-ICP-MC-MS and TIMS) has provided successful applications of U-Pb dating on early and late diagenetic cements (Fig. 2.18). This is a powerful tool that will certainly become very attractive and will help in placing the various dated diagenetic phases on the burial curve (such as the one shown on Fig. 2.23). Through this approach, and together with other diagenetic information (deduced from stable and radiogenic isotopic and fluid inclusion analyses), the burial model can even be further calibrated (Mangenot et al. in press).

Characterizing diagenetic phases, and especially pore space, has been mostly achieved on 2D thin sections, leading in most of the cases to erroneous shapes and imprecise volumes. A significant future development involves the possibility to image—and characterize—the pore space in the three-dimensions by means of X-ray computed tomography (see further in Claes 2015). I have presented this method and related workflows based on the work of De Boever et al. (2012) on typical carbonate reservoir rocks. The details of CT and micro-CT approaches coupled with 3D-image analyses are tackled through describing the utilised setup, image reconstruction and segmentation, as well as building equivalent pore space networks (Fig. 2.21). This method overlaps with those discussed in the following chapter on 'quantitative diagenesis'. Qualitative characterization of pore space segmentation and inter-connectivity could still be done on micro-CT images. The more quantitative applications are discussed in Chap. 3.

CT and micro-CT techniques are very promising and will be further developed in the

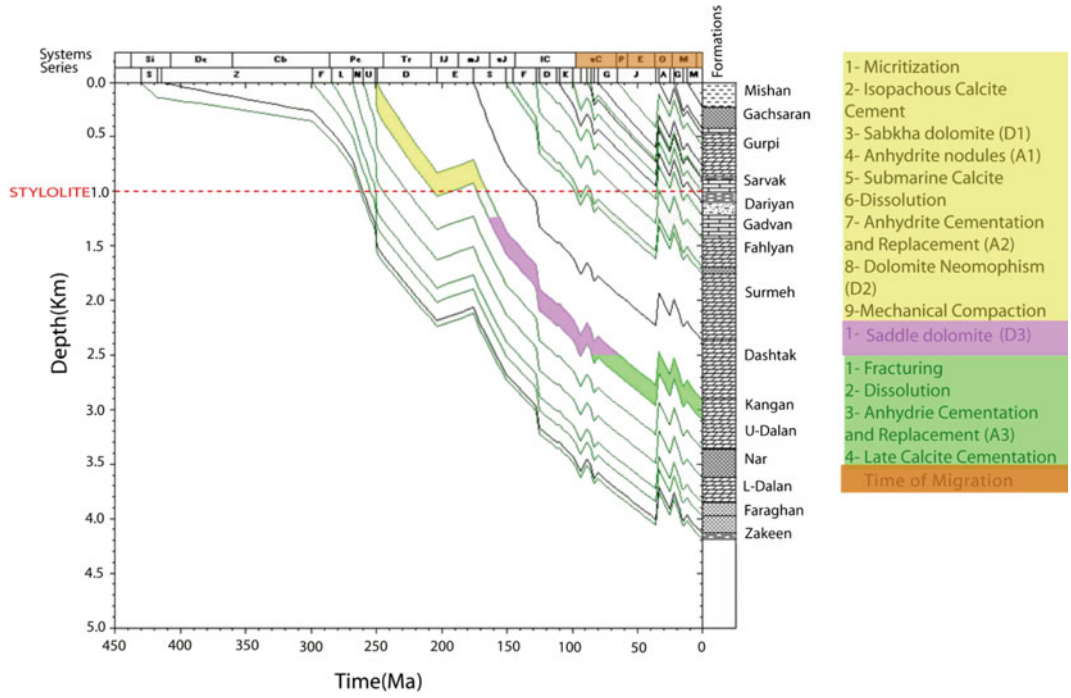

Fig. 2.23 Burial model for a well intercepting Khuff equivalent reservoirs (Kangan Formation) in the Salman field, offshore Iran. A simplified form of presenting the various diagenetic phases superposed on the burial model is also illustrated (for more details refer to Peyravi et al. 2014)

near future for capturing the pore space in 3D (applied for instance through EOR research projects). Scanning resolution needs to be enhanced to capture micro-porosity within grains. In addition, improved intensity separation is needed to be able to better distinguish diagenetic phases. We have also argued the importance of integrating such approach with SEM, microprobe and XRD techniques (De Boever et al. 2012). The eventual perspective of 3D pore space characterization is to come up with new porosity classification schemes taking into account the real dimensions and connectivity of pores.

The new generation of porosity assessment methods (and possible diagenetic minerals volumetric determination) is believed to be associated to the micro-CT technique coupled with computer-based image analysis. Still, an important challenge is associated to defining the representative elementary volume, which has been introduced in Chap. 1 and will be further discussed in the following chapter dedicated to methods of quantitative diagenesis. How to characterize vuggy porosity, if the vugs are larger than the sample under investigation? And what methods to follow to make sure that the analysed sample can represent the reservoir rock? Besides, thin sections and sample-plugs do not take into account fracture porosity, which is known to have crucial impact on carbonate reservoirs. This is commonly addressed, while constructing reservoir models, by making use of oil/gas fields production tests and geophysical-based extrapolations, failing to capture the finer-scale of lithofacies and diagenesis distributions. Alternatively, 'upscaling' in reservoir modelling remains very challenging. In many cases, it reverts to simplified average values representing mixed lithofacies of contrasting reservoir properties. REVS and 'upscaling' are two research subjects form important scientific challenges for achieving multi-scale numerical models of diagenesis.

2.4 Advancement in Characterization of Diagenesis

Several approaches and methods are becoming very attractive for improving our capability of characterizing carbonate reservoir rocks at various scales. Diagenetic processes with their impacts on rock properties need to be further understood. The diagenetic phases (outcome of diagenetic processes) can be precisely described by means of a variety of methods. The most commonly used methods combine petrographic, geochemical and fluid inclusion analyses. They result in characterizing the diagenetic phases and the prevailing physico-chemical conditions at the time of their formation. Thus, available analytical methods—and enhanced techniques—not only lead to better diagenesis characterization but they also unravel the mechanisms of related processes, and eventually their impacts on reservoir properties.

Field observations (and/or well cores investigations) are the starting point of any diagenesis research project. Therefore, improved field (well cores) data-collection, whereby considerable investigation/observation is made at outcrop (and/or on well cores) should be achieved. Based on my experience, there should be a trend towards decreasing the number of samples (and materiel), while increasing their representative significance. In addition, defining the Representative Elementary Volumes (REVs) needs to be attempted for each study.

One of the future developments that will also improve the efficiency and precision of diagenesis characterization is related to computer-assisted petrographic analyses (on conventional microscopic techniques as well as SEM-EDS, EMPA) and image analyses. The key targets will be to undertake faster, and more systematic characterization (of sedimentological and diagenetic features—including porosity).

New analytical techniques for geochemical and mineralogical assessment of the host rocks as well as diagenetic phases are still needed. EMPA is a powerful tool to characterize the distribution of mineralogical variability in carbonate rocks. Mg- and clumped-oxygen isotopic analyses start to be applied to constrain the nature of diagenetic fluids and temperatures of precipitation of diagenetic phases, respectively. U-Pb method has proved to be suitable for dating diagenetic phases. Clumped-oxygen isotope analyses coupled with U-Pb dating provide not only more precised characterization of diagenetic phases, but also suitable proxies for burial history calibration. This will be very much needed for adequately overlaying the diagenetic stages on burial models and for adjusting associated numerical simulations.

Three-dimensional scanning of cores and samples (via computed tomography) is certainly expected to achieve better performance and higher resolutions (e.g. capturing cement phases). Porosity description and classification has always been associated to the host rock textures. Today's technology allows the characterization of the pore space directly, and in 3D (e.g. micro-CT). This will lead inevitably to a new, innovative approach to describing and classifying the pore space in reservoir rocks. The new classification scheme should have a better connection with related permeability.

Quantifying Diagenesis

3

Classical diagenesis characterization methods and conceptual models are qualitative and do not yield quantitative data to be directly used by reservoir engineers for rock-typing and geological modelling. The three-steps workflow (Characterization-Quantification-Simulation), which is illustrated in Fig. 1 (page x), aims at predicting the impact of the relevant diagenetic processes on reservoir properties. The practical purpose of such approach is to improve rock-typing and carbonate reservoir modelling. Based on well-defined diagenetic processes, several approaches could be followed for the quantitative assessment of their impacts on reservoir rocks (e.g. Jones and Xiao 2005; Youssef et al. 2007; Algive et al. 2009; Consonni et al. 2010; Lapponi et al. 2011; Barbier et al. 2012; De Boever et al. 2012).

'Quantitative diagenesis' may be regarded as a field of studies aiming at providing numerical values to the results (impacts) of diagenetic processes on pre-existing carbonate sediments/rocks. While 'Characterization' concerns with describing and classifying diagenetic processes (Chap. 2), here we focus on various techniques adapted to produce quantitative and/or semi-quantitative data. Such information is substantial not only for constructing meaningful numerical models, but also for being able to validate the resulting simulations. They also provide a more subtle link with reservoir engineering and petrophysics.

3.1 State of the Art (Quantitative Diagenesis)

3.1.1 Petrography—Plug/Sample Scale

The classical description of diagenetic phases and porosity—especially by means of petrographic analyses—has to be achieved with a quantitative approach rather than qualitatively. First hand quantitative estimations of rock matrix, allochems/grains and porosity can be done by visual estimations and comparison with %-distribution charts. Image analysis can also help, as it provides a rapid proportional estimation of such rock constituents. It is now common to use software packages such as "JMicroVision", a freeware designed to describe, measure, quantify and classify components of all kinds of images allowing to analyse high definition images of rock thin-sections (http://www.jmicrovision.com). Matlab™ can also be used for undertaking quantitative measurements on photomicrographs or scans of thin sections. Calcite, dolomite and anhydrite, as well as quartz, feldspars and clay may be quantified accordingly. Petrographers go even further as they routinely apply the same methods to quantify the types of allochems or grains (crinoids, algae, forams, gastropods, etc.), cements, and replacive mineralogical phases. Usually, some of

F.H. Nader, *Multi-scale Quantitative Diagenesis and Impacts on Heterogeneity of Carbonate Reservoir Rocks*, Advances in Oil and Gas Exploration & Production, DOI 10.1007/978-3-319-46445-9_3

these phases are estimated semi-quantitatively by using abundance classes (e.g. rare, common, abundant).

Porosity types also may be quantified following the same methods (visual estimations, image analyses). Practically, a first run estimates the overall porosity in a sample (thin section). Then the various types of porosity (e.g. primary, secondary, and sub-types discussed above) are estimated. Their total sum should be made equal to the overall porosity per cent value of the investigated sample. SEM is very useful here to assess, even if qualitatively, the connectivity of the porosity types including micro-porosity (found usually in grains). Besides, SEM images of thin-sections can be acquired with very high resolution.

The SEM images of carbonate rock textures have been used to produce quantitative assessment of specific types of pore space (e.g. inter-granular macro-porosity, intra-granular micro-porosity) as well as cements types (e.g. rim cement around grains, equant cement filling dissolved grains) (Fig. 3.1). Recently, such approach has been coupled with petrophysical analyses (e.g. MICP, NMR; Fleury et al. 2007), and micro-focus Computer Tomography scanning (micro-CT) (e.g. Youssef et al. 2008). Van der Land et al. (2013) employs the SEM 2D images on thin-sections to build pore-network models capable of simulating permeability evolution in carbonate rocks. In terms of quantitative diagenesis, these approaches provide robust links between 2D investigation and bulk rock petrophysical analyses (e.g. MICP) as well as 3D models.

The ending products of quantitative description of thin sections are usually tables featuring all per-cent values and abundance classes of the various investigated elements (Tables 3.1, 3.2 and 3.3). This has been done since decades by petrographers at oil companies, resulting in huge wealth of data. For example, a typical oil or gas field in the Middle-East will have tens of cored and logged wells (up to a few hundreds). Well cores are nowadays CT-scanned (and some are even scanned with micro-CT). Then, the well cores are sampled every foot providing plug-samples for non-destructive petrophysical measurements (Fluid Porosity, Helium Permeability). Thin sections are prepared from these plugs and analysed by means of classical petrography. Destructive petrophysical analyses (e.g. MICP) are later on applied on remaining sample material. The results of quantitative and qualitative microfacies descriptions together with corresponding petrophysical data (Tables 3.1, 3.2 and 3.3) are organized in Microsoft Excel files, presented on log spread-sheets, and used for statistical analyses. They are, moreover, used together with the associated well-log suites to identify distinct electrofacies and rock-types.

3.1.2 Petrography—Reservoir Scale

The quantitative/qualitative description of microfacies (e.g. lithology, texture, cement, porosity) may result in about 80 parameters (e.g. dolomite%, dolomite size, anhydrite cement%, vugs porosity) for each thin section. Typical well cores from the Arab C and Arab D reservoirs (Jurassic, Middle East) with total thicknesses in the order of 100 ft (~30.5 m) and 500 ft (~152.4 m) respectively, may represent 100–500 sample plugs and thin sections (from one well). The resulted description tables include, respectively, 8000 and 40,000 values for the depth-organized thin sections and descriptive parameters (Tables 3.1, 3.2 and 3.3). Subsequently, huge data-bases are expected for oil/gas fields including a great deal of information.

Statistical analysis software packages (e.g. EasyTrace™, IFP Energies nouvelles) are used routinely to analyse such huge databases together with available well logs, and to suggest relationships. Wells are defined and their core data (and logs) are discretized and organized, enabling appropriate correlation across the investigated oil/gas field. For instance, key wells representing distinct depositional environments across the Arab D Member in an oilfield show the vertical and lateral quantitative (%) distribution of lithologies (i.e. calcite, dolomite, anhydrite) (Fig. 3.2). Moreover, the relationships of

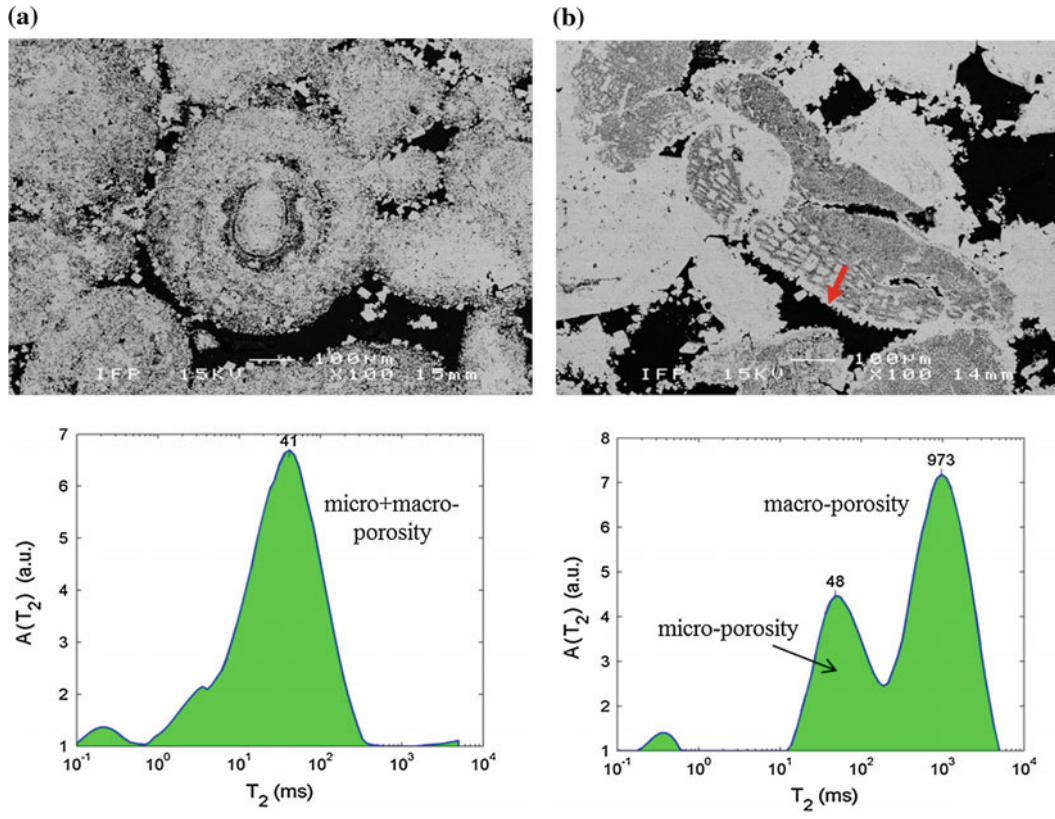

Fig. 3.1 Scanning electron microscope (SEM) photomicrographs coupled with nuclear magnetic resonance (NMR) T_2 distribution graphs of two typical carbonate rocks with bimodal pore size distribution (micro/macro-porosity). **a** Lavoux limestone (grainstone) has a somehow connected micro- and macro-porosity, resulting in one peak on the T_2 distribution diagram (Por. = 28.7 %; Perm. = 90 md). **b** Estaillade limestone (grainstone) shows calcite cement rim around the grains (*arrow*), disconnecting intragranular micro-pores from intergranular macro-pores – illustrated with two peaks on the T_2 distribution diagram (Por. = 24.7 %; Perm. = 273 md) (courtesy of IFPEN Petrophysics group; from Fleury et al. 2007; Youssef et al. 2008)

the prevailing rock texture, lithologhy, and porosity (among other parameters) can be directly assessed through the observation of such well logs. Figure 3.2 represents data from at least 1500 thin sections (with about 7500 values for 5 parameters).

Statistical analysis software packages are also used in order to better classify rock types (and electrofacies). Histograms and charts are plotted accordingly to demonstrate the impacts of certain sedimentologic and diagentic phases on porosity and permeability (Fig. 3.3). Correlation of the data-sets across several wells in a field can also be done. By correlating the data corresponding to certain parameters, trends can be defined. The huge, wide-spread distribution of data (values) can be then sub-grouped into classes with a set of logical relationships. For example, by analysing a data-set representing some 10,000 thin sections from a dozen of wells in one oilfield, all within the Arab D reservoirs (Jurassic, Middle East), one can readily notice that common to abundant syntaxial cement are associated with grain-supported rock textures, limestone lithology with relatively high porosity and permeability values (Fig. 3.3).

Maps of proportional distributions provide an approach to display the quantitative/qualitative data. The estimated data, which are well constrained by depth (and stratigraphic position), are

Table 3.1 Various lithological and textural categories for describing carbonate microfacies (thin sections)

Study/Date Well # Sample # Depth (ft/m) TVD (ft/m) Reservoir Unit	Lithology (%)	Rock Texture (Digital Code)		Grains (Digital Code)	
				Skeletal	Non-Skeletal
	Limestone	Grainstone		Forams	Peloids
	Dolomite	Packstone		Algae	ooids
	Anhydrite	Wackestone	Grain Size	Sponges	Intraclasts
	Silica	Mudstone	Sorting	Echinoids	Extraclasts
	Clay	–		Ostracods	Opaque
				–	quartz
					Clay
	Sedimentary Structures (Digital Code)				
	Stromatolites	Fenestrae	Bioturbation	Dessication	Stylolites

Lithologies (e.g. limestone, dolomite) are often presented in % format; while the abundance of other categories (e.g. grainstone, sorting, sponges, ooids) are described qualitatively with digital codes. Digital codes are selected to represent the most representative value (1 = Mudstone; 2 = Wackestone; 3 = Packstone; 4 = Grainstone), or to represent abundance (0 = absent; 1 = rare; 2 = common; 3 = abundant)

Table 3.2 Categories for describing cement in microfacies (thin sections)

Study/Date Well # Sample # Depth (ft/m) TVD (ft/m) Reservoir Unit	Calcite Cement (%/DC)	Dolomite and Anhydrite Cement (%/DC)			Other Cement/Fill
	Total (%)	Total Dolomite Cement (%)			
	Acicular/Fibrous (DC) Dog-Tooth/Bladed (DC) Blocky-Equant/Drusy (DC) Syntaxial Overgrowth (DC)	Dolomite Replacement		Dolomite Cement	Bitumen (%) Siderite (%)
		Shape	Size		
			Crypto (<16 μm)		
			Micro (16–64 μm)		
		Anhedral (DC)	Fine (64–250 μm)	Primary Porosity Fill (%)	
		Sunhedral (DC)	Medium (250–500 μm)	Secondary Porosity Fill (%)	
		Euhedral (DC)	Coarse (>500 μm)		
			Packing		
		Total Anhydrite Cement (%)			
		Anhydrite replacement		Anhydrite Cement	
		Shape	Size		
		Blocky	Fine (64–250 μm)	Primary Porosity Fill (%)	
		Felted	Medium (250–500 μm)	Secondary Porosity Fill (%)	
		Lath	Coarse (>500 μm)		

Total amounts of cements (calcite, dolomite, anhydrite, …) are usually presented in %; while the abundance of other categories (e.g. cement type, shape, size, …) are described qualitatively with digital codes. Digital codes are selected to represent the most representative value (1 = Anhedral; 2 = Subhedral; 3 = Euhedral), or to represent abundance (0 = absent; 1 = rare; 2 = common; 3 = abundant)

Table 3.3 Categories for describing reservoir properties in microfacies (thin sections)

Study/Date Well # Sample # Depth (ft/m) TVD (ft/m) Reservoir Unit	Primary Porosity		Secondary Porosity		
	Total (%)		Total (%)		
	Intergranular (DC) Skeletal (DC) Non-Skeletal (DC)	Cemented (DC) Cement Nature (C*)	**Dolomite**		**Cracks**
			Intercrystalline	Cemented (DC)	Cemented (DC)
			Vugs	Cement Nature (C*)	Cement Nature (C*)
			Calcite		**Fractures**
			Intraganular	Cemented (DC)	Cemented (DC)
			Matrix (Pinpoint)	Cement Nature (C*)	Cement Nature (C*)
			Molds		
			Vugs		
	Associated Bulk Porosity and Permeability				
	Total (%)	Connected (DC)	Isolated (DC)	Fluid porosity (%)	Helium Permeability (mD)

Total amounts of porosity (primary, secondary, bulk) are usually presented in %; while the abundance of other categories (e.g. porosity type, cemented/filled, connected, …) are described qualitatively with digital codes (DC; 0 = absent; 1 = rare; 2 = common; 3 = abundant). Cement Nature (C*; within primary/secondary porosity) may be represented with letter-codes (e.g. calcite, C; dolomite, D; anhydrite, A). The corresponding Fluid Porosity (%) and Helium Permeability (mD), undertaken on the plug-sample by means of petrophysical analyses, are also added to the description lists

used to draw such proportional maps by means of ArcView GIS, GOCAD, or any other similar software (Liberati 2010; Nader et al. 2013). The position of the well represents the exact (estimated) value, while the area between wells will be given relative values based on proportional methods. These maps can be also upgraded using geostatistical numerical methods (discussed below, Chap. 4).

Using the same data-set (illustrated in Fig. 3.3) for the Arab D reservoirs, maps of proportional distributions for dolomite% have been constructed for a specific stratigraphic sequence and according to the prevailing rock textures (Fig. 3.4). The Arab D reservoirs are known to include very low amounts of dolomites and consist predominantly of limestones (Morad et al. 2012). Considerable distributions of dolomites (>20 %) are only observed on the northern (upper) part of the map for mud-supported textures (Fig. 3.4c), whereas, no important dolomite % are found in grainy textures (Fig. 3.4a, b).

Maps can also be constructed for relative abundance of certain diagenetic phases. The syntaxial overgrowth cement, which has been demonstrated statistically to relate to higher porosity and permeability in the Arab D limestones (see Fig. 3.3), has interesting relative abundance distribution across the study area (Fig. 3.4). Since it is found mainly in grainy rock textures, the map corresponding to its proportional abundance in mud-supported rock textures (where dolomite is also found; Fig. 3.4c) is of no value (Fig. 3.4f). The highest relative abundance of this cement is in the northwestern (upper left) part of the study area for packstone-grainstone and northern/central for the wacke-packstone. Interestingly, These mapped zones overlap with interpreted original lagoon and shoal depositional environments (see index map—Fig. 3.2a; Morad et al. 2012).

The above maps show the proportional distribution of dolomites in mud-supported rock textures and the relative abundance of syntaxial calcite cement in mostly grain-supported (limestone) rock textures. If dolomitization is demonstrated to enhance of the reservoir properties of the Arab D member, similar

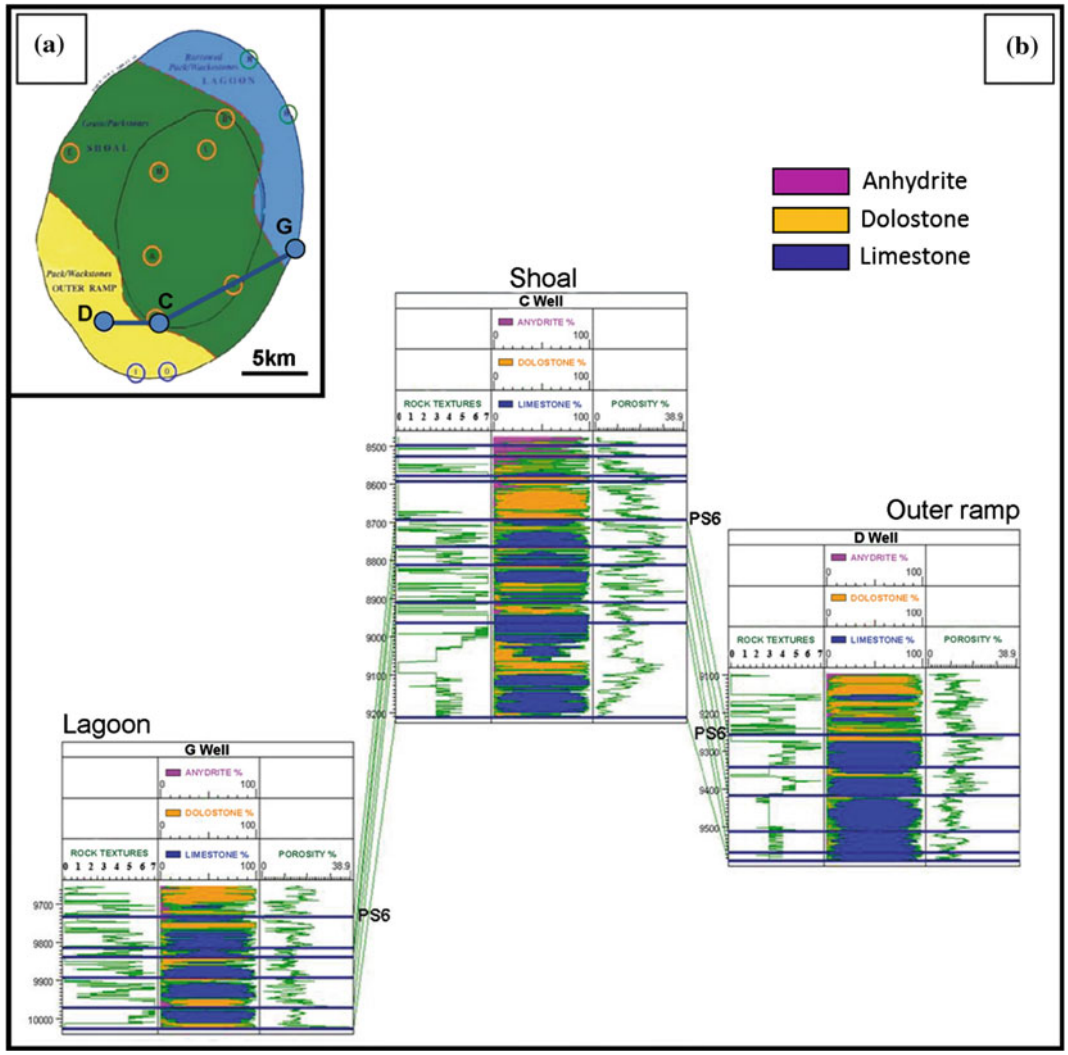

Fig. 3.2 Correlation cross-section (constructed by Easy-Trace™ software based on petrographic analyses of thin sections) showing the distribution of main rock textures (DC = 0 to 7; see Legend in Fig. 3.3), lithologies (%) and porosity (%) across the depositional environments. The location of the wells across the oilfield is indicated in inset map (A)

quantitative/qualitative maps allow to show the areas where enhanced reservoir properties might be found. Similarly for the grain-supported (limestone) facies (which pre-dominate the Arab D member), assuming that the abundance of syntaxial calcite cement can be taken as proxy for more permeable reservoir rocks. This is an example of the quantitative (or semi-quantitative) assessment microfacies data at the field-scale. No predictive approach for reservoir properties is proposed here, rather a static interpolation is invoked to present geo-localized data and deduce reservoir- and diagenetic-trends.

3.1.3 Mineralogical Analyses (X-Ray Diffraction)

The X-ray Diffractometry technique coupled with cell and Rietveld refinements enables

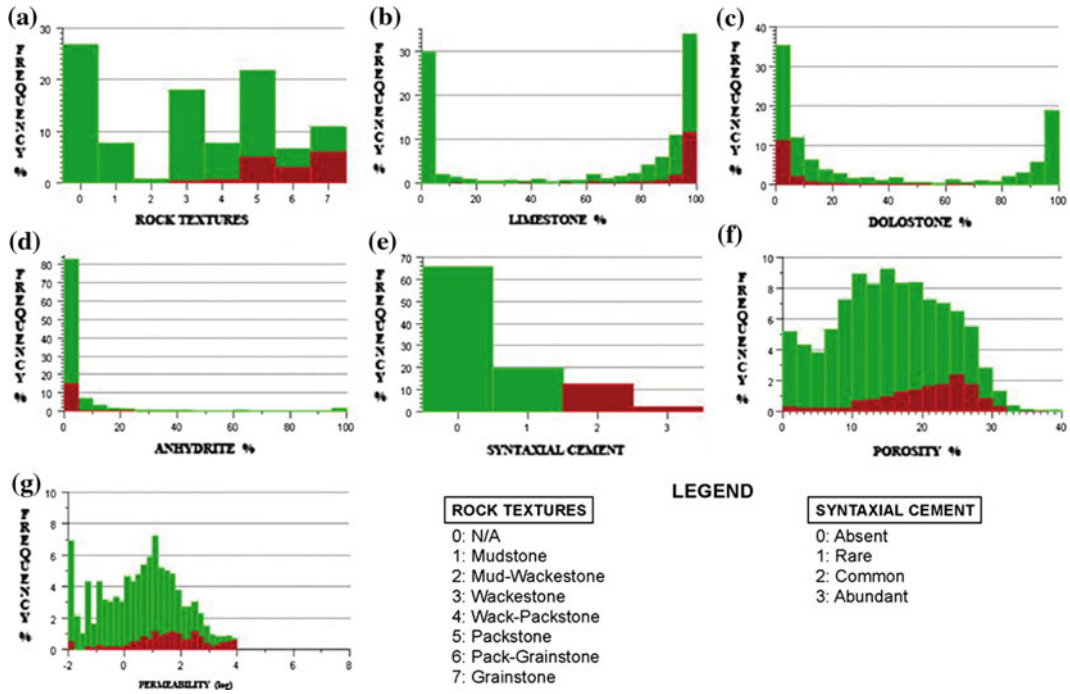

Fig. 3.3 Statistical analyses of well data based on 10,000 thin sections (and samples) from 13 wells (Arab D, Middle East). Resulting histograms represent **a** rock textures, **b** limestone %, **c** dolostone %, **d** anhydrite %, **e** syntaxial calcite overgrowth cement [SCO], **f** fluid porosity, and **g** permeability. Note that the populations of data corresponding to [common] and [abundant] SCO are selected (coloured in *red*)

mineralogical quantification, crystallographic investigation, and assessment of dolomite stoichiometry (e.g. Turpin et al. 2012). Basically, this technique is used for qualitative assessment of the mineralogical phases in a sample (Chap. 2). With proper calibration, the observed peaks on an X-ray diffractogram may be used to quantify the amount of mineral species with respect to the original powdered sample (Fig. 3.5). This is achieved by mixing the powdered sample with a known quantity of an internal pure mineral standard (e.g. Alumina NIST), and by running the analysis on the whole weighted sample.

The sample's representative thin section is first investigated with SEM-EDS techniques and/or EMPA in order to assess its mineralogical composition. It is possible to characterize the mineralogical stoichiometric (or structural) variability through these methods. Subsequently, coupled XRD-Rietveld approach allows precise, quantitative mineralogical determination (Turpin et al. 2012).

Cation substitutions in dolomite crystals, in particular Ca and Mg, which commonly occur during diagenetic processes, modify the mineral stoichiometry. This can be assessed by measuring the cell parameters (a = b and c in Å) of the dolomite crystals and by applying the 'Lumsden (1979) equation' (presented in Chap. 2, p. 23). Turpin et al. (2012) proposed a procedure based on a comprehensive literature review, which compiles the crystallographic data concerning the cell parameters related to the lattice Ca percentage of various dolomites. Then, using the dolomite cell parameters determined by cell refinement, dolomite stoichiometry can be calculated (Fig. 3.6).

Turpin et al. (2012) further investigated the stoichiometry and cell parameters of the Triassic Upper Muschelkalk and Lettenkohle dolomites

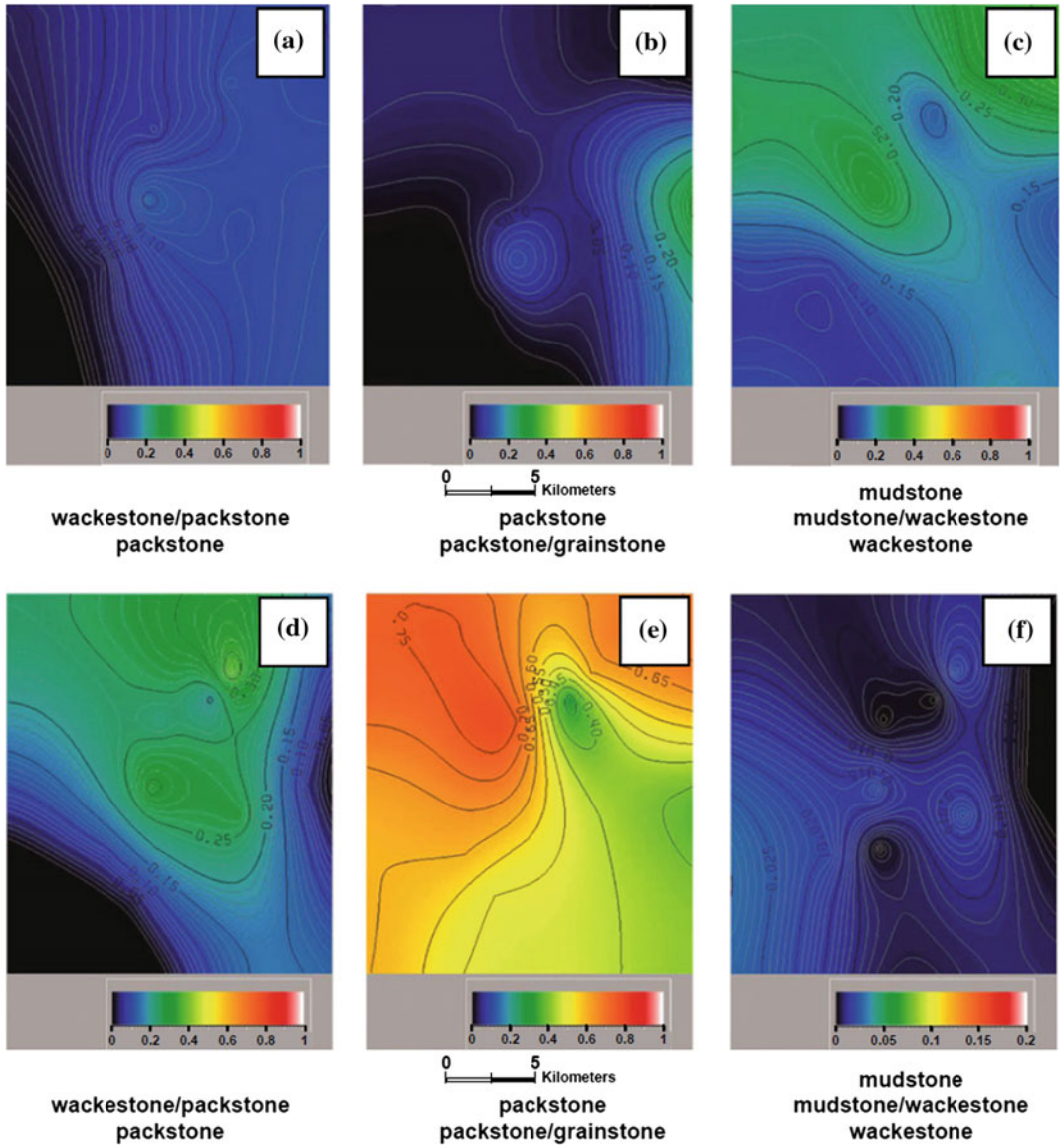

Fig. 3.4 Diagenetic maps showing: (i) the dolomite proportional distribution (**a** Wackestone-Packstone; **b** Packstone-Grainstone; **c** Mudstone-Wackestone); and (ii) the relative abundance of the syntaxial calcite overgrowth cement; **d** wackestone-Packstone; **e** Packstone-Grainstone; **f** Mudstone-Wackestone) in the Arab D member of an investigated oilfield offshore Abu Dhabi (UAE). Average depth of the maps ranges between 3000 and 4000 m (Nader et al. 2013)

in the French Jura (Fig. 3.7). The latter dolomites, associated to anhydrite in sediments, are related to smaller and less variable lattice parameters (calculated by Rietveld refinements). The deficiency of larger Ca ions in the unit cell of Lettenhkohle dolomites compared to Upper Muschelkalk dolomites is potentially a cause for the contraction in the "a" parameter (see Rosen et al. 1988). The expansion of the "c" parameter has been previously related to cation disordering (Reeder and Wenk 1983) or other lattice defects (Miser et al. 1987). This is an explanation for the "c" variability of Upper Muschelkalk dolomites and could be caused by a faster crystallisation

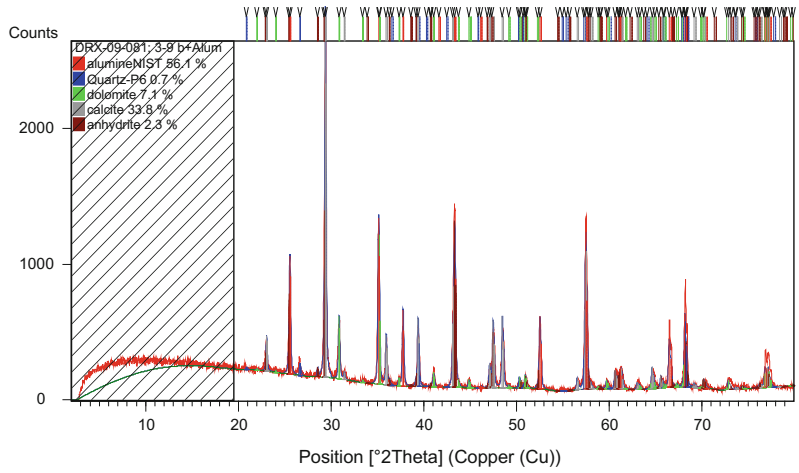

Fig. 3.5 XRD and Rietveld diagram showing the quantitative assessments of calcite, dolomite and anhydrite in a Triassic carbonate rock from the French Jura (Turpin et al. 2012)

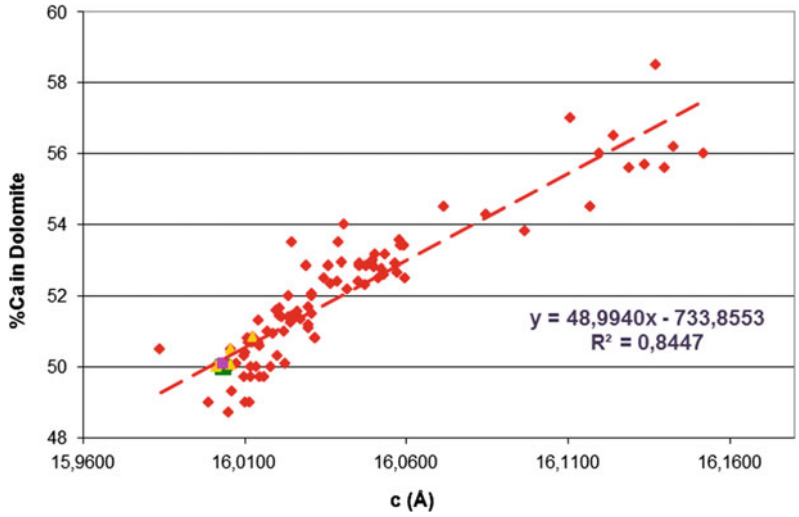

Fig. 3.6 Cross-plot diagram of dolomite stoichiometry (%Ca in dolomite) versus dolomite cell parameter (c in Å) featuring data from various sources (*yellow triangles* represent investigated dolomites, *purple square* is Eugui dolomite standard, and *red lozenges* are published data). The best fit line can be used in order to determine the dolomite stoichiometry (Turpin 2009)

(Rosen et al. 1988) compared to Lettenkohle dolomites. The near-ideal stoichiometry and the small variability of the "c" parameter in Lettenkohle dolomites is in agreement with Warren (2000) proposing that dolomites formed early, in evaporitic settings—and then underwent burial—tend toward ideal stoichiometry and to a generally better ordered crystal lattice. The faster precipitation (calcite-replacement) of the Muschelkalk dolomites is here attributed to a later diagenetic process.

Eugui reference dolomite sample contains Fe and Mn, similar to Lettenkohle and Upper Muschelkalk dolomites. The %Ca calculated on Eugui, Upper Muschelkalk and Lettenkohle dolomites by this new approach are consistent

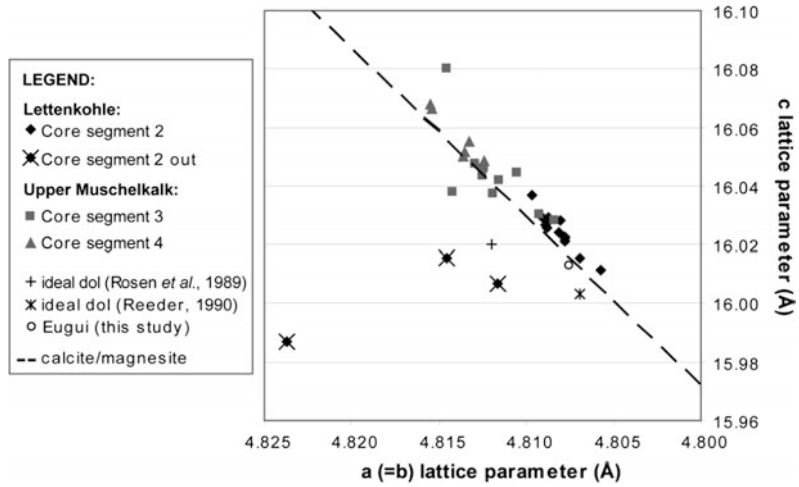

Fig. 3.7 Unit cell dimensions of Upper Muschelkalk and Lettenkohle dolomites. The *dark dashed line* connects the unit cell values of calcite to magnesite. Ideal dolomites (from Rosen et al. 1989; Reeder 1990) are situated below this line due to the unit cell contraction when dolomite is well ordered. Eugui dolomite standard is also indicated (Turpin 2009)

with EMP and AAS analyses and results from previous studies on Eugui dolomites (Turpin et al. 2012). Therefore, it is here proposed that this method can be equally applied to dolomites showing low Fe% and Mn% in their lattice. Care must be taken, however, when dolomites display higher Fe and Mn contents and tend toward the ankerite pole (see also Fig. 2.9).

3.1.4 Geochemical Analyses—Thin Section Scale

By definition, typical geochemical analyses produce quantitative data (e.g. wt% of Ca, Mg, Fe, Mn) representing the chemical traits of the investigated rocks. The difficult step would be in transforming the resulted chemical data into useful information about the original fluids. This is mainly due to the fact that the prevailing physico-chemical conditions at the time of mineral precipitation are unknown. Still, independent arguments can be employed to suggest such conditions. Here, the major and trace element analyses, isotopic measurements and fluid inclusions may provide considerable quantitative data-sets. Quantitative approaches may be used to map geochemical traits at the microscopic scale (Fig. 3.8) and at the scale of an outcrop (Fig. 3.10).

SEM-based punctual chemical analysis method, similar to micro-probes (see Chap. 2), can be used in order to achieve mineral mapping at the micro-scale (Fig. 3.8). The first step is to undertake EDS analyses featuring the major elements composition of the sample. Then, the corresponding mineral assemblages are mapped. Backward reconstructions of dissolution and cementation phases from such 2D mineral maps help in quantifying diagenetic evolution through time (Deschamps et al. 2012).

3.1.5 Geochemical Analyses—Reservoir Scale

Detailed geological (diagenetic) mapping of dolomite fronts (as presented in Chap. 2), can yield invaluable quantitative data. Figure 3.9 shows a detailed geological map of a typical high temperature dolomite front below an erosional unconformity horizons (Nader et al. 2007). The petrographic and geochemical investigations of these dolomites led to the proposal of a

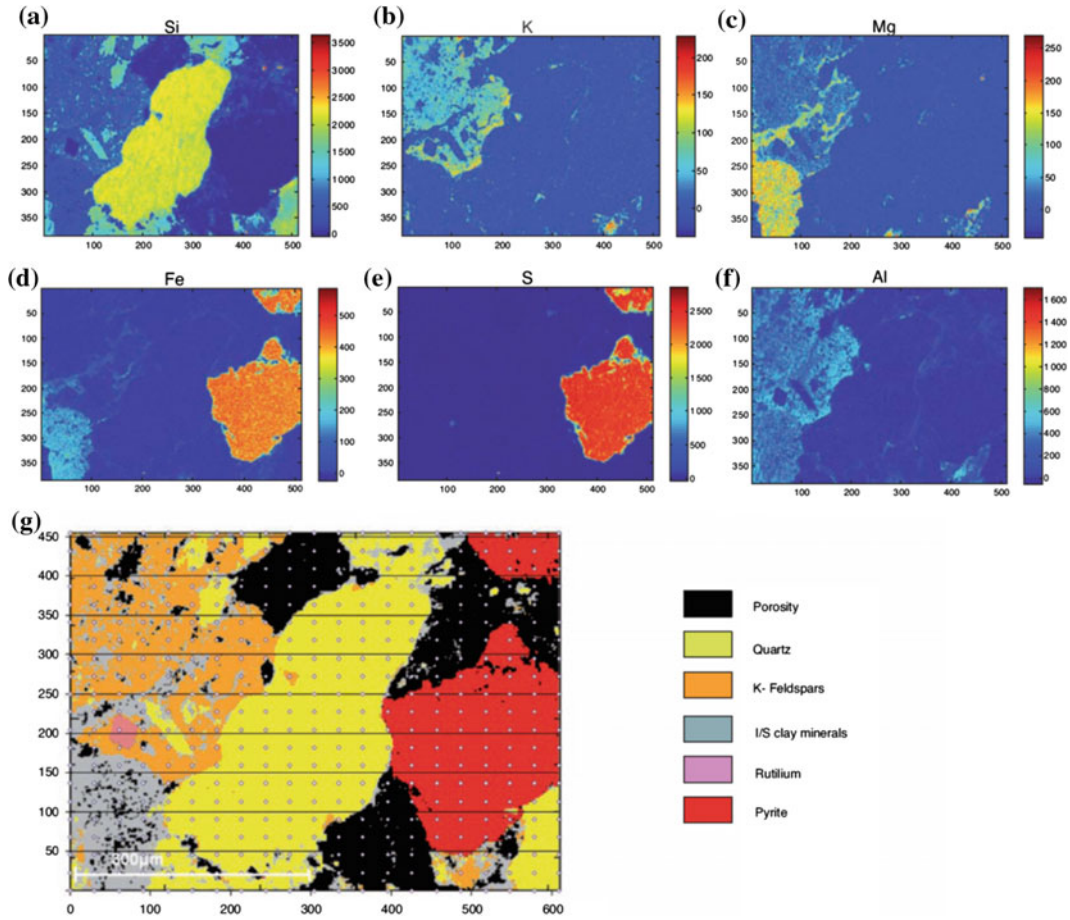

Fig. 3.8 Spectral analysis and resulting mineralogical mapping of a sandstone sample from the Lower Cretaceous Upper Mannville Formation (Alberta, Canada): **a** silica, **b** potassium, **c** magnesium, **d** iron, **e** sulfur, and **f** aluminium spectral analyses; and **g** the minerals distribution map obtained by a statistical cluster analysis (from Deschamps et al. 2012)

conceptual model of dolomitization and a paragenetic sequence, as well as the characterization of the dolomitizing fluids (cf. Fig. 2.11; Chap. 2). Further sampling across the dolomite object allowed us to map its geochemical characteristics and to deduce significant diagenetic trends.

The Fe and Mn concentrations (in ppm) of the samples across the dolostone front were used to draw contour maps for both elements (Fig. 3.10 a). These contour maps show that most of the highest Fe and Mn values plot on the southeastern portion of the dolomite object. This coincides with the interface of the dolostone body with the overlying Upper Jurassic oolitic limestone of the Salima Formation, and the sandstone of the Lower Cretaceous Chouf Formation along an erosive surface (Fig. 3.9).

The Fe versus Mn crossplot for the major components of the dolostone front exhibits a linear covariation (Fig. 3.10b). The Bikfaya Formation limestones (Jurassic host rock) show the lowest Fe and Mn contents (generally up to 1000 and 100 ppm, respectively). The overlying Salima Formation dolostones (intraclasts) have Fe concentrations in the order of 28,000 ppm and Mn concentrations of ca. 1300 ppm. The dolomitized burrows have Fe and Mn concentrations that plot within the field of Fe–Mn values for the beige dolostones, which range from 5000 to 30,000 ppm for Fe and from 100 to 1600 ppm

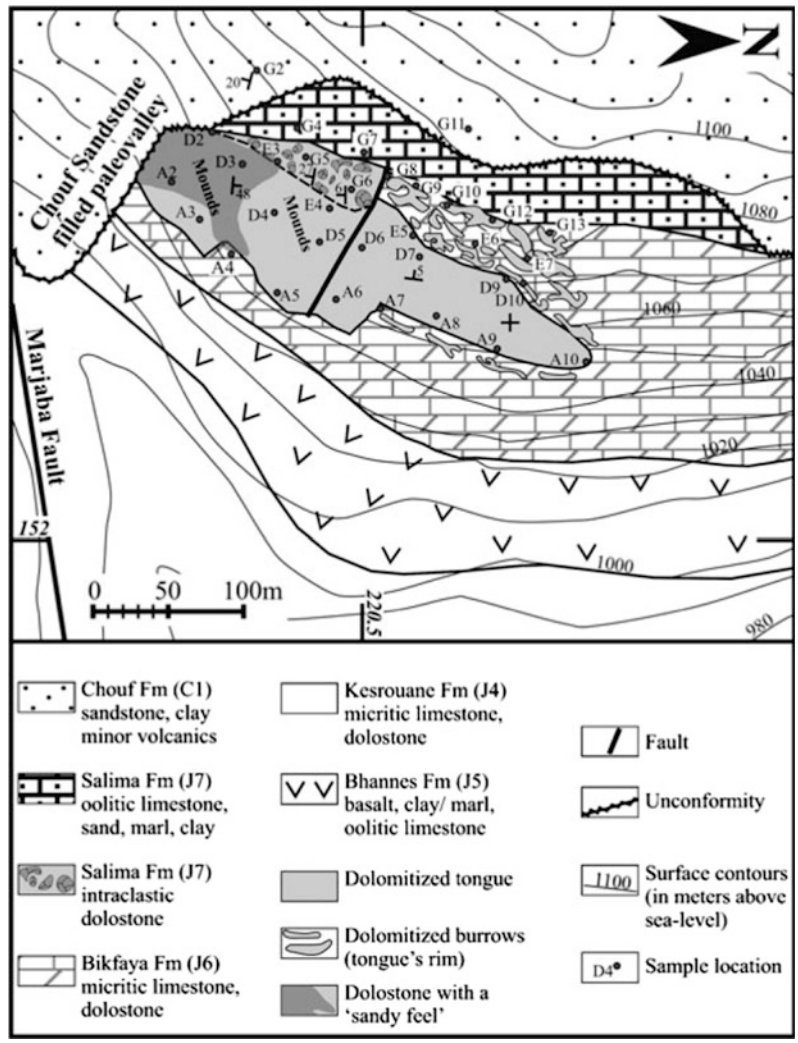

Fig. 3.9 Detailed geological map of the Marjaba dolostone front and its surrounding limestone host-rock (from Nader et al. 2007). The various dolostone facies and their distribution are also presented

for Mn. The highest Fe–Mn concentrations (40,000 and 1800 ppm, respectively) are associated with the 'zoned' dolomites, whose values partly overlap with the Salima intraclasts, the beige dolomite and the dolomitized burrows.

These high concentrations are interpreted to reflect the presence of late diagenetic Fe–Mn-oxi/hydroxides, as observed in the thin sections and SEM analyses (Nader et al. 2007). In fact, selective intracrystalline dissolution of growth zones in the pre-existing front dolomites occurred and was followed by a phase of Fe–Mn oxi/hydroxide precipitation. The Fe and Mn are believed to originate from the oxic, soil-related near surface fluids—explaining their highest concentrations near the interface with the erosional surface (Fig. 3.10a). With subsequent deposition of overlying units and deeper burial, the fluids became reducing and the iron resulted in the precipitation of the ferroan dolomite phase. Consequently, mapping the Fe/Mn concentration values across the dolomite front led to better understanding the diagenetic evolution of the dolomite front. In particular, it helped in constraining the timing of the formation of the dolomite front (or 'beige dolostone'; check also Nader et al. 2004) and the prevailing conditions during subsequent diagenetic alterations.

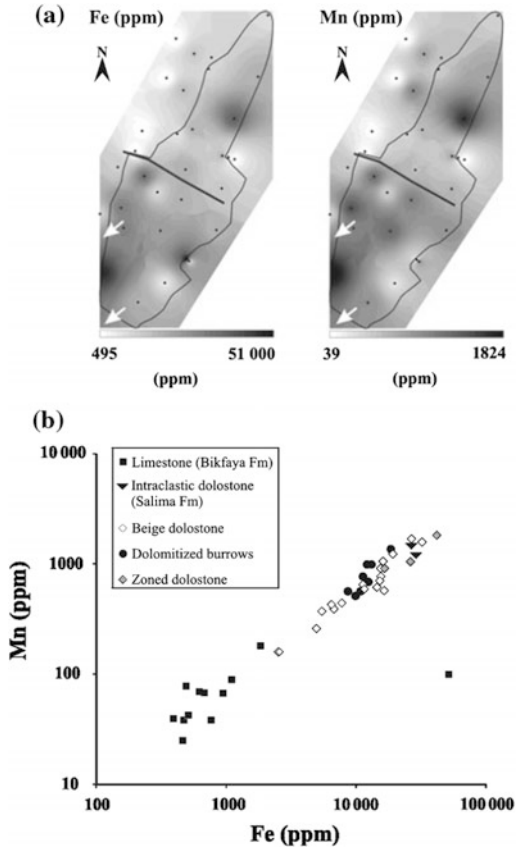

Fig. 3.10 Fe and Mn concentration contour maps (**a**) and cross-plot (**b**) for the Marjaba HDT front (central Lebanon; concentrations in ppm). *Arrows* point towards the interface with the overlying sandstone rock unit, interpreted to be responsible for chemical weathering of the dolomites and enrichment in Fe and clays (Nader et al. 2007). For scale in (**a**) refer to Fig. 3.9

Accordingly, Nader et al. (2007) suggest that near-surface, oxic and soil-related water percolated through the beige dolostones close to the erosional surface before the deposition of the Early Cretaceous Chouf sandstones, resulting initially in dolomite dissolution, then in the precipitation of Fe–Mn-oxi/hydroxides within the dissolved space. Thus, the beige dolomitization pre-dates the Lower Cretaceous Chouf Formation (ca. pre-Valanginian). This invokes that enhanced reservoir properties associated with dolomitization were achieved before further burial during later Cretaceous times. Still, the geochemical mapping at the reservoir-scale of the dolomite front may better explain the internal heterogeneities of this geobody. Zoned dolomites along the erosional surface have been clearly filled by Fe–Mn oxi/hydroxide phases and clays and would make baffle zones within the dolomite reservoir unit—similar to the initial anhydrite precipitates commonly associated with reflux dolomitization.

3.1.6 Geochemical Analyses—Basin Scale

Fontana et al. (2014) documented the fluid flow history and diagenetic evolution of Permo-Triassic carbonate rocks in the northern United Arab Emirates (UAE). These rocks may be considered as analogues of the gas-bearing reservoirs of the Khuff Formation in the subsurface Arabian Plate. Large scale carbonate platform depositional facies appear to have been over-printed by diagenesis. Add to that, the effects of structural evolution and associated fluid-rock interactions, the reservoir properties of the Khuff Formation are very difficult to comprehend and predict (e.g. Videtich 1994; Ehrenberg 2006; Ehrenberg et al. 2007; Rahimpour-Bonab 2007; Moradpour et al. 2008; Esrafili-Dizaji and Rahimpour-Bonab 2010; Koehrer et al. 2010; Rahimpour-Bonab et al. 2010; Koehrer et al. 2011).

Basin-wide early diagenetic processes, such as aragonite dissolution and host-rock dolomitization, are known to increase the porosity and permeability of Khuff carbonates. Conversely, chemical compaction and associated cementation commonly occluded porosity to varying degrees during the burial history (e.g. Breesch et al. 2009, 2011; Callot et al. 2010). Fontana et al. (2014) provided detailed information concerning the associated diagenetic fluid systems at the basin-scale by integrating fracturing analyses,

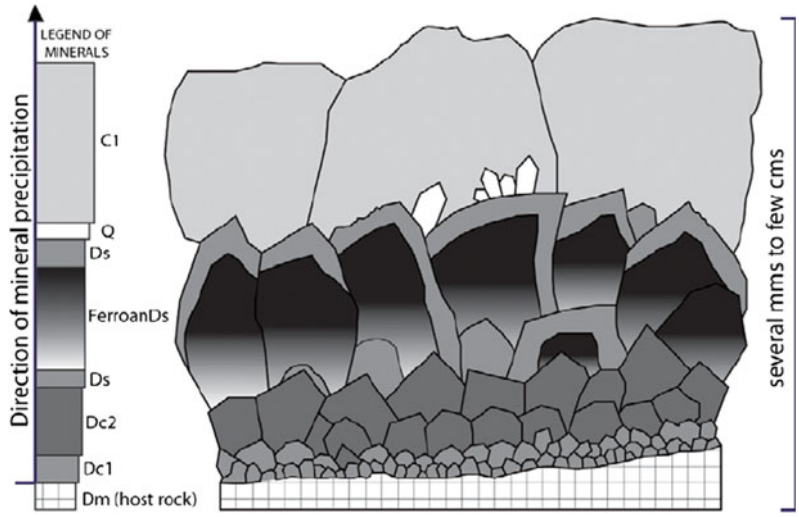

Fig. 3.11 Schematic illustration representing the typical fracture-filling cement stratigraphy (Fontana et al. 2014). The host rock fractures that are filled by several types of dolomite cements (Dc1, Dc2, Ds, Ferroan Ds), quartz (Q) and calcite (C1). Figure 2.3 (Chap. 2) includes photographs of stained slabs featuring this cement stratigraphy

fracture-fill cement stratigraphy, and fluid-inclusion microthermometry as well as basin modelling.

The diagenetic cement phases (dolomite, quartz, calcite) have been investigated with the classical petrographic and geochemical techniques (cf. Chap. 2). Figure 3.11 shows the observed fracture-fill cement stratigraphy. The main cement phases were sampled for stable oxygen and carbon isotopic analyses. Fluid inclusions found in the same phases were also analysed (Fontana et al. 2010).

Using the fractionation equations of calcite and dolomite, the homogenization temperatures of fluid inclusions, and the oxygen stable isotopes of the main carbonate diagenetic phases (Fontana et al. 2010), it is possible to constrain the evolution of the $\delta^{18}O$ (relative to SMOW) composition of the prevailing, original diagenetic fluids. Furthermore, by constraining the relative-timing of the precipitation of each cement phase, the evolution of the diagenetic fluids may be deduced. For the Khuff reservoirs, salinity of the basinal fluids increased with increasing temperature through time as the fluids evolved from a marine signature (about 0 ‰ SMOW) to further $\delta^{18}O$-enriched compositions following the order of cement precipitation (illustrated in Fig. 3.11). Throughout the consecutive precipitation of the early dolomite cements (Dc1, Dc2, Ds), $\delta^{18}O$ VSMOW values of dolomitizing fluids remained between +4 and +8 ‰, while the prevailing temperature increased from 110 to 180 °C. Subsequently, the calcite cement (C1) formed from a fluid with higher salinity (average 21.3 NaCl% equivalent; n = 64) and $\delta^{18}O$ values during progressive increase in temperature (150–200 °C; Fig. 3.12).

The relatively high $\delta^{18}O$ VSMOW values of the fluids considered responsible for the precipitation of the dolomite and calcite cements are in good agreement with the high salinities measured in the fluid inclusions. They retrace a general progressive increase in fluid salinity since their deposition in marine environment (up to 6 × sweater salinity) and associated temperatures (up to 200 °C). The Khuff reservoirs across the Arabian/Persian Gulf appear to have been affected—to a certain extent—by a similar burial/diagenetic evolution with increasingly saline and hot fluids (e.g. Peyravi et al. 2014). An abrupt increase in formation temperatures has been

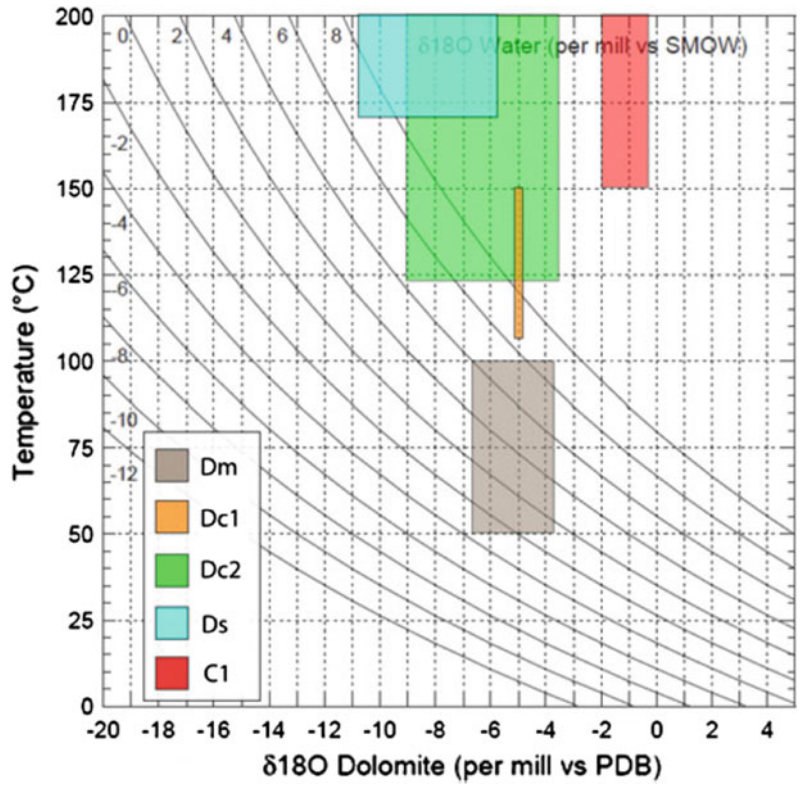

Fig. 3.12 Calculated oxygen stable isotopic composition ranges of the 'parent' diagenetic fluids (expressed in $\delta^{18}O$ VSMOW) for dolomite and calcite cement phases (Legend in Fig. 3.11). Temperatures of precipitation are constrained by microthermometry analysis of fluid inclusions, while oxygen isotopic values of the same cement are reported in $\delta^{18}O$ VPDB values). Fractionation equation used for calcite is from Friedman and O'Neil (1977) and for dolomite from Land 1983)

linked to the major regional thrusting and rapid overburden in the latest Cretaceous (Hawasina tectonic nappe; Fontana et al. 2014). Such quantitative information will help in constraining basin (numerical) models and allows a better understanding of the related diagenetic processes affecting the Khuff reservoirs. The constructed diagenetic evolution is, indeed, adequately constrained by the basin-scale settings. Here, diagenesis is demonstrated to be primarily controlled by the interplay of the burial thermal evolution of the basin and the regional tectonic history.

Finally, it is worth recalling here, that the 'clumped' oxygen isotopic technique (described in Chap. 2, pp. 27–29) helps tremendously constraining the temperature of precipitation for the investigated diagenetic phases (some of which unsuitable for fluid inclusion analysis). This technique (as well as U-Pb dating) would have certainly added value to the above presented study, particularly in constraining the constructed basin models and related thermal simulations.

3.1.7 Fluid Inclusion Analyses—Petroleum Systems

Trapped fluids within crystals may well be petroleum. Petroleum fluid inclusions constitute excellent evidence associated to the oil/gas charge of reservoirs. Today, microthermometry, confocal laser scanning microscopy and Raman microspectroscopy are frequently used to investigate both aqueous/brine and petroleum inclusions and to associate them to diagenetic phases and petroleum systems. Combined to 1D burial modelling, timing of trapping such inclusions can also be defined.

In some mineral phases (e.g. fracture-filling cement), inclusions may contain liquid water plus vapour and liquid petroleum plus vapour, or even the three together. These fluid inclusions are highly valuable, as they may allow the estimation of trapping temperatures and pressures from homogenization temperatures by using the crossed isochores method (e.g. Emery and Robinson

1993). Assumption of PVT properties of the petroleum inclusions has to be done, usually on the basis that they correspond to the petroleum found (and produced) in the field. The liquid water nature might be also estimated by microthermometry. Besides, both liquid petroleum and liquid water in a single inclusion are supposed to have been trapped together (i.e. at the same time). The intersection of the two sets of isochores represents the range of pressures and temperatures within which all inclusions should have been trapped. Note that usually the resulting values are exaggerated (i.e. higher than real values).

The scenario of petroleum and water trapped in co-precipitated minerals during the filling of a reservoir—with the assumption that the related fluid inclusions were unaltered after trapping—has also been simulated in the laboratory (Pironon 2004). Due to pressure or temperature stress, occurring after trapping, the fluid inclusions usually re-equilibrate by stretching (i.e. volumes of inclusions increase) and/or by leakage (i.e. loss of fluid). Such fluid inclusions record only the last maximum stress event with a new set of PVTx conditions.

Commonly, fluid inclusion analysis is combined with numerical burial models (1D). The pressure and temperature conditions at the trapping time can be further constrained (with evidence of larger basin-scale). The hydrostatic or lithostatic pressure regime during trapping can be as such estimated on the related PT diagram (Bourdet et al. 2010; Fig. 3.13). Here, isopleths and isochores of unaltered (Fig. 3.13a) and re-equilibrated (Fig. 3.13b) aqueous and petroleum fluid inclusions can be plot. The intersections of isochores correspond to the trapping PT conditions for the unaltered (preserved) inclusions and the later stress event for the re-equilibrated ones. Since, the evolution of the pressure regimes (hydrostatic and lithostatic) and temperature can be calculated by 1D burial modelling (Fig. 3.13c), one needs simply to combine both methods. Thereafter, the isochores intersection point of the unaletered inclusions, in the area between hydrostatic and lithosthatic curves (Fig. 3.13d) defines the pressure and temperature, as well as the time of trapping. The timing of the last maximum pressure and/or temperature stress is defined similarly for the re-equilibrated fluid inclusions (Fig. 3.13e).

Ong (2013) provided new insights on the diagenesis of the deeply buried siliciclastic reservoirs of oil fields in the Viking Graben (North Sea) by similar fluid inclusion analyses combined with burial modelling. PVTx of fluid inclusion trapping together with numerical basin modelling allowed indeed the reconstruction of fluid migration pathways associated with fluid overpressures in the investigated reservoir (Ong et al. 2014). Hence, the impact of basin-scale regional fluids on diagenesis and reservoir properties could be estimated.

Probably the most interesting advancement of the techniques related to fluid inclusion analysis concerns the experimental procedures (Caumon et al. 2014). Synthetic analogues of aqueous fluid inclusions (e.g. FSCC, Fused Silica Capillary Capsule; Chou et al. 2008) have been used to mimic fluid inclusions (Ong et al. 2013). Thus, a mineral can be made to trap fluids at specific temperature and pressure conditions. Somehow, this approach may represent what happens at the scale of an oil/gas field and can also be used to constrain basin models.

Girard et al. (2014), presented at the "Journée Thématique ASF" conference on the 4th of July 2014 in Paris, a powerful new approach (the PIT-AIT) that consists of the synthesizing co-genetic petroleum and aqueous fluid inclusions and reconstructing their pressure and temperature paths. Henceforth, applications of this approach are to be applied to petroleum reservoirs and is capable to constrain the timing of the hydrocarbon charge, overpressure development as well as the exact P-T conditions of trapping.

3.1.7.1 3D Scanning (CT and Micro-CT) and Image Analysis

Classical petrographical techniques may provide a detailed, quantitative description of the diagenetic phases, but limit observations to two dimensions arbitrarily chosen during preparation of thin sections. X-ray (micro-focus) computed tomography (micro-CT) offers a tool to image

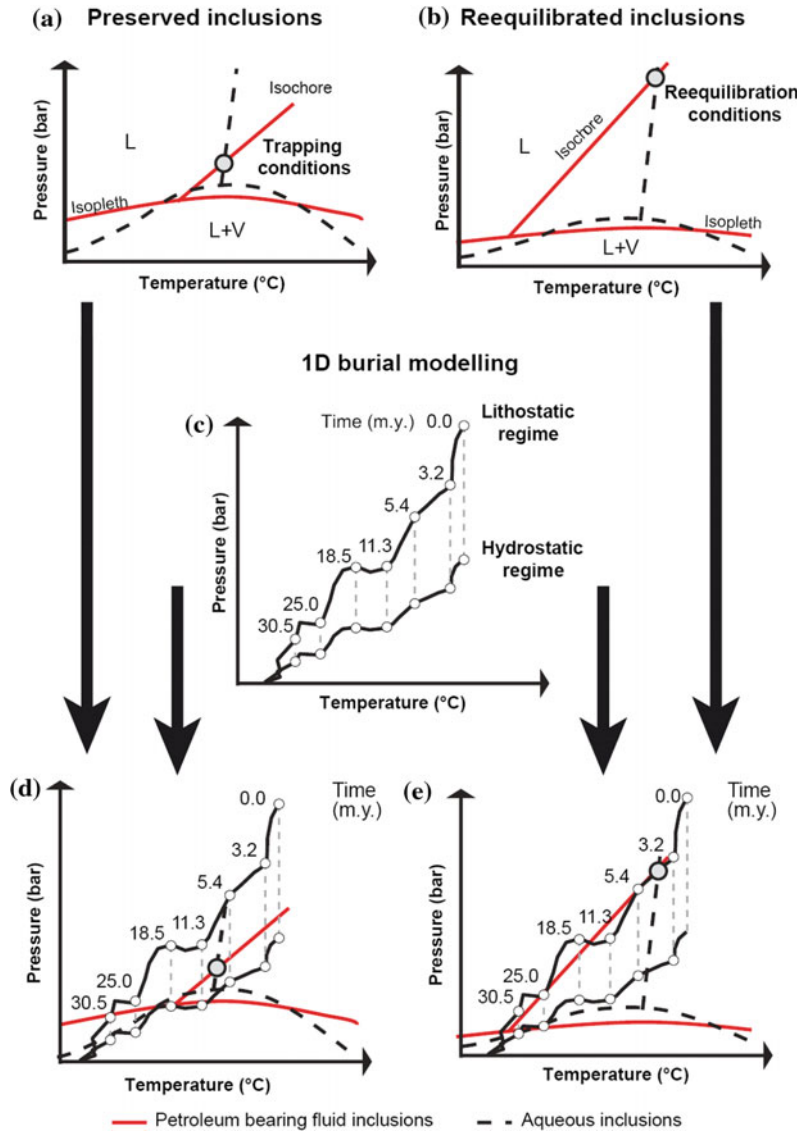

Fig. 3.13 Workflow for dating unaltered (preserved, **a** and **d**) and re-equilibrated (**b** and **e**) fluid water (aqueous) and petroleum inclusions by means of petrography, fluid inclusion analysis and 1D numerical burial modelling (**c**) (from Bourdet et al. 2010)

and quantify the 3D rock fabrics and describe in detail complex 3D pore network geometries (Mees et al. 2003; Youssef et al. 2007, 2008; Claes 2015). De Boever et al. (2012) used micro-CT to quantify the major components of typical carbonate reservoir rocks, and achieved a realistic description of the geometry of the 3D pore structure at different steps in the diagenetic evolution. A good agreement can be achieved between porosity and quantitative XRD measurements (coupled with SEM-EDS and EMPA), and the micro-CT image-based quantification results for a representative sample sub-volume. Further validation of the reconstructed equivalent 3D pore network by comparison of simulated and measured absolute permeability and mercury injection capillary pressures (MICP) show a reasonable agreement, as obtained earlier for other real sandstone and carbonate core material (Knackstedt et al. 2006; Youssef et al. 2007). Still such techniques are hampered by the increasing needs for higher resolutions,

subjective image treatment (e.g. definition of REV), and varying scale of porosity types. These are considered today as future perspective research themes.

Pore space models can also be created from 2D input images produced by analysing thin sections under SEM-EDS (e.g. van der Land et al. 2013). These images are of much higher resolutions (compared to similar scale CT images; check Fig. 3.1), and can be used to derive statistics of the spatial distributions of the diagenetic components in order to construct 3D images (Fig. 3.14). This has been achieved by means of stereology using either multipoint-statistic techniques (e.g. Al-Kharusi and Blunt 2008) or using stochastic approach (Wu et al. 2008).

Rock textures (as well as diagenetic phases) and ancient pore structures are also reconstructed and quantitatively described based on 3D micro-CT images. The equivalent pore networks extracted for relevant diagenetic steps serve as input for pore network models that can quantify the petrophysical properties at these time steps. This allows us to define the flow characteristics of realistic reservoir rocks at specific time steps during diagenesis.

First, the CT setup has to be adapted by tuning the workflow to specific mineralogy recognition and/or porosity cut-offs (Rosenberg et al. 1999). Samples consisting of one mineral species do not yield useful information on existing diagenetic phases by means of CT scanning. In fact, since the mean atomic numbers of the various dolomite or calcite phases are very close respectively, the resulting CT images show no clear difference in grey scale. Hence, the resulting images represent a uniform matrix. The pore space can still be perfectly investigated.

Following CT scanning, the 3D-images are reconstructed. Once the fabrics and pore distribution of the investigated sample appear homogeneous in CT images of the 23 mm diameter plugs, a 5 mm diameter miniplug could be drilled for high-resolution micro-CT. The exact location of the miniplug is often subjectively decided, based on visual investigation of the 23 mm plug CT scans. A couple of adjacent 1000 × 1000 × 1000 pxls volumes are extracted, for instance in the middle part of the 5 mm diameter miniplug

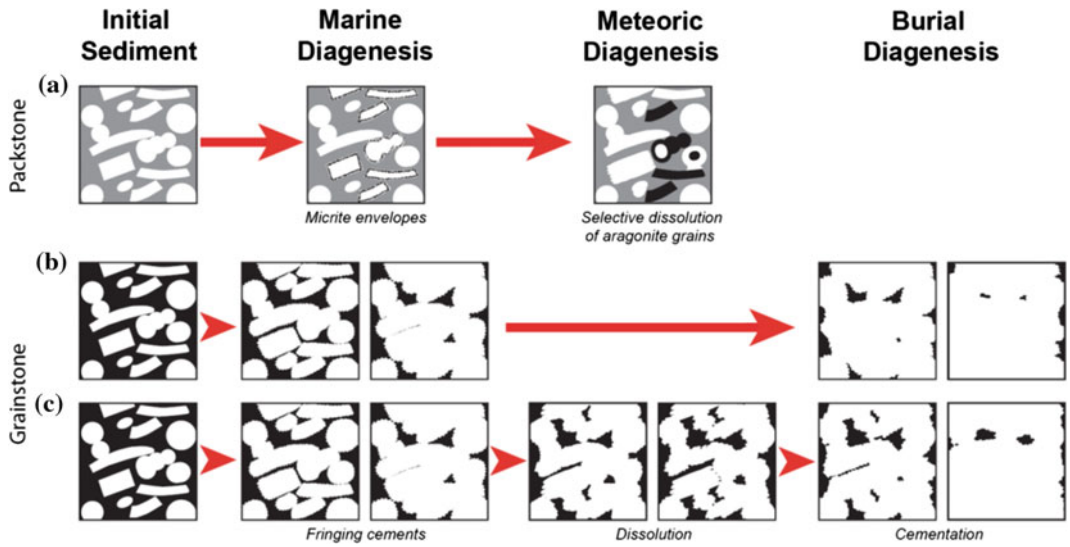

Fig. 3.14 Examples of training images of carbonate rock textures for constructing 3D models of pore space (with evolving diagenesis): **a** Packstone with selective grain micritization during marine diagenesis followed by meteoric aragonite dissolution; **b** Grainstone affected by marine and burial cementation; **c** Grainstone with marine cementation, followed by meteoric dissolution, and then burial cementation. Solids are in *white*, pores in *black* and *grey* represents micrite matrix. Slightly modified from van der Land et al. (2013)

(total volume of a few mm^3). The porosity% is, then, calculated for several volumes of increasing size (Fig. 3.15) indicating a representative elementary volume (REV) size; ca. 5.4 mm^3 (check Fig. 1.10, Chap. 1). This REV value does not take into account vugs which usually span a broad range of sizes (some falling beyond the REV itself). The mercury intrusion capillary pressure (MICP) curve of the same sample is also used to assess the significance of the resolution. For instances, for a resolution of 3 µm, only 63 % of the (effective) porosity is captured in the investigated typical Arab C dolostone. Such a resolution is not enough to capture the intercrystalline micro-porosity which has been detected by MICP measurements of the same samples. Hence, a double detector scan was used to increase the resolution to 1.5 µm, to capture 90 % of the porosity and allows imaging clearly the fine intercrystalline pore connections. There is nevertheless a constant need to increase the resolution of the micro-CT scanning (below 0.5 µm).

Thousands of images are produced for a sample of some 5 mm diameter. These constitute the basic images that are used to reconstruct a 3D-volume. In a second step, the image treatment and quantitative analysis of the reconstructed 3D-volumes consists of (i) visualizing, isolating (segmentation) and quantifying the resolved pore space and different mineral phases, (ii) the reconstruction of an equivalent pore network and description of its parameters, and (iii) the reconstruction of pore networks. Finally, numerical simulation of mercury intrusion and permeability can be done. Following pore space partitioning, a connection matrix is built that is used to simulate mercury intrusion and calculate the permeability. This remains a major research field on its own involving complicated algorithms (e.g. Youseef et al. 2007; Talon et al. 2012). A full drainage curve is obtained through a step by step invasion of an entire pore volume that is accessible via its throat radius for a fixed capillary pressure (Pc). Comparison of simulation results with lab permeability and Purcell mercury porosimetry measurements are used to validate the quality of the reconstructed pore network and pore partitioning.

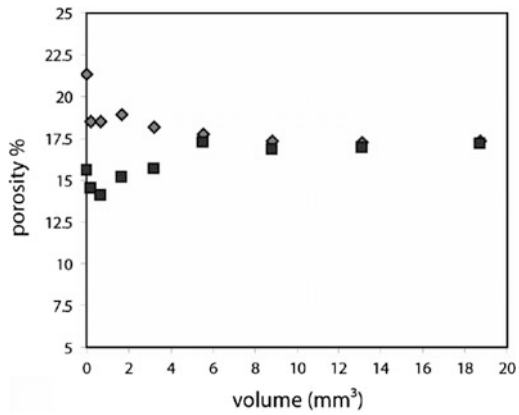

Fig. 3.15 Calculation of porosity% for increasing volumes to investigate the representative elementary volume of the studied sample. The two curves represent two sampling schemes for the volumes: increasing volumes around the centroid (*gray diamonds*) and volumes increasing downwards from the upper surface (*black squares*) of the dataset—check Fig. 1.9 (De Boever et al. 2012)

The grey scale CT, micro-CT images show the different mineral constituents and porosity (Fig. 3.16). The grey scale histogram shows the corresponding peaks, and can be successfully improved by applying a noise reduction filter (Check Fig. 2.20b, Chap. 2). Volumetric percentages of each phases (as well as porosity), calculated after somehow subjective segmentation, can thus be done and compared with other techniques (e.g. XRD, EMPA, MICP).

Different steps of the pore network building, such as segmentation, volume extraction, skeletonization, the definition of minimum diameters and pore space partitioning (cf. Fig. 1.6, Chap. 1). Following skeletonization and pore partitioning, the quality of the partitioning is appreciated qualitatively and validated quantitatively through the comparison between simulated and measured petrophysical properties. First, mercury injection curves are compared (cf. Fig. 2.22, Chap. 2). In a second and more sensitive step, the permeability value is calculated from the equivalent network and compared to the experimental permeability value measured on the 23 mm diameter plug sample.

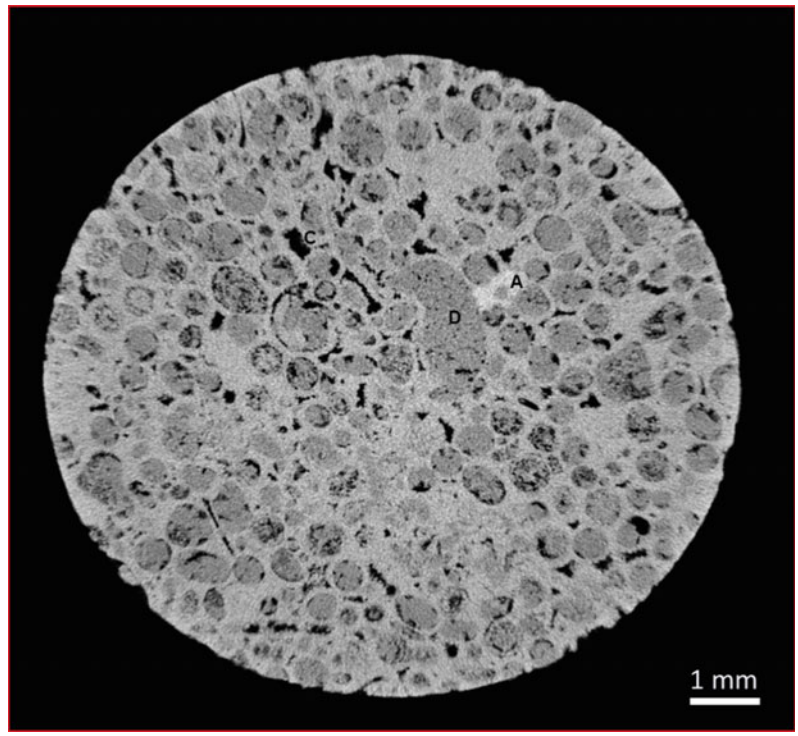

Fig. 3.16 2D-grey scale view of CT scan of a typical dolomitized grainstone. *Darker grey* is dolomite (with micro-porosity, *D*) forming the rock matrix. Calcite cement rims around the dolomitized grains are in *lighter grey* (*C*). Anhydrite is *white* (*A*), while the porosity is *black*. Courtesy of the IFPEN Petrophysics group

The pore partitioning step allows furthermore to calculate statistics on the pore size and pore connectivity, which can aid in a quantitative 3D rock fabric description. Pore radius refers to the radius of a volume-equivalent sphere of the pore. *In finé*, this method is capable to a certain extent to quantify in three-dimensions the volume of allochems (grain constituents of rock matrix), various diagenetic phases (with different grey-scale, i.e. mineralogy), and porosity. The associated permeability can be assessed through different types of numerical modelling (e.g. PNM, Pore Network Models).

3.1.8 Geophysics (Seismic and Wireline Log Data)

Seismic and wireline data are usually integrated in order to achieve quantitative characterization of facies and to investigate the impacts of diagenesis on porosity distribution across heterogeneous reservoirs (Fig. 3.17; Fitch 2010). Diagenesis of carbonate reservoirs may have characteristic responses on well logs (such as Gamma Ray, Density, Acoustic, Compensated Neutron, and True Formation Resistivity).

Stratigraphic markers are picked and correlated across well logs, providing a first step towards sequence stratigraphy and defining the major rock units. The stratigraphic markers are commonly used in combination with petrographic and petrophysical analyses (see for example Fig. 3.2). In addition, sonic and density logs as well as petroacoustic data can be used to generate synthetic seismograms that are tied to the seismic data (Sagan and Hart 2006; Bemer et al. 2012). Hence, log picks could be associated with seismic reflectors which have specific attributes such as dip angle, azimuth, and curvature. The seismic reflectors/horizons—which also reflect diagenesis—are, thus, calibrated by well logs. Faults are preferential pathways for fluids, and they are commonly mapped on seismic cubes using amplitude and coherency attribute maps of the seismic data (e.g. Ghalayini et al. 2016).

Lai et al. (2015) demonstrated that diagenetic facies can be "translated" to well log responses,

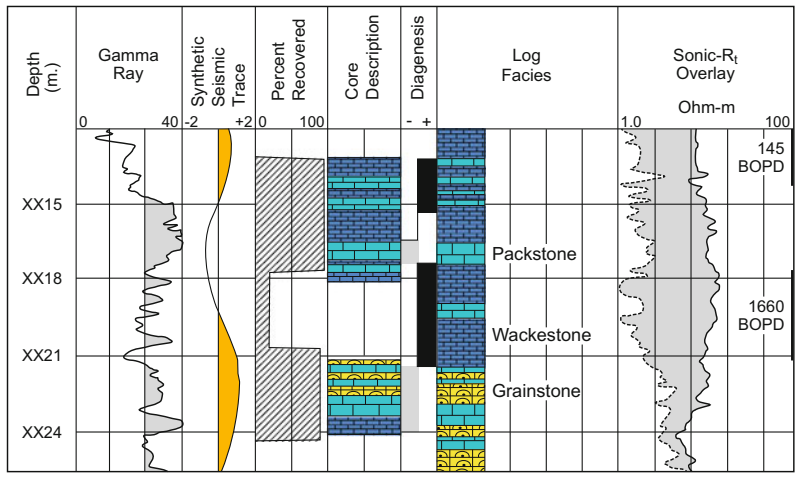

Fig. 3.17 Facies interpretation based on well log data and sedimentologic/petrographic description of cores, allowing facies to be mapped across a carbonate field using other logged wells without cores (Akbar et al. 1995)

and associated to porosity and permeability ranges which are commonly determined from core analyses. Secondary porosity (due to diagenesis) can be estimated by comparing neutron-density crossplots and sonic compressional measurements. Subsequently, the heterogeneity of carbonate reservoirs might be better 'visualized'. Petroacoustic analyses (P- and S- wave phase velocities) coupled with NMR measurements are also used to better predict fluids saturation in carbonate reservoirs (Rasolofosaon and Zinszner 2003; Bemer et al. 2012).

Hydrothermal dolomite are defined seismically using geometric criteria (e.g. sags of key horizons, fault patterns) as well as changes in amplitude or frequency of the seismic data. Sagan and Hart (2006) demonstrated how quantitative seismic methods together with well logs can be used to predict reservoir properties in carbonate rocks, resulting mainly from faulting and fluid-rock interactions (Fig. 3.18).

3.2 Future Perspectives

'Quantitative diagenesis' is a rising field of research on its own as it combines new developments in analytical equipment and creative workflows and techniques. If the objective of characterization of diagenetic processes is to link the processes to the resulted phases (and vice versa), here the main goal is to be able to assign numerical values for such phases. There are several possible key future perspectives and potentially interesting quantitative methods. Some of which have already been introduced in the State if the Art section (above). The following venues are only arbitrarily selected based on my experience.

3.2.1 Remote Sensing and Photogrammetry

State of the art techniques for quantitative diagenesis studies at the plug sub-scale, the subsurface fields, and geological basins have been briefly presented above, still outcrop analogues are needed to fill in the gaps in this broad spectrum. Studying surface-exposed geobodies allows constraining their geometry, internal architecture and constituents associations (e.g. fracturing and lithofacies, dissolution and erosive surfaces) of heterogeneous reservoir rocks. New technological breakthroughs in remote sensing and imaging (some are still under development; e.g. lidar scanning, photogrammetry) attempt not only to capture the spatial dimensions (architecture or structural patterns) of diagenesis-related features that are exposed at outcrops, but also to quantify them (e.g. Kurz et al. 2012).

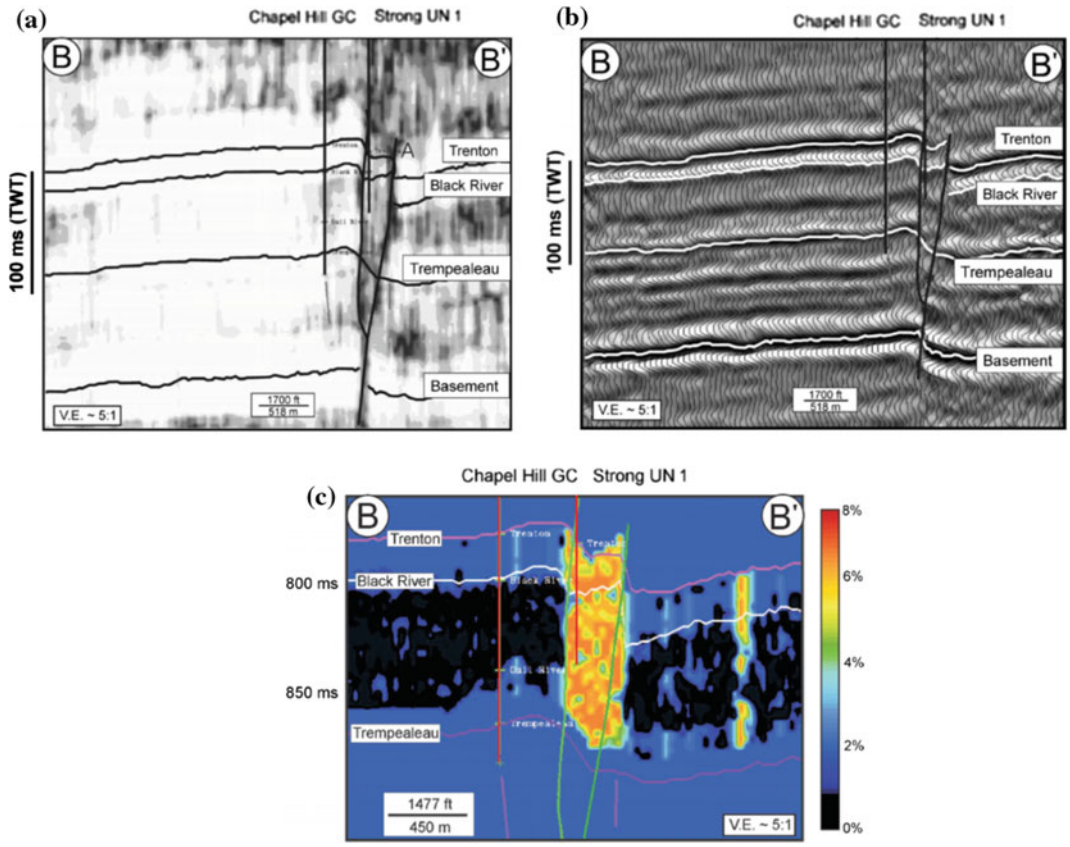

Fig. 3.18 Porosity mapping of fault-related hydrothermal dolomites based on quantitative seismic methods: **a** cross-section of a fault with flower structure through seismic coherency volume; **b** same cross-section with seismic amplitudes; and **c** calculated porosity volume showing the highest developed porosity within the flower structure (from Sagan and Hart 2006)

Remote sensing techniques are coupled with numerical image analysis in order to provide 3D mapping of the sedimentary/diagenetic objects of sub-seismic scales. Today, related remote acquisition is done by means of lidar or photogrammetry. IFPEN has been involved in optimizing ground- and drone-based photogrammetry workflows that are capable of capturing sedimentary structures in detail with high resolution and transforming the images into geo-referenced, gridded models (reservoir-scale). Fracturing and diagenetic features can also be explored and quantitatively assessed. IFPEN's Smart Analog approach for 3D geomodels representing outcrops are built up at the reservoir scale (Fig. 3.19; Schmitz et al. 2014).

First the field aerial- and ground-based geo-referenced acquisitions (hundreds of geo-tagged photographs) are undertaken, resulting in an outcrop model. Interpretation follows by property painting (e.g. facies), drawing objects (e.g. dolomite fronts), including structural information (e.g. fractures-and bedding strike/dip values). The corresponding geomodels are directly worked out from the outcrop 3D models and further statistical and/or geostatistical computation can be applied to fill in where information is lacking. Finally, reservoir modelling can also be applied and compared to the actual subsurface reservoirs (e.g. facies/stratigraphy, seismic attributes, petrophysical properties).

Lidar scanning with hyperspectral imaging and image analysis (e.g. Fig. 3.20) have proved to provide a successful technique in mapping diagenetic phases of distinct chemical and

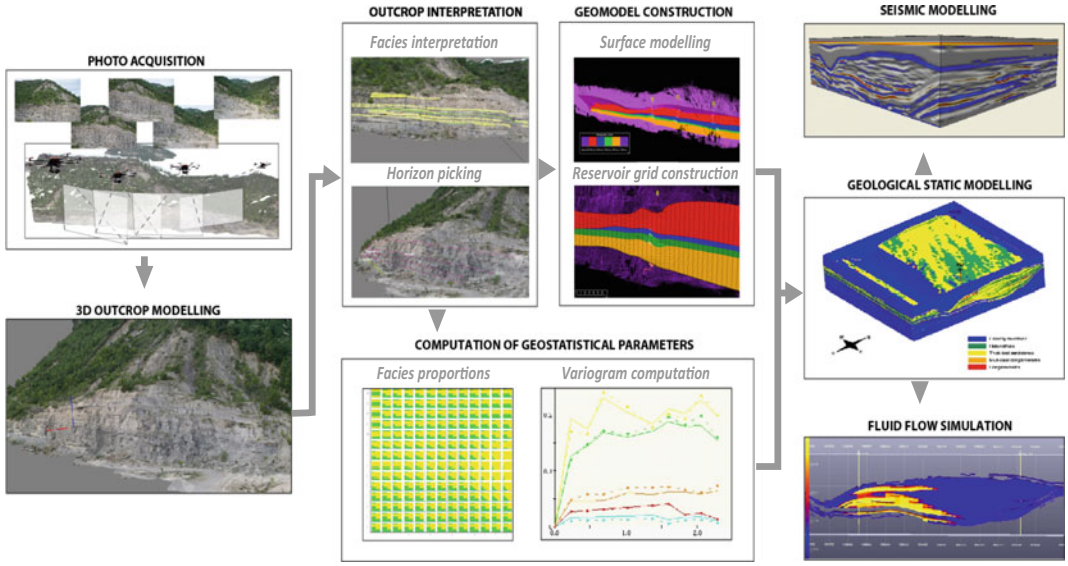

Fig. 3.19 Integrated workflow for reservoir models based on 3D photogrammetry of outcrop analogues: from field acquisition through characterization to numerical modelling (from Schmitz et al. 2014)

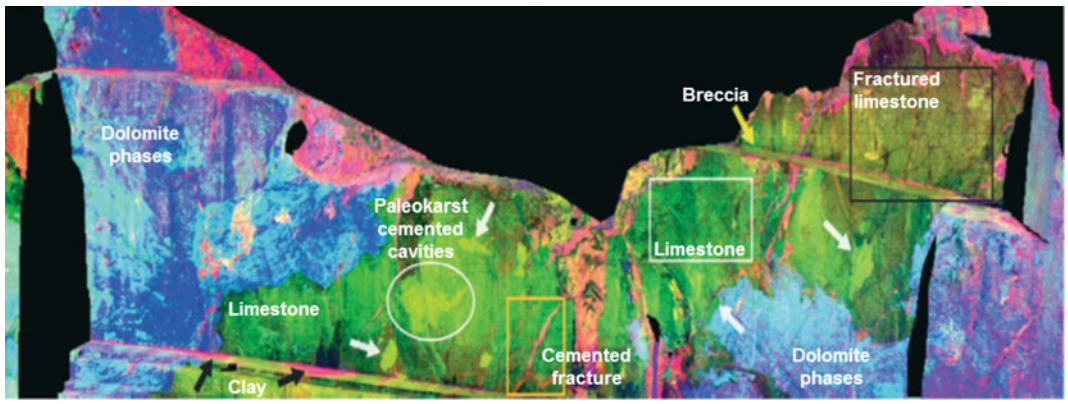

Fig. 3.20 Hyperspctral image analysis and interpretation of the main face of the Pozalagua Quarry (Ranero, NE Spain; from Kurz et al. 2012)

mineralogical nature at the Pozalagua Quarry (northern Spain; Kurz et al. 2012). This new workflow is certainly going to be further improved and applied in the near future. It will certainly allow constructing robust geo-referenced numerical models of reservoir-analogues.

Kurz et al. (2012) were able to map various diagenetic phases, such as ferroan-dolomites, filled/cemented paleokarst cavities and fractured zones by means of combined lidar scanning and hyperspectral imaging. This quantitative approach results in a direct volumetric estimations when surveys can be achieved in three-dimensions.

3.2.2 Integrated Data Analysis Tools

Today, huge petrographic and petrophysical data-bases are available in the industry. A typical oilfield in the Middle East may have about 500 wells (10 % of which are cored and sampled

every foot). Such large data-bases need integrated analytical tools in order to be properly used. I have tried in this chapter to present workflows including software such as EasyTrace™ and GOCAD capable of analysing the petrographic and associated petrophysical data from the plug to the well and field-scale (cf. Figs. 3.2, 3.3 and 3.4). Still, these may as well be improved and encompass other types of information (e.g. well logs, seismic data, fracturing models). Well log suites and interpreted electrofacies coupled with the petrographic and petrophysical investigations (presented above) provide an efficient tool to achieve pertinent quantitative rock-typing.

In addition, invaluable quantitative geochemical and mineralogical data could help in better understanding the reservoir heterogeneities and the impacts of diagenesis (or fluid-rock interactions) on the flow properties evolution. Indeed, temperature and pressure conditions as constrained by isotopic analyses and fluid inclusions may provide the link with numerical basin models.

There is a need at the industry to have an integrated tool (based on software) that is capable of managing all such data in a smart way that highlights their inter-relationships. Accordingly, upscaling would be better conceived and reservoir models could include diagenetic trends and impacts.

3.2.3 Pore Space Models

Investigations of pore space and fluid flow properties in reservoir rocks will certainly attract a considerable number of research groups in the coming years. Diagenesis plays a major role in the (re)distribution of porosity and permeability in carbonate rocks. If better quantitative understanding of the porosity/permeability relationship is generally reached, reproducing the porosity evolution of reservoir rocks could be accomplished with the related permeability changes—still a very challenging task. The new technological breakthroughs (e.g. micro-CT) may lead to directly focusing the pore network evolution rather than investigating the rock textures (and subsequently deducing pore space).

The paleo-pore architecture can be generated today in the three-dimension with high resolution (down to 0.5 μm in certain laboratories) from 2D binarized images (cf. Fig. 3.14; van der Land et al. 2013) or from 3D micro-CT scanned mini-plugs (see above; e.g. De Boever et al. 2012). The latter is succeeded only when the investigated sample contains distinct minerals (host matrix vs. cementing phases), while the former approach using 2D petrographic images can be applied to several diagenetic phases irrespective of its mineralogical heterogeneities. In both cases, the pore space evolution is tied to a certain paragenesis. Pore systems are converted into pore networks which are used to calculate flow properties. 3D pore space structures can be used for modelling complex single and two-phase flows through direct numerical flow simulations (Talon et al. 2012). Such modelling workflows are based directly on the binarized 3D images. Darcy's law and viscosity energy dissipation are applied in order to compute permeability in distinct porous media at the micro-CT scale (e.g. straight channels, 2D model porous media, sandstone). For additional details refer to Talon et al. (2012).

Alternatively, a Pore Network Model (PNM) approach can be used to estimate the permeability values for the reservoir rock at several phases during its paragenesis (e.g. Algive et al. 2012; De Boever et al. 2012). Yet, the derived pore networks are only approximations of the real networks at specific steps during diagenesis. Besides, such networks are often very heterogeneous in nature and reproducing such heterogeneities in previous states remains very difficult. Nevertheless, combining 3D imaging with PNM (and geochemical simulations; discussed in Chap. 4) is believed to be worthwhile for quantitative rock-typing of reservoir rocks and numerical modelling of diagentic impacts on flow properties. Could such an approach also address upscaling?

3.3 Discussion

'Characterization' of diagenesis involves—as discussed in Chap. 2—the description and classification of diagenetic phases and subsequently

their related processes. When describing diagenetic phases/processes implicates numerical values, 'Quantitative diagenesis' studies are invoked. In this chapter, the state of the art for applying quantitative description of diagenesis is presented. Similar general methods with respect to the ones used for qualitative characterization of diagenesis (Chap. 2) are employed (i.e. petrography, mineralogy, geochemistry, fluid inclusion analyses and petrophysics). However, the resulting descriptive data and sometimes the tools are different. For quantitative methods I have also distinguished the investigation scales. For instance, whether the applied methods involve petrography or geochemistry, examining objects of thin section-, reservoir- or basin-scales requires different approaches. With respect to multi-scale diagenesis studies, 'Quantitative diagenesis' occupies a central position, which is based on adequate characterization methods and definition of concepts, and relates to numerical modelling tools (three-stages workflow illustrated in Fig. 1, page x). Indeed, quantitative data are necessary during the construction of numerical models (Chap. 4) and to validate the resulting simulations. We shall see, also, in the next chapter, that modelling aims to consolidate the conceptual models (based on diagenesis characterization) and can lead to their improvement.

Petrographic analyses produce a great deal of data, which remain the basic building blocks of modern diagenesis studies. They involve mostly 2D thin sections and they are presented on logs or in tables and spread-sheets. I have presented two procedures to quantify sedimentary and diagenetic features from scanned images of thin sections and photomicrographs. These are applied by means of Matlab™ scripts (Claes 2015), and through the common use of JMicroVision freeware. These tools help in relatively rapidly and systematically quantifying distinguished features of allochems, cements, and porosity. Images of scanning electron microscopy can be also used for quantitative assessments. They are often combined to petrophysical measurements (e.g. MICP, NMR) achieved on the same samples from which thin sections are made (check Fig. 3.1). Still, most of the industrial petrographic analyses lack this degree of quantification and rely on visual estimation percentages, abundance classes (absent to abundant), and even just occurrences (binary codes: 1 = present, and 0 = absent). Based on my experience in the framework of numerous projects in the Middle East (UAE and Iran), I have compiled three tables (Tables 3.1, 3.2 and 3.3) presenting the various commonly described categories for lithologies and textures, cements, and reservoir properties. Thousands of thin sections and associated samples (plugs) are quantitatively and semi-quantitatively described by filling tables with such categories. They may provide huge amounts of numerical values (up to 80 parameters per thin section) which can be used to statistically study diagenetic phases and relate them to rock-typing.

Having such considerably vast petrographic and petrophysical data-bases from wells across a field can be used to apply reservoir-scale quantitative diagenesis. Of course, they can be coupled with well logs (and, subsequently electrofacies). Quantified diagenetic phases can be correlated through produced cross-sections and help in providing statistical "trends". I have presented the workflow that we applied on the Jurassic Arab D reservoirs at the scale of an oil field in offshore Abu Dhabi (see Fig. 3.3). Here we had a data-set based on 10,000 thin sections from ten wells, which allowed statistical analyses and drawing proportional maps featuring the distributions of the diagenetic phases (Nader et al. 2013). At this stage, in order to avoid repeating the geological discussion of these results—which is well presented above, and in Nader et al. (2013)—I will only focus on the rationale of the dual statistical and mapping approaches.

Statistical analyses—undertaken with appropriate software such as EasyTrace™—lead to better understanding the inter-relationships of some diagenetic phases (e.g. type of cements, mineral replacements) and reservoir properties (porosity and permeability). I have called "drivers" the diagenetic phases that appear to be associated with certain trends of reservoir properties. For example, in Fig. 3.3, we can observe

that where syntaxial calcite overgrowth cement (SCO) is abundant, higher permeability values occur. Therefore the SCO is a "driver" for higher permeability trend.

Mapping of rock textures and lithofacies at the reservoir-scale are undertaken routinely in the industry. What we elaborated further is drawing the proportional distribution of the quantified diagenetic phases (Fig. 3.4). Proportional maps can be, therefore, constructed based on numerical values (%) or relative abundance (absent to abundant). They are valuable tools to visually, geographically associate the various parameters. Besides, such maps are also valuable for constructing numerical models (discussed on the same case study in Chap. 4).

X-ray diffractometry technique coupled with Rietveld refinement and a special sample preparation and analytical methods, which we describe in Turpin et al. (2012), resulted in quantitative assessments of calcite, dolomite and anhydrite contents of Muschelkalk and Lettenkohle carbonate rocks. While the documented procedure may be applied quite rapidly on a large series of samples, we advise that preliminary investigations with SEM-EDS and/or EMPA to be applied on selective samples in order to constrain the mineralogical compositions ahead of massive XRD measurements. The idea was also to compare the resulting quantitative mineralogical compositions with lithology distribution classically presented on well logs. This remains a task to be attempted in the future, I still believe that such approach (including organic matter quantitative analysis) can be used to improve calibration of well logs. Besides, the identification and quantification of carbonate mineral species using Rok-Eval pyrolysis has been achieved recently (Fig. 3.21; Pillot et al. 2014) and can serve to this end too. Combining the results of such analytical techniques and well log suites remains an excellent venue for future research projects.

Spectral analyses by means of electron microprobes result in geochemical mapping at the scale of thin sections. These are also coupled with the new generations of SEM-EDS (punctual chemical analysis) and they can lead also to mineralogical mapping. We have undertaken this approach on sandstone samples from the Lower Cretaceous Upper Mannville Formation (Alberta, Canada; Deschamps et al. 2012; check Fig. 3.8). Alternatively, mapping geochemical attributes (e.g. major and trace element compositions) on bulk-rock samples can be applied on reservoir-scale objects. I have used this approach to quantitatively characterize hydrothermal dolomite fronts (Figs. 3.9 and 3.10), and subsequently refine the associated paragenesis (check Fig. 2.11; Nader et al. 2007). As far as fluid flow operates at the larger basin-scale, the resulting cement stratigraphy may reveal the evolution of geochemical composition of diagenetic fluids (e.g. stable oxygen and carbon isotopes, strontium isotopes, estimated salinity in fluid inclusions). We have applied this approach on the Permo-Triassic Khuff equivalent rock sequence in the UAE (Fontana et al. 2014).

Fluid inclusion analyses have been introduced in Chap. 2, in the general framework of characterizing the original diagenetic fluid by coupling microthermometry and stable oxygen isotopic measurements. In this chapter, I present the same technique, applied on inclusions trapping liquid water as well as petroleum liquid/vapour. This results in a very powerful approach that is still under development with advanced confocal laser scanning microscopy, Raman microspectroscopy, and numerical modelling (check Fig. 3.13). Consequently, we are becoming capable of constraining the timing of trapping of inclusions in the mineral phases (i.e. potentially the precipitation of the mineral—if inclusions are primary), and the prevailing pressure and temperature conditions. In addition, the timing and nature of the hydrocarbon charge can be known. This method and associated workflows will develop further in the near future and certainly allow us to further constrain placing the diagenetic phases (and processes) on the burial history curve (cf. Fig. 2.13).

X-ray computed tomography techniques coupled with image analysis can lead to quantitative volumetric assessment of mineral phases and porosity. Here limitations, which I have discussed in Chap. 2, principally relate to resolution and intensity. The approach of van der Land

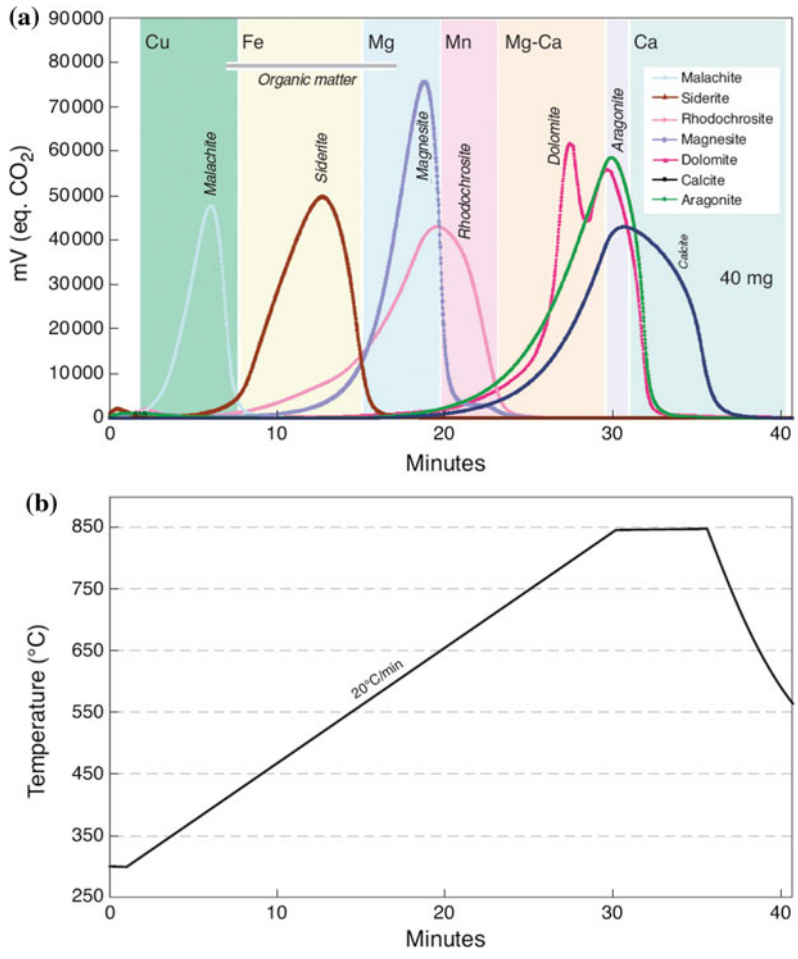

Fig. 3.21 Rock-Eval pyrolysis results for identifying and quantifying carbonate species: **a** Obtained mV (equivalent CO_2) peaks, representing pure mineral standards (malachite, siderite, magnetsite, rhodochrosite, dolomite, aragonite and calcite); **b** the corresponding heating ramp of 20 °C/min between 300 and 850 °C (Pillot et al. 2014)

et al. (2013), which consists of creating 3D pore space models based on high resolution input SEM-EDS training images, is presented above. What attracts my attention to this approach is the potentials it has in incorporating diagenesis-based porosity evolution (Fig. 3.14). I have also presented above the detailed procedure that we have followed to quantify the volumes of anhydrite in dolostones as well as the pore space at IFPEN (De Boever et al. 2012). Here, again the problem of Representative Elementary Volume (REV) is faced, pleading to the need to be addressed in future research projects. The best approach, and the one that I would encourage, is the integration of a variety techniques of acquisition (e.g. micro-CT, SEM-EDS) and image analyses.

Most of the above discussed methods and associated workflows can be still considered under development and continuous improvement. 'Quantitative diagenesis' remains currently a rising field of research. I have selected three subjects which, based on my personal experience, appear to be very promising in the near future. First, remote sensing and photogrammetry methods have proved to be effective in providing detailed outcrop analogue models with high resolution (capturing sedimentary, structural and diagenetic features). Integrated workflows can lead to the construction of appropriate reservoir models that can be compared to 3D reflection seismic cubes and used for fluid flow simulations (IFPEN, Schmitz et al. 2014). Lidar scanning and hyperspectral imaging may result in powerful

'diagenetic mapping' of outcrops (check Fig. 3.18; Kurz et al. 2012). These methods are combined with field work, which is the fundamental activity for sound diagenetic studies. I have discussed above the combined statistical and mapping analyses of huge petrographic and petrophysical data-bases, which are achieved by means of several software tools. It makes sense to propose new integrated data analysis tools (and/or upgrade existing ones) that are capable of managing such data and other types of information (geochemical, geophysical, production tests, etc.). This is certainly a challenge for future software developers, and it will benefit research projects on diagenesis and potentially "upscaling" in reservoir models. The third subject for future development in quantitative diagenesis studies concerns pore space models. Clearly, this line of research is very attractive and will benefit from improved technologies in acquisition and image analyses. I did mention on a final note the pore network modelling (PNM) approach, which is also developed at IFPEN, and has been used to estimate permeability evolution resulting from cementation and dissolution processes (Algive et al. 2012).

Eventually, numerical modelling of diagenesis (Chap. 4) requires further developments in the fields of robust analogue model constructions at the reservoir scale, integrated data analysis software capable of incorporating a maximum amount of quantitative data, and improved 3D assessment of pore space and fluid flow properties.

3.4 Advancement in Quantitative Diagenesis

New methods and workflows are emerging for quantitative assessment of diagenetic phases/processes and their impact on reservoir rocks at various scales. These techniques are significant for providing numerical data that can be used by reservoir engineers as entry (input) data and for validating the results of numerical simulations in order to reach meaningful predictive geomodels capable of constraining reservoir heterogeneities. Most of the methods and workflows presented in this chapter can be still considered as under development and will witness significant improvements in the near future.

I intended to draw the attention through this chapter to the huge wealth of semi-quantitative to quantitative data that come from the industry, and to propose certain ways to organize such data (Tables 3.1, 3.2 and 3.3). Development of software and numerical tools is still needed to cope with the vast geophysical (well logs), petrographic, geochemical and petrophysical data-bases. Enhanced numerical tools should be linked to basin geo-modelling software packages. The reward, will certainly be a better quantification of diagenesis and its impacts on reservoir properties. Similarly, I believe that outcrop analogue studies (through remote sensing and photogrammetry) can help in providing the missing link to understanding subsurface reservoir heterogeneities. This invokes technological breakthrough and building integrated workflows benefitting from a variety of methods and data-sets (such as geophysical and fluid flow simulations). Potentially, such workflows can address the "upscaling" problem in reservoir modelling, especially that at outcrops the luxury of acquiring different scales and determining the REVs might be possible.

At the scale of rock samples (and thin sections), quantitative analyses of diagenetic phases with the integration of SEM-EDS, XRD and EMPA are potentially prone to further enhancement. The new generations of XRD equipment are capable of quantifying minerals with high resolution, yet they need to be combined with SEM-EDS or EMPA to narrow the mineralogical ranges. Besides, quantitative assessment can be done for varying mineralogical assemblages (e.g. ferroan dolomite/calcite). Quantitative dating of diagenetic processes needs to be improved as well and associated to basin history. Further work is expected on understanding the anisotropy evolution of flow properties by means of quantitative assessments of the cement crystal growth and deduced stress fields (e.g. back-scatter SEM analyses, calcite twinning, magnetic susceptibility).

Three-dimensional scanning of cores and samples (via computed tomography) will

continue to develop in order to quantify with higher resolution the mineralogical constituents (matrix and cement) as well as macro- and micro-pore space. Better subjective image treatment and possibilities to deal with varying scales of porosity types constitute real actual and future challenges. Permeability modelling based on pore space and related networks seems to me an important step. For instance, adequate quantitative assessment of flow properties along the paragenetic paths (forward or backward) will help in understanding the diagenetic effects on permeability. A challenging future task would be to distinguish the impacts of burial and tectonic compaction on the evolving pore space.

Numerical Modelling of Diagenesis

4

Techniques for characterizing diagenesis and assessing quantitatively its impact on sedimentary rocks are quite available (some examples are presented in Chaps. 2 and 3). Numerical modelling of diagenesis remains under development and the near future will certainly witness concrete innovations in this field. *In Finé,* a numerical model is expected to deliver a better distribution of petrophysical properties based on the understanding and predictability of the diagenetic processes, and their impacts on the sedimentary rocks. At this stage, the key objective must not be limited to the capability of simulating the exact processes under investigation. It should rather provide a tool able to test certain scenarios and to draw concluding statements that could enforce or dismiss the proposed conceptual model, and guide further reservoir modelling.

Previous and on-going research work aimed at modelling diagenesis to constrain the heterogeneity of carbonate reservoirs (e.g. Caspard et al. 2004; Whitaker et al. 2004; Jones and Xiao 2005; Rezaei et al. 2005; Barbier et al. 2012). Forward modelling to simulate early meteoric diagenesis affecting isolated platform have been proposed by Whitaker et al. (1997a, b). More recently, basin-scale modelling codes taking into account the impact of the residence time of phreatic water lenses and karst on early diagenesis has been undertaken (e.g. Paterson et al. 2008; Hydromel—IFP Energies nouvelles). Caspard et al. (2004), Whitaker et al. (2004), Jones and Xiao (2005), and Consonni et al. (2010) used reactive transport modelling to simulate dolomitization. Calcite dissolution by mixing of fresh and marine waters has been calculated by Rezaei et al. (2005). Dissolution of carbonates and karst processes are very attractive to various multi-disciplinary research groups applying numerical modelling (e.g. Labourdette 2007; Rongier et al. 2014). Only a few published articles make use of geostatistical methods to model diagenesis and associated reservoir heterogeneity (e.g. Doligez et al. 2011; Barbier et al. 2012; Hamon et al. 2013).

Three major numerical approaches for modelling diagenesis processes—focussed on carbonate reservoir rocks—are presented here: (i) geometry-based, (ii) geostatistical, and (iii) geochemical.

4.1 State of the Art (Numerical Modelling of Diagenesis)

4.1.1 Geometry-Based Modelling

By ‘geometry-based modelling’, object-distance and geometric-association simulations are meant. For instance, the object-distance simulation method (ODSIM) that is proposed by Henrion et al. (2010) models a three-dimensional envelope around a skeleton. Such methods have been proposed to

F.H. Nader, *Multi-scale Quantitative Diagenesis and Impacts on Heterogeneity of Carbonate Reservoir Rocks*, Advances in Oil and Gas Exploration & Production, DOI 10.1007/978-3-319-46445-9_4

model dolomitized rocks, cemented veins and karstic networks (e.g. Rongier et al. 2014).

4.1.1.1 Karst Networks Modelling

Underground karst networks represent a major late diagenetic process involving the dissolution of carbonate rocks. Such networks play a significant role in the underground flow distribution in aquifers and reservoirs (Chaojun et al. 2010). Besides, modelling such features can be validated by speleological mapping of accessible karst conduits. The hydrothermal karst systems inlcude some of the most outstanding karst networks—where very rapid dissolution takes place (e.g. Klimtchouk 2007; Palmer 2007). Besides, such hydrothermal dissolving fluids are usually accessible, and have been often associated to nearby hydrocarbon fields (Palmer 2007). Karst networks provide excellent applications for numerical modelling (e.g. Dreybrodt et al. 2005). They have been also investigated by means of geometry-based methods. The latter is capable of modelling the three-dimensional patterns of such geological objects, leading to improved sustainable groundwater utilization, better hydrocarbon exploration/production, and overall optimal management of the subsurface. Besides, one can compare the cavernous karstic networks to the vuggy porosity and even the microscopic pore space networks: it's all a matter of scale.

Skeletons of the karstic network are usually provided either by speleological mapping (i.e. two- and/or three-dimensional maps with measured lateral and vertical dimensions; Fig. 4.1), or by stochastic simulations taking into account the location uncertainties of the actual conduit (Dreybrodt et al. 2005). The ODSIM method computes an Euclidean distance field around the skeleton, which is then refined by means of a random threshold—generated by stochastic methods such as the Sequential Gaussian Simulation (SGS; see below).

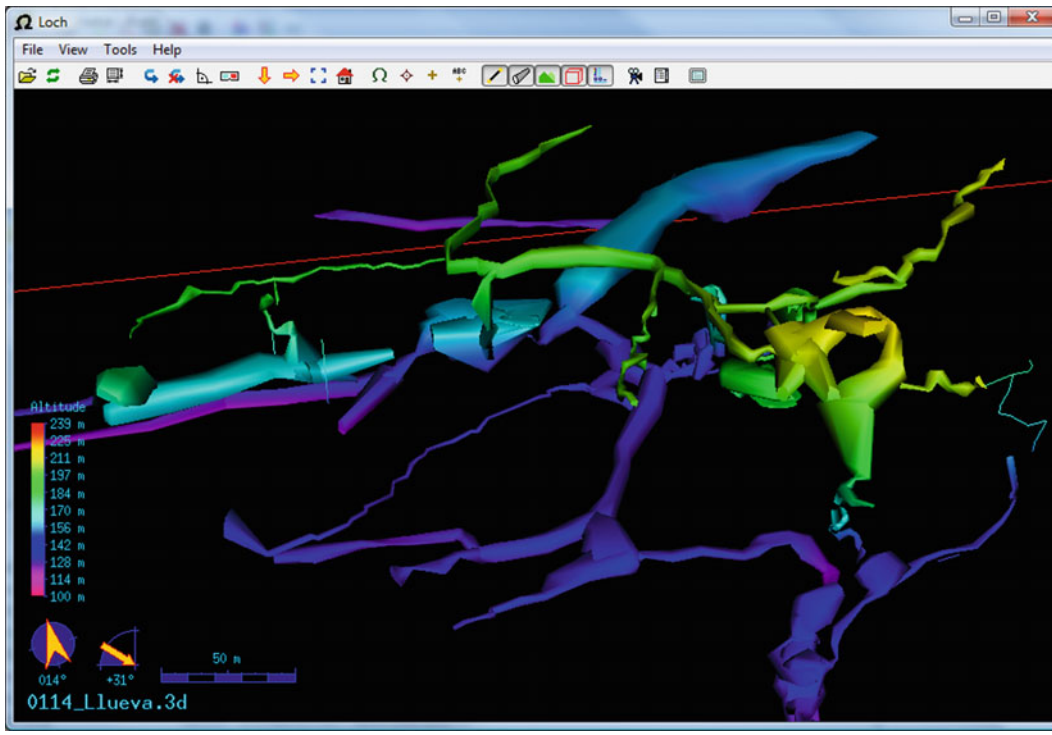

Fig. 4.1 An example of a 3D speleological map of underground karstic networks (Llueva cave, Spain) with Survex and supported by Therion software packages (www.survex.com; http://therion.speleo.sk/index.php). This 3D survey is based on classical speleological mapping

Rongier et al. (2014) presented a new methodology based on ODSIM (as a plugin of the GOCAD software), capable of integrating a series of geological features known to influence conduit shapes. They used a custom distance field generated by a fast marching method, which

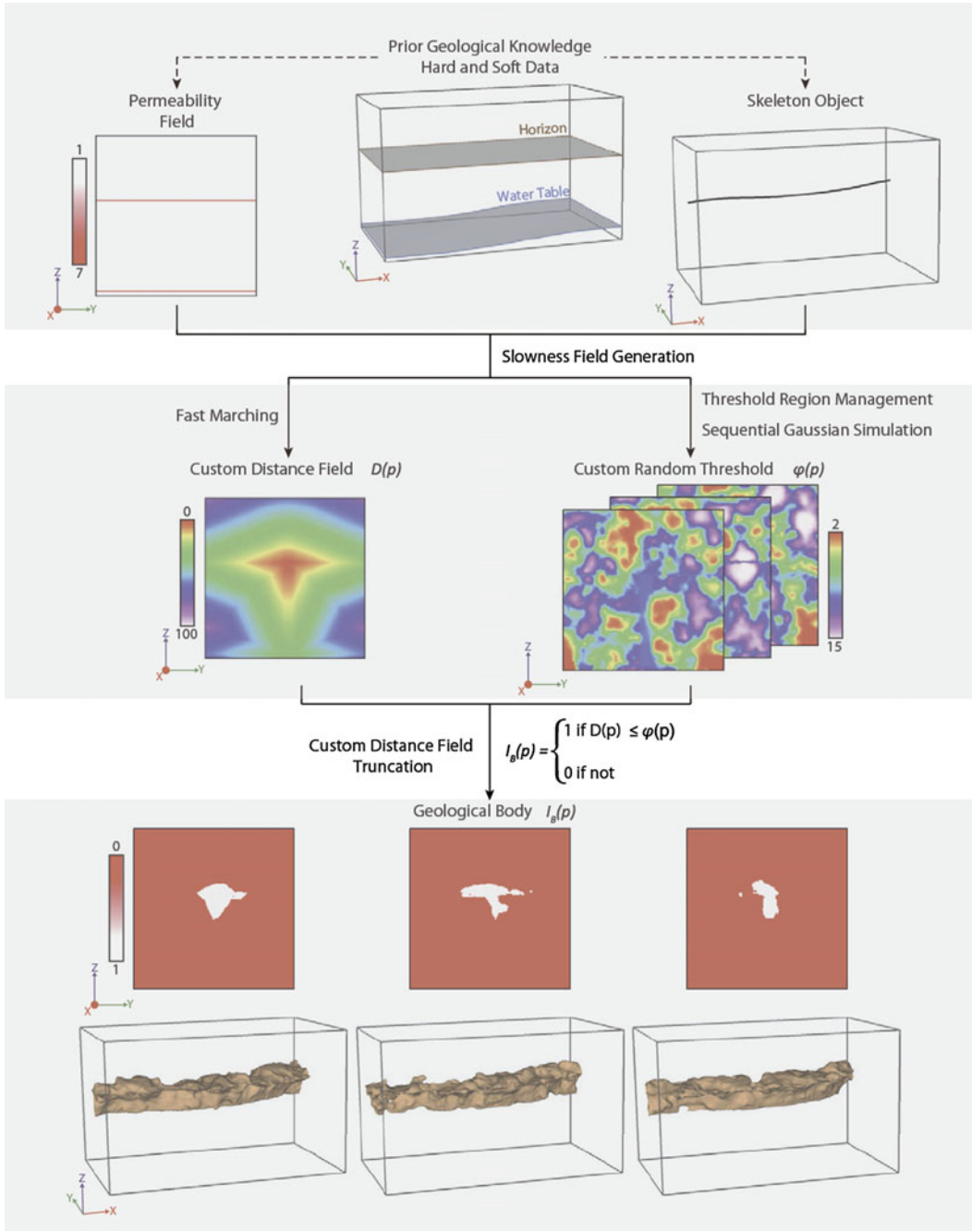

Fig. 4.2 Improved workflow for ODSIM of karstic networks (see text for details, refer to Rongier et al. 2014). Geological data are taken into account, prior to applying numerical methods to constrain the geometry of the simulated geological body (here a karstic conduit)

concerns the propagation of a "front" with known speed, and constrained to geomorphological data. Then a random threshold is built by combining different variograms or distributions (Fig. 4.2).

The above presented workflow is applied for each element known to have a certain control on the shape geometry (e.g. bedding planes, faults), and result in the varying patterns of the produced envelopes for the karstic conduits. Consequently, a variety of karst morphologies can be modelled; e.g. lensoidal bodies along bedding and fault planes, symmetric vertical conduits, keyhole passages, longitudinal notches (Fig. 4.3).

4.1.1.2 Fracture-Related Hydrothermal Dolomite Modelling

Geometry-based modelling of fracture-related dolomitization have been attempted on the Ranero dolostone outcrops (see Fig. 2.1, Chap. 2). The geological model was first constructed featuring the various sedimentological facies and the structural architecture of the Ranero study areas (using GOCAD software). Fractures and faults were further modelled by means of Fraca™ and were subsequently imported into the geomodel (Dumont 2008).

Field observations demonstrated that NW-SE oriented faults (and fractures) are associated with the major hydrothermal dolomitization process (i.e. flow pathways of dolimitizing fluids). Besides, the distance of the dolomite bodies away from such major faults can be measured (from field mapping and satellite image analysis). Hence, similar to the ODSIM method (presented above), the Ranero dolomite objects could be modelled, whereby the NW-SE oriented fractures represent preferential sites of presence of dolomites (Fig. 4.4).

The resulting model distributes similarly the dolomites along the simulated fractures in both northern and southern zones of the study area (outlined in black on Fig. 4.4). This is contradictory to the field observation whereby the southern zone has relatively narrow dolomite corridors in the limestone host-rock (see Fig. 1.8, Chap. 1). In addition, the northern zone consists of two subzones (a higher plateau and a slope; Fig. 4.5), with quite distinct distribution of dolomite bodies around the same major Ranero fault. The plateau is structurally and stratigraphically higher than the slope (Nader et al. 2012), and thus, the larger volume of dolomite might represent the general geometry of hydrothermal dolomites (Davies and Smith 2006; with larger dolomite bodies upwards along faults) (Fig. 4.5). The more considerable distribution of dolomites in the plateau area could also be related to a stratigraphic facies with higher permeability before dolomitization occurred (Dewit 2012).

The concept of fault-related dolomitization with decreasing volume of dolomite bodies with depth from a preferential horizon (e.g. top of host-rock formation) can be modelled with geometry-based methods.

Accordingly, field mapping and aerial image analysis together with conceptual understanding of the fault-related hydrothermal dolomitization (e.g. Nader et al. 2012; Shah et al. 2012; Swennen et al. 2012), provided in the case of Ranero further constraining parameters which concern the size and geometry of the dolomite objects. By applying these constraints together with the distance-to-fractures, the resulting model is more realistic, as it shows larger dolomite geo-bodies in the northern zone of the study area (Fig. 4.6), as observed in the field.

The geometry-based modelling methods do not directly result in a predictive genetic realization, they rather provide static numerical models. They make use of associations of geometric features to constrain their distribution in a realistic way. Eventually, a well-constrained geomodel is constructed and expresses the level of understanding of the spatial distribution and volumes of the simulated objects. This workflow needs to be validated with robust methods—e.g. mapping karstic networks, aerial photogrammetry of outcrops, otherwise it suffers from crucial uncertainties.

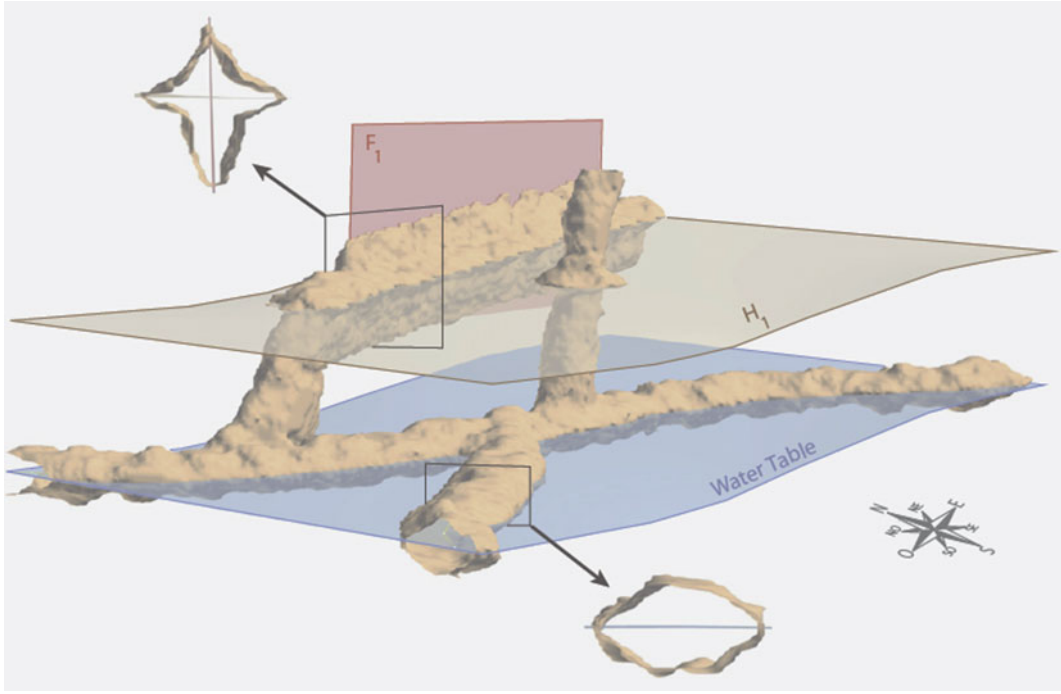

Fig. 4.3 Simulated envelope of a karstic network skeleton obtained by taking into account the bedding plane (H_1)—a stratigraphic feature, a fault (F_1)—a structural feature, and an 'attraction level' (water-table) coinciding with the lowest conduits (from Rongier et al. 2014)

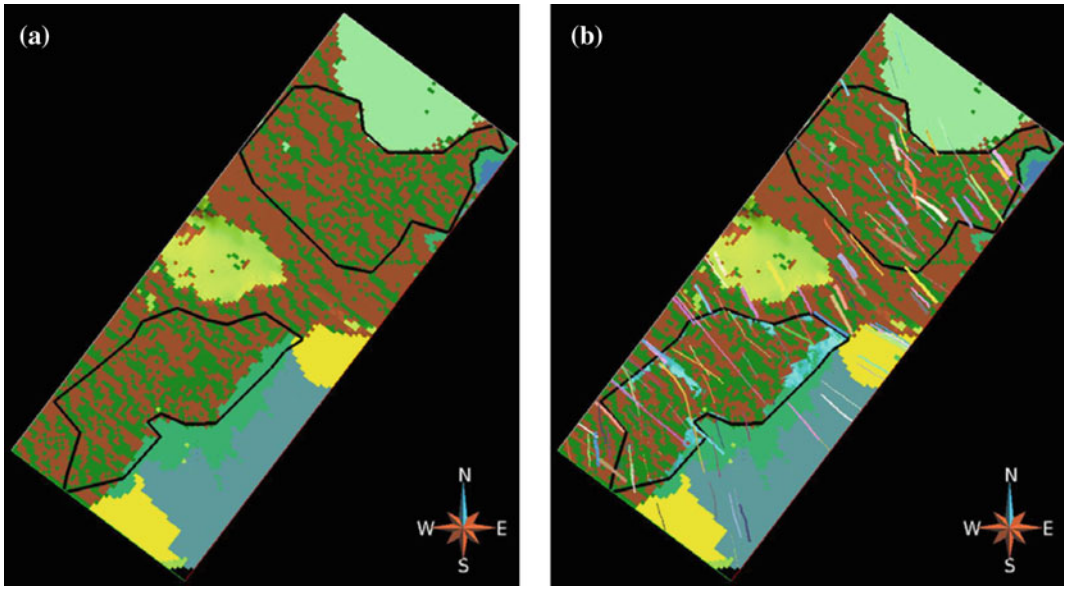

Fig. 4.4 *Top views* of the Ranero model (6000 × 2000 m) showing the two study areas (outlined in *black*) and the distribution of dolomites (*brown*) within the original sedimentary facies (*green*: limestone; *blue*: shale; *yellow*: sand). The simulated dolomite distribution is associated laterally to NW-SE oriented fractures/faults (seen in **b**) (Dumont 2008)

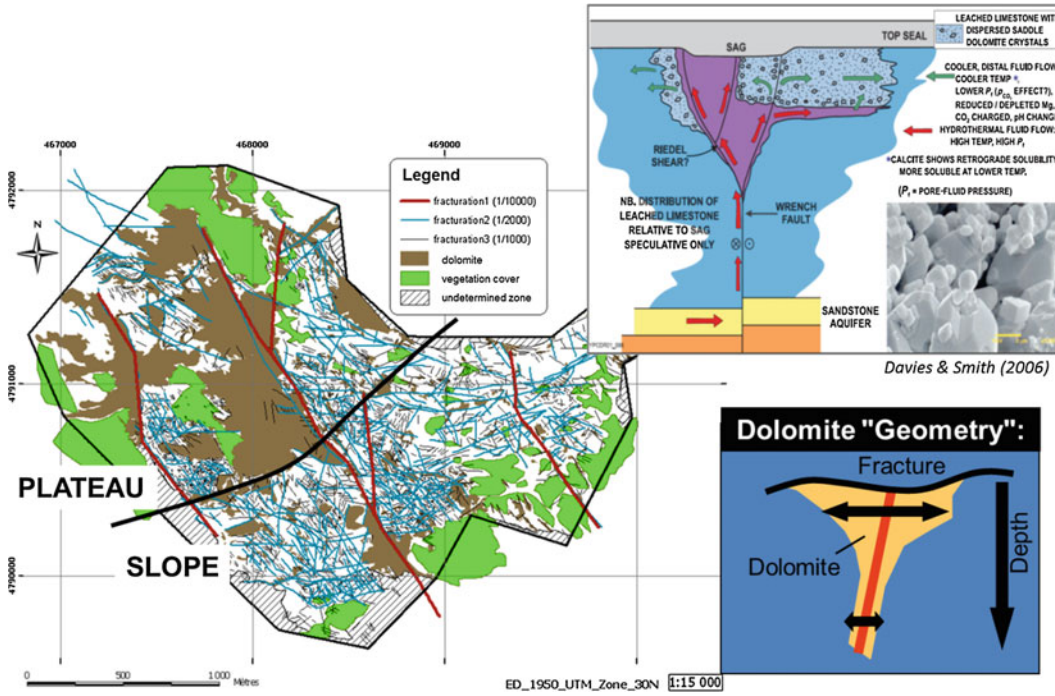

Fig. 4.5 Based on field data and conceptual models, the Ranero fault-related dolomites can be further constrained by applying a distance decreasing control for the dolomite occurrence along faults/fractures with increasing depth from a preferential horizon (ca. top seal, Davies and Smith 2006)

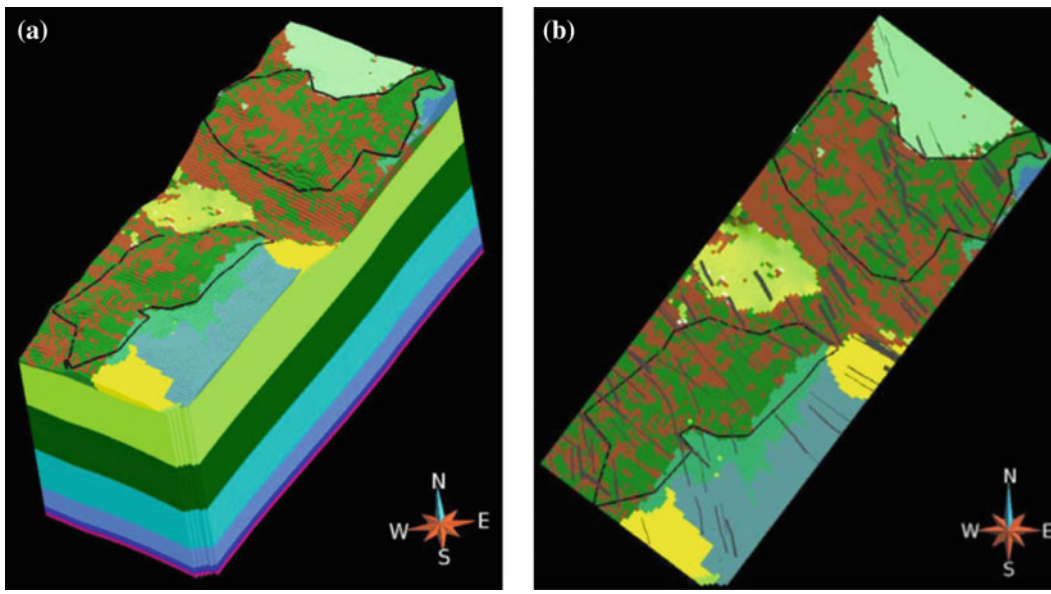

Fig. 4.6 Dolomite distribution simulation of the Ranero model (6000 × 2000 m) taking into account the NW-SE faults and the vertical geometry constraining factors: **a** cube view of the 3D model showing the modelled dolomite distribution near the surface—the northern study area (outlined in *black*) features relatively larger dolomite volumes (in *brown*) compared to the southern area; **b** *Top view* of the model showing the simulated dolomite distribution and the NW-SE faults (compare this map with Fig. 4.4b)

4.1.2 Geostatistical Modelling

Geostatistical methods are often used for reservoir-scale modelling—preferably based on considerable amount of data. Geostatistical simulations make use of stochastic approaches (e.g. plurigaussian, multiple point) to fill in the space between control points (e.g. wells, outcrop logs) with known 'exact' or 'hard' data (Doligez et al. 1999). Hence, the resulting models consist of cells filled with the most probable facies/phase and/or petrophysical properties. This is not a predictive approach but rather an extrapolation workflow based on probability. It certainly helps in illustrating probability-based heterogeneities across reservoirs (cf. Fig. 1.11).

Geostatistical modelling workflows have been investigated to simulate sedimentary facies and associated diagenesis overprints (e.g. Pontiggia et al. 2010; Doligez et al. 2011). The quantitative assessment of diagenetic imprints is analysed by means of different geostatistical workflows to obtain final simulations reproducing both sedimentary facies, diagenetic trends, and resulting petrophysical characteristics in reservoir models.

The general idea is to first generate a model of rock texture distribution that can be controlled by the conceptual knowledge of the depositional environments. The diagenetic imprint distribution is generated afterwards using the relationship characterized between the initial rock textures and their subsequent alteration (diagenesis). If no relationship is evidenced, two independent stochastic realizations can be required for both texture and diagenesis.

The classical facies modelling algorithms are usually shared between object-based and pixel-based (also named cell-based) algorithms. Here variogram-based methods and multiple-point geostatistics are commonly applied. For instance, Matheron et al. (1987) applied this technique successfully to model deltaic reservoirs (in Doligez et al. 2009).

4.1.2.1 Methodology: Geostatistical Parameterization Steps

Discretization The process of which a continuous data set is partitioned into categories sampled on a grid is called discretization. Accordingly, the well paths are converted into cells of the grid by an averaging method. Discretized well trajectories are required as an input to the log discretization. Well log discretization enables one to have the well log information on the stratigraphic grid. Therefore, properties such as dolomite%, porosity, and permeability as well as classical well logs—e.g. neutron, gamma-ray—can be discretized. Depending on the nature of the quantitative data, two different averaging methods for discretizing properties are generally used, "*Mean Value*" (e.g. for dolomite%), and "*Most Represented Facies*" (e.g. for rock textures, cement and porosity types).

Rock texture and diagenetic phase definition The rock textures, cement and porosity are usually associated by means of statistical analysis (e.g. through the use of EasyTrace™ software). For instance, rock textures may be grouped into muddy-, packstone-, and grainy textures, while the cement types into absent, rare, common and abundant classes.

Vertical proportion curves The amount of each discretized category (e.g. rock texture) as a function of depth (along the discretized well trajectory) is quantified by means of the Vertical Proportion Curves (VPC). These are computed along layers of the grid and the results are presented as a graph showing, for instance, the proportion of each rock texture at each level (Fig. 4.7). In order to avoid sharp boundaries the VPCs can be smoothed.

Vertical proportion maps As a VPC is a stacked bar diagram (Fig. 4.7), which represents the vertical distribution (function of depth) of the percentages of all the rock textures in all wells,

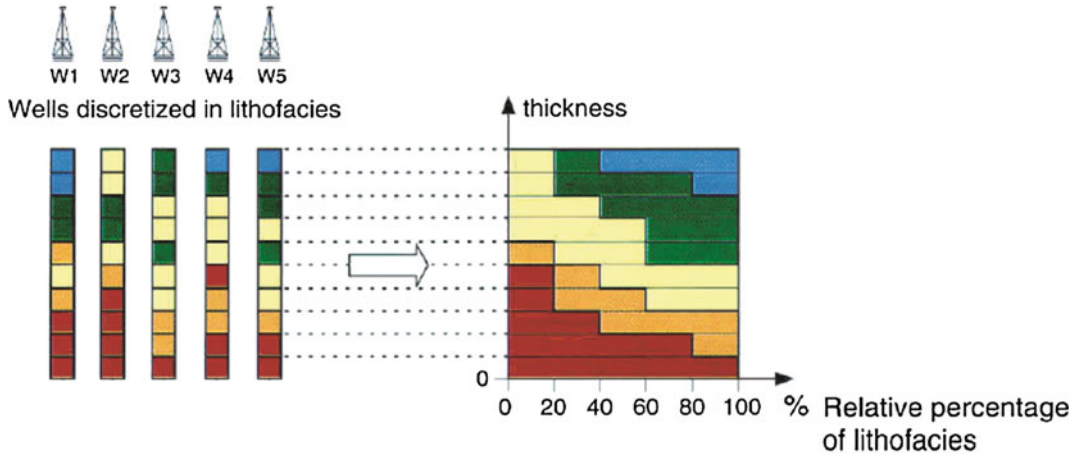

Fig. 4.7 The principle of computing a vertical proportion curve (VPC). The VPC shows the relative proportion of discretized data, such as rock textures, with depth (from Doligez et al. 1999)

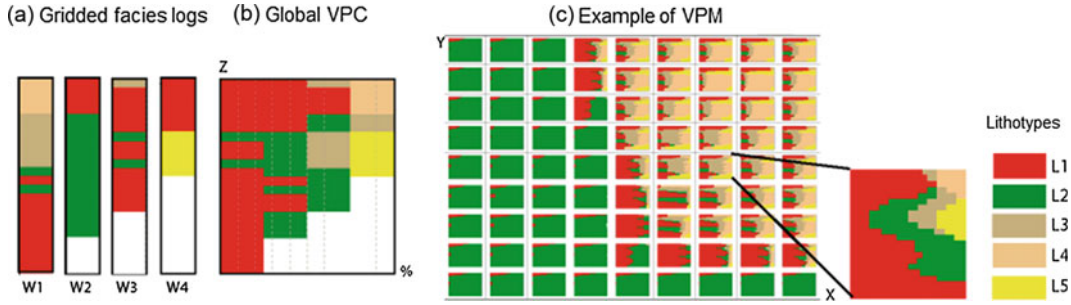

Fig. 4.8 Schematic representation of the computation of VPCs and VPMs: **a** Initial gridded (discretized) well logs with five different lithotypes; **b** resulting Vertical Proportion Curve (VPC) taking into account the gridded facies logs; and **c** computed Vertical Proportion Matrix (VPM), based on **a** and **b** as well as additional geological information. The VPC is computed as global proportions of each facies at specific depth. The VPM is computed from local VPC and additional geological and seismic information, resulting in realistic constrained zonation

the vertical proportion matrix is a set of macro cells (Fig. 4.8), each of which contains one VPC. During the simulation, the related VPC is used in each macro cell. So, if only one VPC is used in a stochastic simulation, it is assumed that the rock textures have no lateral variation. Different methods for computing the proportion matrix can be used: (i) computing the proportion matrix from VPCs; and (ii) designing areas within the grid on which the VPCs are assigned. Property maps can be used to constrain the computation of the matrix of proportions for certain facies and/or diagenetic phases.

Variograms A variogram (Fig. 4.9) is a tool for analysing the spatial correlations and spatial continuity between observations. In other words, the variogram is a measure of "geological variability" versus distance. There is a quite large difference between the horizontal and vertical directions in the "geologic variability". The vertical variability is related to the characteristics (e.g. continuity, thickness) of stratigraphic layers and/or geologic bodies. The horizontal spatial correlation corresponds to the extension of the geological bodies. A single variogram for a specific distance and direction is uncomplicated

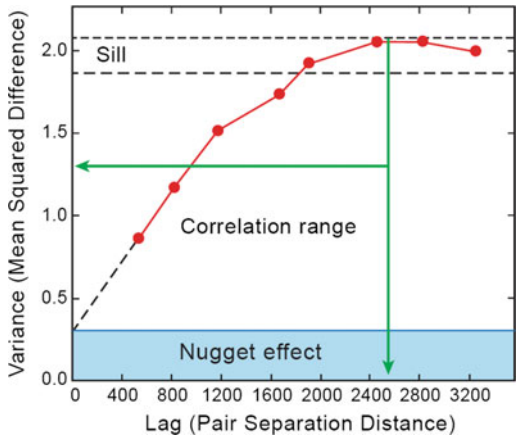

Fig. 4.9 An example of a variogram showing its characteristic parameters: sill, range, and nugget effect (from Yarus and Chambers 2006)

to interpret, but when several distances and directions are taken into account, practical difficulties arise (e.g. Gringarten and Deutsch 1999 and 2001).

In some cases geological variations seem to have no spatial correlation, which could be explained by deterministic geological processes. The type of variogram behaviour when only a small part of the variability is explained by random behaviour is called the *nugget effect* (Fig. 4.9).

Petrophysical properties are often spatially correlated to depositional environments. The spatial correlation decreases with increasing distance, and finally at a certain distance there will be no more spatial correlation. This is called the *range* (Fig. 4.9).

The sill (Fig. 4.9) is the variance of the variogram when no trend exists in the data. The sill is the data variance.

Variogram Model The experimental variogram that is computed from data values as a function of distance between data is fitted with a model (mathematical function of distance). The definition (i.e. type) of this model will have a direct impact on the continuity of the distribution of the simulated property. The most classical models are: exponential, spherical, and Gaussian. They result in more or less continuous distributions (Fig. 4.10). Variogram models can also account for anisotropy (Le Ravalec et al. 2014).

Geologic trends A trend is usually given to the petrophysical property distribution by a geological process (e.g. fining or coarsening upward or the decrease in reservoir quality from proximal to distal parts of the depositional system). These trends might create a variogram that has negative correlation at large distances; e.g. the high porosity at a base of a fining upward package will be negatively correlated to the low porosity at the top of the unit (e.g. Gringarten and Deutsch 1999 and 2001).

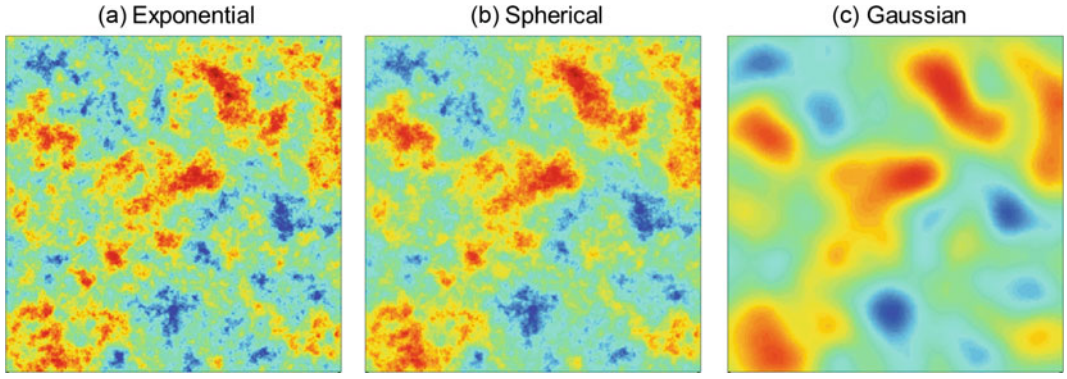

Fig. 4.10 Influence of variogram model type (**a** Exponential; **b** Spherical; and **c** Gaussian) on the resulting distribution of modelled properties. The grid consists of 200 × 200 cells, and the Range is set at 40 cells (from Le Ravalec et al. 2014)

4.1.2.2 Methodology: Geostatistical Simulation Methods

Methods for indicator/categorical variables

Sequential indicator simulation SIS is based on the indicator approach (Fig. 4.11). When a rock texture (i.e. a categorical variable) is simulated, the indicator approach transforms each rock texture into a new variable. Then, the probability of simulating related rock texture (e.g. mudstone, pack-wackestone, grainstone) at a given position, is computed using hard data (e.g. well data) and already simulated values. The values of the variable corresponding to the rock texture present is set to 1, and the rest is set to 0 (Falivene et al. 2006). A random path is defined to go through the grid.

Truncated Gaussian simulation This method is based on the truncated Gaussian simulation algorithm and needs a preliminary estimation of facies proportions to define thresholds (Doligez et al. 1999; Falivene et al. 2006), which are used to back-transform the values of the underlying Gaussian Random Function (GRF) into facies (Doligez et al. 1999). Two steps summarize the process (Fig. 4.12): (1) GRF is produced by the use of variogram models, which are fitted into the experimental variograms calculated either from wells and/or seismic data; and (2) the GRF is truncated using thresholds, so that the random variable is divided into classes; above, in between, and below the thresholds. Depending on the geological setting, the thresholds are either constant or variable. In the case of stationary

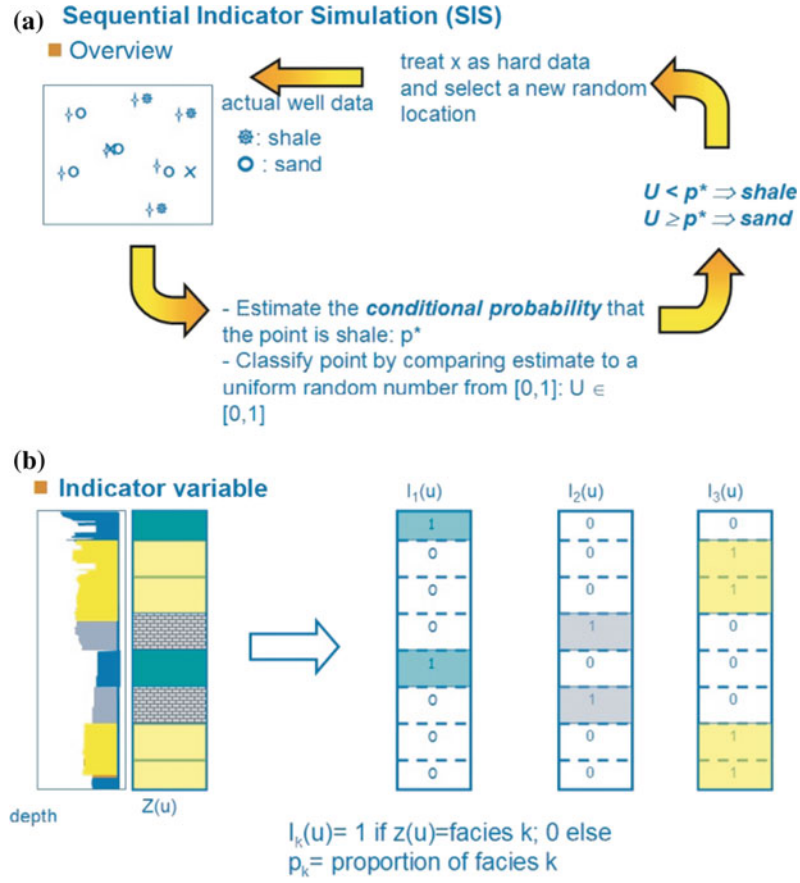

Fig. 4.11 **a** The principles of the Sequential Indicator Simulation (SIS). **b** The way categorical variables are transformed into indicator functions (Le Ravalec et al. 2014; courtesy of Doligez, IFPEN)

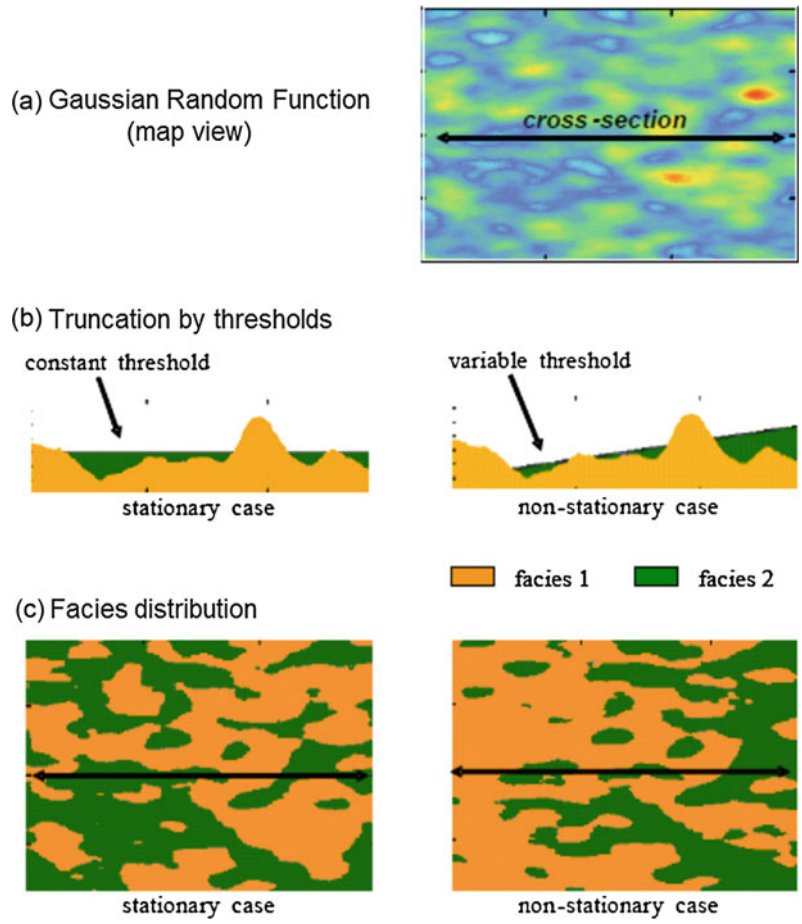

Fig. 4.12 The principle of truncated Gaussian approach: **a** Generation of the Gaussian random function; **b** Truncation of both a variable and constant threshold along a vertical section; **c** Resulting facies distribution for both stationary and non-stationary case (from Lerat et al. 2007)

configurations, heterogeneities are assumed to be homogeneously distributed, and the thresholds are constant in the lateral direction and computed level by level from VPC (Fig. 4.7). The other option is to use a non-stationary configuration, this means that lateral trends can be seen in the facies distribution and that the thresholds are variable. In this case, the algorithm can use more than a single VPC and instead deals with a 3D proportion matrix, which represents the spatial variations of the facies proportions (Fig. 4.8). Hence, the truncation thresholds in the GRF are now variable in space and the simulated facies will follow these variations (Doligez et al. 1999).

PluriGaussian simulation The plurigaussian model, consists of simultaneously truncating two (or more) Gaussian variables, which may be correlated or not (Doligez et al. 2009). The basic principle is to use two (or more) Gaussian variables (G1 and G2, Fig. 4.13a) to condition the spatial structure of two (or more) different sets of lithotypes (e.g. rock textures). The contact (and transition) relationships between the lithotypes are determined by the lithotype rule (index box- and pie-charts in Fig. 4.13b, c) that defines the truncation diagram. The practical values of truncation are computed on the base of this diagram, still honouring the proportions of lithotypes (Fig. 4.13). Normando et al. (2005) demonstrated that the plurigaussian simulation algorithm is capable of reproducing the initial reservoir characteristics as it respects the lithofacies proportion, proportion matrix and the lithotype rule.

This method has been used to model heterogeneous media for petroleum reservoir

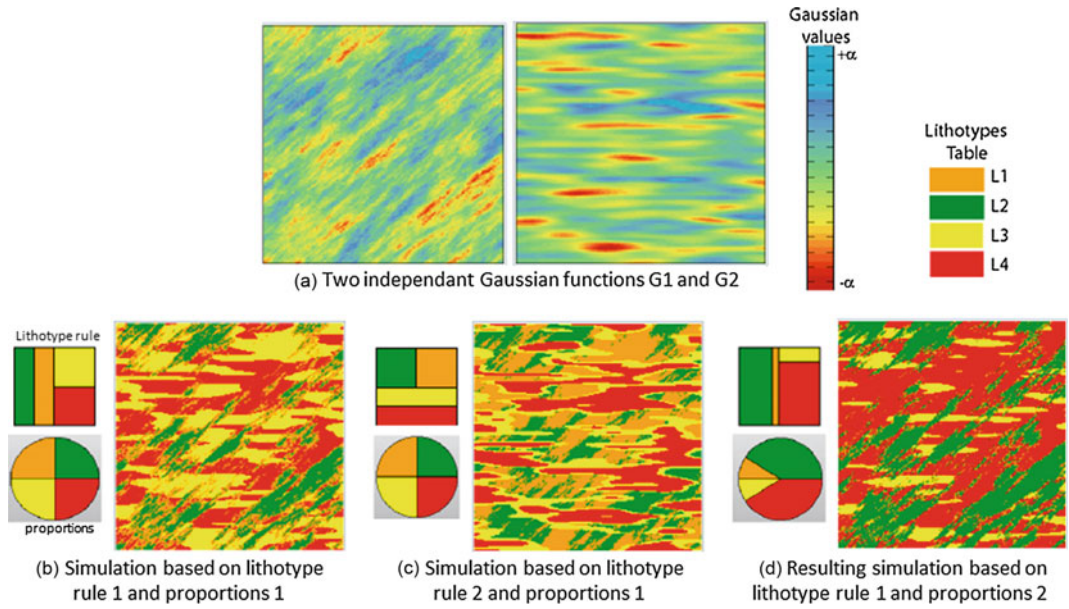

Fig. 4.13 The plurigaussian method and related parameters: **a** Two independent Gaussian functions (G1 and G2); **b**, **c** Different simulations based on distinct lithotype pattern rules (1, 2), but similar proportion patterns of lithotypes (proportions 1); **d** Resulting simulation with lithotype proportions (2) and adjusted lithotype rule 1. Note the effects of changing lithotype rules and proportions on the resulting simulations

characterization, mining or hydrogeological models (e.g. Pelgrain de Lestang et al. 2002; Fontaine and Beucher 2006; Galli et al. 2006; Emery and Gonzales 2007; Doligez et al. 2009; Mariethoz et al. 2009). Extensions to bi-PGS has been proposed (Doligez et al. 2011; Hamon et al. 2013) to co-simulate two categorical variables (i.e. sedimentologic facies and diagenetic imprints) in one step using, potentially correlated parameters for each of them.

In a typical plurigaussian workflow, the relative proportions of the different lithotypes that will be simulated, have to be well defined. These proportions are usually estimated by analysing wells or outcrops data, and computed as a global vertical proportion curve (VPC) which represents the vertical succession and distribution of facies in one stratigraphic unit.

Generally, the proportions are not constant over the domain and vary laterally because of the existence of trends in the geological/diagenetic processes. This non stationarity is captured by providing variable proportions over the domain in a grid of vertical proportions or VPM which is computed from the well data and additional geological information (e.g. sequence stratigraphy, conceptual depositional/diagenetic models, seismic data). It can be considered as a 3D probability volume of lithotypes, giving the local probability of getting a particular facies or diagenetic phase at a particular location (e.g. Ravenne et al. 2000).

Multiple Points Geostatistics simulation

MPS is able to reproduce complex geological patterns (e.g. channels) which cannot be modelled by simple variograms. Instead of using 2-point statistics from a variogram model (e.g. SIS), the MPS approach borrows multiple-point statistics from a conceptual geological model defined as a training image (Tahmasebi et al. 2012). The borrowed multiple-point patterns from training images, are then anchored to 'hard' data (e.g. subsurface well logs, outcrop images, seismic data). MPS remains a stochastic method. Therefore, the principles of stationarity and ergodicity do not allow an arbitrary choice of such training images. Caers and Zhang (2002)

demonstrated that modular training images can be used to build complex reservoir models by means of multiple-point geostatistics. New emerging approaches for multipoint-multiscale with coarse and fine training images have been proposed by Gardet et al. (in press) and Le Ravalec et al. (2014) (Fig. 4.14).

Object-based methods Object models are built from geometrical objects randomly distributed in space, whereby probability laws depict the locations, shapes and orientation of these objects. Fracture networks are often represented by this approach. For example, the NW-SE faults in the Ranero case were modelled

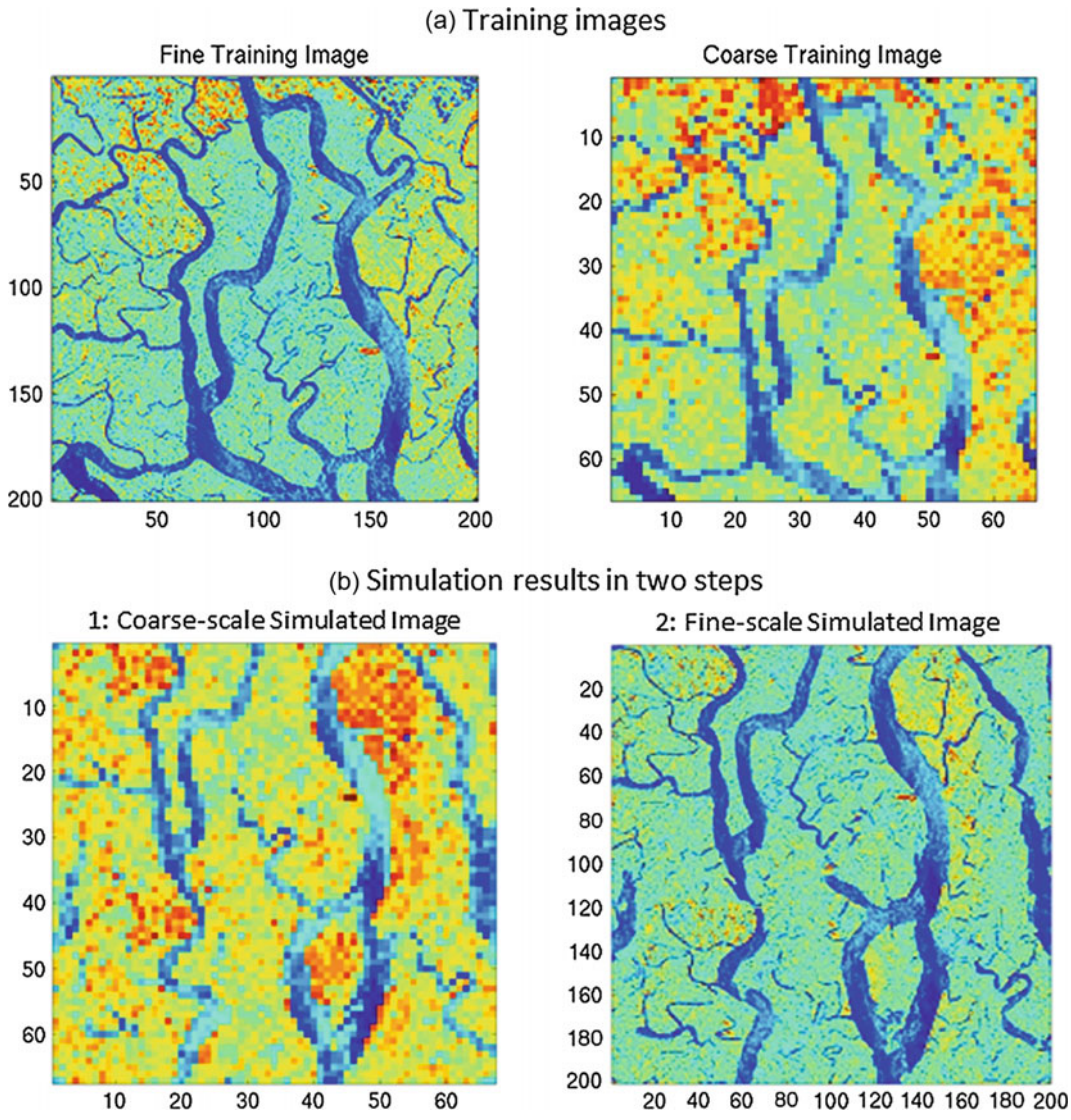

Fig. 4.14 The multiple-point geostatistics applied on channels: **a** Training images (at fine and coarse scales); **b** Simulation results in two steps; first at the coarse scale then at the fine scale given the realization simulated at the coarse scale (from Gardet et al. in press—courtesy of M. Le Ravalec, IFPEN)

according to this method (check Fig. 4.6). Object-based models can be combined with the above listed pixel-based models (i.e. simulations based on indicator/categorical variables), in order to get better representation of the investigated geological formations.

Methods for continuous variables

The above presented methods are used on indicator or categorical variables such as rock textures (i.e. mudstone vs grainstone), whereby the data is in the form of codes (check Table 3.1, Chap. 3). Other type of data are in the form of continuous numbers, e.g. dolomite%, porosity%, and well logs. These continuous variables are usually treated with sequential Gaussian and FFT-MA simulation methods.

Sequential Gaussian simulation SGSim is a widely used method involving the definition of a random path visiting all grid blocks of the model. For each block, SGSim determines the local distribution from simple kriging. Then it draws a value from this local distribution—assigned to the current grid block. Finally, it adds the simulated value to the data set. This method is efficient and it can be applied on any sort of grids. It provides conditional realizations (Le Ravalec et al. 2014).

FFT-MA simulation This method combines the moving average method with the fast Fourier transformation. The method performs the convolution product of the moving average method in Fourier space, making the computation of the moving averaging easy and fast. The FFT-MA method can generate efficiently large Gaussian realizations of any stationary covariance function (Le Ravalec et al. 2000; Hu and Ravalec-Dupin 2004).

4.1.2.3 Case Study: Geostatistical Modelling of the Upper Jurassic Arab D Reservoir Heterogeneity, Offshore Abu Dhabi, United Arab Emirates (Morad 2012)

The aim of this study is to statistically analyse the impact of diagenesis on reservoir-quality and to propose a specific workflow for modelling the spatial distribution of rock textures, diagenetic trends, and reservoir properties at a typical oil-field scale. Petrographic and petrophysical data from nine wells in a field offshore Abu Dhabi were first analysed. Then the distribution of facies/diagenetic phases and reservoir properties were modelled.

Geological Settings

The Arab Formation consists of four members, from bottom to top Arab D, C, B and A. The maximum flooding surface at the base of the formation (Arab D) is dated within the middle Kimmeridgian (about 153.5 Ma; MFS J70, Sharland et al. 2001), and the maximum flooding surface at the top of the formation (Arab A) overlaps with the Kimmeridgian-Tithonian boundary (150.75 Ma; MFS J100; Ehrenberg et al. 2007). In offshore Abu Dhabi the Arab Formation measures an average thickness of about 770 ft (235 m; Alsharhan and Magara 1994). Arab D and C members are the main reservoirs. The Arab B and A members, together with the overlying Hith Formation provide the appropriate sealing for the underlying reservoirs. The Arab D member is further subdivided into four layers (D5, D4, D3, D2; from bottom to top) (Morad et al. 2012).

A regressive part of a second-order supersequence represents the whole Arab Formation. The supersequence is composed of four-fold hierarchy ranging from sequences to cycles,

which due to the presence of barrier islands and a slope, were deposited on a distally steepened ramp characterized by an offshore break (Morad et al. 2012). Extensive lateral and vertical variations in the lithofacies are observed within the Arab D member depending on the location within the ramp (Al-Suwaidi and Aziz 2002). Supratidal algal laminated mudstone/evaporite and lagoonal evaporite, wackestones, and packstones are found on the inner ramp. The ramp crest comprises high energy deposits such as foraminiferal packstones, grainstones, floatstones, and intraclastic rudstones. The slope and outer ramp comprises open-marine bioturbated wackestones and mudstones (Fig. 4.15).

The evaporite content increases towards the top of the formation due to the generally prevailing isolated to semi-isolated lagoon. Fluctuations in relative sea level are interpreted to have been the main controls of the distribution and lithology patterns of the inner ramp deposits of the Arab Formation (Al Silwadi et al. 1996).

The Arab D member consists of five parasequence sets (PS), which have a shallowing-upward trend (Fig. 4.16). Each of these PSs starts with a deepening component (TST), which is overlain by a MFS/condensed section (CS), finally topped by a shallowing component (HST; Azer and Peebles 1998; Morad et al. 2012). A typical parasequence set (PS3; partially equivalent to Arab D3) of the Arab D limestone reservoirs are further analysed in this study.

Statistical Analysis

The PS3 succession comprises rock textures with the highest porosity and permeability values with respect to all investigated parasequences of the Arab D Member (Morad 2012). The available data of this parasequence set (PS3; Fig. 4.17) consisted of well core data (petrographic and petrophysical data) representing 600 depth-corresponding samples from nine wells. These "samples" (and corresponding values) have been statistically quantified and analysed (check Figs. 3.2, 3.3, 3.4, Chap. 3).

The PS3 stratigraphic interval includes four sedimentological depositional facies across the studied field (from northeast to southwest: lagoon, shoal, outer shoal, and outer ramp); all of which are intercepted by wells that are part of the data set (Fig. 4.17). Vertically, the PS3 comprises the cycles of D3L1 and D3L2, and ranges from 17 to 55 m in thickness (Fig. 4.16). The data set (~600 samples) in PS3 is characterized by considerably good reservoir properties, represented especially by high permeability values in grain-supported textures. PS3 includes a TST overlain by an important HST (Fig. 4.16).

The lagoon facies in PS3 (Fig. 4.17) has an average thickness of 17 m, and consists predominantly of packstone rock textures (Fig. 4.18a). Where grainstones prevail, considerable inter- and intragranular porosity (14–18 %) are observed, with low abundance of cement (e.g. syntaxial calcite overgrowth cement—SCOC; Fig. 4.18b).

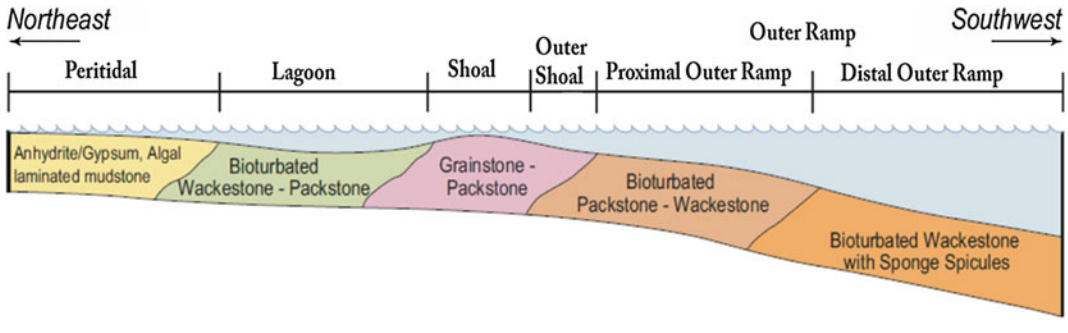

Fig. 4.15 Schematic depositional model of the Arab D and C members (from Morad et al. 2012)

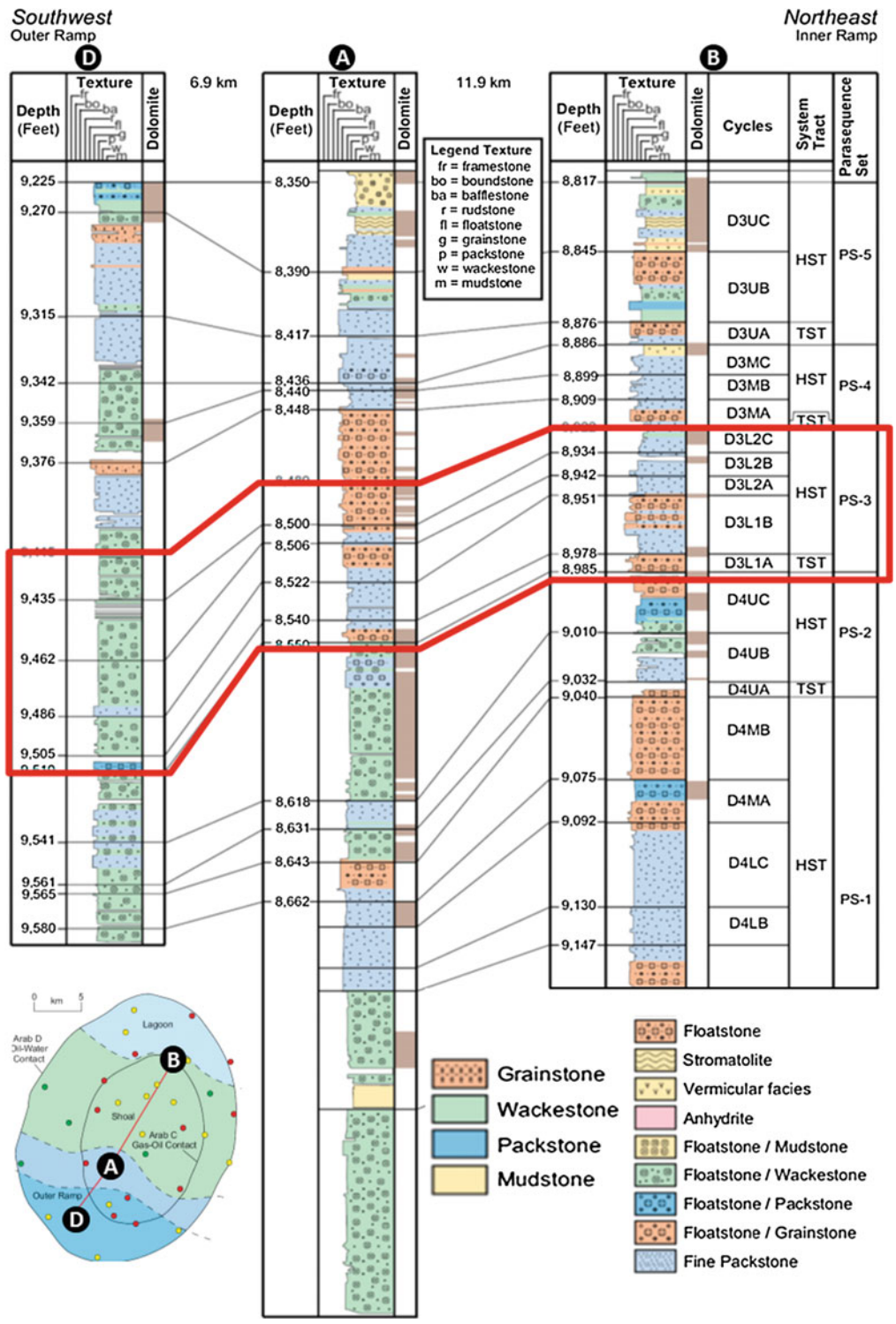

Fig. 4.16 Three well-logs from southeast outer ramp to the northeast inner ramp across the investigated field, showing the rock texture distribution of the investigated parasequence set (PS3, *red outline*)—from Morad et al. (2012)

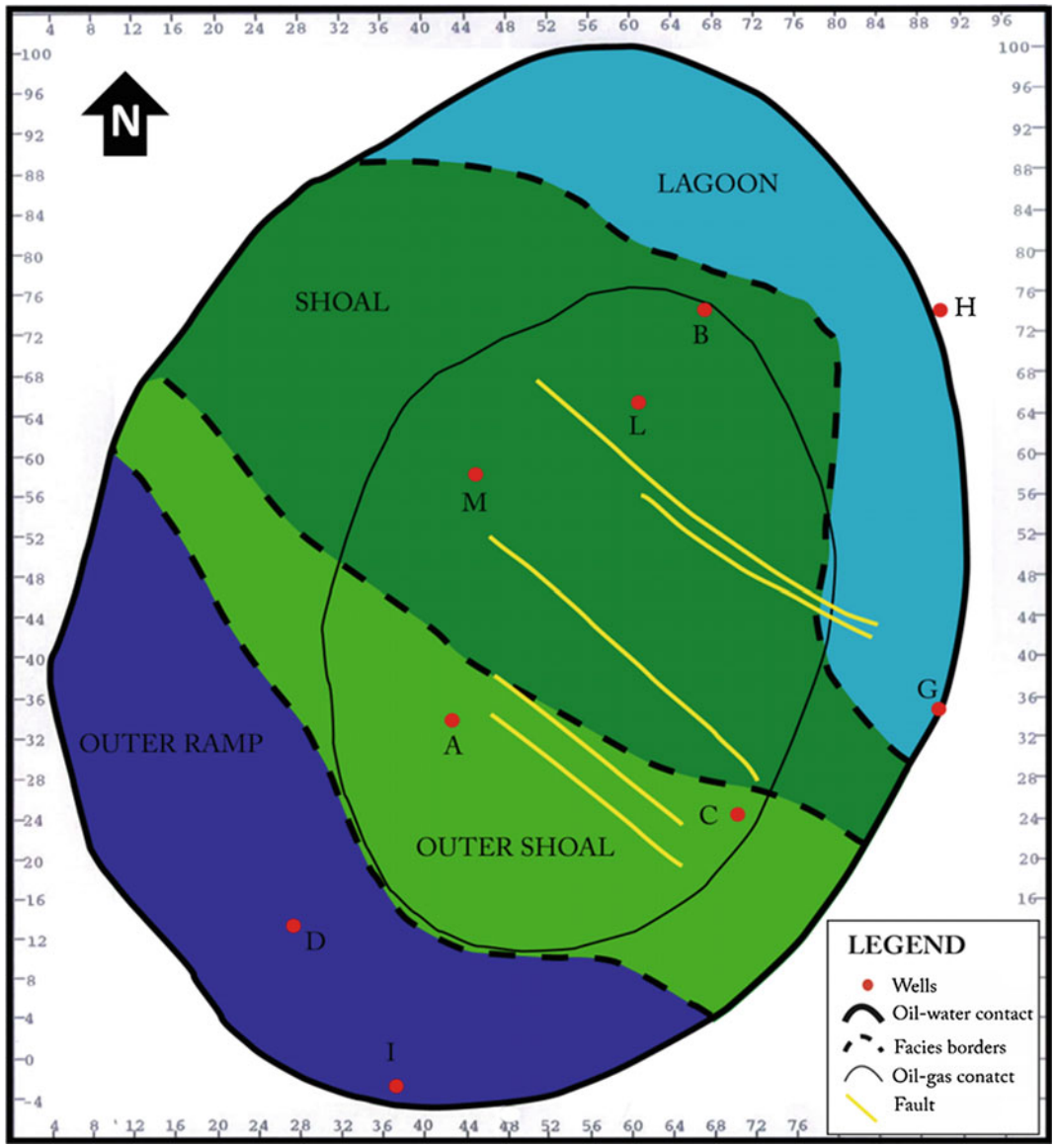

Fig. 4.17 Simplified map showing the investigated field (~20 × 25 km) at the PS3 interval, the extent of the depositional facies, as well as the locations of wells

Muddy textures with relatively sparse dolomite content (low permeability, ca. 2 mD) also characterize the lagoon facies in PS3.

The thickness of the shoal facies in PS3 ranges from 19 to 55 m. Here, the most permeable grainy textures (around 1600–3900 mD) within the investigated database (for PS3) are observed. These rock textures are characterized by relatively larger intergranular macro-porosity and common abundance of SCOC (occurring almost in half of the investigated samples) (Fig. 4.19a). The syntaxial calcite cement grows especially around crinoids fragments and appears to be associated with considerable intergranular porosity. Packstone textures are also found and they are characterized by low abundances of cement and dolomite (Fig. 4.19b). The shoal facies also include partially dolomitized muddy

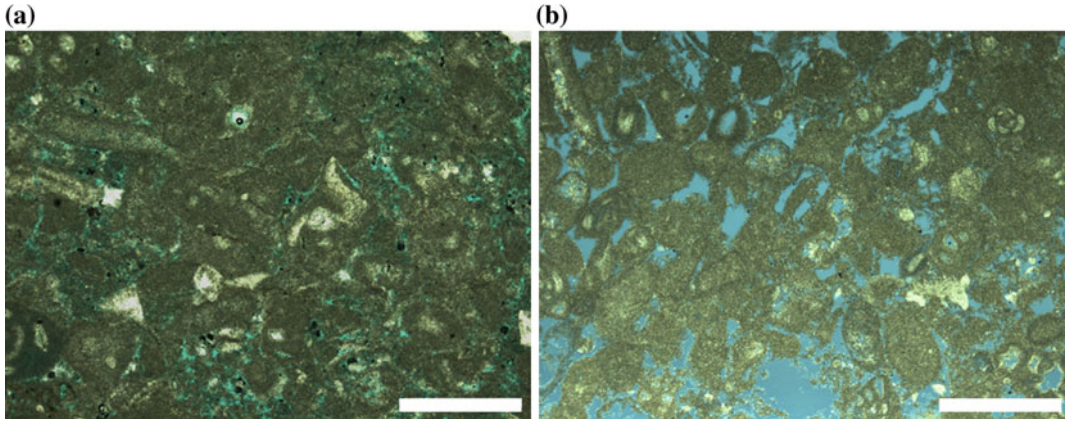

Fig. 4.18 Photomicrographs (PPL) displaying characteristic lagoon microfacies in PS 3: **a** Packstone with low inter- and intragranular porosity in well H, 9967 ft (~3038 m); **b** Grainstone containing relatively high inter- and intragranular porosity in well H, 8955 ft (~2729 m). Scale bars represent 1 mm

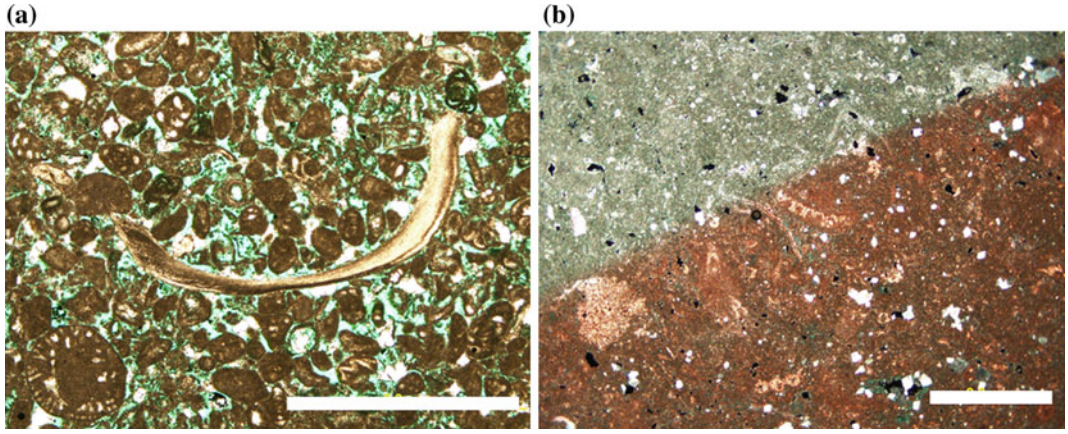

Fig. 4.19 Photomicrographs (PPL) displaying examples of shoal microfacies in PS 3: **a** Grainstone with high porosity in well L, 11731 ft (~3576 m); **b** Wackemudstone with bioclasts in well L, 10768 ft (~3282 m) (partially stained thin section; *red* is calcite, *white* is dolomite). Scale bars represent 2 mm

textures with significant porosity and permeability values (14–22 % and up to 184 mD).

The thickness of the outer shoal facies of PS3 ranges from 21 to 29 m, while the main rock textures are grain-supported (Fig. 4.20a). They resemble their equivalent in the shoal, but with considerably lower permeability values (one order of magnitude lower). The packstone textures are characterized by relatively good reservoir properties and with rare/common SCOC (Fig. 4.20b). Moderately dolomitized muddy textures, with relatively low flow properties are also found, still to a lesser extent.

The outer ramp facies in PS 3 has a thickness of 29–30 m. Muddy textures (mudstone/wackestone), with low dolomite content and low reservoir properties dominate the related dataset (Fig. 4.21a). To a lesser extent, packstone and wackestone textures are also found in the outer ramp facies (Fig. 4.21b). They are characterized by relatively low flow properties.

The statistical analysis of petrographic and petrophysical data (from well cores) is summarized in Table 4.1 (check also Fig. 3.3, Chap. 3). Data are organized by depositional facies (distributed across the oilfield) and rock textures.

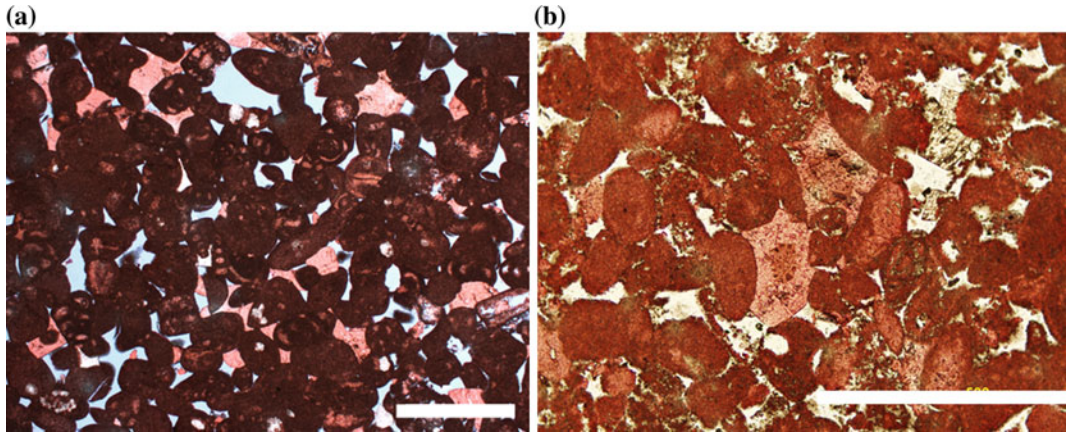

Fig. 4.20 Photomicrographs (PPL) displaying characteristic outer shoal microfacies in PS3: **a** Grainstone/packstone with relatively low intragranular and mouldic porosity and with relatively abundant SCOC in well C, 8845 ft (~2696 m); **b** Grain-Packstone with SCOC in well A, 8523 ft (~2598 m) (stained thin section; *red* is calcite, *white* is dolomite). Scale bars represent 1 mm

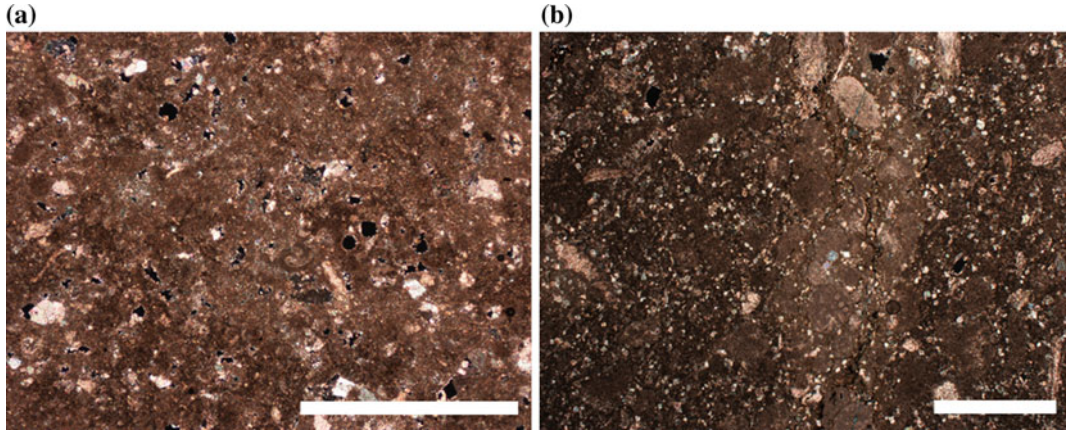

Fig. 4.21 Photomicrographs (PPL) displaying characteristic outer ramp microfacies in PS3: **a** Wackestone with scattered calcite cemented moulds in well I, 10,060 ft (~3066 m); **b** Moderately dolomitized wacke-mudstone in well I, 10,033 ft (~3058 m). Scale bars represent 1 mm

Then, those rock textures with specific diagenetic phases such as partial cementation (SCOC) and dolomitization are presented separately with the corresponding porosity and permeability values.

The highest observed porosity in the PS3 generally occurs in the grainstones and packstones of the shoal and outer shoal facies (average ~20–25 %). Such grainy rock textures (grainstones and packstones), show a higher average porosity (5–15 %) where syntaxial calcite cement (SCOC) is common (grown typically around fragments of crinoids commonly found in deeper shoal and outer shoal depositional environments) (Fig. 4.22a, c). Muddy textures show relatively lower (macro-)porosity values in the shoal facies (17 %), where scarce dolomite content (<10 %) is associated with relatively higher porosity values (Fig. 4.22d). The lagoon and outer ramp are characterized by relatively lower porosity values (9–14 %).

The highest observed permeability values occur in the grainy textures of the shoal facies in

Table 4.1 The quantitative impact of diagenesis on reservoir quality for the various depositional facies and rock textures in PS3

Facies (wells)	Diagenetic process		Av. Φ (%)	Av. K (mD)	Nr of samples	Thickness (ft)	Frequence (%)
Lagoon (G, H)						55 - 56	
Muddy textures	>>>		10	2	17		24
Packstone textures	>>>		14	13	38		59
Packstone textures	>>> Common SCOC	>>>>	14	24	4		
Grainy textures	>>>		14	59	10		17
Grainy textures	>>> Common SCOC	>>>>	18	568	2		
Shoal (B, L, M)						62 - 181	
Muddy textures	>>>		14	7	27		19
Muddy textures	>>> Dolomite < 10%	>>>>	22	184	18		
Packstone textures	>>>		22	106	75		38
Packstone textures	>>> Common/Abundant SCOC	>>>>	26	609	15		
Grainy textures	>>>		26	1644	50		43
Grainy textures	>>> Common/Abundant SCOC	>>>>	24	3907	53		
Outer Shoal (A, C)						70 - 96	
Muddy textures	>>>		9	1	10		13
Muddy textures	>>> Dolomite > 75%	>>>>	12	7	3		
Packstone textures	>>>		20	61	20		35
Packstone textures	>>> Common SCOC	>>>>	22	200	15		
Grainy textures	>>>		15	128	22		52
Grainy textures	>>> Common/Abundant SCOC	>>>>	25	285	28		
Outer Ramp (D, I)						95 - 99	
Muddy textures	>>>		9	1	156		83
Packstone textures	>>>		9	0,7	31		17

Values without any impact of diagenesis are shown first for each rock texture, followed by values that take diagenesis into account (in bold). SCOC—syntaxial calcite overgrowth cement

PS3 (up to 3900 mD). The same textures have values of one order of magnitude lower in the lagoon and outer shoal facies. The packstone textures are relatively high-permeable in the shoal and outer shoal. The common/abundant occurrence of SCOC seems to be associated with higher permeability values generally in grainstone and packstone textures (Fig. 4.22a; check also Fig. 3.3). Muddy textures show only good permeability in the shoal, where values are considerably higher (from 7 to 184 mD; Table 4.1) in samples that undergone slight dolomitization (<10 %; Fig. 4.22b).

Geostatistical Simulations

The distribution of the above presented rock textures across the investigated field (constrained by their depositional environments spatial configuration) together with the impacts of specific diagenetic trends on petrophysical properties, has been achieved through geostatistical modelling. The diagenetic trends refer to observed relationships ("rules") made upon quantitative and statistical analyses (above), whereby the presence of a specific type of cement (i.e. SCOC) in grainstones/packstones and the extent of dolomitization in wackestones/mudstones appear to co-relate to "samples" with relatively higher reservoir properties, compared to those similar rock textures in the same depositional environments. Accordingly, we called "drivers" or "proxies" these (semi-)quantified diagenetic phases that appear to impact the reservoir properties (and imply "diagenetic trends").

The followed workflow for modelling the depositional facies distributions and diagenetic trends of the PS3 interval of Arab D reservoirs in the investigated field involved several steps (Fig. 4.23). First, a statistical analysis has been undertaken to investigate quantitatively the rock

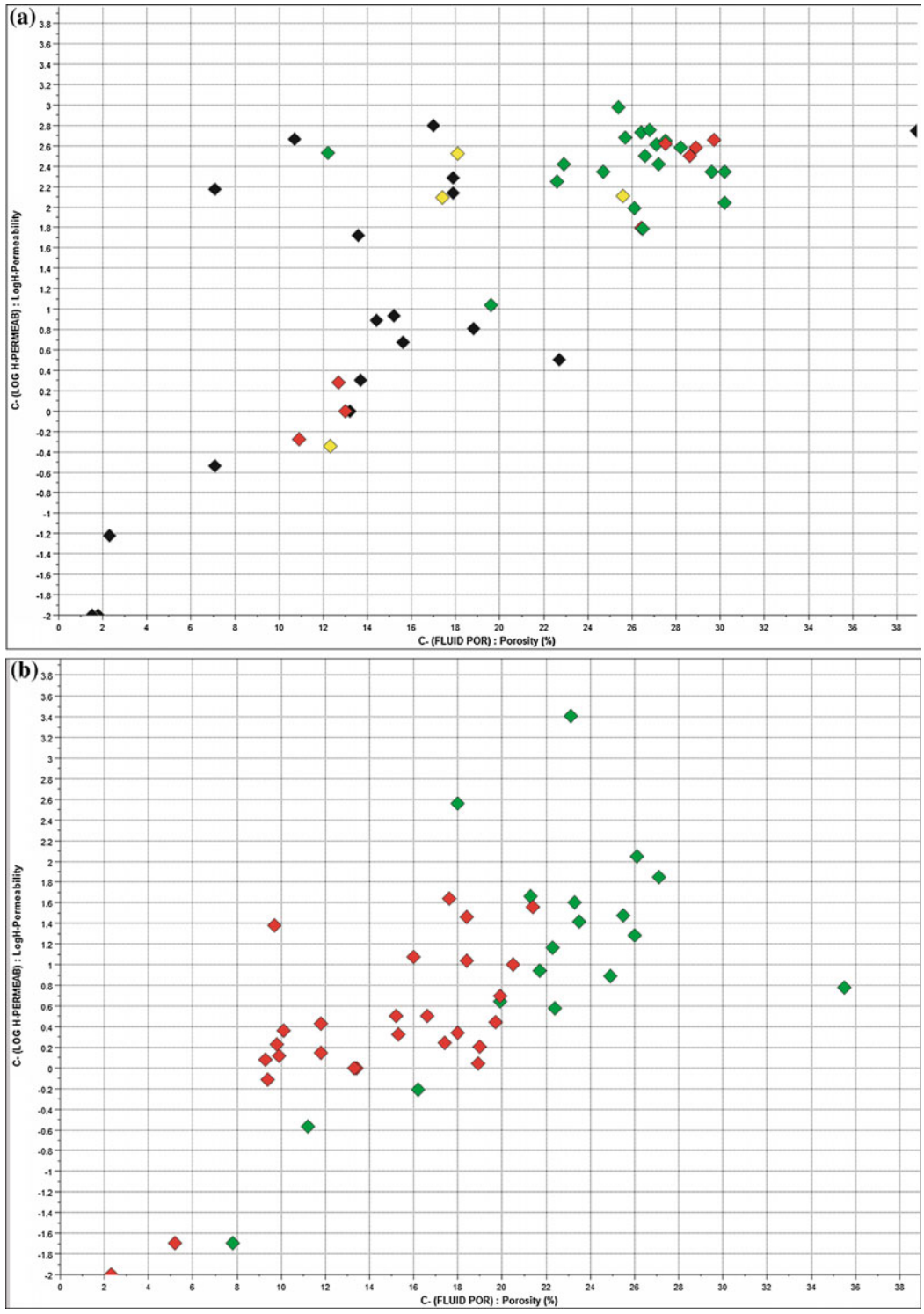

Fig. 4.22 Cross-plots of bulk porosity (%) versus log-permeability analysed based on the abundance of SCOC and dolomite% within the PS3: **a** Poro/perm plot featuring highest porosity and permeability values for grainy textures of the outer shoal in PS3 with common/abundant SCOC (*Red* = abundant, *green* = common, *yellow* = rare, *black* = absent); **b** Most of the samples with minor dolomite content (<10 %, *green*) have relatively moderate to high poro/perm values compared to those with higher dolomite content (>10 %, *red*)

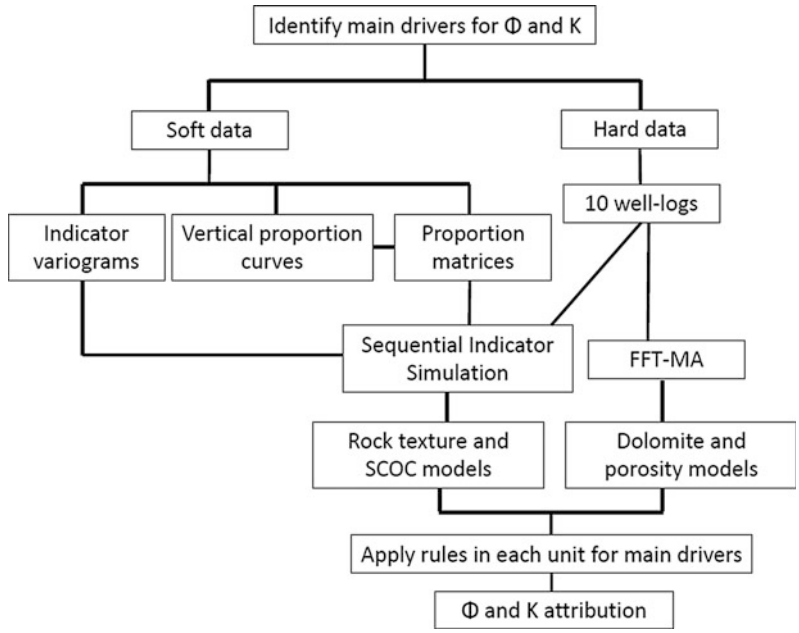

Fig. 4.23 Geostatistical modelling workflow for the distributions of rock textures (in three classes: grainy, packstone, muddy), the SCOC (in four classes: absent, rare, common, abundant), dolomite (%) and porosity (%) in PS3 (from Morad 2012). In order to investigate the diagenetic trends (impacts of diagenesis on reservoir properties), rules linking diagenetic drivers (e.g. SCOC, dolomitization) to observed changes of the corresponding reservoir properties have been applied, and resulted in attributed porosity and permeability distributions in a geomodel

textures distribution and to identify the main diagenetic drivers for porosity and permeability (e.g. SCOC/Dolomite%, see above). Then, the gridded model (of the studied field) was constructed including the available hard data (discretized well logs)—soft data will be interpolated. Simulations (multi-realizations) were achieved to infer the soft data distribution between cells informed with hard data; e.g. (semi-)quantitative distributions of rock textures (Grainy-Packstone-Muddy), SCOC (absent/rare to abundant), dolomite (%), and porosity (%). This step involves the definition of variograms, vertical proportion curves VPC, and vertical proportion matrices VPM (see above). Simulations were achieved by the SIS and FFT-MA methods to reproduce the distribution of rock textures and SCOC as well as dolomite% and porosity, respectively (Fig. 4.23). Rules for the main diagenetic drivers of porosity and permeability, are thereafter proposed and applied. For instance, where "common or abundant SCOC" is present, in grainstones and packstones, the average permeability values is doubled, based on the statistical analysis (Table 4.1). Finally, the applied rules are used to attribute porosity and permeability values across the reservoir model taking into account the simulations (realizations) for rock textures distribution.

Rock Textures Distribution First, it has to be noted that the rock textures distribution of PS3 is related to the geographic configuration of the depositional environments (see Fig. 4.17), which shows a NW-SE orientation (here, defined as azimuth N110°) of a ramp system (discussed above).

The workflow for the geostatistical simulation of the rock textures distribution, was therefore based on the depositional facies map (Fig. 4.17) and the computed vertical proportion curves (VPCs) of the discretized wells at the PS3 interval (Fig. 4.24). In order to better constrain the distribution of rock textures as a function of

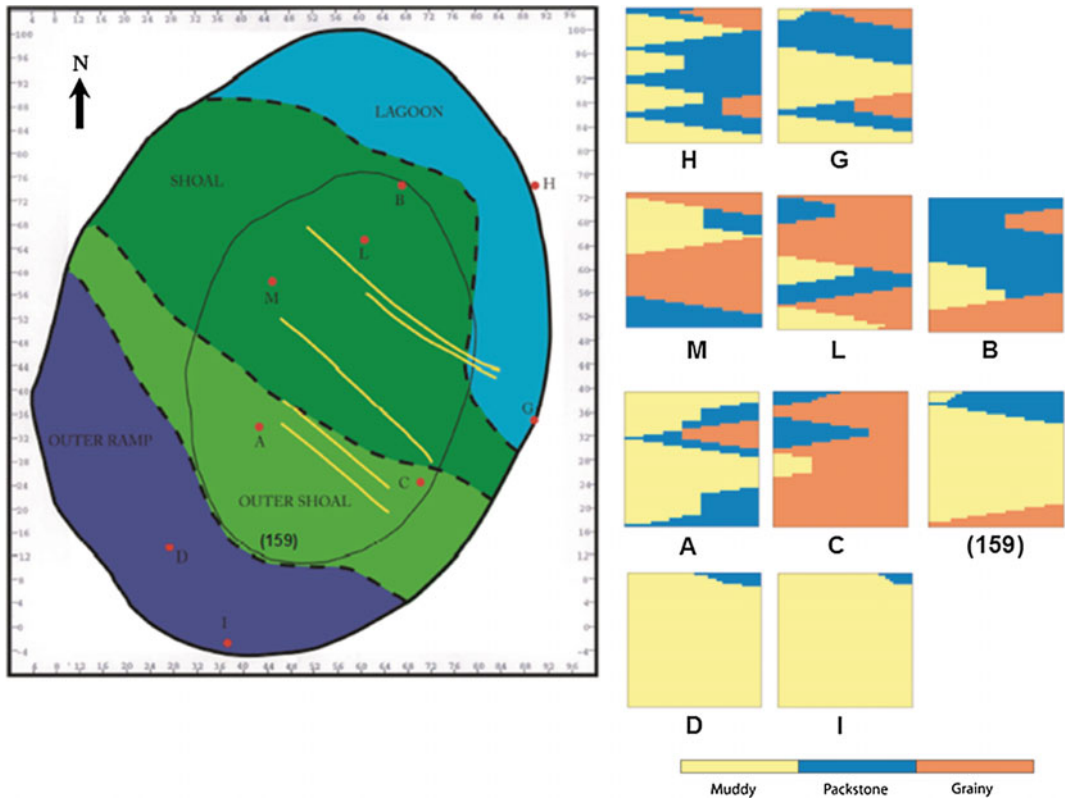

Fig. 4.24 *Left* Depositional facies map showing the location of the wells (hard data) across the investigated field. *Right* Computed vertical proportion curves (VPCs) representing the vertical rock textures distributions in each of the ten wells

the extent depositional, a property map was created (Fig. 4.25). This map consists of four areas corresponding to the lagoon, shoal, outer shoal and outer ramp environments. With this constraining map and VPCs (corresponding to well hard data), the proportion matrix (Fig. 4.26) was produced (for more details, check Methodology section above).

The used method for simulations of rock texture distribution is the Sequential Indicator Simulation (SIS; for further information check Methodology above). A specific orientation was adopted (azimuth N110°) based on the known depositional facies spatial configuration (Table 4.2). Other simulation parameters such as ranges (X, Y and Z) and sill were defined arbitrarily based on data range of magnitudes and trial and errors.

Once the variogram parameters are defined and the proportion matrix computed, the simulation of the distribution of rock textures in PS3 was achieved (Fig. 4.27). It illustrates the pre-dominance of grainy textures in the areas representing the shoal and lagoon facies. To a lesser extent, grainy textures are also found in the outer shoal facies in the south-eastern part of the studied field. Packstone rock textures characterize lagoon, outer-shoal and outer-ramp areas (compare Fig. 4.27 and Fig. 4.24). The muddy rock texture are predominant in the outer ramp area. They are also found in the lagoon area.

Geostatistical modelling resulted in correctly distributing the rock textures according to the selected simulation method (here, SIS) between the wells (control points). The statistical data collected from well cores has been honoured at the well locations. The property map, is a constraining tool proposed by the sedimentologist in order to group those wells that are believed to penetrate facies relating to specific depositional

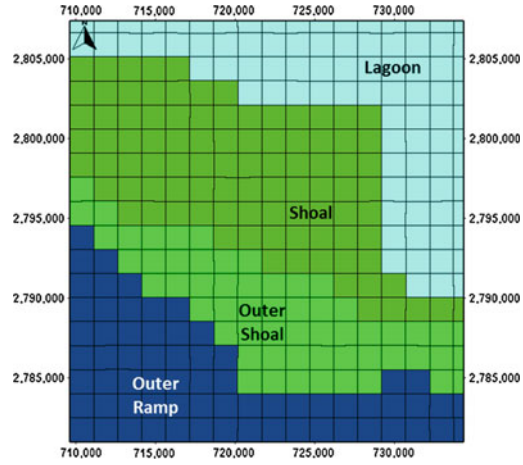

Fig. 4.25 Property map showing the extent of the depositional environments (i.e. areas). Through the implementation of these areas, the computed VPCs for the corresponding wells will be grouped (e.g. Wells H and G assigned for Lagoon Area). The computed proportion matrix (VPM; Fig. 4.26) will honour this geographical zonation

environments. It is important to note that this modelling method remains stochatsic (non-deterministic) and will not result in precise allocation of the exact rock textures in the geomodel. Each realization (simulation) will show different rock textures distributions. Yet, all of

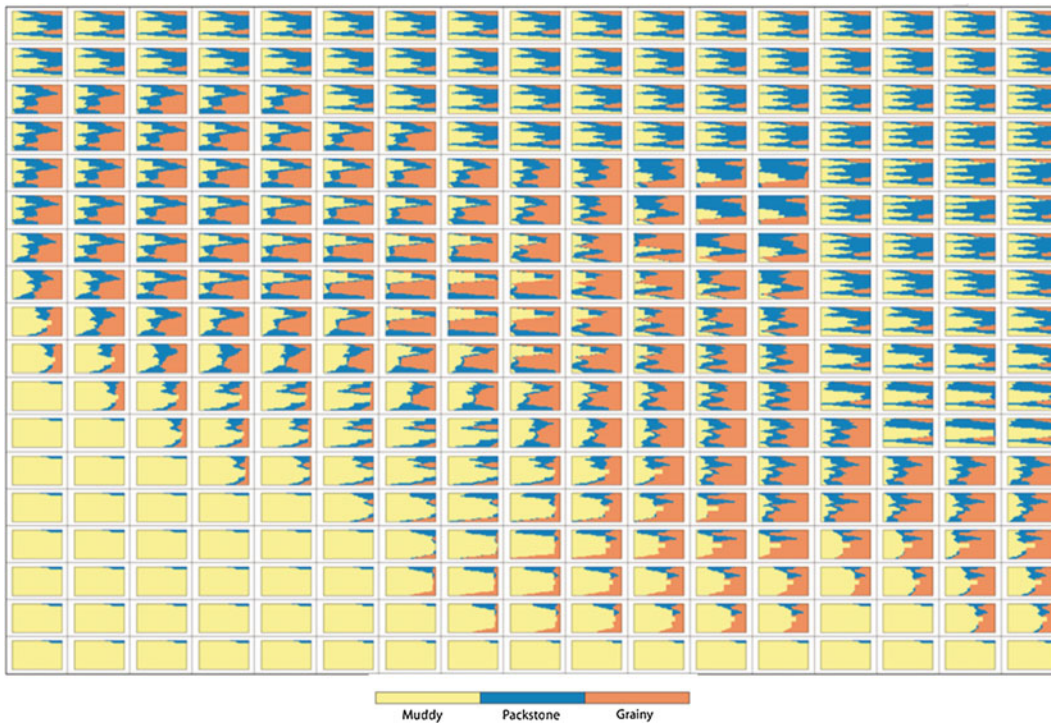

Fig. 4.26 Constrained proportion matrix (VPM) for rock textures in PS3 with a grid of 10 × 10 for X and Y. Grainy textures dominate in the shoal and in some parts of the outer shoal facies, as expected

Table 4.2 The simulation method and variogram values for the rock textures distribution of PS3

Method	RangeX	RangeY	RangeZ	Azimuth	Sill
SIS	6000	3000	1	110	0.10

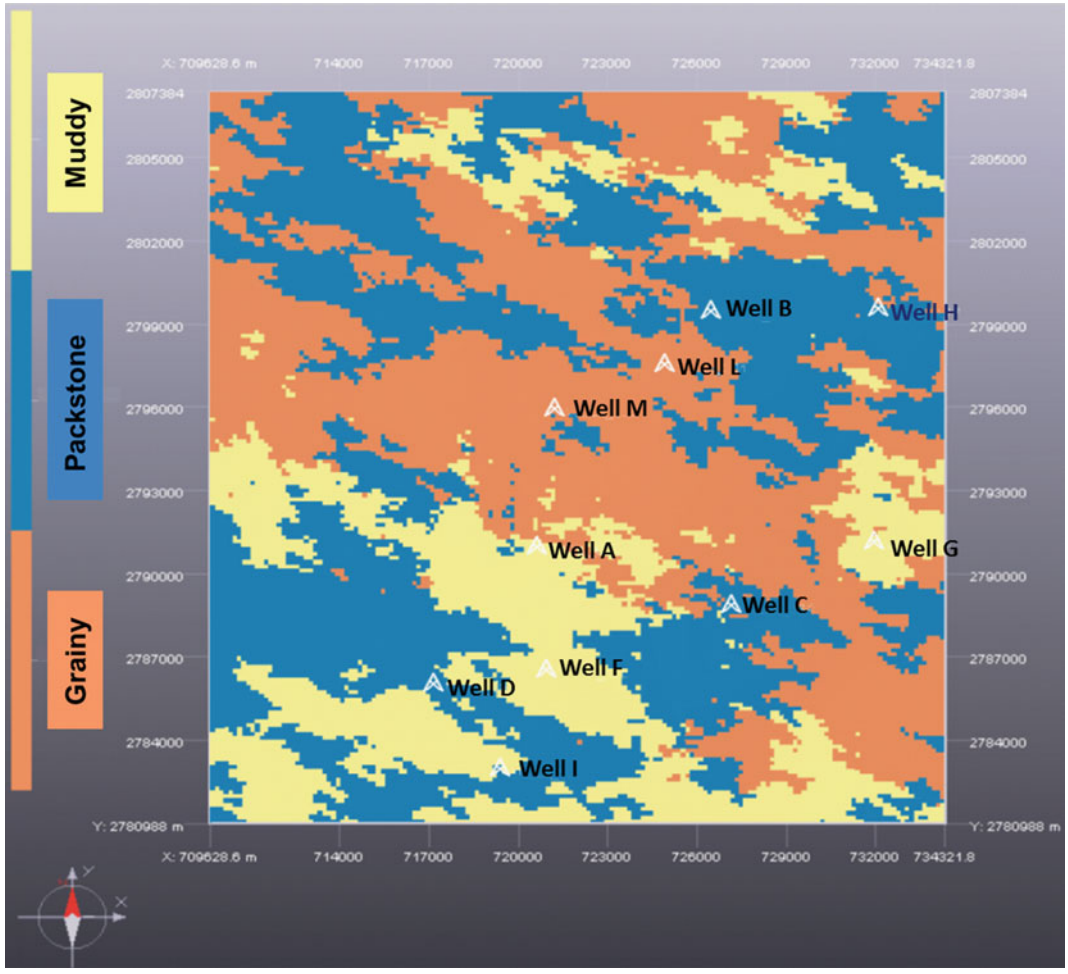

Fig. 4.27 *Top view* of the modelled rock textures distribution in PS3 (see text for details). While this realization illustrates the heterogeneous distribution of rock textures across the PS3, predominance of grainy and muddy textures in the areas where the shoal and outer ramp have been assigned has been correctly produced

them will portray the geostatistical rules that were implemented and will therefore present logical, probable distributions.

Syntaxial Calcite Overgrowth Cement (SCOC) Distribution The occurrence of common/abundant SCOC was used as a discrete property. The SCOC was imported as classes: 1 = absent, 2 = rare, 3 = common, and 4 = abundant. The same workflow, which was followed to model the rock textures distribution (see above), has been used for the SCOC distribution modelling (Fig. 4.28).

The abundance of the syntaxial calcite overgrowth cement (SCOC) is related to the rock textures (mostly in grainstones and packstones) and the presence of crinoids (as it grows on

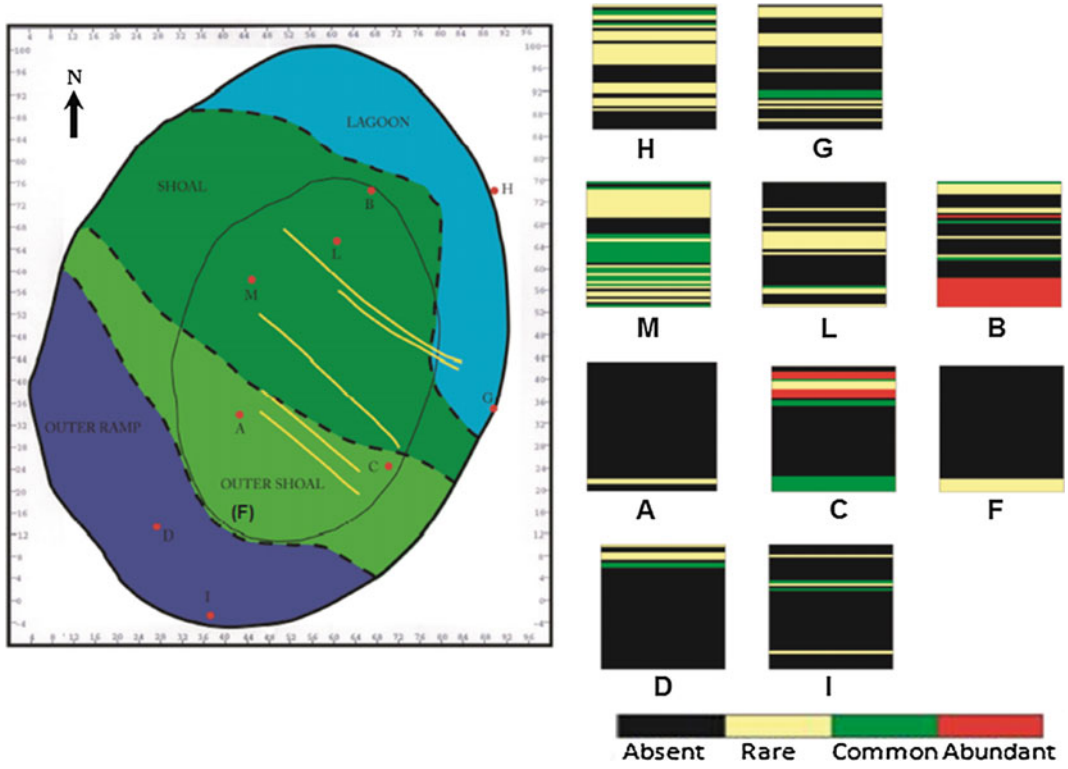

Fig. 4.28 *Left* Depositional facies map showing the location of the wells (hard data) across the investigated field. *Right* Reported well-logs data representing the vertical SCOC abundance distributions in each of the ten wells

fragments of crinoids in deeper outer-marine depositional realms). Therefore, the quantitative proportional abundance map of SCOC in grain-supported rock textures across the field (check Fig. 3.4), has been used as a constraining property map (Fig. 4.29) for the computation of the proportion matrix (VPM; Fig. 4.30).

The proportion matrix (VPM) was computed taking into account the proposed constraining property map. In this case, the values on the map of constraint are used as quantitative data in the kriging system to compute the proportion matrix. To model the distribution of SCOC across the study area (field), we chose a similar method as used for the simulation of rock texture distribution (i.e. Sequential Indicator Simulation, SIS). Since, the modelled cement is genetically associated to the rock textures, the same specific orientation was adopted (azimuth N110°) (Table 4.3). Other simulation parameters such as ranges (X, Y and Z) and Sill were defined arbitrarily based on data range of magnitudes and on trial and errors.

The simulation of SCOC distribution in the PS3 suggests patches of common occurrences in the northern and western part of the field (Fig. 4.31). The simulation does not show clear occurrence of abundant SCOC; this may be explained by very low frequency of "abundant" SCOC in the data set (check Figs. 3.3 and 3.4, Chap. 3). The simulation results are coherent with the proportion matrix and the VPCs. SCOC is commonly found in the northern and western parts of the grid (field; Fig. 4.31). The modelled distribution is quite heterogeneous (patchy) as it obeys to the statistical scattering computed from well data and the constraining property map. One should not consider the resulted simulation as an

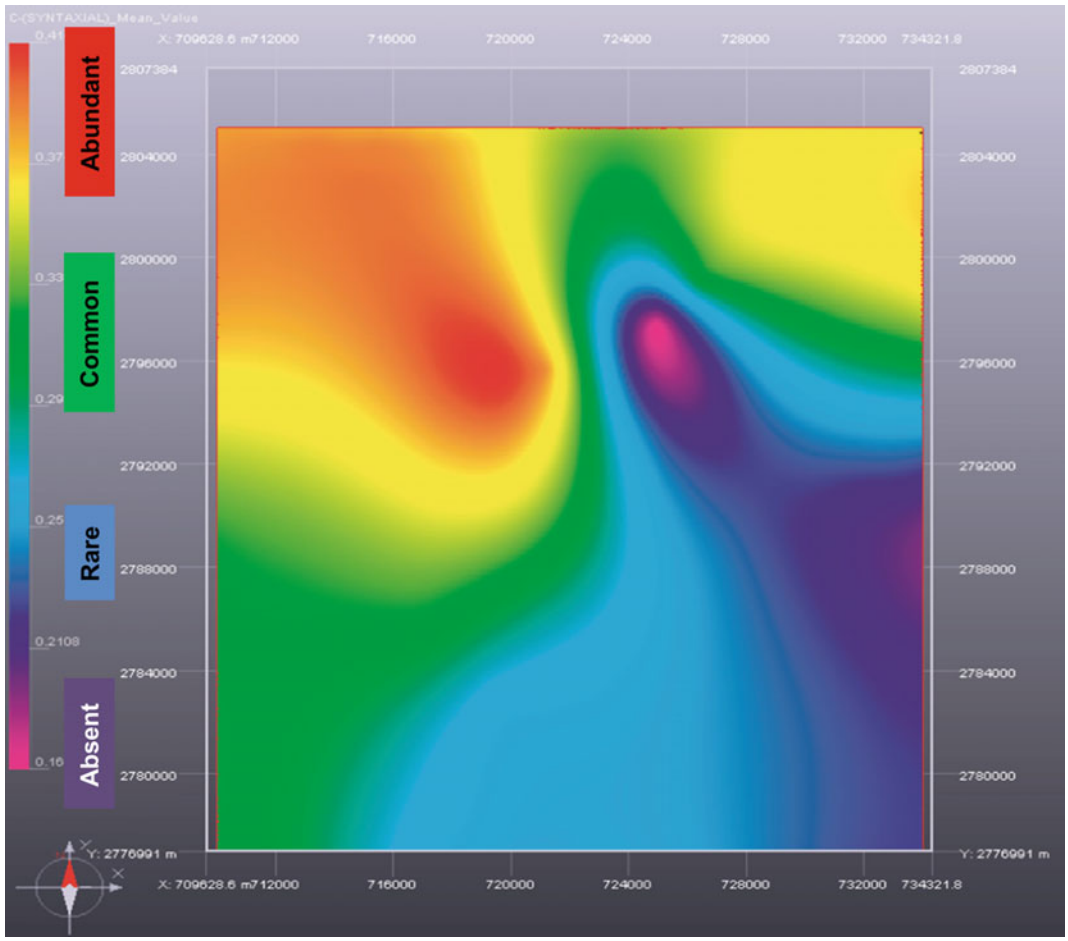

Fig. 4.29 Property map for constraining the distribution of SCOC in PS3. The map shows the proportional abundance of the SCOC in grain-supported rock textures in Arab D member interpolated from well data (cumulated proportions of the SCOC in the stratigraphic unit). We assumed that the PS3 (typical rock sequence of the Arab D member) will have similar abundance distribution

exact map of the common presence of SCOC, rather as a logical probable distribution.

The syntaxial calcite overgrowth cement, whose presence in the grain-supported textures have been co-related to relatively higher permeability values (see above), seems to be common in the areas corresponding to lagoon, shoal and outer shoal. Besides, Fig. 4.31 shows that within these areas only the northern and western parts display common SCOC.

Dolomite Distribution Since the amount of dolomite in the investigated samples (well data) is a continuous property (in % of bulk rock) we chose to simulate it by using the FFT-MA method (see above for details, Methodology). A quite similar workflow (to the above presented workflows for rock textures and SCOC distributions) was followed to model the dolomite % distribution across the investigated field. The resulting simulation represents the heterogeneous patchy distribution of dolomite across in PS3 (Fig. 4.32). Relatively, larger patches of considerably high dolomite% are found on the eastern and southern parts of the grid (areas corresponding principally to lagoon and outer ramp depositional facies; Fig. 4.32).

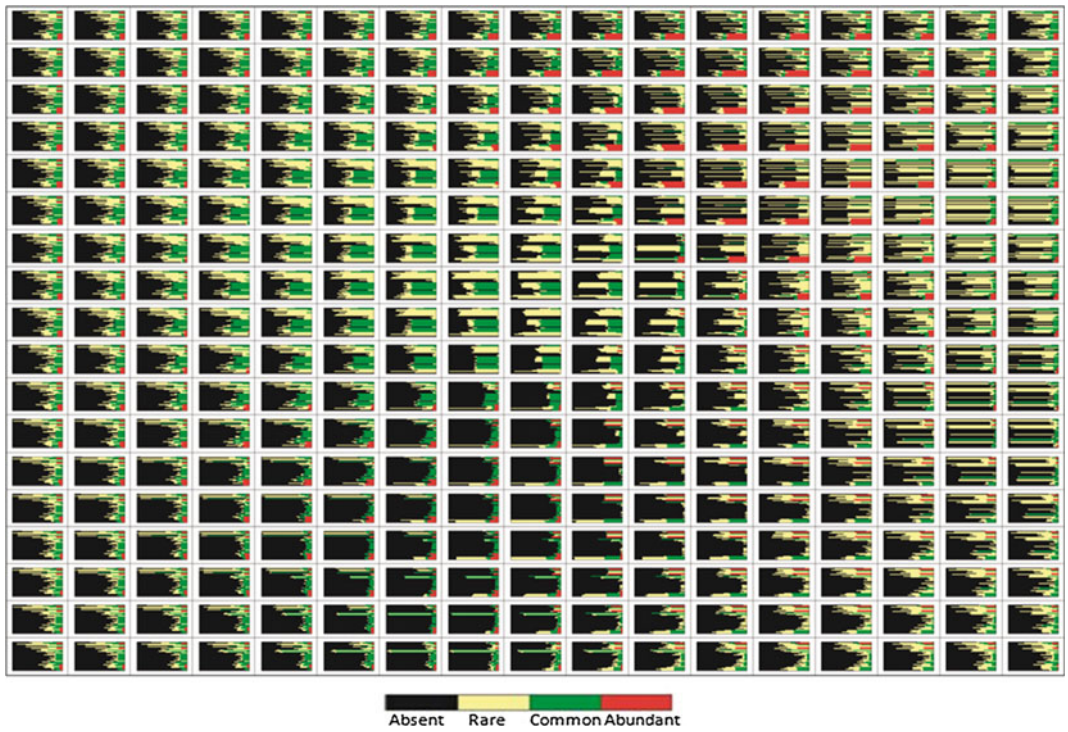

Fig. 4.30 Constrained proportion matrix (VPM) for SCOC in PS3 with a grid of 10 × 10 for X and Y. Abundant (*red*) and common (*green*) occurrences of cement are principally observed in the northern part of the grid

Table 4.3 The simulation method and variogram values for the SCOC distribution of PS3

Method	RangeX	RangeY	RangeZ	Azimuth	Sill
SIS	6000	3000	1	110	0.10

Porosity and Permeability Attribution The attribution of petrophysical properties (porosity and permeability) is based on the results of the statistical analysis that was undertaken on the available data-set (summarized in Table 4.1). Results of the geostatistical modelling (rock textures, classes of SCOC, proportion of dolomite) performed for PS3 were used for the assignment of porosity and permeability average values according to the rules defined for the diagenetic drivers (i.e. SCOC and dolomite).

Practically, the geomodel represents the geostatistical distribution of the rock textures (grainy, packstone, and muddy) together with the patchy distribution of SCOC classes and dolomite%. The average values of porosity and permeability for each rock texture categories (presented in Table 4.1) was attributed in this geomodel. Values were rounded off to nearest 5 % ratio.

In order to map the spatial impact of diagenesis on the reservoir properties, the diagenetic "drivers" (i.e. SCOC and dolomite, whose distribution has been modelled) are used to propose "rules" linking their presence with altered porosity and permeability values.

Two simplified rules were applied for redistributing the porosity and permeability: (i) Porosity and permeability average values for samples with "common" and "abundant" SCOC (bold in Table 4.1), are attributed to cells with

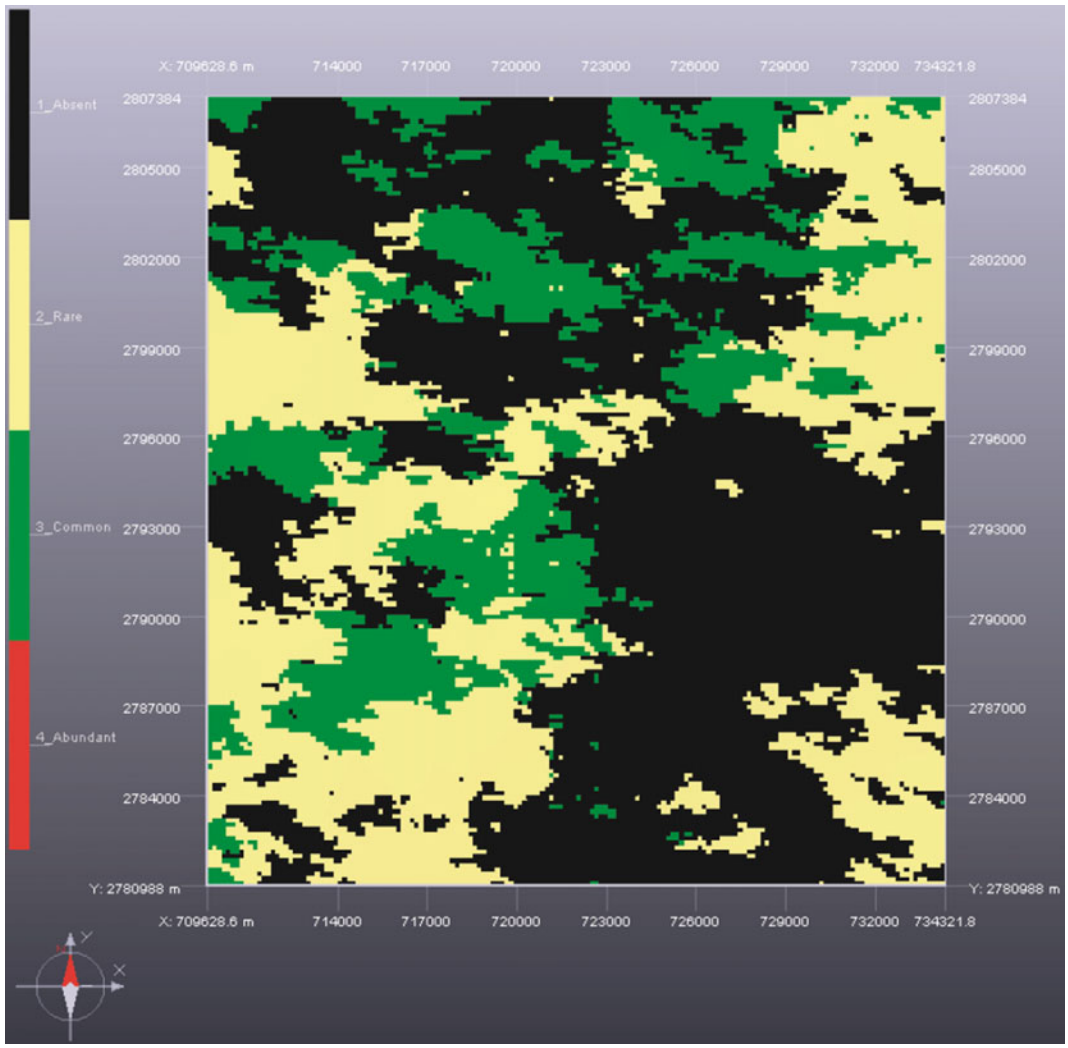

Fig. 4.31 *Top view* of the modelled SCOC distribution in PS3 (see text for details). Common occurrence (in *green*) of this cement is mostly noticed in the northern and western part of the grid

grainy and packstone rock texture in PS3, instead of the overall average porosity and permeability values; (ii) Porosity and permeability average values associated with dolomite% (bold in Table 4.1) are similarly attributed to muddy rock textures in the geomodel.

The resulting simulations (Figs. 4.33 and 4.34) illustrate the realistic aspect of heterogeneities of the PS3 reservoirs and the impact of diagenetic trends on porosity, and especially permeability. Modelling results of PS3 illustrate the heterogeneous central part of the investigated field, where the highest porosity and permeability values are observed, particularly in areas where grainy textures are present. Areas with high dolomite content are generally associated with lower porosity and permeability values, except in the outer shoal facies, where high dolomite content seems to enhance the permeability values (Fig. 4.34).

The constructed geomodel was capable of reproducing a heterogeneous distribution of reservoir rocks based on the original depositional facies and known diagenetic trends. This

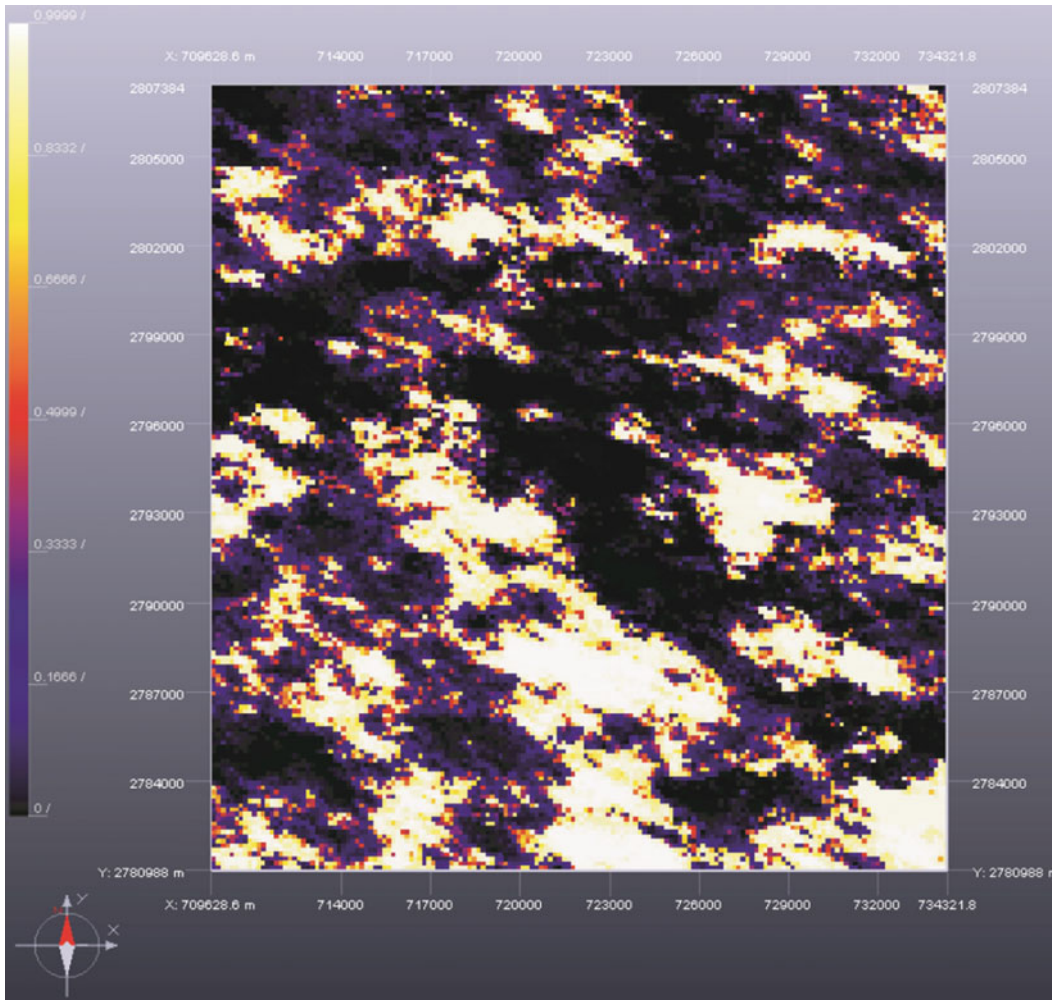

Fig. 4.32 *Top view* of the modelled dolomite distribution in PS3 (see text for details). Here, completely dolomitized (large patches in *white*, up to 100 % dolomite) are observed mainly in the southern part of the grid, in the areas which correspond to the outer shoal and outer ramp facies. *Black shades* represent almost 0 % dolomite

has been done following several steps and combining methods and software packages (EasyTrace™, CobrafLow™, GOCAD). Still, the resulted simulations/realizations are not deterministic. They represent logical, highly probable distributions that are governed by the input 'hard' well data, geological constraints (depositional environment maps, diagenesis), and statistical analysis of petrographic and petrophyscial data.

Although, the shoal facies includes the most optimal reservoir rocks, their heterogeneity in terms of porosity and permeability values is difficult to assess. The proposed workflow helps in illustrating such heterogeneity and applying specific controls on its stochastic distribution. Particularly, the grain-supported limestone textures (pack-/grainstones and grainstones) characterize chiefly the shoal and outer shoal facies. These represent the best reservoir rocks, where

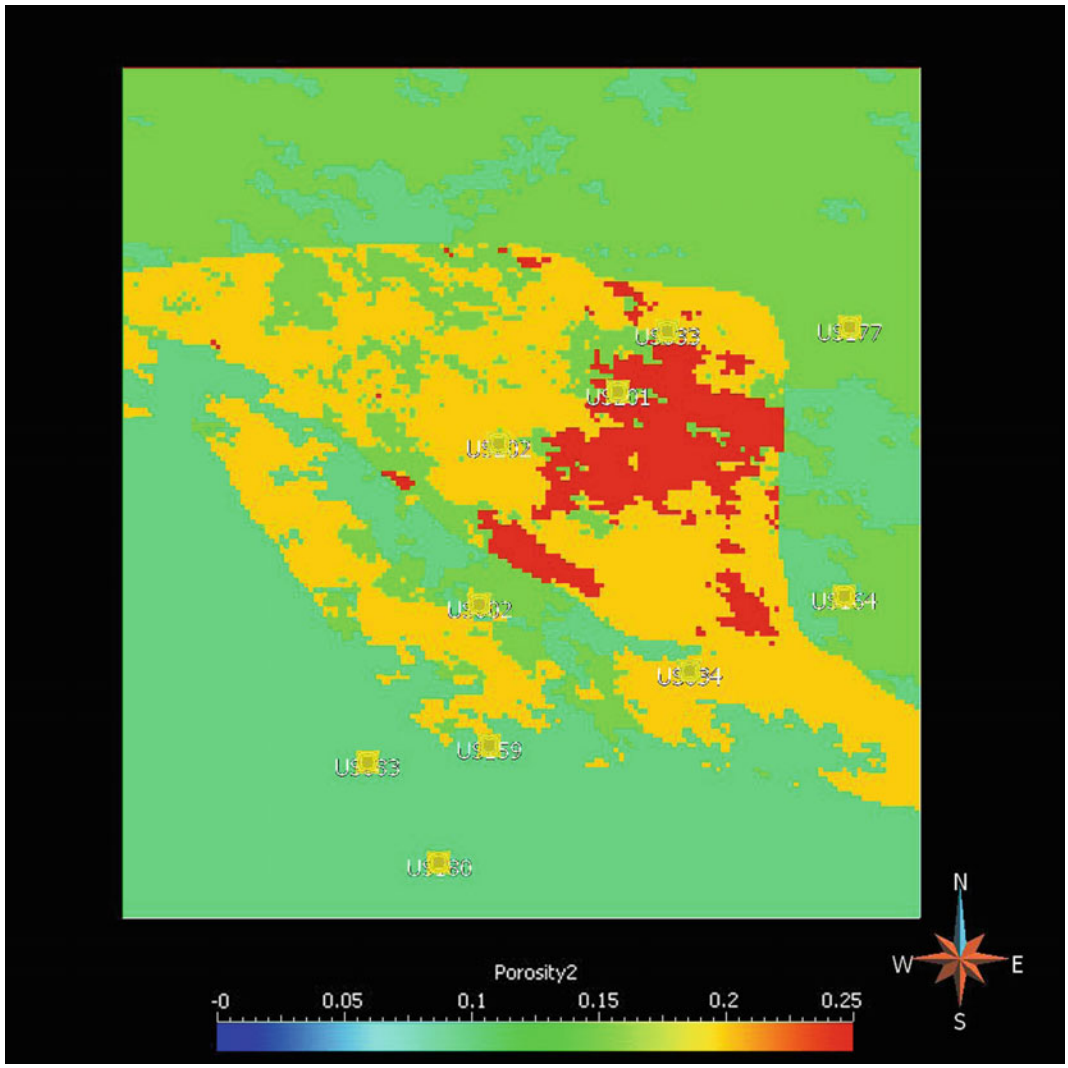

Fig. 4.33 View of the porosity attribution in PS3, based on the modelled distributions of rock textures, SCOC and dolomite as well as the diagenetic drivers rules. Here, the lagoon facies (north) has relatively low porosity values ranging between 10 and 15 %. The shoal facies shows a heterogeneous patchy porosity distribution, with values ranging between 15–25 %. The highest values are seen in the *red*, where grainy textures prevail. The outer shoal facies have similar porosity values to those of the shoal facies, but slightly lower. The outer ramp facies is characterized by lower porosity values (~10 %). The porosity scale-bar spans 0 to 25 %

they have relatively high amounts of scattered syntaxial calcite overgrowth cement (SCOC) and are less affected by dolomitization. Dolomitization generally enhances porosity and permeability in mud-supported limestone textures of the proximal outer ramp and outer shoal facies, where reflux dolomitization is inferred (see Morad et al. 2012).

4.1.2.4 Alternative Workflow for Geostatistical Modeling of the Arab D Reservoir Heterogeneity

The above described modelling workflow and results for the depositional facies distributions and diagenetic trends of the PS3 interval of Arab D reservoirs involved the SIS and FFT-MA

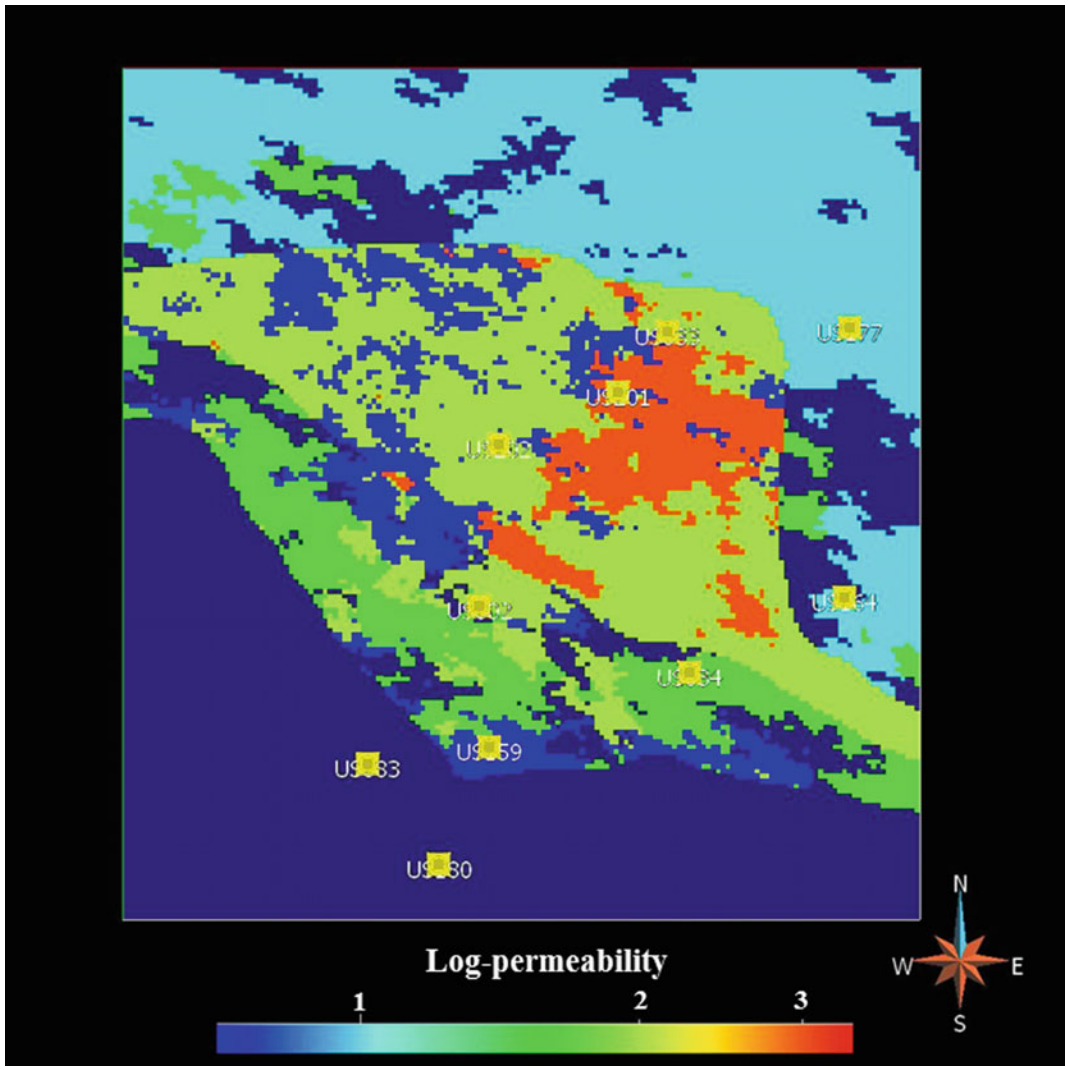

Fig. 4.34 View of the permeability attribution in PS3, based on the modelled distributions of rock textures, SCOC and dolomite as well as the diagenetic drivers rules. The lagoon facies has relatively low permeability values. Relatively high permeability values are found in the shoal facies. Where grainy textures dominate and no dolomite is present, the highest permeability values occur. The heterogeneity of the outer shoal facies resembles the shoal facies, but with lower values. The outer ramp facies is characterized by lower permeability values

geostatistical methods. Rules for the main diagenetic drivers of porosity and permeability were applied based on the statistical analysis of well data (Table 4.1), organized by depositional facies (i.e. grainy, packstone, muddy). Accordingly, such applied rules were used to attribute porosity and permeability values across the reservoir model.

An alternative workflow is proposed to achieve the same objectives—namely, to model the reservoir porosity/permeability heterogeneity of the PS3 interval, by cross-relating the depositional facies, the diagenetic driver, as well as the porosity and permeability distributions. This workflow makes use of the plurigaussian method which involves two Gaussian simulations for

modelling the depositional facies. It provides a simpler and faster way to distribute the reservoir properties between the wells across the oil field.

Alternative Workflow

The alternative workflow is presented in Fig. 4.35. It consists of four distinct yet inter-related modelling steps: (1) facies distribution through a plurigaussian simulation; (2) porosity distribution by depositional facies type by means of the FFT-MA method; (3) diagenetic driver (SCOC, see above) distribution by depositional facies and correlated with modelled porosity through the collocated cokriging; and (4) permeability distribution by depositional facies, calculated based on the simulated porosity and diagenetic driver (SCOC). This last step reproduces the semi-arbitrary "attribution" that was done in the previous workflow (above).

The plurigaussian method—with Gaussian variogram model—was preferred here for rock textures (facies) simulations because it results in less pixelated features (with respect to SIS, above) representing a simplified view of the related depositional environments (check Fig. 4.10); whereby the shoal includes predominantly grainy textures, the lagoon features packstones and muddy, and the outer ramp is mainly made up of muddy textures. Since the PS3 facies are dominated by shoal and outer shoal grainstones with the major diagenetic driver being the syntaxial calcite overgrowth cement (SCOC) which is itself rather correlated with grainy textures, the porosity and SCOC simulations were constrained by the simulated facies (rock textures). In addition, the SCOC distribution was correlated with porosity, since such cement is highly common in grainy and rare to absent in muddy textures. The above rules are based on the geological observations (check Figs. 4.17, 4.18, 4.19, 4.20 and 4.21, and Table 4.1).

Simulations and Results

Facies Distribution As mentioned above the plurigaussian method was used in order to model the distribution of rock textures (facies) across the study area. This is done by using two Gaussian simulations with the first one representing the general azimuth of structures (N110°), and the second smaller structures with perpendicular (N020°) orientation (Fig. 4.36).

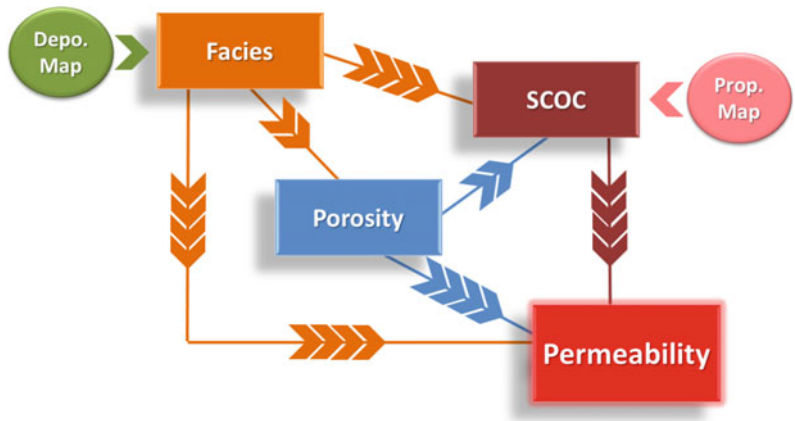

Fig. 4.35 Geostatistical modelling workflow for the distributions of facies (rock textures in three classes: grainy, packstone, muddy) by means of plurigaussian method, constrained by depositional environments map; porosity with FFT-MA correlated to the similauted facies; the SCOC (in four classes: absent, rare, common, abundant) constrained by general proportion relative abundance map and correlated to porosity—simulations with collocated cokriging, and permeability calculated by facies based on modelled porosity and SCOC. The arrows point to the relationship between the four modelling steps. For example porosity simulations are constrained by facies simulations and constrain the SCOC and permeability simulations

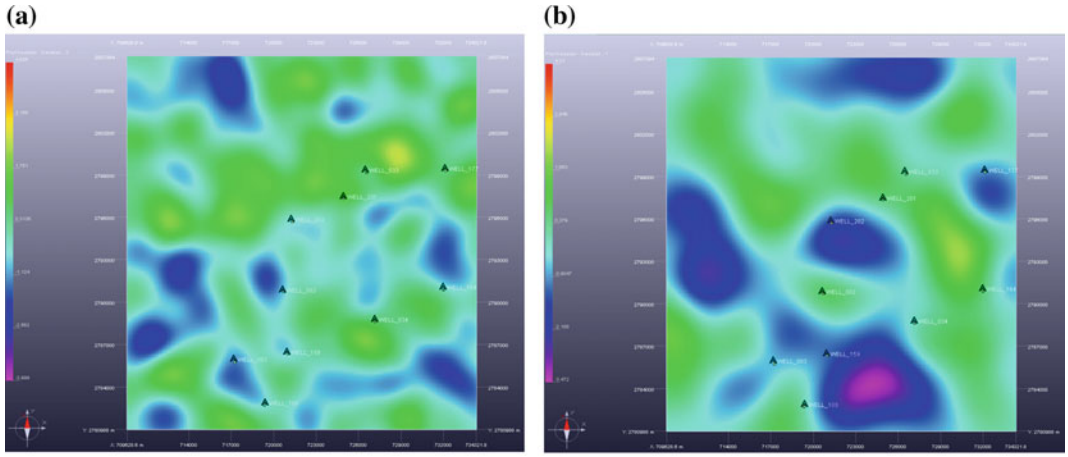

Name	Structure	RangeX	RangeY	RangeZ	Azimuth
G1	Gaussian	6000	6000	1.02	110
G2	Gaussian	4000	4000	1.02	20

Fig. 4.36 Results of the two Gaussian simulations (**a**: G1; **b**: G2) across the study area for the rock textures (facies). The well locations (control points) are indicated. The parameters used for each simulation are also listed—these were defined based on data range and on trial and errors. The colour scale bars range from −4.0 to 4.6 for **a** and −3.5 to 4.2 for **b**, *red* representing the highest values)

These orientations were defined based on the known depositional facies spatial configuration.

Similarly to the SIS simulation of the distribution of rock textures (above), the depositional facies map (Fig. 4.17) was honoured. Vertical proportion curves (VPCs) of the discretized wells at the PS3 interval were computed. The proportion matrix (VPM) was produced by using the same constraining property map representing the lagoon, shoal, outer shoal and outer ramp depositional environments (cf. Fig. 4.25). Thereafter the variogram parameters were defined and the facies simulation was achieved (Fig. 4.41a).

Porosity Distribution The porosity values consist of a continuous property (in % of bulk rock) and therefore were simulated by means of the FFT-MA method. A similar workflow was followed (see above), yet three simulations were provided corresponding respectively to the grainy, packestone, and muddy rock textures (facies). The variogram model parameters are presented in Table 4.4.

SCOC Distribution The quantitative proportional abundance map of SCOC in grain-supported rock textures across the field (check Figs. 3.4 and 4.29), was used as a constraining property map for the computation of the proportion matrix (VPM). Still, the collocated cokriging method was used here (instead of the SIS), providing three simulations corresponding to the three groups of rock textures (facies). The conditioning dataset was the available well data. In addition, the simulated porosity was used as a secondary property with defined correlation coefficients of 0.5 and 0.8 for packstone (Table 4.5) and grainy rock textures (Table 4.6). A very low (and null) correlation coefficient was used for the muddy textures since no syntaxial overgrowth cement is found in this facies.

Permeability Distribution The major controlling parameter for the permeability distribution for the PS3 interval (of the Arab D Member) across the study area is believed to be the prevailing rock textures (facies). Indeed, the best

Table 4.4 Variogram model for the porosity (FFT-MA) simulations

Structure	RangeX	RangeY	RangeZ	Azimuth	Sill
Spheric	6130	6560	1.02	110	0.10

The parameters of the variogram model were defined based on data range and on trial and errors

Table 4.5 Parameters for the collocated cokriging simulations of the SCOC distribution in packstone rock-textures across the study area, and constraints for the variogram model

Parameters for collocated cokriging					
Conditioning dataset		Second property		Correlation coefficient	
DSW_PS3_F (wells)		Porosity-FFTMA		0.5	
Variogram model					
Structure	RangeX	RangeY	RangeZ	Azimuth	Sill
Spheric	6130	6560	1.02	110	0.10

Note that a moderate correlation between SCOC and porosity has been applied. These parameters were defined based on data range and on trial and errors

Table 4.6 Parameters for the collocated cokriging simulations of the SCOC distribution in grainstone rock-textures across the study area, and constraints for the variogram model

Parameters for collocated cokriging					
Conditioning dataset		Second property		Correlation coefficient	
DSW_PS3_F (wells)		Porosity-FFTMA		0.8	
Variogram model					
Structure	RangeX	RangeY	RangeZ	Azimuth	Sill
Spheric	6130	6560	1.02	110	0.10

Note that a high correlation between SCOC and porosity has been applied. These parameters were defined based on data range and on trial and errors

reservoir rocks statistically are those of grainy textures (commonly in the shoal environment). Yet, these show significant heterogeneities in terms of their porosity and permeability (as observed above). The working hypothesis is that such heterogeneity can be predicted using a diagenetic driver (here the SCOC distribution, which is itself associated to the porosity). Based on the porosity-permeability laws for micro-, meso-, and macro-porosity proposed by Lønøy (2006), the permeability distribution has been calculated for muddy, packstone and grainy textures (Table 4.7). The simulated porosity values were used to calculate the permeability (between the wells). According to the statistical analysis of well data (presented in Table 4.1), the permeability values seem to be more than double when the packstone and/or grainy textures include common to abundant SCOC. Thus, the respective Lønøy (2006) equations were modified (by multiplying by 2).

Synopsis

The alternative workflow succeeded in modelling the distributions of facies (rock textures), porosity, SCOC and resulted permeability for the PS3 interval (Upper Jurassic Arab D Member) across the study area (Fig. 4.37). Where muddy rock textures (mostly representing the outer ramp and parts of the lagoon depositional environments; Fig. 4.37a) prevail, porosity and permeability values are relatively low (Fig. 4.37b, d). Minor

Table 4.7 Applied conditional formulas for calculating permeability values based on simulated porosity per rock texture (facies) taking into account the SCOC distribution

MUDDY	Patchy Micro- Intergranular Porosity (Lønøy, 2006): k= 10^(1.4955*ln({Porosity})-3.2488)
PACK	Patchy Meso- Intergranular Porosity (Lønøy, 2006): k= 10^(1.5253*ln({Porosity})-2.5953) IF Common/Abundant SCOC → 2x k: k= if({Syntaxial}>1.6, 2*(10^(1.5253*ln({Porosity})-2.5953)), 10^(1.5253*ln({Porosity})-2.5953))
GRAINY	Patchy Macro- Intergranular Porosity (Lønøy, 2006): k= 10^(1.8095*ln({Porosity})-3.074) IF Common/Abundant SCOC → 2x k: k= if({Syntaxial}>1.6, 2*(10^(1.8095*ln({Porosity})-3.074)), 10^(1.8095*ln({Porosity})-3.074))

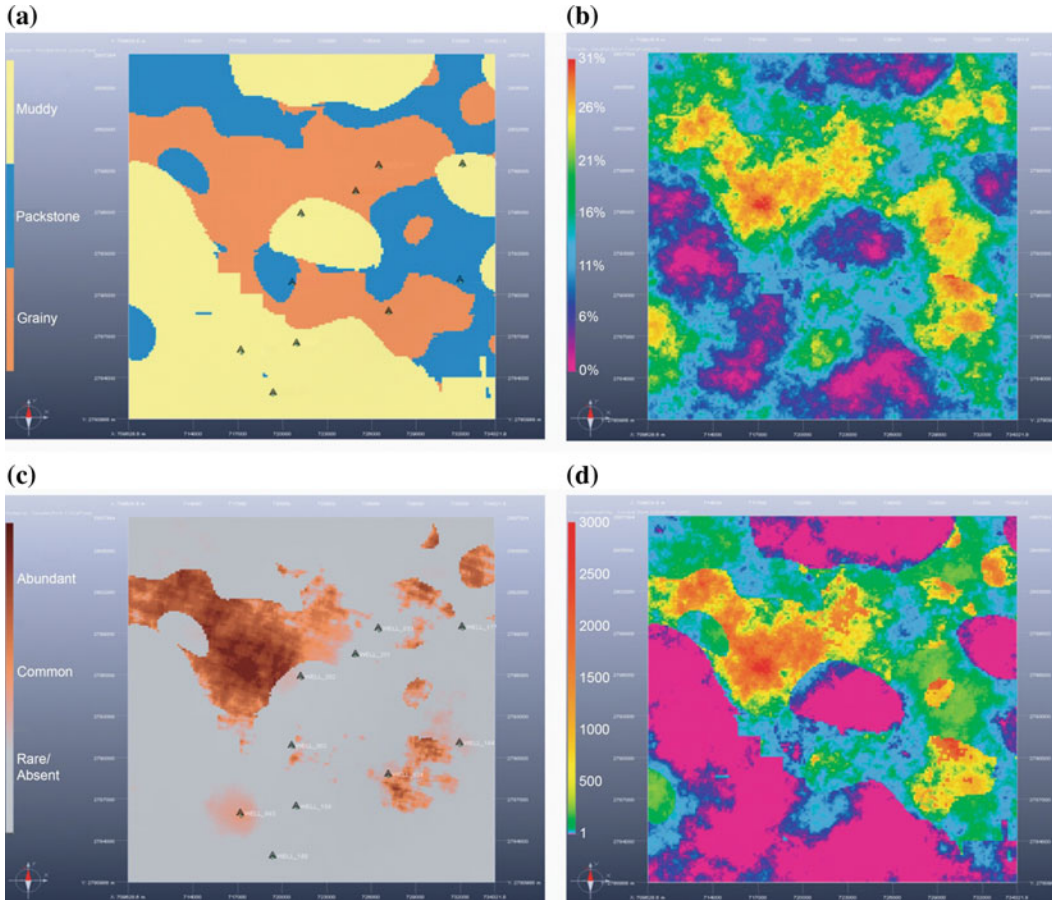

Fig. 4.37 Distributions of rock textures (facies; **a**), porosity in % (**b**), SCOC (**c**) and permeability in mD (**d**) based on geostatistical modelling involving plurigaussian, FFT-MA, collocated cokriging methods for the PS3 interval (Upper Jurassic Arab D member). Low porosity and permeability dominate the muddy textures, while the packstone and grainy textures portray the highest permeability where SCOC is common to abundant. Maps are view of layer 40 of the 3D model

exceptions can still be observed where well data show the opposite (probably due to minor dolomitization—not taken into account with this modelling workflow). For grainy and packstone textures mainly representing the shoals, the permeability is a function of simulated porosity and the SCOC distribution (check Fig. 4.37b–d). Thus, where porosity is relatively high and SCOC is common to abundant, the permeability is higher.

4.1.3 Geochemical Modelling

Geochemical modelling employs thermodynamic and kinetic rules (from data-bases, e.g. USGS; Palandri and Kharaka 2004) to examine chemical reactions and fluid-rock interactions. This can be done through a 0D model (e.g. ArXim, PHREEQ-C), whereby the viability of a certain chemical reaction is tested and analysed. Furthermore, coupling geochemical modelling with reactive-transport (RTM) allows the simulation of fluid-flow and associated fluid-mineral processes in 1D, 2D and 3D configurations. Geochemical RTM are attractive as they provide forward simulations of fluid-rock interactions and resulting diagenetic phases. Yet, they need to be validated since most of these processes occurred in different, usually unknown temporal and physico-chemical conditions. This remains currently a challenging task for achieving useful geochemical models of diagenetic processes. Nevertheless, geochemical modelling is capable of providing invaluable answers to specific questions concerning the fluid-rock interactions. Henceforth, it is very appropriate to use this technique in order to support or refute proposed conceptual models and inferred diagenetic impacts on reservoir properties.

Within the larger framework of diagenesis studies, numerical modelling plays an important role for analysing quantitatively certain concepts. Diagenetic processes need, first, to be well investigated and characterized. Their impacts and/or resulting phases have to be further quantified in order to provide input-data for the numerical models.

Dolomitization conceptual models include two major groups. The first group represents early seawater-related—sometime abhydrite associated—dolostones. The second illustrate later dolomitization processes associated with basinal-fluids at higher temperatures and depths. A typical example of early seawater-related dolomitization model is that of the reflux involving gravity-flow of seawater-modified brines (cf. Adams and Rhodes 1960). The burial (compaction) model of dolomitization (e.g. Illing 1959; Jodry 1969; Hood et al. 2004) involves pumping of basin formation waters from the basin (undergoing burial and compaction) into adjacent permeable carbonate rocks.

4.1.3.1 0D Geochemical Modelling: Dissolution/Precipitation Rates

De Boever et al. (2012), applied 0D geochemical modelling to obtain an estimate of dolomite dissolution and anhydrite precipitation rates in a typical Arab Formation reservoir rock, at the micro-scale (combined with micro-CT investigations; see above, Chap. 3). The evolution of an open geochemical system, changing at a rate governed by the fluid and rock composition and reaction kinetics, has been modelled with ArXim software (EMSE-IFPEN), which is an open source program for multiphase speciation, equilibrium and reaction calculations between minerals, aqueous solutions and gases.

The reactions take place in a box with the size of a small plug (2.5 cm^3), which is representative of the scale of samples studied—from Arab Formation, Abu Dhabi (UAE). The geochemical calculations include the solid phases calcite, dolomite and anhydrite. Quantitative XRD results allow deriving the volume% of solid phases and porosity present at the onset of the reaction. The grain diameter of solid phases was adjusted to meet the total pore surface at the onset of reaction. Fluid compositions are described by their pH and the concentration (mol/kg) of seven components involved in calcite-dolomite-anhydrite reactions. The concentrations of geochemical components are based on formation water data from the Arab Formation in the UAE (Morad et al. 2012), detailed brine compositions in equilibrium with the Jurassic

Table 4.8 Geochemical compositions of the fluids (associated to dolomite dissolution and anhydrite precipitation) used in reaction path calculations (from De Boever et al. 2012)

Component mol/kg	Dolomite dissolution		Anhydrite precipitation		
Cl^-	3.3	3.3	3.3	3.3	3.3
SO_4^{2-}	0.051	0.047	0.047	0.054	0.052
CO_2(aq)	0.0077	0.008	0.027	0.0018	0.0019
Na^+	3 381	3 381	3 372	3 390	3 390
K^+	0.01	0.01	0.01	0.01	0.01
Mg^{2+}	0.00014	0.000075	0.00092	0.00042	0.00043
Ca^{2+}	0.0089	0.0051	0.0061	0.0045	0.00024
pH	6.5	6.7	5.7	6.9	7.0
Temperature (°C)	85	95	95	95	105

Smackover Formation (Moldovanyi and Walter 1992) and actual, surface Abu Dhabi sabkha waters (Wood et al. 2002). The Smackover Formation in the Southern Reservoirs encloses a carbonate-evaporite sequence with a similar mineralogical assemblage as the Arab C Member (calcite, anhydrite, dolomite) and is presently buried at depths between 2765 m and 3250 m. The compositions of fluids in equilibrium with the rock assemblage, used as a basis in the calculations are listed in Table 4.8.

The typical Arab Formation water has Na^+ and Cl^- concentrations well above that of typical seawater; it has also high SO_4^{2-} and HCO_3^- concentrations. It inherited its main characteristics from evaporative waters that caused early reflux dolomitization and equilibrated with a dolomite-calcite-gypsum/anhydrite rock sequence. Solutions' ionic strengths are higher than 3.0 and (Pitzer 1973) equations are used to compute aqueous activity coefficients. The USGS database (Palandri and Kharaka 2004) is used for the kinetic constants.

Geochemical modelling parameters were constrained by the inferred geological burial curve as well as the pressure (P) and temperature (T) during which different cementation/dissolution events took place. Advective fluid flow velocities were varied between 0.1 m/y and a few tens of m/y. Constraints were obtained from (Machel 2004; Whitaker et al. 2004) who compiled information on different fluid flow rates for different hydrological drives in basin studies. Because of the uncertainties associated with the fluid composition and reaction conditions, T, P, fluid composition (Mg^{2+}, Ca^{2+}, SO_4^{2-}, CO_2 concentration and salinity) and fluid flow velocity (m/y) were changed as part of a sensitivity study.

The simulations represent thermodynamic-kinetic reaction path calculations in a box with length dx (m), on which an advective flow with velocity u (m/y) is imposed. At first, a fluid in-place is created and modelled to be in thermodynamic equilibrium with the mineralogical assemblage at given T and P. During dynamic simulations, a fluid that is out of equilibrium as a result of small changes in the fluid chemistry (Mg^{2+}, Ca^{2+}, SO_4^{2-}, CO_2 concentration or salinity) and/or temperature (°C), is injected. Temperature and pressure conditions remained constant during each simulation. A closed system run allows determining the equilibration time of the fluid with the rock. Then, the advective velocities implied during open system, dynamic runs are chosen as such that the fluid leaves the volume, with length dx, prior to full equilibration. The 3D volume that is dissolved or precipitated during a specific diagenetic event is obtained (for validation) from the CT-images (Table 4.9; see above, Chaps. 2 and 3).

Each simulation addresses one dissolution or precipitation reaction at a time (Table 4.10). No replacement processes or concurrent dissolution of two phases (calcite and dolomite) have been considered. Each diagenetic process is simulated,

Table 4.9 Quantitative diagenesis of three samples from the Arab Formation (Abu Dhabi—UAE) by means of micro-CT image analyses and XRD (from De Boever et al. 2012)

Sample	Resolution	Volume		Total porosity (%)	µ-porosity (%)	vol largest percolating cluster (%)	Dolomite (%)	Anhydrite (%)	Celestine (%)	Calcite (%)	Pyrite (%)	Bitumen (%)
Sample A	3 µm	27 mm³	vol%	14.3	5.5	0.7	85.3	3.7		9.6	0.1	
			wt%				86.4	3.7		9.7	0.1	
			XRD wt%				87.3	1.5		10.6	0.6	
Sample B	7 µm	0.8 cm³	vol%	22.7		22.0	53.5	24.0		/		4.5
			wt%				69.0	31.0				5.5
			XRD wt%				71.4	22.4		1.5		4.7
Sample C	1.5 µm	6.7 mm³	vol%	16.4		15.2	74.4	8.1	1.1			
			wt%				88.1	10.0	1.8			
			XRD wt%				95.4	3.6	1.0			

Table 4.10 Sample chemical and physical input parameters for reaction path simulations

Dolomite dissolution time 0 to time 1		
Δporosity	0,07	
Grain radius (m)	0,01	
Duration	Unknown (assume 40 My)	
CO_2 (mol/kg)	0,015	0,050
Velocity effective (m/y)	10,0	20,0
Cooling	ΔT=10°	
Temperature	85 °C	95 °C
Anhydrite cementation time 1 to time 2		
Δporosity	0,09	
Grain radius (m)	0,01	
Duration	40 My	
SO_4^{2-} (mol/kg)	0,07	
Ca^{2+} (mol/kg)	0,005	
Velocity effective (m/y)	0,1	2,0
Na^+ (mol/kg)	3,42	2,82
Cl^- (mol/kg)	3,3	3,7
Temperature	95 °C	105 °C

In gray: values of input parameters that were varied for sensitivity analysis (see also Table 4.8) (Boever et al. 2012)

according to one or more scenarios. Selected scenarios are based on background literature of the geological history of the study area. The maximum geological duration of the diagenetic events (in m.y.) helps in eliminating unrealistic scenarios.

The calculated reaction rates (dolomite and anhydrite volumes dissolved/precipitated per time unit) reflect the rate of dissolution/precipitation in a realistic geochemical space, but are independent of changes in the pore structure and assume 'perfect mixing'. The 3D volume of dissolution or cementation obtained from CT images and the maximum geological duration of the diagenetic event (in m.y.), as described in literature and/or validated by basin modelling (burial history), demonstrate the necessity to study far-from-equilibrium geochemical systems at a small scale in order to achieve sufficiently fast reaction progress with time.

Eventually, this approach provides a way to calculate the impact of diagenetic processes (i.e. dissolution of dolomite and anhydrite cementation, Table 4.10) on the host-rock mineralogy and porosity with no fluid transport simulations. Results were used to attempt constraining reactive pore network modeling (R-PNM; De Boever

et al. 2012). The same workflow can also be applied on larger basin-scale, whereby the relative amount of porosity destruction (cementation/plugging) or porosity enhancement (dissolution) can be assessed. At this stage, the results are burdened with several uncertain parameters, but they can lead to meaningful trends.

4.1.3.2 2D Geochemical Reactive Transport Modelling: Reflux Dolomitization

Dolostones are known worldwide to reservoir significant amount of hydrocarbon. In the prolific Middle East region, major hydrocarbon accumulations are in dolostone reservoirs either of, or related to, reflux origin (e.g. Permian Khuff, Jurassic Arab Formations, Fontana et al. 2014). A reflux system refers to a conceptual model whereby downward gravity-flow of brines (highly saline fluids) results in dolomitization (cf. Adams and Rhodes 1960). The heterogeneous distribution of reflux dolostones and their overall impact on reservoir properties (porosity and permeability) have to be properly understood for constructing reservoir models and applying improved/enhanced oil recovery (IOR/EOR) methods. The reflux dolostones are inherently associated with the platform interior evaporites (sabkha) and are believed to occur relatively early, after sediment deposition. They are associated with evaporitic conditions and often contain anhydrite.

Figure 4.38 illustrates the chief characteristics of the reflux dolostones: association to platform interior (and sequence boundaries), decreasing dolomite downwards, good lateral continuity versus poor vertical continuity, and abundant patchy non-dolomitized zones (evaporite and muddy sediments) (Adams and Rhodes 1960; Sun 1995; Cantrell et al. 2004). The evaporite content in the reflux dolostones is usually absent—particularly at outcrops—either by dissolution or by replacement (calcite, dolomite and/or silica). This does not mean that at the time

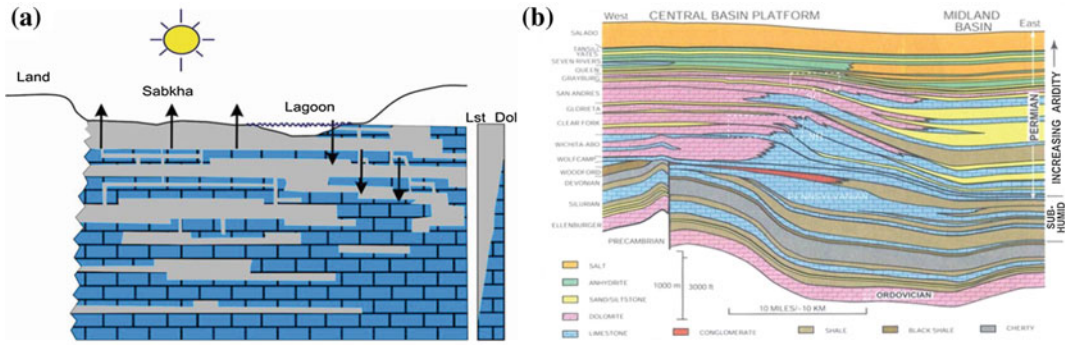

(c)

PROCESS	CAPILLARY EVAPORATION EVAPORITIVE PUMPING	GRAVITY REFLUXING BRINES
DISTRIBUTION/ GEOMETRY	STRATIFORM ALTERNATION OF LST. and DOL.	
	DECREASING DOLOMITE CONTENT DOWNWARDS	
BARRIERS TO FLOW	ABUNDANT { evaporites, muddy sediments	
RESERVOIR CONTINUITY LAT	GOOD	
RESERVOIR CONTINUITY VERT.	POOR	

Fig. 4.38 General characteristics of reflux dolomite model: **a** Schematic illustration showing the lateral and vertical dolomite distribution (*arrows* represent fluid flow); **b** Reflux dolomites (in *pink*) are associated with platform interiors and can be inferred from interpreted seismic sections and sequence stratigraphy models; **c** Key characteristics of reflux dolomite reservoirs (from various sources; see text for details)

of dolomitization it did not occur, and that it was not genetically associated to the dolostones. Moreover, several workers modified the reflux model to include mesohaline fluids, which do not result in the precipitation of evaporite (e.g. Simms 1984; Whitaker and Smart 1990; Melim and Scholle 2002). Geochemical numerical modelling can help in determining whether evaporite minerals—such as anhydrite—could have precipitated and to what extent.

Predictive tools are necessary in order to capture the spatial and temporal emplacement of the dolomite front, together with the anhydrite content (Fig. 4.39). This certainly plays an

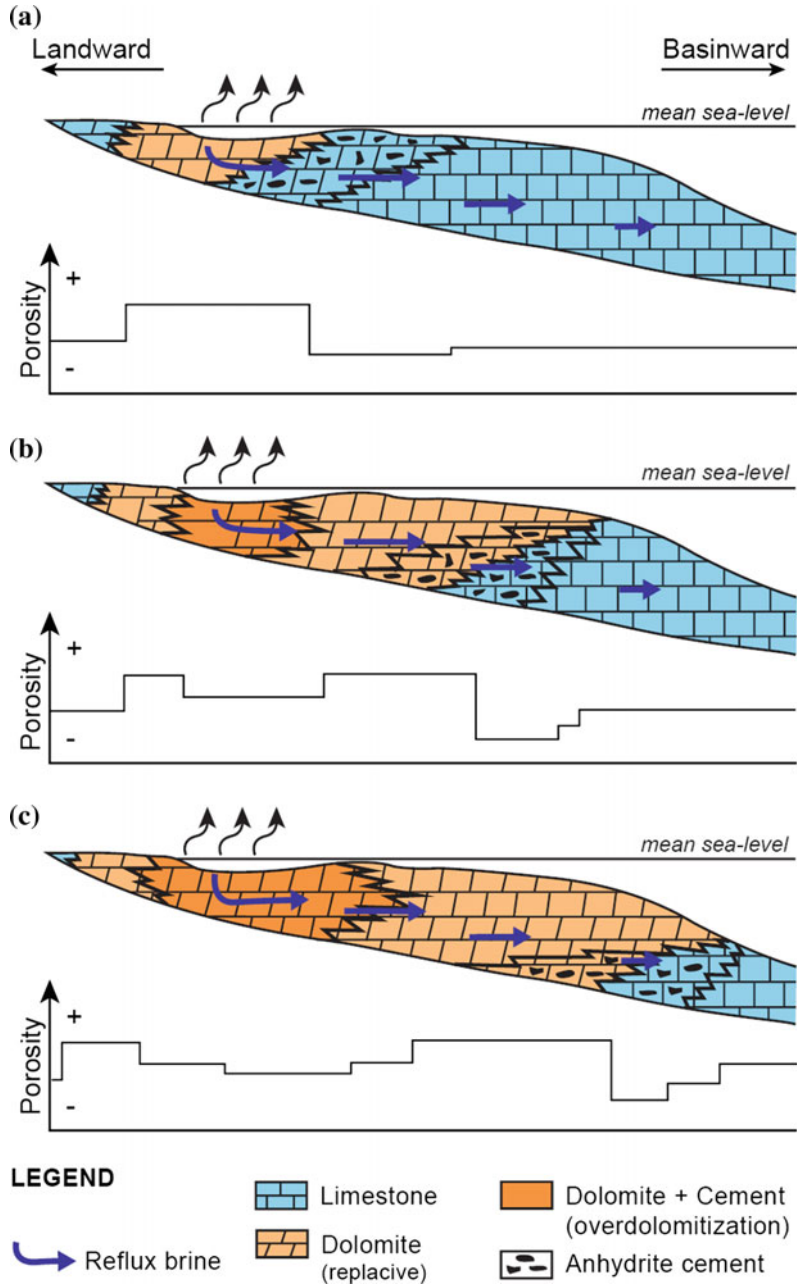

Fig. 4.39 Conceptual model of reflux dolomitization, including both processes of replacement of calcite and precipitation of dolomite cement (overdolomitization). The spatial and temporal distributions of dolomite and the anhydrite together with their impacts on porosity, are illustrated along three time steps (**a**–**c**) illustrating the propagation of the reflux dolomite front (from Jones and Xiao 2005)

important role in the partitioning of the reservoir, with un-dolomitized muddy layers and anhydrite acting as barriers. Another pertaining issue is that of overdolomitization (plugging of intercrystalline porosity with dolomite cements), which may play an important role in producing impermeable zones within the dolomite geo-body. All of these observations (which are investigated and characterized at outcrops) have to be taken into account.

Jones and Xiao (2005) used a two-dimensional numerical reactive transport model (by means of Xt2; Bethke 1996, 2002) to investigate systematically the temporal and spatial distribution of replacement dolomitization, dolomite cementation, anhydrite cementation, and porosity evolution in a reflux system (Fig. 4.40). Both hypersaline and mesohaline fluids have been tested and resulted in reflux dolomitization. The produced 2D model showed that anhydrite cements are spatially and temporally associated with dolomitization and resulted in reducing the porosity. The 2D model was used as a numerical tool to run several sensitivity analyses. Accordingly, Jones and Xiao (2005) demonstrated that the rates of dolomitization and anhydrite cementation are chiefly associated to flow rate and brine chemistry. They also highlighted that the temperature and reactive surface area control the rate of dolomitization (Fig. 4.41).

The 2D geochemical reactive transport model proposed by Jones and Xiao (2005) shows the propagation of dolomitization front with the related anhydrite and dolomite cementations (Fig. 4.40). A major interest in similar models (which were also replicated at IFPEN with ArXim-Coores^{TM}; Masoumi 2009) concerns the forward simulations of the mineral heterogeneities and porosity during the formation of such fronts. This does not imply necessarily

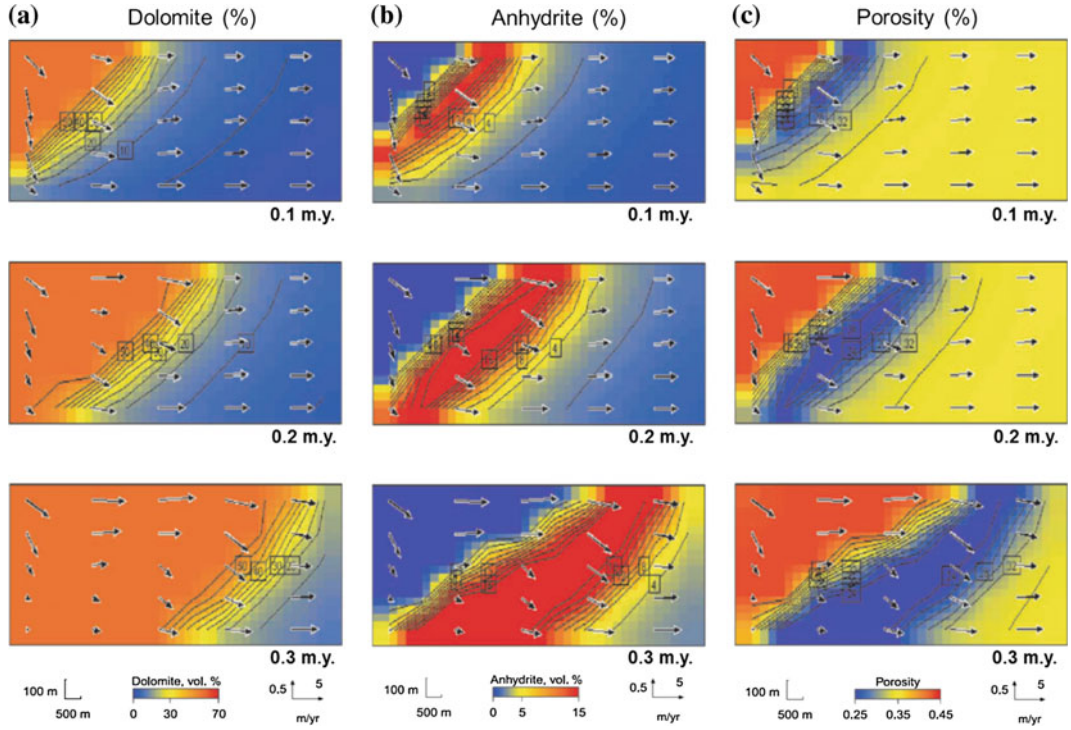

Fig. 4.40 Simulation results of reflux dolomitization 2D geochemical RTM with the original brines at 50 °C and in three time steps (0.1, 0.2 and 0.3 m.y. after the start of fluid injection); from Jones and Xiao (2005): **a** Propagation of the reflux dolomite front (contour interval = 5 %); **b** Migration of the anhydrite cement belt at the front of the dolomite body (contour interval = 2 %); and **c** Porosity evolution during the propagation of the dolomite front and anhydrite cement precipitation (contour interval = 0.02)

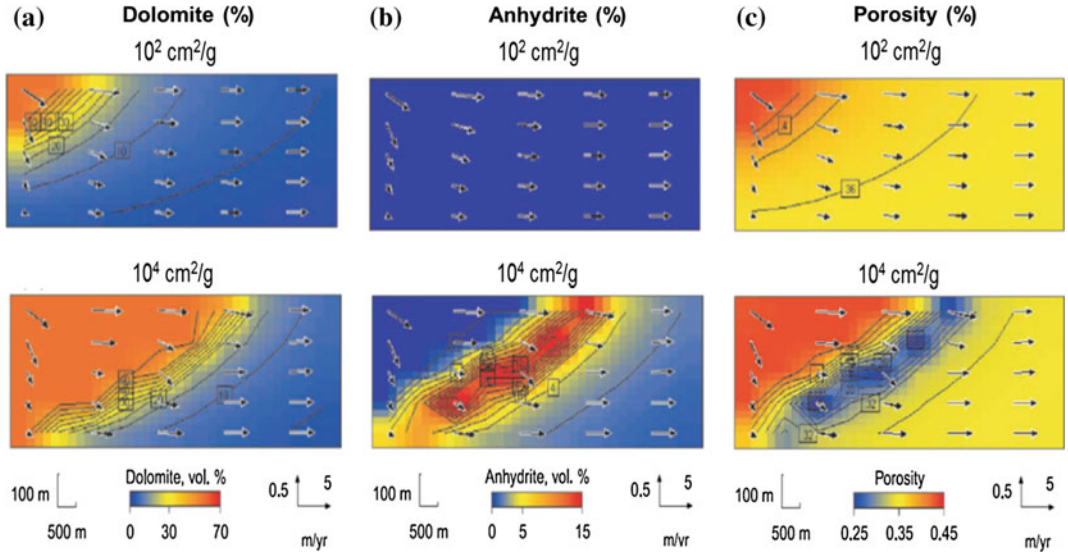

Fig. 4.41 A typical example of sensitivity analyses demonstrating the influence of the reactive surface areas (10^2 and 10^4 cm^2/g) on the modelled dolomite and anhydrite precipitations as well as porosity; from Jones and Xiao (2005): **a** The dolomite front is clearly larger with higher values if reactive surface area (contour interval = 5); **b** No anhydrite precipitates for the lower value of reactive surface area (contour interval = 2); and **c** Major impacts on porosity magnitude and extent result based on the selected value of reactive surface area (contour interval = 0.02). All figures represent the simulation results at the same time step (0.2 m.y. after the start of fluid injection)

absolute results in terms of quantitative distributions, but mainly diagenetic trends explaining the observed reservoir heterogeneities in similar geo-bodies.

RTM can also be used to test the significance of certain controlling factors on the dolomitization process. For example, the extent of reactive surface area is demonstrated to considerably affect the amount of dolomitization and anhydrite precipitation (Fig. 4.41). Consequently, such models can be excellent tools to further investigate and prioritize the key controlling factors of specific diagenetic processes (tempo-spatially).

4.1.3.3 3D Geochemical Reactive Transport Modelling: Compactional Dolomitization

Geochemical reactive transport modelling can be also used with 3D configurations in order to probe the effects of fluid flow paths and related fluid-rock interactions. Besides, this can be achieved—to a certain extent—on various scales (basin, reservoir, plug; e.g. De Boever et al. 2012). Consonni et al. (2010) applied numerical greochemical RTM to a case of compaction-driven dolomitization affecting the Jurassic Malossa paleohigh in the Po Plain (Italy; Fig. 4.42). They aimed at investigating the origin and evolution of the dolomitizing fluids and to provide a better understanding of the distribution of potential reservoir dolomitized bodies in the Po Plain.

The working hypothesis (or conceptual model) of Consonni et al. (2010) involves compaction of basinal sediments and water escape from the basin upslope to the nearby paleohigh shelf carbonates (Fig. 4.42). Thus, these compactional fluids are believed to be driven through the western margin of the Canonica Basin (slope breccia) and the adjacent Malossa Paleohigh porous carbonates.

First, a numerical basin model was constructed covering the study area (about 30 × 30 km); i.e. the basin and adjacent paleohigh (Fig. 4.43). The model included the

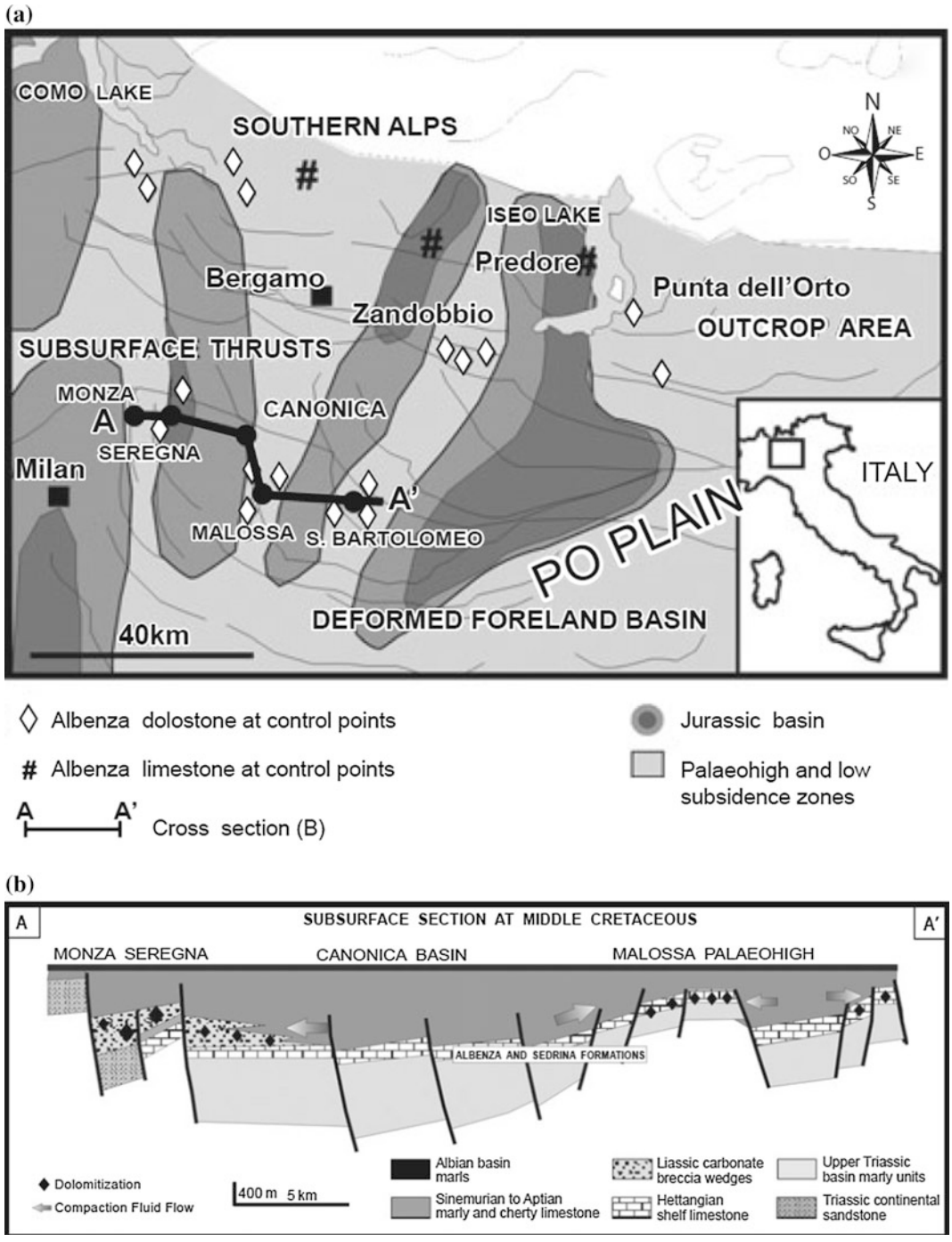

Fig. 4.42 Simplified map and cross-section showing the paleogeographic configuration at the Jurassic times of the Po Plain and the southern Alps (from Consonni et al. 2010): **a** Basins and paleohighs distributions—the location of the cross-section in **b** is indicated; **b** Subsurface cross-section at the Middle Cretaceous showing the Malossa Paleohigh affected by the and suggested basinal compaction fluid flow (*arrows*)

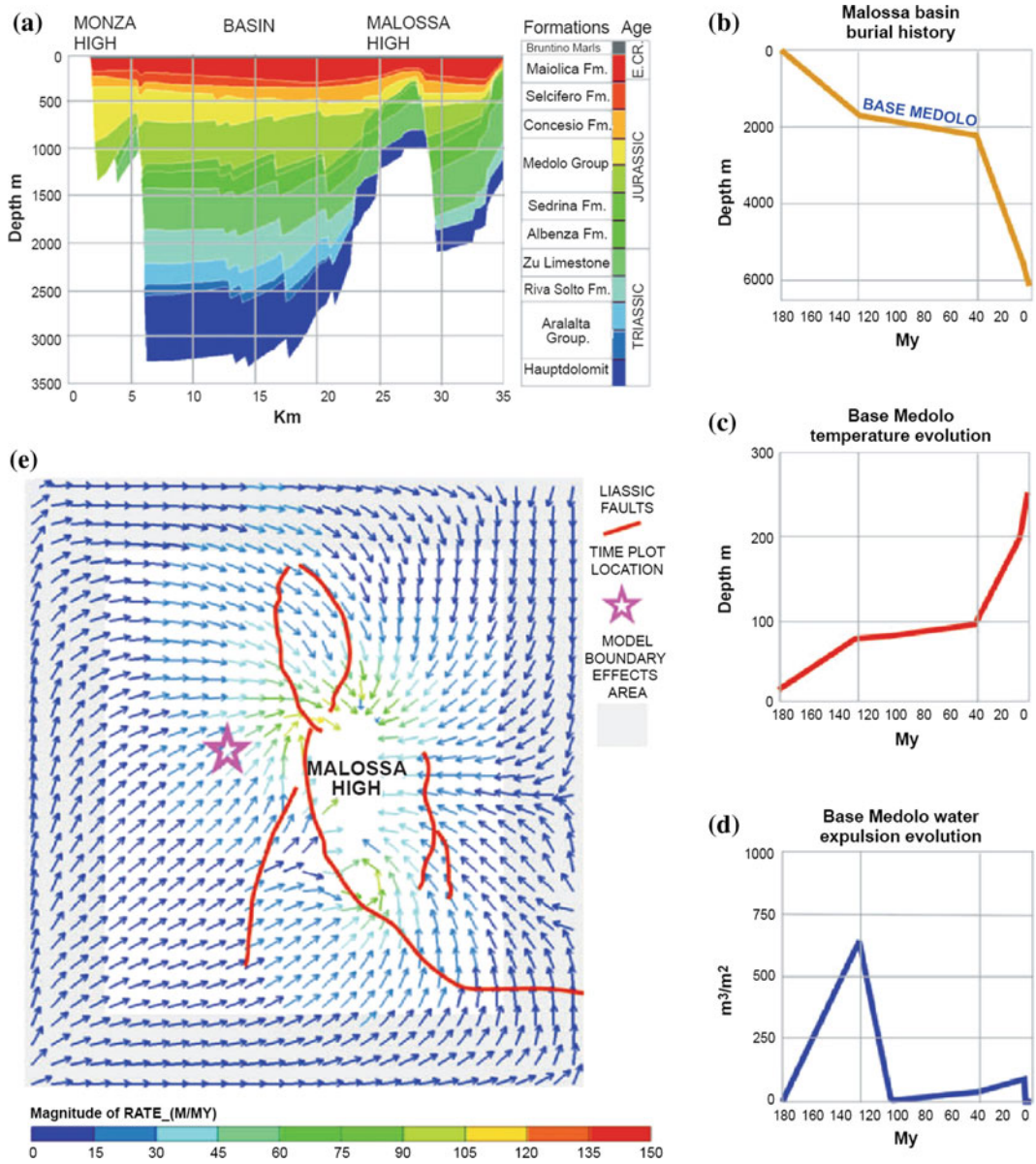

Fig. 4.43 Basin (burial) modelling results across the Canonica basin and Malossa Paleohigh (Po Plain, Italy; from Consonni et al. 2010): **a** 2D (East–West) burial model featuring the basin and paleohigh, datum to top Early Cretaceous; **b**–**c**) Burial/Thermal history curves at the base of the Medolo Group (for location check the star in **e**; **d** Fluid expulsion history curve during burial and compaction of the Medolo Group—high expulsion rates appear to have lasted 20 m.y.; **e** Map showing the simulated fluid flux at the Malossa paleohigh within the basin model—the basin area is about 30 × 30 km

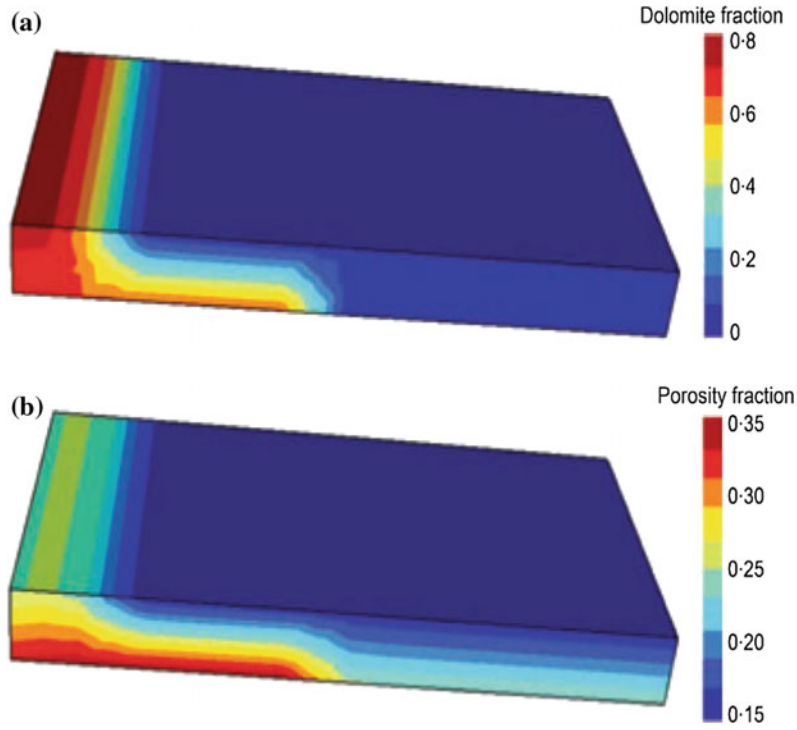

Fig. 4.44 Results of the 3D geochemical reactive transport model (RTM; with TOUGHREACT code) covering the Malossa Paleohigh (nested within and constrained by the regional basin model)—the time of fluid flow is set at 2 m.y. (from Consonni et al. 2010): **a** Dolomite volume% configuration with faster propagation of the dolomitization front in the more permeable lower layers (Albenza Formation); **b** Porosity volume% at the end of the simulation showing an increase in the Albenza Formation from 25 to 35 %, following dolomitization

stratigraphic interval of interest: base of Medolo Group (Jurassic) to top of Maiolica Formation (Early Cretaceous).

While the compactional fluids are believed to come from the Medolo Group, the topmost part of the model (Early Cretaceous) is sealed by marls. Hence the system is properly confined upward. The basin model allowed the calculations of the burial and thermal evolutions in the basin, as well as the related fluid expulsion history (Fig. 4.43). This means that it allowed constraining the amount of fluid expelled and the time range of expulsion towards the paleohigh. The fluid flux could be subsequently mapped across the model and across the paleohigh, where it is supposed to have led to pervasive dolomitization (Fig. 4.43e).

Once these constraining parameters have been defined, the geochemical reactive transport model covering the Malossa Paleohigh (nested in the larger regional basin model) was constructed. Several scenarios and tests were undertaken to investigate the resulted dolomitization and associated porosity evolution (Fig. 4.44).

Since dolomitization is chiefly affected by fluid flow, faults would make pertinent flow paths. The constructed model was used as a tool in order to investigate the impacts of faults (i.e. pathways with higher original permeability) on the dolomite front propagations (Fig. 4.45). In particular, the effects of the orientations of the faults with respect to flow were analysed. Dolomitization is believed in this study to increase the porosity% (see above), the resulting configurations of the dolomite fronts with respect to fractured zones presence and orientations yield considerable impacts on reservoir properties and extent.

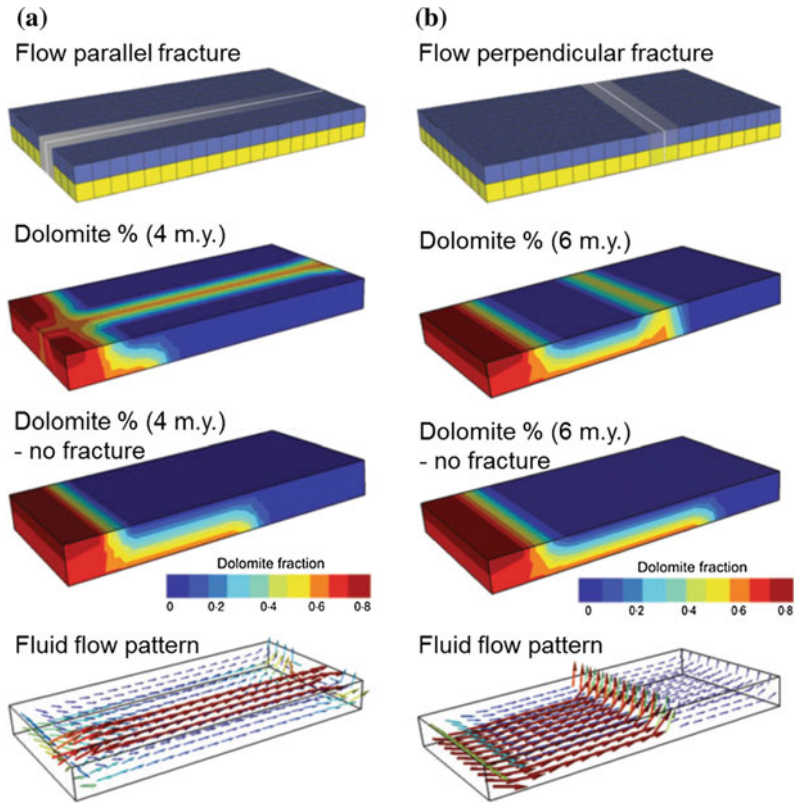

Fig. 4.45 Results of the 3D geochemical reactive transport model of the Malossa Paleohigh highlighting the impact of two different configurations of faults/fractures (from Consonni et al. 2010): **a** Dolomitization in 4 m.y. with a flow parallel fracture; **b** Dolomitization in 6 m.y. with a flow perpendicular fracture. In both cases, dolomite % distribution with no fracture is illustrated for comparison. In addition the respective fluid flow patterns are presented. The dolomite front evolution is highly affected by the presence and orientation of the fractured zones with respect to the flux sources. Such configurations have been demonstrated to result in distinct distributions of reservoir properties—e.g. porosity%

4.2 Future Perspectives

Numerical modelling of the fluid-rock interactions (diagenesis) is actually an expanding discipline in geosciences. The three distinct approaches for modelling diagenetic features and effects of diagenesis on host-rocks, which were presented above are still under development and will provide further advancement in the years to come. Numerical tools have to cope with further complicated algorithms and workflows in order to produce workable solutions that take into account key diagenetic processes which affect reservoir properties. This is not only needed for the hydrocarbon industry—today expressed by the development and application of enhanced oil recovery (EOR) techniques and the like—but also for the better use of the underground, such as water, gas, and oil storage (e.g. CCS), and geothermal energy production.

4.2.1 Geometry-Based Modelling

Karst networks represent the consequence of diagenetic dissolution mainly in carbonate rocks. Today, these are properly modelled with geometry-based approaches (described above). With advanced techniques in 3D mapping of

accessible networks and stochastic generation of conduit envelopes and validation (at least partially within an explored karstic network), future perspectives would aim at examining the impact of the generated geometries and associated fluid-flow (Rongier et al. 2014). This is actually being achieved on micro-CT scale and hence can be foreseen for larger scales. In addition, once the fluid-flow simulations are achieved within karst conduits, sedimentation therein could be assessed leading to a predictive conduit flow/filling evolution. This type of studies can be adapted for hydrogeology and geotechnical purposes, as well as other underground processes involving conduit flow (e.g. hydrothermal diagenesis).

Modelling geo-bodies based on their geometry or on their spatial inter-relationships, like the case of the Ranero hydrothermal dolomite outcrops (described above), represent a powerful method for characterizing reservoir analogues. This can well be integrated with remote sensing and photogrammetry approaches (described in Chap. 3). Once a geomodel is produced and subsequently validated by field data, it can be applied to subsurface reservoirs known to include similar diaganetic phases. This will certainly induce uncertainty which needs to be addressed properly.

4.2.2 Geostatistical Modelling

Modelled distributions of rock textures, diagenetic phases, and petrophysical properties across a reservoir interval within an oilfield offshore Abu Dhabi (UAE), by means of geostatistical approaches (discussed above), have provided a meaningful representation of the spatial heterogeneous distribution of porosity and permeability. The depositional facies does not alone constitute the prime parameter controlling the petrophysical properties in a carbonate reservoir, because these properties are overprinted by a prolonged diagenetic history (e.g. Labourdette 2007). Therefore, specific workflows including several steps were developed in order to model the impact of diagenesis on reservoir porosity and permeability across the studied field for specific parasequence intervals. The main goal for such geostatistical modelling is to fill in data between control points (e.g. wells) in a meaningful way.

While further advancement in terms of algorithms development for specific diagenetic processes is ongoing (i.e. new geostatistical methods), integration of a variety of types of data (such as well logs and seismic data) is believed to result in better reconstruction of the rock texture distribution (e.g. Lerat et al. 2007). The bi-PGS and adapted nested approaches which take into account the sedimentary facies (rock textures) and associated diagenetic phases at the same time is under development and will result in very interesting outcomes.

Different simulation methods exist today and several ones have been used and are presented above. It is strongly recommended to test distinct values for the applied variograms (i.e. the vertical, major horizontal, and minor horizontal ranges) and different simulation methods (e.g. plurigaussian and sequential indicator simulation, SIS) in order to create the most realistic facies distribution. The reason why a certain method would be eventually selected depends on the results being geologically reasonable.

A resulting simulation (e.g. Figs. 4.27 and 4.37) represents only one possible image of the simulated interval among numerous realizations. The variability of the simulation results is associated with several configuration parameters and uncertainties, such as: (i) uncertainties on the quantification of % of rock textures, cements, etc.; (ii) confidence on relationships between properties (rock textures-diagenesis-petrophysics); (iii) number of wells used in the simulation workflow; (iv) geostatistical approach which can be more or less well-suited to the case study; and (v) geostatistical parameters—e.g. rock texture proportions, maps of properties used as constraints, variogram ranges and azimuths.

Henceforth, to better evaluate the impact of methods and parameters, sensitivity studies (including uncertainty analyses) have to be integrated to geostatistical modelling of diagenesis. For industry projects, this approach may lead to probability or risk maps featuring the most

likelihood of finding a certain facies, diagenetic driver, and/or reservoir properties in a specific cell. In addition, blind wells could be used to check the predictability of simulated parameters.

4.2.3 Geochemical Modelling

Reactive transport modelling (RTM) are being used frequently to address specific processes of diagenesis (e.g. reflux dolomitization, described above). This process-based approach is still inhibited by the fact that it is difficult to validate quantitatively the simulation outcomes, by several kinetic and thermodynamic uncertainties, and due to the poor understanding of porosity/permeability relationships—mainly in altered carbonate rocks. These three issues will certainly be attractive venues of research in the near future.

At this stage, the geochemical modelling (with or without transport) can still be used for understanding certain diageneic processes and their impacts on the host rock mineralogy and porosity (and to a lesser extent permeability). This can be done at different scale from pore to reservoir and basin—depending on the process (its extent and duration) and the numerical tools (e.g. Jones and Xiao 2005; Consonni et al. 2010; De Boever et al. 2012).

Geochemical reactive transport modelling (RTM) has also become very attractive nowadays (e.g. Jones and Xiao 2005; Consonni et al. 2010, see above). They are expected to be further developed in the near future and integrated to reservoir simulators. Several approaches have been carried out at IFPEN with further development of ArXim and COORES^{TM} software packages. Thus, dolomite front propagation (reflux and hydrothermal) as well as fracture-related dolomitization have been successfully reproduced numerically. The difficulty remains in adequately validating the simulation results.

4.2.4 Towards Integraded Geomodels

Numerical modelling of diagenesis will certainly play major role in the future within the new generation of integrated geomodels. The sedimentary facies are distributed by means of process-based stratigraphic modelling software (e.g. Hawie et al. 2015). Subsequently, basin models can be constructed based on the optimal facies distribution and taking into account the burial history at the scale of the basin (providing as such temperature and pressure conditions as well as fluid flow, among other parameters; cf. Consonni et al. 2010). Approaches like the Local Grid Refinement (LGR) in basin modelling packages can bring the larger grid-cells to smaller dimensions, allowing the reservoir model to be nested in the broader basin model (with constrained boundary conditions). Diagenesis studies will help in plotting the sequence of rock-fluid interactions (paragenesis) along the burial curves. Quantitative diagenesis provides "diagenesis maps" featuring the proportions and volumes of investigated diagenetic phases. The distribution of the diagenetic phases and their impacts on reservoir properties could be simulated by geostatistical methods and/or by geochemical reactive transport models. The final outcome will be a reservoir model with well-constrained diagenesis-related heterogeneities nested in the larger-scale basin model (Fig. 4.46).

4.3 Discussion

Through the previous chapters, workflows as well as adequate classical and emerging methods for characterizing diagenetic processes and quantifying their results and impacts on sedimentary rocks have been discussed. From a practical point of view, both characterization and quantification stages are necessary to be able to propose geologically sound numerical models

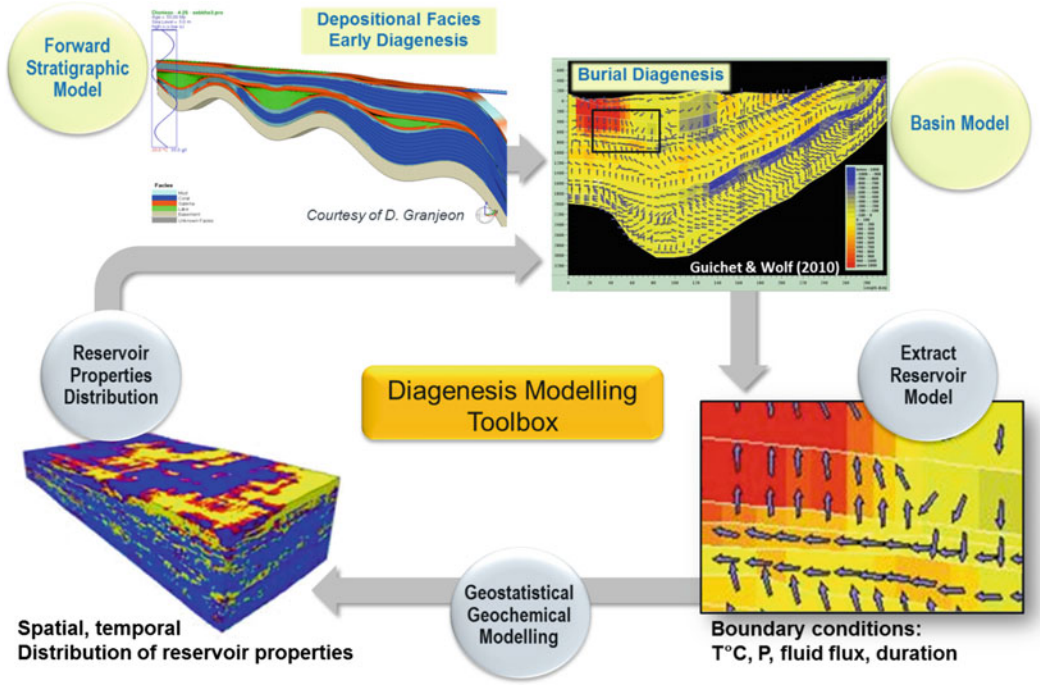

Fig. 4.46 Towards integrated basin/reservoir geomodels: Schematic workflow for integrating basin- and reservoir-scale methods. Basin-scale modelling provides constraints related to the sedimentary facies distribution and fluid evolution covering the basin's complicated history. The investigated reservoir is nested within the basin geomodel and benefits from computed boundary conditions. Geostatistical and/or geochemical RTM methods can be used to infer about reservoir heterogeneities taking into account quantitative diagenesis

that are capable of testing specific hypotheses. Here, numerical models are regarded as tools that are employed to provide additional arguments to enforce or dismiss the conceptual models of diagenesis. Ultimately, some modelling techniques could be expected to result in quantitative simulations of the distributions and evolutions of reservoir properties. Therefore, they are proposed as an evident step towards improved reservoir models capturing complex heterogeneities. In contrast to the previous chapters, the theme of numerical modelling of diagenesis still is in its early development phase.

Geometry-based modelling involves object-distance and geometric association simulations resulting in static models. The application of such methods (improved ODSIM—object-distance simulation method) has been achieved on simulating the 3D envelopes around skeletons of karstic networks (Fig. 4.2; Rongier et al. 2014). Similar methods are under development and they can be regarded as attractive future research lines. They have a large range of applications spanning over hydrogeology, environmental sciences, and reservoir engineering. I have alluded the similarities of karst networks simulations to the pore space modelling at the micro-scale. By investigating the larger, accessible karst networks, we can improve pore space modelling and related flow simulations at a varying scale in reservoir modelling (think again about "upscaling"!). Another application of geometry-based modelling, which is presented above concerns the surface-exposed Ranero dolomite geo-bodies (northern Spain; Fig. 1.7). Results of the conceptual and quantitative diagenetic studies of these fracture-related hydrothermal dolomites are discussed in the previous chapters and several published contributions (Shah et al. 2012; Dewit 2012; Swennen

et al. 2012). Based on the field-scale mapping of the exposed dolomites and fractures by means of aerial and satellite photographs (Fig. 2.1), as well as other geological studies, we were able to construct a 3D static model featuring the lithofacies and dolomite distributions. The latter were distributed based on geometric relationship with faults (i.e. walk away distance from fractures) and the conceptual dolomitization model. This is not a predictive technique, rather a way to meaningfully distribute diagenetic features. Besides, it is quite limited to the quantitative data that is made available. For instance, the depth/vertical extent is weakly validated with studies made on surface exposures. Advanced analogue studies (as discussed in Chap. 3)—coupled also to other methods, e.g. reflection seismic surveys) can play an important role in improving this approach and propose better solutions for further constrained reservoir models.

Geostatistical methods have gained increasing attention in the recent years and they are commonly used for reservoir modelling. These methods do not lead to predictive forward simulations, but they improve the static distribution of properties based on probability. The exact science behind the algorithms that are developed for geostatistical methods are beyond the scope of this book. Nevertheless, I tried to summarize the basics for common parameterization and simulation methods. For more detailed discussion on methodologies, the readers are referred to Le Ravalec et al. (2014) and other references inserted in Sect. 4.1.2 (Geostatistical modelling). I would rather emphasis on grouping of the common geostatistical methods based on the type of simulated data (i.e. categorical, continuous). For example, where the entry data are "categorical" (or "indicator"), certain methods are to be applied (SIS, Truncated and PluriGaussian, MPS, see above). Semi-quantitative data of sedimentary facies, rock textures, cements, and even porosity, represented as occurrences and abundance classes (Chap. 3), are considered categorical variables. Other methods such as Sequential Gaussian (SGSim) and FFT-MA are better used for continuous data (e.g. percentage values, dolomite%, porosity%; numeric values, permeability in mD). Using the most appropriate method—which is somehow controlled by the type and amount of entry data—will secure reaching meaningful output realizations. This is a red flag that I rise for the fellow researchers who would like to explore geostatistical modelling.

The general idea is to produce a model of rock texture distribution that is controlled by the conceptual knowledge of sedimentology and depositional environments, then simulate the associated diagenesis overprints. While theoretically, this approach is feasible, several limitations exist. One of the direct problem relates to the fact that the investigated samples have already been overprinted by a complex sequence of diagenetic phases. Here, the significant role of "quantitative diagenesis" is emphasized for distinguishing the real impacts of diagenetic phases (overprints) separately. Since this is also very difficult to achieve, the statistical analyses (as discussed in Chap. 3) may provide certain "trends" that could be further tested with geostatistical modelling. We have applied this rationale on the Arab D reservoirs from an oilfield offshore Abu Dhabi, UAE (MSc of Daniel Morad 2012). Based on the previous projects describing and quantifying diagenesis across the field (Liberati 2010; Morad et al. 2012; Nader et al. 2013), we were able to prepare a robust data-set that can be used to undertake a case study for constructing a sound reservoir model capable of capturing the Arab D reservoir heterogeneities by means of geostatistical methods (CobraFlow™ prototype). I reminded, above, the geological settings of the investigated rock sequence across the oil field (otherwise discussed in Nader et al. 2013). Then, basic elements of petrographic and statistical analyses are presented, highlighting two proposed diagenetic "drivers" for enhanced reservoirs properties. These are related to abundance of syntaxial calcite overgrowth cement (SCOC) and dolomitization degree (dolomite%) in mud-supported rock textures (Table 4.1).

First the distribution of rock-textures (in three categories: mudstone/wackestone, packstone, grainstone; Fig. 4.27) were modelled for the

investigated rock sequence, across the study area (oil field). This was achieved by taking into account the extent of the depositional environments. Then the syntaxial overgrowth calcite cement (SCOC) and dolomite distributions were modelled (Figs. 4.31 and 4.32). The mapped abundance proportional maps of the SCOC (check Fig. 3.4) were used as property maps to constrain the geostatistical simulation of SCOC distribution. Prior statistical analyses (with EasyTrace™) which are illustrated in Chap. 3 (Fig. 3.3), and summarized in Table 4.1, resulted in estimating average porosity and permeability values for the various rock textures with or without the "drivers". These average values together with the simulated distributions of rock textures and diagenetic "drivers" were used in order to attribute simplified reservoir properties (porosity and permeability) across the model (Figs. 4.33 and 4.34). There is no guaranty, at this stage, that resulting maps reflect the exact distributions in the oil field. Still, the main emphasis that I would like to make concerns the feasibility of the workflow. Blind well tests can be applied to improve this workflow. In addition, sensitivity analysis of certain used parameters and uncertainty studies can be very rewarding. Ultimately, the outcome simulations can be regarded as probability maps of distributions.

From a geological point of view, the Arab D modelling case study, showed that the shoal facies of the Arab D member (known to have the best reservoir rock-types with respect to the other, lagoon, and outer ramp facies) possess quite impressive reservoir heterogeneities. The undertaken geostatistical modelling helped in illustrating generalized distributions of such reservoir heterogeneities. An alternative workflow, based on cross-relating rock textures, diagenetic "drivers", and porosity was applied making use of other geostatistical modelling methods (e.g. PluriGaussian).

Geochemical modelling methods are process-based, aimed to result in predictive, forward simulations of chemical reactions and fluid-rock interactions through timely constrained durations. Simulations can be the outcome of dimensionless (0D) models (by means of ArXim, PHREEQ-C), whereby chemical reactions and results can be tested. For instance, could normal seawater at temperatures higher than 100 °C precipitate dolomites? And to what extent? This can be viewed as a box, in which the chemical interactions of liquid, mineral and gas phases are calculated at specific temperatures and pressures for a certain period of time. This method has been applied on the framework of quantitative characterization of anhydrite plugging cement in dolostone reservoirs through micro-CT and image analyses (De Boever et al. 2012). Tables 4.8, 4.9 and 4.10 present the quantitative entry data and prevailing conditions (e.g. temperatures) that were used in order to run 0D simulations capable of reproducing the dolomite dissolution and anhydrite cementation. This workflow was coupled to reactive pore network modelling (PNM-R) in order to estimate permeability values associated to the ArXim simulated porosity per diagenetic steps (see De Boever et al. 2012).

Geochemical reactive transport models (RTM) couple geochemical modelling with reactive transport and allow subsequently the simulation of fluid-flow and associated fluid-mineral interactions in dimensional contexts (1D to 3D). Inherently, porosity/permeability relationships have to be taken into account in RTM, yet their precision remains a challenging issue—and a good subject for future projects. Two case studies concerned with 2D and 3D geochemical RTM of distinct mechanisms of dolomitization are presented in this chapter—i.e. Jones and Xiao (2005) and Consonni et al. (2010), respectively. Similar 2D geochemical RTM, using ArXim-Coores, was applied on the Marjaba hydrothermal dolomite front, which was described in Chaps. 2 and 3 (Fig. 4.47).

Through geochemical RTM, the temporal and spatial distributions of replacement and cement dolomites, anhydrite cement and porosity for dolomite fronts can be achieved (Jones and Xiao 2005). First, the resulting anhydrite cementation front surrounding the dolomite growing front (also observed in Fig. 4.47) could explain the presence of anhydrite cement in the adjacent

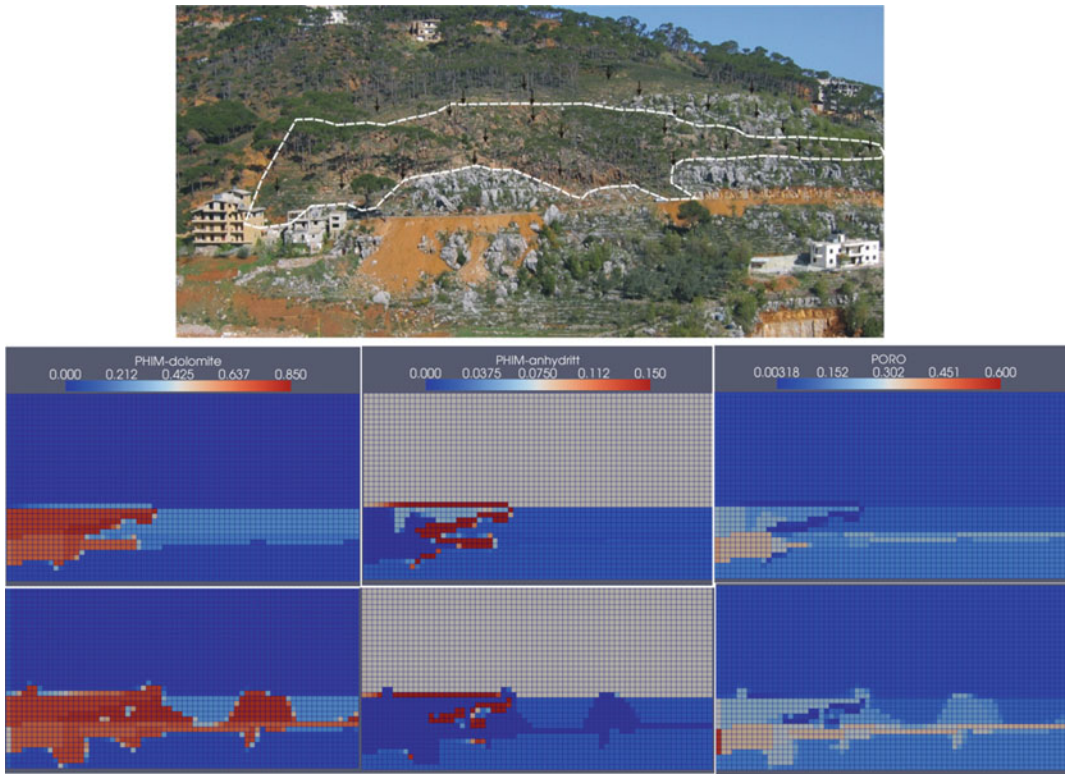

Fig. 4.47 Results of geochemical RTM simulations achieved by ArXim-Coores^{TM} representing the formation of hydrothermal dolomite fronts (dolomite, anhydrite and porosity%), based on the Marjaba HTD outcrop in central Mount Lebanon (check also Fig. 3.9). The model is about 340 m wide (68 cells; cell = 5 m) and 144 m thick. The Marjaba HTD (above photograph) is about 250 m long

undolomitized limestones and dolomitized part. Thus, the heterogeneous aspect of such dolostone geo-bodies could be further understood. A second remarkable outcome is the resulting over-dolomitization (dolomite cementation plugging gained porosity) at the input source of dolomitizing fluids, which without eventual fracturing would stop the fluid flow, and subsequently the further growth of the dolostone front. This also plays an important role for reservoir characterization, since those area near the input of dolomitizing fluids would be tight. In addition to all that, the model proposed by Jones and Xiao (2005) can be used to apply sensitivity analyses and prioritize the input parameters that play a significant role in the resulting simulations. A typical example of such sensitivity analyses is illustrated in Fig. 4.41 concerning the remarkable influence of the reactive surface areas on the resulted volumes of dolomite and anhydrite through the simulations.

The second case study consists of a larger, integrated project where basin modelling was applied in order to extract boundary conditions constraining a 3D reservoir-scale geochemical reactive transport model (Consonni et al. 2010). This workflow was applied on assumed compaction driven dolomitization process that is believed to have affected the Jurassic Malossa paleohigh (Po Plain, Italy). Consonni et al. (2010) provide arguments that the resulting simulations of dolomitization and porosity evolution (Fig. 4.44) are validated by well cores. They emphasis on the role of faults and fractures (presence and orientations) in the resulting volumes and shapes of dolomite geo-bodies (Fig. 4.45). The main interest in this study stems from its attractive workflow with regards

to nesting a reservoir RTM in the larger basin-scale model in order to allow constraining the boundary conditions which are required to reach viable results. This is a workflow that will certainly be further applied in the framework of basin/reservoir integrated research projects.

Recently, integrated numerical modelling schemes of diagenesis at the various scales and with different tools have been proposed (Fig. 4.46). Here again, the scale of the investigation (whether quantitative analysis—see Chap. 3, or modelling—this chapter) determines the approach and the tools. For instance, we could envisage forward stratigraphic and burial models to distribute the rock textures and prevailing pressure and temperature conditions at the larger, basin scale. Here 0D geochemical modelling can help in testing potential presence or absence of certain diagenetic processes (which could be even constrained by paragenesis—as discussed in Chap. 2). Geochemical models capable of proposing quick, simple estimations of porosity evolution in hydrozones (marine, meteoric, and mixing) typically affecting carbonate platforms (Paterson et al. 2008) have been generated. Eventually, the built workflow may be associated to forward stratigraphic models of carbonate platforms, allowing to include impacts of early diagenesis. In addition, reservoir-scale models could be nested in the larger basin-scale benefitting from general boundary conditions (discussed above). Here the scale is smaller and different methods will be applied to quantitatively characterize diagenesis and apply geostatistical and/or geochemical transport reactive models. The resulting simulations would illustrate the reservoir heterogeneities and can be placed again—through Local grid Refinement (LGR) techniques—in the basin model, where by simulation fluid flow resumes.

4.4 Advancement in Numerical Modelling of Diagenesis

New modelling tools, methods and workflows are emerging for numerical simulation of diagenetic phases/processes and their impacts on reservoir rocks at various scales. Whether the approach is geometry-based, geostatistical or geochemical, the outcomes are not necessarily the exact reproduction of the natural objects, it should rather provide certain solutions to specific problems.

In "numerical modelling terms", the parameters associated to "diagenesis" are different with respect to the method used. When applying geostatistical (and geometry-based) methods, simulations concern final states of co-existing variables (cements, porosity, permeability). The modelling approach tries to spatially distribute these variables based on geological concepts and probability (e.g. correlating depositional facies and specific diagenetic phases). Process-based geochemical modelling methods treat the diagenetic variables as continuously evolving with time; such as continuous dissolution of calcite while precipitation of dolomite. Therefore, the spatial/temporal continuous distribution of diagenetic phases can be simulated, leading to validating and testing the proposed concepts. Eventually, the proposed paragenesis—already quantified (Chap. 3)—becomes dynamic through such numerical process-based models.

Generally speaking, new algorithms capable of dealing with complicated computations of diagenetic processes should be proposed (e.g. nested facies/diagenesis geostatistical approach; Doligez et al. 2011). Still, resulted simulations (e.g., geometry-based, geostatistical, geochemical reactive transport modelling) must be validated—this is a crucial pre-requisite. Then, adequate uncertainty analyses that are capable of assessing the probability of success of modelling realizations are to be applied (e.g. Koek et al. 2015).

I have presented several geostatistical approaches which are based on industrial data (from mature producing fields), to achieve geologically meaningful distribution of diagenetic phases and their impacts on reservoir properties (check Fig. 4.37). The resulting realizations did not necessarily replicate nature, but they deliver the major trends and provide further suggestions for defining key parameters for sensitivity analyses.

We have used geochemical modelling combined with micro-CT and PNM in an attempt to quantify and predict the 3D pore space evolution in carbonate reservoir rocks (De Boever et al. 2012). Recently, simple examples of fluid-rock geochemical simulations have been achieved with ArXim, providing straight forward estimations (0D simulations) of porosity destruction or enhancement in hydrozones during carbonate platform growth. Such modules can be eventually plugged in forward stratigraphic modelling tools and help in predicting the effect of diagenetic processes during the growth of a carbonate platform according to residence times of specific hydrozones (e.g. Paterson et al. 2008). Dolomite front propagations have been modelled with geochemical RTM techniques—e.g. Jones and Xiao (2005) and Consonni et al. (2010). The eventual goal for geochemical RTM is to be able to predict the impacts of diagenesis on reservoir properties.

In a practical approach, a simplified paragenesis (time-defined key diagenetic processes/phases) could be integrated into the burial history within basin and reservoir models. Subsequently, adequate tools need to be developed to allow for chain simulations of successive key processes of diagenesis. Such tools need to be able to: (i) integrate fluid flow and geochemical species (e.g. Mg, Si, NaCl contents) transfer across basin-scale and reservoir-scale models; (ii) define robust porosity/permeability relationships and implement them properly—e.g. reactive transport models; and (iii) apply adequate uncertainty analyses.

Finally, integrating basin and reservoir models remains a major objective for future advancement on modelling diagenesis. Bringing the large-scale constraining parameters (temperature, pressure, fluids) to the scale of reservoir—as input data, is necessary to construct viable numerical models of diagenesis. Subsequently, the simulated reservoir heterogeneities can be brought back to the basin-scale. Could a simulation at the scale of the basin take into account the alterations resulting from a specific diagenetic phase? This is the challenge that I set for future research projects.

Conclusions

5

This contribution concerns the general theme of diagenesis and related impacts on the heterogeneity of reservoir rocks. It is both a review and a look to the future, covering those aspects of studies that have been well understood so far, and highlighting future challenges for better predicting quantitatively diagenesis on a broad range of scales. The lessons that I learnt—and which contributed to the collective scientific advances—from all the research work that I have been involved in, since a decade, are discussed in detail in specific sections of the above chapters.

New techniques and recent advances in numerical modelling will provide better tools for achieving time-constrained, quantitative diagenetic studies. Future operational workflows consist of three main stages in an iterative way (Fig. 5.1): (i) constructing a conceptual diagenesis model, (ii) quantifying the related diagenetic phases, and (iii) modelling the diagenetic processes. Proposed solutions to specific problems and expected innovations related to the three stages are discussed below.

Basin analysis and modelling appears to be a crucial step in providing the larger framework for reservoir studies. Therefore, two major clusters for future research programmes on modelling diagenesis will consist of: (i) numerical modelling of fluid-rock interactions, and (ii) integrated basin-reservoir modelling. In order to undertake these programmes, a series of developments still need to be attained in each of the above mentioned stages (Fig. 5.1).

5.1 Characterization Techniques and Workflows

Classical diagenesis studies make use of a wide range of descriptive analytical techniques leading to conceptual models that characterize specific, relatively time-framed fluid-rock interaction processes, and deduce their impacts on reservoir rocks. Currently used techniques, which were presented in this book, combine petrographic, geochemical and fluid inclusion analyses. The inferred paragenesis is commonly projected on burial/thermal evolution models, allowing better constrained temperature and pressure conditions, and subsequently, timing of diagenetic phases (e.g. Fontana et al. 2014). Figure 2.23 shows an example of a burial model (1D) over which the main diagenetic phases are placed. By achieving this task, we will be able to test the proposed process associated to the specific phase. For example, if the process of dolomitization is proposed to be hydrothermal, the deduced temperature of precipitation of the dolomites should be higher than the ambient calculated burial temperature at the same time. In addition, this same task (e.g. Fig. 2.23) will help in constructing numerical models of diagenesis, whereby process-based chain-simulations of fluid-rock interactions can be achieved and linked to the basin history (discussed below).

Since characterizing diagenetic features implies analytical descriptive techniques,

F.H. Nader, *Multi-scale Quantitative Diagenesis and Impacts on Heterogeneity of Carbonate Reservoir Rocks*, Advances in Oil and Gas Exploration & Production, DOI 10.1007/978-3-319-46445-9_5

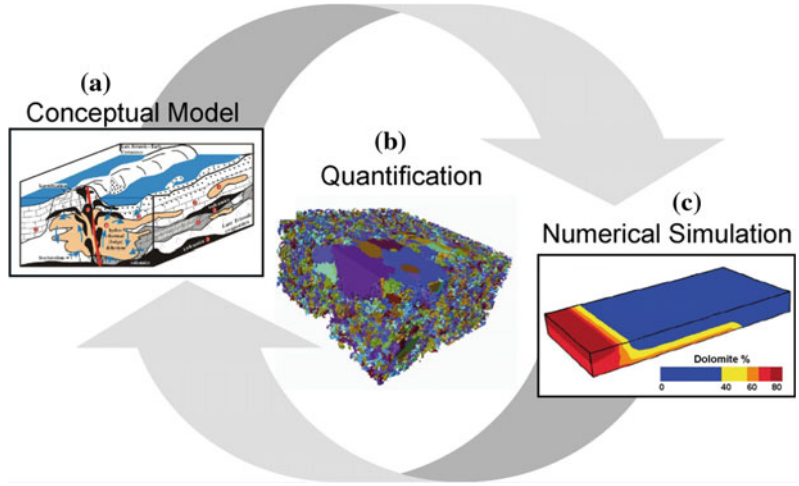

Fig. 5.1 Proposed future operational workflow for tackling diagenesis: **a** Conceptual studies of diagenesis—for example hydrothermal or high temperature dolomitization (HTD; Nader et al. 2004, 2007); **b** Quantitative diagenesis methods—e.g. micro-computed tomography (micro-CT) image analyses (De Boever et al. 2012); and **c** Numerical simulations of diagenetic processes such as reactive transport modelling of dolomitization (e.g. Consonni et al. 2010)

basically on rock samples from expensive well cores and remote field areas (sometimes with difficult access), one of the faced principal limitations concerns data-collection and field observation. New innovative workflows are therefore needed to improve field (well cores) data-collection, aiming to decrease the number of samples (and materiel), while increasing their representativity. Accordingly, characterization of diagenesis should take into account the Representative Elementary Volumes (REVs). Field data collection should be planned in function of the set objectives and the scale of investigation, as well as the tools that will be employed.

Faster and more systematic analytical characterization of sedimentological and diagenetic features would help treating larger amounts of representative data (check Nader et al. 2013). New analytical techniques or advanced developments need to be applied (e.g. Mg- and clumped-oxygen isotopic analyses, U-Pb) in order to decrease uncertainties and provide pertinent descriptions of the diagenetic phases and conditions of their formation (Chap. 2).

Enhanced scanning performance with higher resolution of cores and samples (e.g. computed tomography coupled with image analysis software development) will be crucial in order to succeed in shifting characterization methods towards the three-dimension (e.g. Fig. 2.19). This will certainly operate with new, innovative pore space description and classification schemes, with a better connection to flow properties.

Having all said, new ideas and better conceptual models for diagenetic processes are still being produced. The dolomite "bandwagon" with a variety of proposed models for dolomitization taught us that upon newly investigated natural objects, improved analytical tools, and scientific creativity, new concepts emerge. Understanding the larger tectono-stratigraphic framework seems to me critical to answer several questions related to diagenetic processes. While this is relatively easy on exposed outcrop studies, it is certainly more challenging for subsurface studies.

5.2 Quantitative Techniques and Workflows

Most of the current studies on diagenesis are qualitative and do not yield quantitative data, which are crucially needed for rock-typing and

geological modelling. Innovative approaches are emerging for applied quantitative diagenesis (some of which are presented in Chap. 3). These techniques are significant for providing numerical data that can be used by reservoir engineers as entry (input) data, and for validating the results of numerical simulations. Quantitative diagenesis is a cornerstone for achieving meaningful, predictive geomodels able of constraining reservoir heterogeneities.

A huge wealth of semi-quantitative to quantitative data come from the industry, e.g. well logs and cores from mature oil/gas fields. Today, a crucial task would be to develop software and numerical tools capable of integrating—and statistically analysing—such huge petrographic, geochemical and petrophysical data-bases (e.g. Nader et al. 2013). My experience taught me, that these tools should be linked to basin geo-modelling packages in order to facilitate integrated approaches. On another level, outcrop analogue studies by means of remote sensing and image analysis have proven their utility by providing the missing 3D framework for investigated subsurface reservoirs (e.g. Fig. 3.19). Subsequently, quantitative upscaling and downscaling workflows including the most appropriate way to define the REVs could be envisaged.

On the sample (rock) scale, achieving increased resolution of 3D scanning (e.g. mineralogical constituents—matrix and cement—macro- and micro-pore space) is still needed. This development needs to be accompanied by improved permeability modelling based on pore space and related networks (e.g. De Boever et al. 2012). In addition, quantitative mineralogical and geochemical analyses of diagenetic phases could be further applied with the integration of SEM-EDS, XRD and EMPA (e.g. Fig. 3.8). Rock-Eval pyrolysis can also be used to quantify mineral species (as shown in Fig. 3.21). This last innovation is expected to be further applied in the future.

As far as exact timing of diagenetic phases is still difficult to quantify, important analytical advancements are needed (e.g. U-Pb). This will certainly help in properly placing the investigated diagenetic processes within reservoir and basin frameworks.

5.3 Modelling Techniques and Workflows

Themes relates to the numerical modeling of diagenesis include specially geometric and geostatistical methods as well as geochemical reactive transport simulations of fluid-rock interactions. How to be able to distribute diagenesis-related reservoir heterogeneities in a geologically meaningful way? How to predict the extents and impacts of fluid-rock processes on various scales? These are general scientific questions that might be answered in the near future by means of numerical modelling.

The concept of diagenetic "trends" appears to be, at this stage, the main objective that I would realistically seek with numerical modelling tools. No matter on whether the selected modelling approach is geometry-based, geostatistical or geochemical, its outcomes will not necessarily mimic the natural objects. Instead, modelling results should rather provide reasonable solutions to specific problems; and they should highlight certain plausible trends constraining the extents and impacts of the investigated diagenetic processes on reservoir rocks.

Each numerical modelling approach (geostatistical vs. geochemical) considers differently the parameters representing diagenesis. For geostatistical modelling the diagenetic variables are "static" (final) values that need to be spatially distributed according to pre-set relationships and probability. This is contrasted to the way, diagenesis parameters are considered in process-based geochemical modelling. Through the former approach, the objective is to apply probability-based geometric configurations of sedimentary facies and diagenetic phases. I have contributed by defining statistically proven diagenetic trends (e.g. dolomitization—or increased dolomite%, dissolution—increased porosity values, anhydrite cement—increased anhydrite%). Diagenetic "drivers" could be further proposed based on statistical analyses (e.g. "when syntaxial calcite overgrowth cement is abundant, average permeability values are double than otherwise"; discussed in details in Chaps. 3 and 4). Results of incorporating the above summarized ideas in

geostatistical modelling workflows are promising (Fig. 4.37). I look forward to apply them on case studies, whose resulting simulations can be validated later on. New algorithms capable of treating complicated computations of both sedimentary facies and quantitative diagenetic data, are being developed (e.g. nested facies/diagenesis geostatistical approach; Doligez et al. 2011).

Process-based geochemical modelling considers the diagenetic parameters as dynamic, evolving with time. This predictive approach aims at calculating the spatial-temporal emplacement of diagenetic phases (resulted from chemical reactions). Geometry-based, geostatistical, geochemical reactive transport models must be validated. Alternatively, adequate uncertainty analyses that are capable of assessing the probability of success of modelling realizations must to be applied.

Based on the sedimentological and geochemical studies of Whitaker and Smart (2007a, b), fluid-rock (0D) geochemical simulations were undertaken with ArXim to estimate porosity destruction or enhancement in hydrozones during their residence time in carbonate platform. Such innovative modules (together with possibility to undertake related sensitivity analyses on principal critical factors) can be eventually plugged in forward stratigraphic modelling tools and help in predicting the effect of diagenetic processes during the growth of a carbonate platform.

Attempts to quantify and predict the 3D pore space evolution in carbonate reservoir rocks have been done through geochemical modelling combined with micro-CT and reactive pore network modelling (PNM-R) (De Boever et al. 2012). Two major problems were faced while using R-PNM for modelling diagenesis: (i) difficulty to model micro-porosity inside grains; and (ii) reaching several possible paths for porosity-permeability functions. This second limitation is expressed by the fact that we could calibrate the model on the known time-steps, yet the paths between these steps could not be constrained (De Boever et al. 2012). Additional improvements are still needed for achieving more pertinent results with similarly integrated approaches.

Dolomite front propagations with geochemical RTM techniques—similar to Jones and Xiao (2005), and Consonni et al. (2010)—aim to predict the impacts of diagenesis on reservoir properties. Additional progress in software capabilities is still needed, as well as suitable reference cases for validation. In particular, porosity-permeability laws included into the geochemical RTM tools need to be revised. In addition, dual porosity and fracturing during RTM simulations, which are not taken into account at the moment, have to be properly addressed.

Eventually, we will succeed in integrating the paragenesis (time-defined key diagenetic processes/phases) into the burial history within basin and reservoir models. To reach this end, we need to develop a new methodology that allows chain simulations of successive key processes of diagenesis. Such tools need to be able to: (i) integrate fluid flow and geochemical species (e.g. Mg, Si, NaCl contents) transfer across basin-scale and reservoir-scale models; (ii) define robust porosity/permeability relationships and implement them properly—e.g. reactive transport models; and (iii) apply adequate uncertainty analyses.

5.4 Integrated Modelling Workflows

Integrated basin/reservoir modelling involves forward stratigraphic (source to sink), structural and petroleum system modelling. Lithofacies (simulated by forward stratigraphic methods) are transferred to burial models. Such transfer approach can be optimized by adding further functionalities for stratigraphic modelling with respect to early diagenesis and related impacts on reservoir properties. Hence, fluid flow would be better constrained in the larger basin geomodels, especially across new frontier hydrocarbon provinces—such as the Levant Basin in the Eastern Mediterranean region—where calibration wells are lacking (Nader 2014).

The Levant Basin model (Hawie et al. 2015) can be used as a reference case study to further apply basin-reservoir integrated modelling. Such a workflow may secure the larger-scale boundary

conditions that are needed for pertinent reservoir modelling with emphasis on fluid-rock interactions (e.g. Consonni et al. 2010). It is noteworthy to remind that while most of the concepts of diagenesis operate at the larger, basin-scale, the description of the diagenetic phases (products) and their association with the overall petrophysical evolution of sedimentary rocks remain at reservoir (and even outcrop/well core) scale. Upscaling and the definition of representative elementary volumes will constitute major challenges for sedimentologists and reservoir engineers in the coming decades. Integrated basin-reservoir geomodels can also help in tackling this challenge which includes solving technical problems as well as significant scientific questions.

In order to reach this end, we need to integrate stratigraphic, structural and basin modelling, incorporating organic matter distribution and fluid flow and geochemical species transfer. This latter breakthrough leads to inferring about the plausibility of certain diagenetic processes across the investigated basins. One should not forget fractured reservoirs and the resulting dual flow properties. The significance of the representativity of investigated samples, upscaling and REVs has been highlighted in this book. For modelling fractured reservoirs, production tests are commonly used. Therefore, another challenging issue is to find new ways to model dual, matrix and fracture flow properties in reservoirs.

Through this contribution, I have proposed a basin-reservoir integration workflow, whereby the large-scale constraining parameters (pressure, temperature, fluid fluxes) can be brought to the scale of reservoir as boundary conditions, and implementing the reservoir heterogeneities back to the basin-scale (check Fig. 4.46, Chap. 4). This approach will require applying and improving functionalities such as Local Grid Refinement to render the basin-scale grids closer to those of reservoirs, facilitating the nesting of reservoir models within the larger basin models. A 'Diagenesis Modelling Toolbox' consists of several numerical tools (some of which I have presented above, e.g. geostatistical and geochemical modelling) that will simulate diagenetic processes within this scheme and estimate their influences on the heterogeneity of carbonate reservoirs (Fig. 5.2).

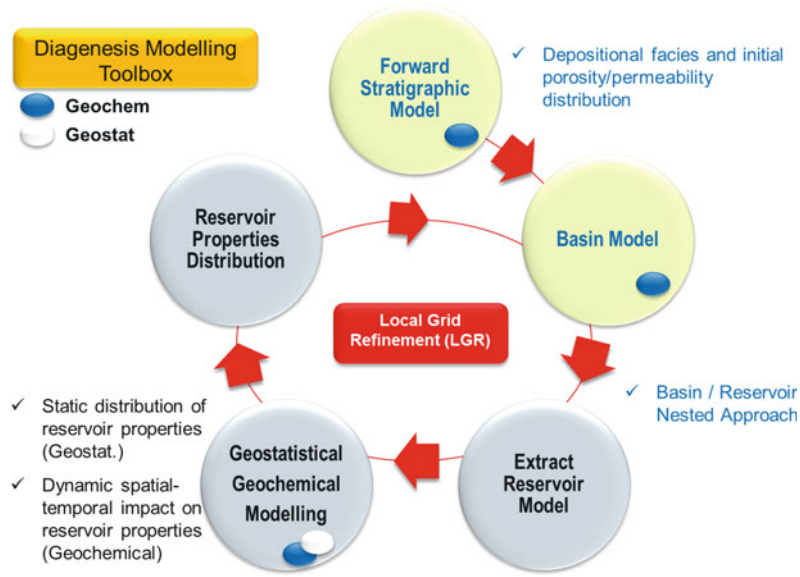

Fig. 5.2 The Diagenesis Modelling Toolbox: Several numerical tools (such as geostatistical methods and geochemical RTM) embedded within the basin-to-reservoir scale loop, capable of simulating diagenetic processes and their impacts on carbonate rocks

5.5 Way Forward

Understanding and predicting subsurface heterogeneities remain of paramount importance for petroleum exploration and production as well as geothermal energy production, underground storage, and environmental remediation. Numerical modelling of quantitative diagenesis and its impact on carbonate reservoir properties will be even more developed in the near future. Therefore, the way forward with respect to carbonate diagenesis scientific research seems evident to me as the integration of a variety of numerical workflows at different scales: from a basin-scale (using seismic data, outcrop-analogues, well cores, etc.) to a reservoir-scale, and eventually the plug-scale.

'Scale' remains the parameter that has been less investigated and cross-correlated. A multi-scale approach is, henceforth, necessary to constrain pertinently diagenetic processes. The challenge consists in defining the representativity of the investigated scale (e.g. REVs) and succeeding meaningful upscaling. In other words, we need to increase efficiency and avoid data information loss through upscaling. Based on the adopted scale of investigation, specific methods are to be used. Thus, the choice of the efficient methods for quantitative diagenesis is a function of the modelling scale.

Results of numerical modelling are to be validated by quantitative data with respect to diagenetic processes. In order to achieve this task, reference study cases should be characterized properly by means of modern quantitative techniques (some of which are still under development; e.g. clumped isotopes, U-Pb). In particular, there is a necessity for an innovative way in classifying pore space in carbonate rocks based on the 3D pore geometry rather than the surrounding texture.

Curriculum Vitae

Fadi Henri Nader
Email: fadi-henri.nader@ifpen.fr
Born: September 4, 1972

Geologist Expert at IFP Energies Nouvelles

Key Competencies

- 16 years of experience in research associated to hydrocarbon exploration and production
- Expert in sedimentology, carbonate rock diagenesis and reservoir characterization
- Skills in integrated sedimentology/stratigraphy, structural geology and geochemistry
- Teaching at universities, oil companies, and supervising students (M.Sc., Ph.D., Post-Doc)
- Co-author of more than 40 peer reviewed international publications
- Leader, mentor and coach of young geologists, geophysicists and reservoir engineers

Membership

- Member of the **International Association of Sedimentologists (IAS)** since 2001
- Fellow of the **Geological Society of London** since January 2004
- Active Member of the **AAPG** since January 2005. Delegate at the House of Delegates
- Member of the **Société Géologique de France** since January 2008
- Co-Leader of Task VII (Sedimentary Basins) of the **International Lithosphere Program**

Awards

AAPG Middle East "Distinguished Service Award", March 6, 2016.

Qualification

2015 Université Pierre et Marie Curie (UMPC, Paris VI University): Diplôme d'Habilitation à diriger la Recherche (HDR)—Multi-scale diagenesis and impacts on heterogeneity of reservoir rocks

2003 KU Leuven University (Belgium) : Ph.D. in Geology—Petrographic and

F.H. Nader, *Multi-scale Quantitative Diagenesis and Impacts on Heterogeneity of Carbonate Reservoir Rocks*, Advances in Oil and Gas Exploration & Production, DOI 10.1007/978-3-319-46445-9

geochemical study of the Kesrouane Formation (Jurassic), Mount Lebanon: implications on dolomitization and petroleum geology

2000 American University of Beirut (Lebanon): M.Sc. in Geology—Petrographic and chemical characterization of the Jurassic-Cretaceous carbonate sequence of the Nahr Ibrahim region, Lebanon

1994 American University of Beirut (Lebanon): B.Sc. in Geology

Glossary

ArXim Open source program for multiphase speciation, equilibrium and reaction calculations between minerals, aqueous solutions and gases (EMSE and IFPEN)

Avizo™ 3D analysis software application for exploring and understanding materials structures and properties, in a wide range of materials science research areas (FEI)

CobraFlow™ Software for performing geologically meaningful simulations using geostatistical algorithms (IFPEN and Centre of Geostatistics of the Paris School of Mines)

Coores™ (CO_2 Reservoir Environmental Simulator), a research code designed to study CO_2 storage processes from the well to the basin scale (IFPEN). It simulates multi-component three-phase and 3-D fluid flow in heterogeneous porous media. To take into account mineralogy changes, the transport model is coupled with ArXim

DionisosFlow™ (Diffusion Oriented Normal and Inverse Simulation Of Sedimentation), a deterministic 3D multi-lithology stratigraphic modelling software that simulates depositional processes in a sequence of steps moving forward in time (IFPEN)

EasyTrace™ A multi-disciplinary 1D data processing and editing tool, featuring advanced spreadsheets and a wide range of functionalities for geologists and geophysicists (IFPEN)

EOR Enhanced Oil Recovery

Fraca™ Software capable of characterizing, modelling and calibrating faults and fractures. It builds consistent fracture networks, constrained in 3D by seismic and geological attributes

GOCAD (Geological Object Computer Aided Design), a software package used for building and update, geo-referenced 3D subsurface models (Gocad Research Group, Georessources UMR 7359, Géologie—Université de Lorraine)

InterWell™ Software capable to analyse post, pre stack and 4D seismic data, to compute multi cubes seismic wavelet calibrated at wells and to build a priori seismic impedance cubes honouring wells and stratigraphic data (IFPEN)

JMicroVision A freeware designed to describe, measure, quantify and classify components of all kinds of images allowing to analyze high definition images of rock thin-sections (http://www.jmicrovision.com)

Matlab™ A high level programming language and interactive environment capable of advanced numeric computation, data analysis and visualization, programming and algorithm development and application (Mathworks)

F.H. Nader, *Multi-scale Quantitative Diagenesis and Impacts on Heterogeneity of Carbonate Reservoir Rocks*, Advances in Oil and Gas Exploration & Production, DOI 10.1007/978-3-319-46445-9

PHREEQ-C A computer program designed to perform a wide variety of aqueous geochemical calculations. It implements several types of aqueous models and is capable of undertaking speciation, saturation-index, and transport calculations (USGS)

TemisFlow™ Basin modelling software package for assessing regionally controlled petroleum systems and basin evolutions. It calculates the generation, migration and accumulation of fluids (IFPEN)

References

Abdel-Rahman, A.-F.M. and Nader, F.H. (2002). Characterization of the Lebanese carbonate stratigraphic sequence: a geochemical approach. The Geological Journal, 37, 69-91.

Adams, J.E., and Rhodes, M.L. (1960). Dolomitization by seepage reflux. AAPG Bulletin, 44, 1912-1920.

Ahr, W. (2008). Geology of Carbonate Reservoirs: The Identification, Description and Characterization of Hydrocarbon Reservoirs in Carbonate Rocks. John Wiley and Sons, Inc. New Jersey (USA). 227p.

Akbar, M., Petricola, M., Watfa, M., Badri, M. A., Charara, M., Boyd, A., Cassell, B., Nurmi, R., Delhomme, J.-P., Grace, M., Kenyon, B., and Roestenburg, J.W. (1995). Classic interpretation problems; evaluating carbonates. Oilfield Review, 7, 38-57.

Algive, L., Békri, S., and Vizika, O. (2009). Reactive pore network modeling dedicated to the determination of the petrophysical property changes while injecting CO_2, SPE Paper 124305 presented at the SPE Annual Technical conference and Exhibition, New Orleans, Louisiana, USA, 4-7 October, 2009.

Algive, L., Bekri, S., Nader, F.H., Lerat, O., and Vizika, O. (2012). Impact of diagenetic alterations on petrophysical and multiphase flow properties of carbonate rocks using a reactive pore network modelling approach. Oil & Gas Science and Technology (OGST), 67(1), 147-160.

Al-Kharusi, A.S., and Blunt, M.J. (2008). Multiphase flow predictions from carbonate pore space images using extracted network models. Water Resources Research, 44, W06S01.

Alsharhan, A.S., and Magara, K. (1994). The Jurassic of the Arabian Gulf Basin: Facies, depositional setting and hydrocarbon habitat. Canadian Society of Petroleum Geologists, Memoir 17, 397-412.

Al Silwadi, M.S., Kirkham, A., Simmons, D.S., and Twombley, B.N. (1996). New Insights into Regional Correlation and Sedimentology, Arab Formation (Upper Jurassic), offshore Abu Dhabi. GeoArabia, 1 (1), 6-27.

Al-Suwaidi, A.S., and Aziz, S.K. (2002). Sequence stratigraphy of Oxfordian and Kimmeridgian shelf carbonate reservoirs, offshore Abu Dhabi. GeoArabia, 7(1), 31-44.

Azer, S.R., and Peebles, R.G. (1998). Sequence Stratigraphy of the Arab A to C Members and Hith Formation, Offshore Abu Dhabi. GeoArabia, 3(2), 251-268.

Barbier, M., Hamon, Y., Doligez, B., Callot, J.-P., Floquet, M., and Daniel, J.-M. (2012). Stochastic joint simulation of facies and diagenesis: a case study on early diagenesis of the Madison Formation (Wyoming, USA). Oil & Gas Science and Technology, 67 (1), 123-146.

Bathurst, R.G.C. (1975). Carbonate Sediments and their Diagenesis. Elsevier Science Publ. Co., 660p.

Behar, F., Lorant, F., and Lewan, M.D. (2008). Role of NSO compounds during primary cracking of a Type II kerogen and a Type III lignite. Organic Geochemistry, 39, 1-22.

Bemer, E., Adelinet, Y., Hamon, Y., Dautriat, J., and Nauroy, J.-F. (2012). Petroacoustic Signature of Carbonate Rocks Microstructure. AAPG Hedberg Conference, Fundamental Controls on Flow in Carbonates, July 8-13, 2012, Saint-Cyr Sur Mer, Provence, France, Search and Discovery Article #120036 (2012)

Bethke, C.M. (1996). Geochemical reaction modeling. New York, Oxford University Press, 397p.

Bethke, C.M. (2002). The Xt2 model of transport in reacting geochemical systems. Hydrogeology program: Urbana, Illinois, University of Illinois, 89p.

Bonifacie, M., Calmels, D., and Eiler, J. (2013). Clumped isotope thermometry of marbles as an indicator of the closure temperatures of calcite and dolomite with respect to solid-state reordering of C-O bonds. Mineralogical Magazine, 77(5), 735.

Bonifacie, M., Calmels, D., Pisapia, C., Deschamps, P., Hamelin, B., Brigaud, B., Pagel, M., Katz, A., Gautheron, C., Saint Bezar, B., and Landrein, P. (2014). Une determination originale de la temperature et de l'age des cristaux de calcite dans des brèches et des datation U-Pb sur des cristaux de calcite. In: Proceedings of "Journée thématique ASF. Diagenèse: avancées récentes et perspectives", Orsay, 4 July, 2014. Publication ASF, Paris, 75.

Bosworth, W., Huchon, P., and McClay, K. (2005). The red sea and Gulf of Aden basins. Journal of African Earth Sciences, 43, 334-378.

F.H. Nader, *Multi-scale Quantitative Diagenesis and Impacts on Heterogeneity of Carbonate Reservoir Rocks*, Advances in Oil and Gas Exploration & Production, DOI 10.1007/978-3-319-46445-9

Bou Daher, S., Nader, F.H., Müller, C., and Littke, R. (submitted). Journal of Petroleum Geology, 37 (1), 5-24. Geochemical and petrographic characterization of Campanian – Lower Maastrichtian calcareous petroleum source rocks of Hasbayya, South Lebanon. Marine and Petroleum Geology, submitted.

Bou Daher, S., Nader, F.H., Strauss, H., and Littke, R. (2014). Depositional environment and source-rock characterization of organic-matter rich upper Santonian - upper Campanian carbonates, northern Lebanon. Journal of Petroleum Geology, 37 (1), 5-24.

Boudreau, B.P. (1997). Diagenetic models and their implementation. Springer-Verlag, Berlin, 482p.

Bourdet, J., Pironon, J., Levresse, G., and Tritlla, J. (2010). Petroleum accumulation and leakage in a deeply buried carbonate reservoir, Níspero field (Mexico). Marine and Petroleum Geology, 27, 126-142.

Bowman, S.A. (2011). Regional seismic interpretation of the hydrocarbon prospectivity of offshore Syria. GeoArabia, 16(3), 95-124.

Breesch, L., Swennen, R., and Vincent, B. (2009). Fluid flow reconstruction in hanging and footwall carbonates: Compartmentalization by Cenozoic reverse faulting in the Northern Oman Mountains (UAE). Marine and Petroleum Geology, 26, 113-128.

Breesch, L., Swennen, R., Dewever, V., Roure, F., and Vincent, B. (2011). Diagenesis and fluid system evolution in the northern Oman Mountains, United Arab Emirates: Implications for petroleum exploration. GeoArabia, 16(2), 111-148.

Caers, J., and Zhang, T. (2002). Multiple-point geostatistics: a quantitative vehicle for integrating geologic analogs into multiple reservoir models. Stanford University, Stanford Center for Reservoir Forecasting, Stanford CA 94305-2220, 24p.

Callot, J.P., Breesch, L., Guilhaumou, N., Roure, F., Swennen, R., and Vilasi, N. (2010). Paleo-fluids characterisation and fluid flow modelling along a regional transect in Northern United Arab Emirates (UAE). Arabian Journal of Geosciences, 3, 413-437.

Cantrell, D.L., Swart, P.K., and Hagerty, R.M. (2004). Genesis and characterization of dolomite, Arab-D Reservoir, Ghawar Field, Saudi Arabia. GeoArabia, 9 (2), 11-36.

Cantrell, D.L., Swart, P.K., Robertson, C.H., Kendal, C. G. and Westphal, H. (2001). Geology and production significance of dolomite, Arab-D resrvoir, Ghawar field, Saudi Arabia. GeoArabia, 6(1), 45-59.

Caspard, E., Rudkiewicz, J.L., Eberli, G.P., Brosse, E., and Renard, M. (2004). Massive dolomitization of a Messinian reef in the Great Bahama Bank: a numerical modelling evaluation of Kohout geothermal convection. Geofluids 4, 40-60.

Caumon, M.-C., Robert, P., Laverret, E., Tarantola, A., Randi, A., Pironon, J., Dubessy, J., and Girard, J.-P. (2014). Determination of methane content in NaCl-H2O fluid inclusions by Raman spectroscopy. Calibration and application to the external part of the central Alps (Switzerland). Chemical Geology, 378-379, 52-61.

Ceriani, A., Di Giulio, A., Goldstein, R.H., Rossi, C. (2002). Diagenesis associated with cooling during burial: an example from lower Cretaceous reservoir sandstones (Sirt Basin, Libya). AAPG Bulletin, 86(9), 1573–1591.

Chaojun, Z., Chengzao, J., Benliang, L., Xiuyu, L., and Yunxiang, L. (2010). Ancient karsts and hydrocarbon accumulation in the middle and western parts of the North Tarim uplift, NW China. Pet. Explor. Dev., 37, 263–269.

Chauveau, B., Granjeon, D., and Huc, A. (2013). Depositional model of marine organic matter coupled with stratigraphic forward numerical model (Dionisos) : Application to the Devonian Marcellus Formation. In: Proceedings of AAPG ICE, International Conference and Exhibition (8-11 September 2013, Colombia).

Choquette, P.W., and James, N.P. (1987). Diagenesis # 12. Diagenesis in Limestones-3. The deep burial environment. Geoscience Canada, 14, 3-35.

Choquette, P.W., and Pray, L.C. (1970). Geologic nomenclature and classification of porosity in sedimentary carbonates. AAPG Bulletin, 54, 207-250.

Chou, I.M., Song, Y.C., and Burruss, R.C. (2008). A new method for synthesizing fluid inclusions in fused silica capillaries containing organic and inorganic material. Geochimica Cosmochimica Acta, 72(21), 5217-5231.

Cita, M.B., and Ryan, W.B.F. (1978). Messinian erosional surfaces in the Mediterranean. Marine Geology, 27, 193-366.

Claes, S. (2015). Pore classification and upscaling strategy in travertine reservoir rocks. PhD Thesis, KU Leuven, Belgium, 119p.

Consonni, A., Ronchi, P., Geloni, C., Battistelli, A., Grigo, D., Biagi, S., Gherardi, F., and Gianelli, G. (2010). Application of numerical modelling to a case of compaction-driven dolomitization: a Jurassic palaeohigh in the Po Plain, Italy. Sedimentology, 57, 209-231.

Davies, G.R., and Smith, L.B. (2006). Structurally controlled hydrothermal dolomite reservoir facies: an overview. AAPG Bulletin, 90(11), 1641-1690.

De Andrade, V., Vidal, O., Lewin, E., O'Brien, P., and Agard, P. (2006). Quantification of electron microprobe compositional maps of rock thin sections: an optimized method and examples. Journal of Metamorphic Geology, 24, 655-668.

De Boever, E., Varloteaux, C., Nader, F.H., Foubert, A., Bekri, S., Youssef, S., and Rosenberg, E. (2012). Quantification and prediction of the 3D pore network evolution in carbonate reservoir rocks. Oil & Gas Science and Technology (OGST), 67(1), 161-178.

Dennis, K.J., Affek, H.P., Passey, B.H., Schrag, D.P., and Eiler, J.M. (2011). Defining an absolute reference frame for 'clumped' isotope studies of CO_2. Geochimica et Cosmochimica Acta, 75, 7117-7131.

Dercourt, J., Ricou, L.E., and Vrielynck, B. (1993). Atlas Tethys Paleoenvironmental Maps. Gauthier-Villars, Paris, 307p.

Deschamps, R., Kohler, E., Gasparrini, M., Durand, O., Euzen, T., and Nader, F.H. (2012). Impact of mineralogy and diagenesis on reservoir quality of the Lower Cretaceous Upper Mannville Formation (Alberta, Canada). Oil & Gas Science and Technology (OGST), 67 (1), 31-58.

Dewit, J. (2012). Genesis and reservoir properties of hydrothermal dolomites (HTD), Ramales platform (northern Spain). PhD Thesis, KU Leuven, Belgium, 183p.

Dickson, J.A.D. (1966). Carbonate identification and genesis as revealed by staining. Journal of Sedimentary Petrology, 36, 491-505.

Doligez, B., Beucher, H., Geffroy, F., and Eschard, R. (1999). Integrated reservoir characterization: improvement in heterogeneous stochastic modeling by integration of additional external constraints. In: Reservoir Characterization Recent Advances, R.Schatzinger and J.Jordan eds., AAPG Memoir 71, 333-342.

Doligez, B., Beucher, H., Pontiggia, M., Ortenzi, A., and Mariani, A. (2009). Comparison of Methodologies and Geostatistical Approaches for Diagenesis Quantification, AAPG Convention, Denver, Colorado, 7-10 June.

Doligez, B., Hamon, Y., Barbier, M., Nader, F., Lerat, O., and Beucher, H. (2011). Advanced workflows for joint modelling of sedimentological facies and diagenetic properties. Impact on reservoir quality. SPE Annual Conference and Exhibition in Denver, Colorado, USA, 30 October – 2 November 2011, SPE 146621.

Dolson, J.C., Boucher, P.J., Siok, J., and Heppard, P.D. (2005). Key challenges to realizing full potential in an emerging giant gas province: Nile Delta/Mediterranean offshore, deepwater, Egypt. In: Dore, A.G., Vining, B.A. (eds.), Petroleum Geology: North-West Europe and Global Perspectives-Proceedings of the 6th Petroleum Geology Conference. Petroleum Geology Conferences Ltd. Published by the Geological Society, London, 607-624.

Doummar, J. (2005). Sedimentology and diagenesis of the Albian rock sequence (Upper Hammana-Lower Sannine Formations), northern Lebanon. MSc. Thesis, American University of Beirut, Beirut, Lebanon, 199p.

Dreybrodt, W., Gabrovšek, F., and Romanov, D. (2005). Processes of speleogenesis: a modeling approach. Carsologica 4 (ZRC Publishing, Karst Research Institute – ZRC SAZU, Postojna – Ljubljana, Slovenia), 375p.

Durand, B., and Nicaise, G. (1980). Procedure of kerogen isolation. In: Durand, B. (Ed.), Kerogen, Insoluble Organic Matter from Sedimentary Rocks. Editions Technip, Paris, 13-34.

Ehrenberg, S.N. (2006). Porosity destruction in carbonate platforms. Journal of Petroleum Geology, 29, 41-52.

Ehrenberg, S.N., Nadeau, P.H., and Aqrawi, A.A.M. (2007). A comparison of Khuff and Arab reservoir potential throughout the Middle East. AAPG Bulletin, 91(3), 275-286.

Eiler, J.M. (2007). "Clumped-isotope" geochemistry – The study of naturally-occurring, multiply-substituted isotopologues. Earth and Planetary Science Letters, 262, 309-327.

Emery, X., and Gonzalez, K. (2007). Probabilistic modelling of lithological domains and its application to resource evaluation. Journal of the South African Institute of mining and metallurgy, 107(12), 803-809.

Emery, D., and Robinson, A. (1993). Inorganic Geochemistry: Applications to Petroleum Geology. Blackwell Scientific Publications, Oxford, 250p.

Erickson, A.J., and Von Herzen, R.P. (1978). Downhole temperature measurements, DSDP leg 42A, Initial Rep. Deep Sea Drill. Proj., 42A, 857-871.

Esrafili-Dizaji, B., and Rahimpour-Bonab, H. (2009). Effects of depositional and diagenetic characteristics on carbonate reservoir quality: a case study from the South Pars gas field in the Arabian Gulf. Petroleum Geoscience, 15, 325-344.

Esteban, M., and Taberner, C. (2003). Secondary porosity development during late burial in carbonate reservoirs as a result mixing and/or cooling of brines (in Proceedings of Geofluids IV). Journal of Geochemical Exploration, 78-79, 355-359.

Falivene, O, Arbuès, P., Gardiner, A., Pickup, G., Muñoz, J.A., and Cabrera, L. (2006). Best practice stochastic facies modeling from a channel-fill turbidite sandstone along (the Quarry outcrop, Eocene Ainsa basin, northeast Spain). AAPG Bulletin, 90(7), 1003-1029.

Ferket, H., Guilhaumou, N., Roure, F., and Swennen, R. (2010). Insights from fluid inclusions, thermal and PVT modeling for paleo-burial and thermal reconstruction of the Cordoba petroleum system (NE Mexico). Marine and Petroleum Geology, 28(4), 936-958.

Fitch, P.J.R. (210). Heterogeneity in the petrophysical properties of carbonate reservoirs. Ph.D. Thesis, University of Leicester (UK), 265p.

Fleming, C.A. (1969). The Mesozoic of New Zeland. Chapters in the history of the Circum Pacific Mobile Belt. Quarterly Journal of Geological Society of London, 125, 70-125.

Fleury, M., Santerre, Y., and Vincent, B. (2007). Carbonate rock typing from NMR relaxation measurements. Proceeding of the SPWLA annual Symposium, Austin, June 3-6, 2007.

Fontaine, L., and Beucher, H. (2006). Simulation of the Muyumkum uranium roll front deposit by using truncated plurigaussian method. In : Proceedings of the 6th International Mining Geology Conference, "Rising the challenge", 21-23 August 2006, Darwin, Australia, 11p.

Fontana, S., Nader, F.H., Morad, S., Ceriani, A., and Al-Aasm, I.S. (2010). Diagenesis of the Khuff Formation (Permian-Triassic), northern Uinted Arab Emirates. Arab J. Geosci. (Springer), 3, 351-368

Fontana, S., Nader, F.H., Morad, S., Ceriani, A., Al-Aasm, I.S., Daniel J.-M., and Mengus, J.-M. (2014). Fluid-rock interactions associated with regional tectonics and basin evolution. Sedimentology, 61, 660-690.

Foubert, A., and Henriet, J.-P. (2009). Nature and significance of the recent carbonate mound record: The mound challenger code. Springer-Verlag, Berlin Heidelberg.

Freytet, P., and Verrecchia, E.P. (2002) Lacustrine and palustrine carbonate petrography: an overview. J. Paleolimnol., 27, 221–237.

Friedman, I., and O'Neil, J.R. (1977). Compilation of stable isotopic fractionation factors of geochemical interest. In M. Fleischer (Ed.), Data of Geochemistry. United States Geological Survey Professional Paper, 440-KK, 6th edition, 12p.

Frisia, S., Borsato, A., Fairchild, I.J, and McDermott, F. (2000). Calcite fabrics, growth mechanisms, and environments of formation in speleothems from the Italian Alps and Southwestern Ireland. Journal of Sedimentary Research, 70, 1183-11 96.

Galli, A., Le Loc'h, G., Geffroy, F., and Eschard, R. (2006). An application of the truncated pluri-gaussian method for modeling geology. In Stochastic modeling and geostatistics: principles, methods and case studies. AAPG Computer applications in Geology 5 (2), 109-122.

Gardet, C., Bouquet, S., and Le Ravalec, M. (in press). Multiscale simulation of geological formations with multipoint statistics. Stoch. Environ. Res. Risk Assess., in press.

Gardosh, M., Druckman, Y., Buchbinder, B., and Rybakov, M. (2006). The Levant Basin Offshore Israel: Stratigraphy, Structure, Tectonic Evolution and Implications for Hydrocarbon Exploration. Geophysical Institute of Israel, 1-119.

Gardosh, M., Druckman, Y., Buchbinder, B., and Calvo, R. (2008). The Oligo-Miocene deepwater system of the Levant basin. Geological Survey of Israel, 33, 1-73.

Gasparrini, M., Bechstädt, T., and Boni, M. (2006). Massive hydrothermal dolomites in the southwestern Cantabrian Zone (Spain) and its relation to the late Variscan evolution. Marine and Petroleum Geology, 23(5), 543-568.

George, R., Rogers, N., and Kelley, S. (1998). Earliest magmatism in Ethiopia: evidence for two mantle plumes in one flood basalts province. Geology, 26, 923-926.

Ghalayini, R., Daniel, J.-M., Homberg, C., Nader, F.H., and Comstock, J.E. (in press). Impact of Cenozoic strike-slip tectonics on the evolution of the northern Levant Basin (offshore Lebanon). Tectonics, 10.1002/2014TC003574.

Ghosh, P., Adkins, J., Affek, H., Balta, B., Guo, W.F., Schauble, E.A., Schrag, D., and Eiler, J.M. (2006). $^{13}C–^{18}O$ bonds in carbonate minerals: a new kind of paleothermometer. Geochim. Cosmochim. Acta, 70 (6), 1439–1456.

Girard, J.-P., Ong, A., Caumon, M.-C., Laverret, E., and Pironon, J. (2014). Recent advances in coupling petroleum and aqueous fluid inclusions for diagenesis P-T reconstructions in hydrocarbon reservoirs. In: Proceedings of "Journée thématique ASF. Diagenèse: avancées récentes et perspectives", Orsay, 4 July, 2014. Publication ASF, Paris, 75, 44-47.

Goldsmith, J.R., and Graf, D.L. (1958). Structural and compositional variations in some natural dolomites. Journal of Geology, 66, 678-693.

Granjeon, D. (1996). Modélisation stratigraphique déterministe – conception et applications d'un modèle diffusif 3D multilithologique, Géosciences Rennes. Université de Rennes 1, Rennes, France.

Granjeon, D., and Joseph, P. (1999). Concepts and applications of a 3-D multiple lithology, diffusive model in stratigraphic modeling. Numerical experiments in stratigraphy: recent advances in stratigraphic and sedimentologic computer simulations. SEPM Spec. Publ., 62, 197-210.

Gringarten, E., and Deutsch, C.V. (1999). Methodology for Variogram Interpretation and Modeling for Improved Reservoir Characterization. Society of Petroleum Engineers, SPE 56654.

Gringarten, E., and Deutsch, C.V. (2001). Teacher's Aide Variogram Interpretation and Modeling. Mathematical Geology, vol. 33, no. 4.

Hamon Y., Deschamps R., Joseph P., Schmitz J., Doligez B., Lerat O., Dumont C. (2013). Integrated workflow for characterization and modelling of a mixed sedimentary system: The Alveolina Limestone Formation (Early Eocene, Graus-Tremp Basin, Pyrenees, Spain). In: 14ème congrès français de Sédimentologie (Ed. ASF), 437 p., Paris, France.

Halstenberg, D.B. (2014). Reconstruction of tectonic paleo-heat flow for the Levantine Basin (Eastern Mediterranean); Implications for basin and petroleum system modelling. MSc. Thesis, RWTH Aachen University, 85p.

Hawie, N. (2014). Architecture, geodynamic evolution and sedimentary filling of the Levant Basin: a 3D quantitative approach based on seismic data. PhD Thesis, Université Pierre et Marie Curie (Paris VI), Paris, France, 271p.

Hawie, N., Deschamps, R., Granjeon, D., Nader, F.H., Gorini, C., Muller, C. Montadert, L., and Baudin, F. (in press). Multi-scale constraints of sediment source to sink systems in frontier basins: a forward stratigraphic modelling case study of the Levant Basin. Basin Research, accepted/in press.

Hawie, N., Gorini, C., Deschamps, R., Nader, F.H., Montadert, L., Granjeon, D. Baudin, F. (2013). Tectono-stratigraphic evolution of the northern Levant Basin (offshore Lebanon). Marine and Petroleum Geology, 48, 392-410.

Henrion, V., Caumon, G., and Cherpeau, N. (2010). ODSIM: an object-distance simulation method for conditioning complex natural structures. Math. Geosci., 42(8), 911–924.

Hood, S.D., Nelson, C.S., and Kamp, P. J.J. (2004). Burial dolomitisation in a non-tropical carbonate petroleum reservoir: the Oligocene Tikorangi Formation, Taranaki Basin, New Zealand. Sedimentary Geology, 172, 117-138.

Hu, L.Y., and Ravalec-Dupin, M.L. (2004). Elements for an Intergrated Geostatistical Medeling of Heterogeneous Reservoirs. Oil & Gas Science and Technology (OGST), 59(2), 141-155.

Humphrey, J.D. (1988). Late Pleistocene mixing zone dolomitization, southeastern Barabados, West Indies. Sedimentology, 35, 327-348.

Hutchison, C.S. (1971). Laboratory Handbook of Petrographic Techniques. Wiley-Interscience, New York, 527p.

Hutington, K.W., Budd, D.A., Wernicke, B.P., and Eiler, J.M. (2011). Use of clumped-isotope thermometry to constrain the crystallization temperature of diagenetic calcite. Journal of Sedimentary Research, 81, 656-669.

Illing, L.V. (1959). Deposition and diagenesis of some upper Paleozioc carbonate sediments in Western Canada. Proceedings, Fifth World Petroleum Congress, New York, Section 1, 23-52.

Immenhauser, A., Hillgärtner, H., and Van Bentum, E. (2005). Microbial-foraminiferal episodes in the Early Aptian of the southern Tethyan margin: ecological significance and possible relation to oceanic anoxic event 1a. Sedimentology, 52, 77-99.

Ivanov, M.V., Lein, A.Yu., and Kashparova, E.V. (1976). Oxidized compounds of sulfur in sediments of the PacificOcean; intensity of their formation and diagenetic changes. In: I.I. Volkov (Editor), The Biochemistry of Diagenesis of Ocean Sediments. Akademia Nauk, Moscow, 171-178 (in Russian).

Jodry, R.L. (1969). Growth and dolomitization of Silurian Reefs, St. Clair County, Michigan. AAPG Bulletin, 53, 957-981.

Jones, B., Robert, L.W., and Macneil, A. J. (2001). Powder X-ray diffraction analysis of homogeneous and heterogeneous sedimentary dolostones. Journal of Sedimentary Research, 71, 790-799.

Jones, G.D., and Xiao, Y. (2005). Dolomitization, anhydrite cementation, and porosity evolution in a reflux system: Insights from reactive transport models. AAPG Bulletin, 89(5), 577-601.

Klimchouk, A. (2007). Hypogene Speleogenesis: Hydrogeological and morphogenetic perspective. National Cave and Karst Research Institute, Carlsbad, NM, USA, Special Paper N°1, 106p.

Knackstedt, M.A., Arns, C., Ghous, A., Sakellariou, A., Senden, T., Sheppard, A.P., Sok, R.M., Averdunk, H., Pinczewski, W.V., Padhy, G.S., and Ioannidis, M.A. (2006). 3D imaging and flow characterization of the pore space of carbonate core samples, Paper SCA2006-23 presented at the International Symposium of Core Analysts, Trondheim, Norway, 12-16 September.

Koehrer, B., Zeller, M., Aigner, T., Poeppelreiter, M., Milroy, P., Forke, H., and Al-Kindi, S. (2010). Facies and stratigraphic framework of a Khuff outcrop equivalent: Saiq and Mahil formations, Al Jabal al-Akhdar, Sultanate of Oman. GeoArabia, 15, 91-156.

Koehrer, B, Aigner, T., and Pöppelreiter, M. (2011). Field-scale geometries of Upper Khuff reservoir geobodies in an outcrop analogue (Oman Mountains, Sultanate of Oman). Petroleum Geoscience, 17, 3-16.

Kurz, T.H., Dewit, J., Buckley, S.J., Thurmonds, J.B., Hunts, D., and Swennen, R. (2012). Hyperspectral image analysis of different carbonate lithologies (limestone, karst and hydrothermal dolomites): the Pozalagua quarry case (Cantabria, North-west Spain). Sedimentology, 59, 623-645.

Labourdette, R. (2007). 3D sedimentary modelling: toward the integration of sedimentary heterogeneities in reservoir models. PhD Thesis, Université Montpellier 2, France.

Lai, J., Wang, G., Chai, Y., and Ran, Y. (2015). Prediction of Diagenetic Facies using Well Logs: Evidences from Upper Triassic Yanchang Formation Chang 8 Sandstones in Jiyuan Region, Ordos Basin, China. Oil & Gas Science and Technology (OGST), DOI:10.2516/ogst/2014060.

Land, L.S. (1983). The application of stable isotopes to studies of the origin of dolomite and to problems of diagenesis of clastic sediments. In M.A. Arthur, T.F. Anderson, I.R. Kaplan, J. Veizer and L.S. Land (Eds.), Stable Isotopes in Sedimentary Geology. Society of Economic Paleontologists and Mineralogists Short Course Note 10, 4.1-4.22.

Lapponi, F., Casini, G., Sharp, I., Blendinger, W., Ferna´ndez, N., Romaire, I., and Hunt, D. (2011). From outcrop to 3D modelling: a case study of a dolomitized carbonate reservoir, Zagros Mountains, Iran. Petroleum Geoscience, 17(3), 283-307

Lavoie, D., Jackson, S., and Girard, I. (2011). Understanding hydrothermal dolostone through combined new stable isotope (δMg) analyses with conventional field, petrographic and isotopic data. AAPG International Conference and Exhibition, Milan, Italy, October 23-26, 2011 – Search and Discovery Article #50521.

Lerat, O., Nivlet, P., Doligez, B., Lucet, N., Roggero, F., Berthet, P., Lefeuvre, F., and Vittori, J. (2007). Construction of a Stochastic Geological Model Constrained by High-Resolution 3D Seismic Data - Application to the Girassol Field, Offshore Angola. Society of Petroleum Engineers, SPE 110422.

Le Ravalec, M., Doligez, B., and Lerat, O. (2014). Integrated reservoir characterization and modeling. IFPEN E-book, 2014, DOI:10.2516/ifpen/2014001 http://books.ifpenergiesnouvelles.fr/ebooks/integrated_reservoir_characterization_and_modeling/

Le Ravalec, M., Noetinger, B., and Hu, L.Y. (2000). The FFT Moving Average (FFT-MA) Generator: An Efficient Numerical Method for Generating and Conditioning Gaussian Simulations. Math. Geology, 32 (6), 2000, DOI : 10.1023/A:1007542406333

Li, W., Chakraborty, S., Beard, B.L., Romanek, C.S., and Johnson, C.M. (2012). Magnesium isotope

fractionation during precipitation of inorganic calcite under laboratory conditions. Earth and Planetary Science Letters, 333-334, 304-316.

Liberati, M. (2010). Field-scale distribution of diagenetic phases in the Arab D and Arab C members (Late Jurassic, UAE): quantifying diagenetic processes and inferring their impacts on reservoir heterogeneities. MSc., University of Pavia, Italy, 130p.

Longman, M.W. (1980). Carbonate diagenetic textures from nearsurface diagenetic environments. AAPG Bulletin, 64, 461-487.

Lønøy, A., 2006. Making sense of carbonate pore systems. AAPG Bulletin, 90 (9), 1381-1405.

López-Horgue, M.A., Iriarte, E., Schröder, S., Fernández-Mendiola, P.A., Caline, B., Corneyllie, H., Frémont, J., Sudrie, M., and Zerti, S. (2010). Structurally controlled hydrothermal dolomites in Albian carbonates of the Asón valley, Basque Cantabrian Basin, Northern Spain. Marine and Petroleum Geology, 27, 1069-1092.

Lucia, F.J., (1999). Carbonate reservoir characterization. New York, Springer, 226p.

Lumsden, D.N. (1979). Discrepancy between Thin-Section and X-Ray Estimates of Dolomite in Limestone. Journal of Sedimentary Petrology, 49(2), 429-436.

Machel, H.G. (2004). Concepts and models of dolomitization: a critical reappraisal. In: Braithwaite, C.J.R., Rizzi, G., and Darke, G., eds., The Geometry and Petrogenesis of Dolomite Hydrocarbon Reservoirs: London, Geological society of London. Special Publications 235, 7-63.

Machel, H.G., Mason, R.A., Mariano, A.N., and Mucci, A. (1991). Causes and emission of luminescence in calcite and dolomite. In Barker, C.E. & Kopp, O.C., eds., Luminescence Microscopy and Spectroscopy: Qualitative and Quantitative Applications. SEPM, 9-25.

Machel, H.G., Cavell, P.A., and Patey, K.S. (1996). Isotopic evidence for carbonate cementation and recrystallization, and for tectonic expulsion of fluids into the Western Canada Sedimentary Basin. Geological Society of America Bulletin, 108, 1108-1119.

Macgregor, D.S. (2012). The development of the Nile drainage system: integration of onshore and offshore evidence. Petroleum Geoscience, 18, 417-431.

Mariethoz, G., Renard, P., Cornaton, F., and Jaquet, O. (2009). Truncated Plurigaussian Simulations to Characterize Aquifer Heterogeneity. Groundwater, 47 (1), 13-24, DOI: 10.1111/j.1745-6584.2008.00489.x

Marlow, L., Kornpihl, K., and Kendall, C.G. (2011). 2-D Basin modelling study of petroleum systems in the Levantine Basin, Eastern Mediterranean. GeoArabia, 16(2), 17-42.

Matheron, G., Beucher, H, Fouquet, C., Galli, A.., Guerrilot, D., and Ravenne, C. (1987). Conditional simulation of the geometry of fluvio-deltaic reservoirs. Paper SPE 16753 presented at the SPE Annual Technical Conference and Exhibition, 62, Dallas-TX, 123-130.

McKenzie, J.A. (1981). Holocene dolomitization of calcium carbonate sediments from the coastal sabkhas of Abu Dhabi, U.A.E. Journal of Geology, 89, 185-198.

Mees, F., Swennen, R., Van Geet, M., and Jacobs, P. (2003). Applications of X-ray computed tomograhy in geosciences, in F Mees, R Swennen, M Van Geet, and P Jacobs eds., Applications of X-ray Computed Tomography in the Geosciences: London, Geological Society of London, Special Publications, 215, 1-6.

Melim, L.A., and Scholle, P.A. (2002). Dolomitization of the Capitan Formation forereef facies (Permian, west Texas and New Mexico): seepage reflux revisited. Sedimentology, 49, 1207-1227.

Milliman, J.D., and Syvitski, J.P.M. (1992). Geomorphic/tectonic control of sediment discharge to the ocean: The importance of small mountainous rivers. Journal of Geology, 100, 525-544.

Minster, T., Nathan, Y., and Ravh, A. (1992). Carbon and sulfur relationships in marine Senonian organic-rich, iron-poor sediments from Israel - a case study. Chemical Geology, 97, 145-161.

Miser, D.E., Swinnea, J.S., and Steinfink, H. (1987). TEM Observations and X-Ray Crystal-Structure Refinement of a Twinned Dolomite with a Modulated Microstructure. Am. Mineral., 72, 1-2, 188-193.

Moldovanyi, E.P., and Walter, L.M. (1992). Regional trends in water chemistry, Smackover Formation, southwest Arkansas: Geochemical and physical controls. AAPG Bulletin, 76(6), 864-894.

Moore, C.H. (2001). Carbonate Rservoirs: Porosity Evolution and Diagenesis in a Sequence Stratigraphic Framework. Developments in Sedimentology (Elsevier Science B.V., Amsterdam), 55, 444p.

Morad, D. (2012). Geostatistical Modeling of the Upper Jurassic Arab D Reservoir Heterogeneity, Offshore Abu Dhabi, United Arab Emirates. MSc. Thesis, Uppsala University, Sweden, 113p.

Morad, S., Al-Aasm, I.S., Nader, F.H., Ceriani, A., Gasparrini, M., and Mansurbeg, H. (2012). Impact of diagenesis on the spatial and temporal distribution of reservoir quality in the Jurassic Arab D and C members, offshore Abu Dhabi oilfield, United Arab Emirates. GeoArabia, 17(3), 17-56.

Moradpour, M., Zamani, Z., and Moallemi, S.A. (2008). Controls on reservoir quality in the lower Triassic Kangan Formation, Southern Arabian Gulf. Journal of Petroleum Geology, 31, 367-386.

Nader, F.H. (2003). Petrographic and geochemical study of the Kesrouane Formation (Jurassic), Mount Lebanon: Implications on dolomitization and petroleum geology, Katholieke Universiteit Leuven, 386p.

Nader, F.H. (2011). The petroleum prospectivity of Lebanon: an overview. Journal of Petroleum Geology, 34 (2), 135-156

Nader, F.H. (2014a). Insights into the Petroleum Prospectivity of Lebanon. In: Marlow, L., Kendall, C., and Yose, L. (eds): Petroleum systems of the Tethyan region. AAPG Memoir 106, 241-278.

Nader, F.H. (2014b). The Geology of Lebanon. Scientific Press, 108p.

Nader, F. H. and Swennen, R. (2004a). Petroleum prospects of Lebanon: Some remarks from sedimentological and diagenetic studies of Jurassic carbonates. Journal of Marine and Petroleum Geology, 21(4), 427-441.

Nader, F. H. and Swennen, R. (2004b). The hydrocarbon potential of Lebanon: new insights from regional correlations and studies of Jurassic dolomitization. Journal of Petroleum Geology, 27(3), 253-275.

Nader, F. H., Abdel-Rahman, A.-F. M., and Haidar, A. T. (2006). Petrographic and chemical traits of Cenomanian carbonates from central Lebanon and implications for their depositional environments. Cretaceous Research, 27, 689-706.

Nader, F. H., Swennen, R. and Ottenburgs, R. 2003. Karst-Meteoric dedolomitization of Jurassic carbonates, Lebanon. Geologica Belgica, 6, 3-23.

Nader, F. H., Swennen R. and Ellam, R. (2004). Stratabound dolomite versus volcanism-associated dolomite: an example from Jurassic platform carbonates in Lebanon. Sedimentology, 51(2), 339-360.

Nader, F., Swennen, R, Ellam, R. (2006). Petrographic and geochemical study of the Jurassic dolostones from Lebanon: evidence for superimposed diagenetic events. Journal of Geochemical Exploration, 89, 288-292.

Nader, F.H., Swennen, R., and Ellam, R. (2007). Field geometry, petrography and geochemistry of a dolomitization front (Late Jurassic, central Lebanon). Sedimentology, 54, 1093-1110.

Nader, F.H., Swennen, R., and Keppens, E. (2008). Calcitization/dedolomitization of Jurassic dolostones (Lebanon): results from petrographic and sequential geochemical analyses. Sedimentology, 55, 1467-1485.

Nader, F.H., Lopez-Horgue, M.A., Shah, M.M., Dewit, J., Garcia, D., Swennen, R., Iriarte, E., Muchez, P., and Caline, B. (2012). The Ranero hydrothermal dolomites (Albian, Karrantza valley, northwest Spain): Implications on conceptual dolomite models. Oil & Gas Science and Technology (OGST), 67(1), 9-29.

Nader, F.H., De Boever, E., Gasparrini, M., Liberati, M., Dumont, C., Ceriani, A., Morad, S., Lerat, O., and Doligez, B. (2013). Quantification of diagenesis impact on reservoir properties of the Jurassic Arab D and C members (offshore, U.A.E.). Geofluids, 13, 204-220.

Naylor, D., Al-Rawi, M., Clayton, G., Fitzpatrick, M.J., and Green, P.F. (2013). Hydrocarbon potential in Jordan. Journal of Petroleum Geology, 36 (3), 205-236.

Netzeband, G. L., Gohl, K., Hubscher, C.P., Ben-Avraham, Z., Dehghani, G.A., Gajewski, D., and Liersch, P. (2006). The Levantine Basin crustal structure and origin. Tectonophysics, 418, 167-188.

Nordahl, K., and Ringrose, P. (2008). Identifying the representative elementary volume for permeability in heterolithic deposits using nuerical rock models. Mathematical Geosciences, 40, 753-771.

Normando, M.N., Remacre, A.Z., and Sancevero, S.S. (2005). The Study of Plurigaussian Simulation's Lithotype Rule in Reservoir Characterization Process. Paper SPE 94949-MS presented at the SPE Latin American and Caribbean Petroleum Engineering Conference, 20-23 June, Rio de Janeiro, Brazil.

Ong, A. (2013). Réservoirs silicoclastiques très enfouis: Caractérisation diagénétique et modélisation appliquées aux champs pétroliers du Viking Graben (Mer du Nord). PhD Thesis, Université de Lorraine, pp. 339.

Ong, A., Pironon, J., Carpentier, C., and Girard, J.-P. (2014). Impact of fluid overpressure on reservoir quality of the Tabert sandstones (Middle Jurassic) in the Greater Alwyn Area, Q3 area, Northern North Sea, UK. In: Proceedings of "Journée thématique ASF. Diagenèse: avancées récentes et perspectives", Orsay, 4 July, 2014. Publication ASF, Paris, 75, 81-85.

Ong, A., Pironon, J., Robert, P., Dubessy, J., Caumon, M.-C., Randi, A., Chailan, O., and Girard, J.-P. (2013). In situ decarboxylation of acetic and formic acids in aqueous inclusions as a possible way to produce excess CH_4. Geofluids, 13, 298-304.

Palandri, J.L., and Kharaka, Y.K. (2004). A compilation of rate parameters of water-mineral interaction kinetics for application to geochemical modeling. Open file report 2004-1068, 1-70. 2004. USGS.

Palmer, A.N. (2007). Cave Geology. Cave Books, Dayton, OH, USA, 454p.

Parker, A., and Sellwood, B.W. (1994). Quantitative Diagenesis: Resent developments and applications to reservoir geology. Kluwer Academic Press, Dordrecht, Netherland, 288p.

Paterson, R.J., Whitaker, F.F., Smart, P.L., Jones, G.D., Oldham, D. (2008). Controls on early diagenetic overprinting in icehouse carbonates: Insights from modeling hydrologicql zone residence times using CARB3D + . Journal of Sedimentary Research, 78, 258-281.

Pelgrain de Lestang, A., Cosentino, L., Cabrera, J., Jimenez, T., and Bellorin, O. (2002). Geologically Oriented Geostatistics: an Integrated Tool for Reservoir Studies. Paper SPE 74371 presented at the SPE International Petroleum Conference and Exhibition in Mexico held in Villahermosa, Mexico, 10–12 February.

Peyravi, M., Rahimpour-Bonab, H., Nader, F.H., and Kamali, M.R. (2014). Dolomitization and buriql history of lower Triassic carbonate reservoir-rocks in the Persian Gulf (Salman offshore field). Carbonates and Evaporites, DOI 10.1007/s13146-014-0197-2

Pillot, D., Deville, E., and Prinzhofer, A. (2014). Identification and quantification of carbonate species using Rock-Eval pyrolysis. Oil & Gas Science and Technology (OGST), 69(2), 341-349.

Pironon, J. (2004). Fluid inclusions in petroleum environments: analytical procedure for PTX reconstruction. Acta Petrologica Sinica, 20(6), 1333-1342.

Pitzer, K. S. (1973). Thermodynamics of Electrolytes. I. Theoretical Basis and General Equations. Journal of Physical Chemistry, 12, 268-277.

Ponikarov, V.P. (1966). The Geology of Syria. In: Explanatory Notes on the Geological Map of Syria, Scale 1:200 000. Ministry of Industry, Syrian Arab Republic.

Pontiggia, M., Ortenzi, A., and Ruvo, L. (2010). New integrated approach for diagenesis characterization and simulation. Paper SPE 127236 presented at the SPE North Africa Technical Conference and Exhibition, Cairo, Egypt, 14-17 February.

Powell, JH, and Moh'd, B.K. (2011). Evolution of Late Cretaceous to Eocene alluvial and carbonate platform sequences in Jordan. GeoArabia, 17(3), 29-82.

Rahimpour-Bonab, H. (2007). A procedure for appraisal of a hydrocarbon reservoir continuity and quantification of its heterogeneity. Journal of Petroleum Science and Engineering, 58, 1-12.

Rahimpour-Bonab, H., Esrafili-Dizaji, B., and Tavakoli, V. (2010). Dolomitization and anhydrite precipitation in Permo-Triassic carbonates at the South Pars gasfield, offshore Iran: controls on reservoir quality. Journal of Petroleum Geology, 33(1), 43-66.

Rasolofosaon, P., and Zinszner, B. (2003). Petroacoustic Characterization of Reservoir Rocks For Seismic Monitoring Studies Laboratory Measurement of Hertz and Gassmann Parameters. Oil & Gas Science and Technology (OGST), 58(6), 615-635.

Ravenne, C., Galli, A., Doligez, B., Beucher, H., and Eschard, R. (2000). Quantification of facies relationships via proportion curves. In: Armstrong, M., Bettini, C., Champigny, N., Galli, A. and Remacre, A., Editors. Proceedings of the Geostatistics Sessions of the 31st International Geological Congress.—Quantitative geology and geostatistics, Rio de Janeiro, Brazil, 6–17 August 2000, **12**, Kluwer Academic, Dordrecht.

Reading, H.G., ed. (1996). Sedimentary environments: processes, facies and stratigraphy. Blackwell Science, 704p.

Reeder, R.J., ed. (1990). Carbonates: Mineralogy and Chemistry. Mineralogical Society of America, Rev. Mineral., 11, 399p.

Reeder, R.J., and Wenk, H.R. (1983). Structure Refinements of Some Thermally Disordered Dolomites. Am. Mineral. 68, 7-8, 769-776.

Rezaei, M., Sanz, E., Raeisi, E., Ayora, C., Vásquez--Suñé, E., Carrera, J. (2005). Reactive transport modeling of calcite dissolution in fresh-salt water mixing zone. Journal of Hydrology, 311, 282-298.

Riding, R.E., and Awramik, S.M. (2000). Microbial Sediments. Springer-Verlag Berlin Heidelberg.

Rietveld, H.M. (1969). A Profile Refinement Method for Nuclear and Magnetic Structures. Journal of Applied Crystallography, 2, 65-71.

Roberts, G., and Peace, D. (2007). Hydrocarbon plays and prospectivity of the Levantine Basin, offshore Lebanon and Syria from modern seismic data. GeoArabia, 12(3), 99-124.

Rohais, S., Bonnet, S., and Eschard, R. (2012). Sedimentary record of tectonic and climatic erosional perturbations in an experimental coupled catchment-fan system. Basin Research, 24, 198-212.

Ronchi, P., Jadoul, F., Ceriani, A., Di Giulio, A., Scotti, P., Ortenzi, A., and Fantoni, R. (2011). Multistage Dolomitization in an Early Jurassic Platform (Southern Alps, Italy): insights for the distribution of massive dolomitized bodies. Sedimentology, 58(2), 532-565.

Rongier, G., Collon-Drouiallet, P., and Filipponi, M. (2014). Simulation of 3D karst conduits with an object-distance based method integrating geological knowledge. Geomorphology, 217, 152-164.

Rosen, M.R., Miser D.E., and Warren, J.K. (1988). Sedimentology, mineralogy and isotopic analysis of Pellet Lake, Coorong region, South Australia. Sedimentology, 35, 1, 105-122.

Rosenbaum, J., and Sheppard, S.M. (1986). An isotopic study of siderites, dolomites and ankerites at high temperatures. Geochimica Cosmochimica Acta, 50, 1147-1150.

Rosenberg, E., Lynch, J., Guéroult, P., Bisiaux, M., and Ferreira de Paiva, R. (1999). High resolution 3D reconstructions of rocks and composites. Oil & Gas Science and Technology, 54(4), 497-511.

Roure, F., Swennen, R., Schneider, F., Faure, J.L., Ferket, H., Guilhaumou, N., Osadetz, K., Robian, P., and Vandeginste, V. (2005). Incidence and importance of tectonics and natural fluid migration on reservoir evolution in foreland fold-and-thrust belts. Oil and Gas Science and Technologie (OGST), 60(1), 67-106.

Royse, C.F., Wadell, J.S., and Petersen, L.E. (1971). X-ray determination of calcite-dolomite: an evaluation. Journal of Sedimentary Petrology, 41, 483-488.

Rustad, J.R., Casey, W.H., Yin, Q.-Z., Bylaska, E.J., Felmy, A.R., Bogatko, S.A., Jackson, V.E., and Dixon, D.A. (2010). Isotopic fractionation of Mg^{2+}(aq), Ca^{2+}(aq), and Fe^{2+}(aq) with carbonate minerals. Geochimica Cosmochimica Acta, 74, 6301–6323.

Sagan, J.A., Hart, B.S. (2006). Three-dimensional seismic-based definition of fault-related porosity development: Trenton–Black River interval, Saybrook, Ohio. AAPG Bulletin, 90(11), 1763–1785.

Santerre, Y., (2010). Influence of early diagenesis and sedimentary dynamics on petrophysical properties distribution in carbonate reservoirs. PhD Thesis, IFP and Marseille University.

Schauble, E.A. (2011). First-principles estimates of equilibrium magnesium isotope fractionation in silicate, oxide, carbonate and hexaaquamagnesium(2 +) crystals. Geochimica Cosmochimica Acta, 75, 844–869.

Schenk, H.J., Horsfield, B., Krooß, B., Schaefer, R.G., and Schwochau, K. (1997). Kinetics of petroleum formation and cracking. In: Petroleum and Basin Evolution, eds., D. H. Welte et al. Springer, Berlin, 535p.

Schmitz, J., Deschamps, R., Joseph, P., Lerat, O., Doligez, B., and Jardin, A. (2014). From 3D

photogrammetric outcrop models to reservoir models: an integrated modelling workflow. Extended abstracts in proceedings of the Vertical Geology Conference 2014, 5 – 7 February 2014, University of Lausanne, Switzerland, 143-148.

Shah, M.M., Nader, F.H., Dewit, J., Swennen, R., and Garcia, D. (2010). Fault-related hydrothermal dolomites in Cretaceous carbonates (Cantabria, northern Spain): Results of petrographic, geochemical and petrophysical studies. Bull. Soc. geol. Fr., 181(4), 391-407.

Shah, M.M., Nader, F.H., Garcia, D., Swennen, and Ellam, R. (2012). Hydrothermal dolomites in the Early Albian (Cretaceous) platform carbonates (NW Spain): Nature and origin of dolomites and dolomitising fluids. Oil & Gas Science and Technology (OGST), 67 (1), 97-122.

Sharland, P.R., Archer, R., Casey, D.M., Davies, R.B., Hall, S.H., Heward, A.P., Horbury, A.D., and Simmons, M.D. (2001). Arabian plate sequence stratigraphy. GeoArabia Special Publication, 2, 371p.

Simms, M.A. (1984). Dolomitization by groundwater-flow systems in carbonate platforms. Trans. Gulf Coast Assoc. Geol. Soc., 34, 411-420.

Sømme, T., Helland-Hansen, W., Martinsen, O. J., and Thurmond, J. B., (2009a). Relationships between morphological and sedimentological parameters in source-to-sink systems: a basis for predicting semiquantitative characteristics in subsurface systems. Basin Research, 21, 361–387.

Sømme, T., Martinsen, O. J., and Thurmond, J. B. (2009b). Reconstructing morphological and depositional characteristics in subsurface sedimentary systems: an example from the Maastrichtian-Danian Ormen Lange system, Møre Basin, Norwegian Sea. AAPG Bulletin, 93, 1347–1377.

Steinberg, J., Gvirtzman, Z., Folkman, Y., and Garfunkel, Z. (2011). Origin and nature of the rapid late Tertiary filling of the Levant Basin. Geology, 39, 355-358.

Sun, S.Q. (1995). Dolomite reservoirs: porosity evolution and reservoir characteristics. AAPG Bulletin, 79, 186-204.

Swennen, R., Dewit, J., Fierens, E., Muchez, P., Shah, M. M., Nader, F.H., and Hunt, D. (2012). Multiple dolomitisation events along the Pozalagua Fault (Pozalagua Quarry, Basque – Cantabrian Basin, Northern Spain). Sedimentology, 59, 1345-1374.

Swennen, R., Ferket, H., Benchilla, L., Roure, F. and Ellam, R.M., SUBTRAP Team (2003) Fluid flow and diagenesis in carbonate dominated foreland fold-and-thrust belts: petrographic inferences from field studies of late-diagenetic fabrics from Albania, Belgium, Canada, Mexico and Pakistan. Journal of Geochemical Exploration, 78-79, 481-485.

Tahmasebi, P., Sahimi, M., Mariethoz, G., and Hezarkhani, A. (2012). Accelerating Geostatistical Simulations using Graphical Processing Units. Computers & Geosciences, 46, 51 – 59, doi:10.1016/j.cageo.2012.03.028

Talon, L., Bauer, D., Gland, N., Youssef, S., Auradou, H., and Ginzburg, I. (2012). Assessment of the two relaxation time Lattice-Boltzmann scheme to simulate Stokes flow in porous media. Water Resources Research, 48, W04526, doi:10.1029/2011WR011385

Tucker, M.E. (1988). Techniques in Sedimentology. Blackwell Science Ltd, Oxford, 394p.

Turpin, M., Nader, F.H., and Kohler, E. (2012). Empirical calibration for dolomite stoichiometry calculation: Application on Triassic Muschelkalk-Lettenkohle carbonates (French Jura). Oil & Gas Science and Technology (OGST), 67(1), 77-95.

Van der Land, C., Wood, R., Wu, K., van Dijke, M. I.J., Jiang, Z., Corbett, P. W.M., and Couples, G. (2013). Modelling the permeability evolution of carbonate rocks. Marine and Petroleum Geology, 48, 1-7.

Videtich, P.E. (1994). Dolomitization and H_2S generation in the Permian Khuff Formation, offshore Dubai, U.A. E. Carbonates and Evaporites, 9, 42-57.

Wachter, E., and Hayes, J.M. (1985). Exchange of oxygen isotopes in carbon-dioxide – phosphoric acid systems. Chemical Geology, 52, 365-374.

Ward, W.C., and Halley, R.B. (1985). Dolomitization in a mixing zone of near-seawater composition, Late Pleistocene, northeastern Yucutan Peninsula. Journal of Sedimentary Petrology, 55, 407-420.

Warren, J. (2000). Dolomite: occurrence, evolution and economically important associations. Earth-Sci. Rev., 52, 1-3, 1-81.

Whitaker, F.F., and Smart, P.L. (1990). Circulation of saline groundwaters through carbonate platforms; evidence from the Great Bahama Bank. Geology, 18, 200-204.

Whitaker, F.F., and Smart, P.L. (2007a). Geochemistry of meteoric diagenesis in carbonate islands of the northern Bahamas: 1. Evidence from field studies. Hydrological Processes, 21, 967-982.

Whitaker, F.F., and Smart, P.L. (2007b). Geochemistry of meteoric diagenesis in carbonate islands of the northern Bahamas: 2. Geochemical modelling and budgeting of diagenesis. Hydrological Processes, 21, 967-982.

Whitaker, F.F., Smart, P.L., and Jones, G.D. (2004). Dolomitization: from conceptual to numerical models. In: Braithwaite, C.J.R., Rizzi, G., and Darke, G., eds., The Geometry and Petrogenesis of Dolomite Hydrocarbon Reservoirs: London, Geological society of London. Special Publications 235, 99-139.

White, R.S., and McKenzie, D. (1989). Magmatism at rift zones: the generation of volcanic continental margins and flood basalts. Journal of Geophysical Research, 94, 7685-7729.

Wilson, J.L. (1975). Carbonate facies in geologic history. Springer-Verlag, Berlin, Heidelberg, 471p.

Wu, K., Ryazanov, A., van Dijke, M.I.J., Jiang, Z., Ma, J., Couples, G., and Sorbie, K.S. (2008). Validation of methods for multi-scale pore space reconstruction and their use in prediction of flow properties of carbonate. In: International Symposium of the Society of Core Analysts, Abu Dhabi.

Wygrala, B.P. (1989). Integrated study of an oil field in the southern Po Basin, Northern Italy. PhD thesis, University of Cologne, Germany.

Yarus, J.M., and Chambers, R.L. (2006). Practical Geostatistics-An Armchair Overview for Petroleum Reservoir Engineers. Society of Petroleum Engineers, SPE 103357.

Young, E.D., and Galy, A. (2004). The isotope geochemistry and cosmochemistry of magnesium. Reviews in Mineralogy & Geochemistry, 55, 197-230.

Youssef, S., Rosenberg, E., Gland, N., Skalinski, M., and Vizika, O. (2007). High resolution CT and pore-network models to assess petrophysical properties of homogeneous and heterogeneous carbonates, *Paper SPE* 111427 presented at the *SPE/EAGE Reservoir Characterization and Simulation Conference*, Abu Dhabi, U.A.E., 28-31 October.

Youssef, S., Han, M., Bauer, D., Rosenberg, E., Bekri, S., Fleury, M., and Vizika, O. (2008). High resolution μ-CT combined to numerical models to assess electrical properties of bimodal carbonates, *Paper SCA* 2008 - Temp Paper#A54 presented at the *International Symposium of Core Analysts*, Abu Dhabi, UAE, 29-30 October.

Zeyen, H., Volker, F., Wehrle, V., Fuchs, K., Sobolev, S. V., and Altherr, R. (1997). Styles of continental rifting: crust-mantle detachment and mantle plumes. Tectonophysics, 278, 329-352.

Zilberman, E., and Calvo, R. (2013). Remnants of Miocene fluvial sediments in the Negev Desert, Israel, and the Jordanian Plateau: Evidence for an extensive subsiding basin in the northwestern margins of the Arabian plate. Journal of African Earth Sciences, 82, 33-53.